Gold Mining

Formation and Resource Estimation, Economics and Environmental Impact

Melanie D. Corral
Jared L. Earle
Editors

NOVA

GOLD MINING: FORMATION AND RESOURCE ESTIMATION, ECONOMICS AND ENVIRONMENTAL IMPACT

GOLD MINING: FORMATION AND RESOURCE ESTIMATION, ECONOMICS AND ENVIRONMENTAL IMPACT

MELANIE D. CORRAL
AND
JARED L. EARLE
EDITORS

Nova Science Publishers, Inc.
New York

LIBRARY OF CONGRESS CATALOGING-IN-PUBLICATION DATA

Gold mining : formation and resource estimation, economics, and environmental impact / [edited by] Melanie D. Corral and Jared L. Earle.
p. cm.
Includes bibliographical references and index.
ISBN 978-1-61728-428-1 (E-Book)
1. Gold mines and mining. 2. Gold ores. I. Corral, Melanie D. II. Earle, Jared L.
TN410.G65 2009
622'.3422--dc22
2009013516

Published by Nova Science Publishers, Inc. † New York

CONTENTS

PREFACE

Gold, a chemical element with the symbol Au, is a highly sought-after precious metal, having been used as money, in jewelry, in sculpture, and for ornamentation since the beginning of recorded history. The metal occurs as nuggets or grains in rocks, in veins and in alluvial deposits. Gold mining consists of the processes and techniques employed in the removal of gold from the ground. There are several techniques by which gold may be extracted from the Earth. Since the 1880s, South Africa has been the source for a large proportion of the world's gold supply, with about 50% of all gold ever produced having come from South Africa. Other major producers are the United States, Australia, China, Russia and Peru. The world's oceans also hold a vast amount of gold, but in very low concentrations. At current consumption rates, the supply of gold is believed to last 45 years. This book will present current research on gold mining including methodologies for discovering new deposits of gold as well as economic and environmental issues.

Chapter 1 - The prerequisite condition of gold mining is to find where gold deposits are located within the upper crust of the Earth. Since the existing gold deposits that are found through surface exploration technology will be completely mined in the foreseeable future, it is imperative to explore for new concealed giant gold deposits under the cover of the Earth surface. This requires that new predictive exploration methods be developed for understanding the fundamental mechanisms that control ore body formation and mineralization within the upper crust of the Earth. Towards this end, the computational geoscience methodology has been developed for investigating ore forming mechanisms over the past decade. The main purpose of this chapter is to present a modern mineralization theory that is not only associated with the advanced computational geoscience methodology, but also can be used to explore the potential mineral precipitation patterns in hydrothermal systems within the upper crust of the Earth. The central part of the modern mineralization theory is to consider the interaction between pore-fluid flow, heat transfer, mass transport and chemical reactions that take place within the upper crust of the Earth in a comprehensive manner. For a chemically equilibrium system, the approximate form (i.e. the rock alteration index and the improved rock alteration index) of the mineralization rate concept can be used to predict the mineral precipitation patterns in hydrothermal systems. But for a chemically non-equilibrium system, the detailed interaction between solute advection, solute diffusion/dispersion and chemical kinetics needs to be considered to determine potential mineral precipitation patterns in hydrothermal systems within the upper crust of the Earth.

Several examples are given to demonstrate how the modern mineralization theory is used for predicting mineral precipitation patterns in hydrothermal systems.

Keywords: Formation mechanism, gold deposits, mineral precipitation patterns, computational geoscience methodology.

Chapter 2 - Miners, geologists, and engineers have been solving problems related to geo-spatial data for generations. A major task of mineral exploration consists of mapping the bedrock and surficial geology using traditional field methods, geochemical analysis, geophysical exploration, and aero-photo interpretations. Integration of field survey data and other pertinent information for the purpose of mineral resource estimation can be a time-consuming task. However since the development of Geographic Information Systems (GIS) technology in 1962, most of these tasks can now be accomplished in a more time-efficient manner. With the increasing popularity and functional development of GIS in recent years, many mining companies started using GIS as the preferred tool for mine planning, analysis, and management. The commodities market, environmental regulations and government policies pushed companies to further streamline their operations and become more competitive and cost effective. Moreover, the state and federal agencies involved in the mine permitting process are adopting the GIS format as the standard for communicating spatial data.

This paper presents a case study of GIS application in gold resource estimation. It is a synthesis of a series of previously published works. GIS technology has been applied to compile, integrate, analyze and visualize the offshore marine placer gold deposits at Nome, Alaska. With the help of GIS, information on placer gold deposits can be updated, queried, visualized, and analyzed much more effectively than before. Various geostatastical interpolation methods, such as Inverse Distance Weighted (IDW), Ordinary Kriging (OK), Ordinary Kriging with lognormal transformation (OK-log), Simple Kriging (SK) and Indicator Kriging (IK), were studied and compared to strike for an optimum approach of resource estimation. Ore body boundaries and the resource estimation at various cutoff grades at any given domain can be calculated interactively. In addition, a web-based GIS was developed to facilitate remote users to access the data. The GIS architecture developed in this project was designed for general usage and can be adapted to mineral resource estimation in other study areas.

Chapter 3 - Gold mining from Roşia Montană is located in the Apuseni Mountains, in the west-central part of Romania and can be traced back to approximately 106 a.d. at the beginning of the Roman occupation of Dacia. In the medieval times the sporadic mining activity was mentioned, but accelerated in the XVIII-XIXth centuries. In the last 60 years underground and open surface mining activities were conducted, but presently, due to some Romanian governmental budget constraints, the state-owned mining company develops activities only at a small scale.

The study of Roşia Montană ecosystem was based on zinc, cadmium, lead, copper and manganese concentration determination in the streams, rivers and drinking water. Also, the concentration of gold from two medicinal plants, *Equisetum arvense* and *Achillea millefolium* collected from this region and from the other one was determined. It was observed that the concentrations of heavy metals were above the limits accepted by the Romanian Standard. One of the main pollution source is the solid rock (waste) deposited by the river sides. Acid Rock Drainage (ARD) is a naturally occurring process caused when water and air come into the contact with rocks containing sulphide minerals. Naturally occurring bacteria bring about

acidification which in turn leaches heavy metals from rocks. The acid water produced can disturb the aquatic life and contaminate dinking water supplies.

It is well known from literature, that *Equisetum arvense* is a gold bioaccumulator and it is used as a prospector for its ores. The medicinal plants collected from Roşia Montană district presented a higher concentration of gold than the plants from other regions. From the results obtained it was observed that Roşia Montană District is an ecosystem impacted by the mining industry.

Chapter 4 - Economic evaluation of gold mining projects is a key input to the go/not-to-go decision. This is usually carried out by developing a cash-flow model projecting future revenues, capital and operating costs and other cash flow items. Based on these cash inflows and outflows, net annual cash flows throughout project lifetime are generated and measures of project merit, such as payback period (PB), discounted cash flow internal rate of return (IRR) and net present value (NPV), are estimated. In such conventional economic analysis, annual revenues are estimated assuming that future gold prices and gold production are known with certainty. If the analysis requires dealing with a foreign currency, the conventional practice is to assume certainly-known future exchange rates. In most cases, flat gold prices and exchange rates are applied throughout project life time. As with market variables, future amounts of gold production are assumed to be known with certainty.

In reality, both the market and geological variables are highly uncertain. Given this fact, it is possible that future conditions will be different from what is expected at project start-up time. In this case, management is expected to respond to the new information by revising original operating plans. The important shortcoming of conventional economic evaluation methods, based on static discounted cash flow analysis, is that they ignore this management flexibility to alter or revise production decisions in the future based on the new information. In some cases, the additional value of such management flexibility could be a large proportion of project value and can have a significant impact on the decision-making process.

In contrast to static evaluation methods, the real options valuation (ROV) approach can incorporate the dynamic nature of future operating policy into current value estimates of gold mining projects. In this respect, management flexibility to revise original production plans in the future according to the new information is integrated into the financial evaluation model. This article aims to explore the differences between conventional static economic evaluation methods and the modern ROV technique. A comparison between the two evaluation approaches is provided through a case study of a gold mining project.

Keywords: Gold mining; Economic evaluation; Discounted cash flow; Real options valuation.

Chapter 5 - Ghana is a major player in the gold mining industry globally and in Africa in particular. The country is ranked 11th in the global league of gold producers and the second, only after South Africa, in Africa. Ghana's gold bearing rocks are confined to five parallel bands of metavolcanic and metasedimentary rocks locally called gold belts. The most dominant of these belts is the Ashanti belt, which accounts for nearly 80% of the gold mines and 90% of total annual gold output. Four main kinds of gold deposits exist in these gold-bearing corridors. These are placer or alluvial deposit, which occurs along stream courses draining these corridors, and quartz reef (free milling); extracted mainly by gravity concentration; sulphide ores and the oxidised sulphide ore; both of which are extracted by heap-leach methods. Non-sulphidic paleoplacer (free milling) ore occurs mainly in the Banket conglomerates of the Tarkwaian Formation. The premier valued gold is associated with well

sorted and packed hematite rich conglomerates that occur in the thinner beds. The oxidised ores, associated mainly with the Birimian rock formation, occur in the weathered rocks and are derived from sulphides, principally arsenopyrite,and pyrites and their primary derivatives are the sulphide ores etc. Two main types of mining operations exist- large scale and artisanal mining. The artisanal miners exploit mainly placer or alluvial gold. The chemistry of gold ores, type of mining and processing technologies employed, present considerable challenges to water resources management in these mining area. Almost all surface water bodies within the mining areas are polluted and aquatic life in most of them is extremely low or non existent. Significant number of streams and shallow wells has disappeared due to over abstraction of groundwater for gold processing and dewatering of mines. Acid mine drainage is also a major concern. Though groundwater contamination is not a major concern in the mining areas due to impoverishment of the rocks of heavy metals, isolated cases of high arsenic, mercury, iron, manganese and aluminium concentrations in groundwater are of major concern for drinking water supply. Gold mining has also resulted in severe land degradation and major environmental concerns.

Chapter 6 - Ghana has had a long history of gold production, and is known that in the 18th century gold was shipped by foreign trading ports (e.g., British, Dutch, Danish) from the Ashanti Region of the then Gold Coast. The Ashanti Region is a primary gold producing area; and in the former times the Ashanti goldfields was the source of the wealth of the Ashanti Kings. Today, the gold mining sector in Ghana is one of the most important and fast growing industries earning foreign exchange for the country. It exerts strong physical, socio-economic and cultural benefits on the nation and particularly on the local residents. Unfortunately, gold mining has caused arsenic contamination through the oxidation of sulphide minerals as well as diffuse contamination of mercury to be released into the environment. Consequently, vegetation has become degraded and giant plant species have been dwarfed. Foodcrops are also found to have high content of arsenic. Fruit trees and rootcrops now have longer maturity period and eventually low yields of agricultural products. The result is that malaria, cancer and non-cancer diseases, Buruli ulcer and other skin diseases are prevalent in these mining environments.

Chapter 7 - Although gold production is relatively minor from the Arabian–Nubian shield at present, extensive alluvial and lode fields along the western side of the Red Sea in Upper Egypt and northern Sudan were worked out by the ancient Egyptians for thousands of years. In the Eastern Desert of Egypt, numerous but small gold deposits are generally related to auriferous quartz veins commonly associated with brittle-ductile shear zones, generally cutting through the Neoproterozoic crystalline basement rocks and trending in different directions. Gold mineralization at the Betam mine area, south Eastern Desert, is related to a series of milky quartz veins along a NNW- trending brittle-ductile shear zone cutting through successions of pelitic schists, next to a small granite intrusion. Gold-sulfide mineralization (pyrite, arsenopyrite, galena, subordinate chalcopyrite and gold) is closely associated with a conspicuous hydrothermal alteration halo. Textural relationships, including replacement and crosscutting of mineral phases and quartz veins record a post-foliation alteration assemblage of quartz+sericite+chlorite+ calcite±albite±epidote.

The hydrothermal alteration halo alongside the auriferous quartz veins comprises three distinct zones, namely: (a) distal chlorite-calcite zone (chlorite+calcite±biotite±pyrite± sericite±epidote), (b) intermediate sericite-chlorite zone (sericite+chlorite+pyrite±biotite), and (c) proximal pyrite-sericite zone (quartz+pyrite+sericite±albite). These zones merge to each

other gradually, ending outwards into the unaltered metasediments. The pyrite-sericite zone presents the highest gold grade, especially in zones thickly seamed with sulfide-rich quartz veinlets. Mass balance calculations revealed that the pyrite-sericite zone experienced significant metasomatic changes relative to limited mass and volume changes for the chlorite-calcite zone. The overall picture of chemical gains and losses with increase the intensity of hydrothermal alteration is indicative of: (i) addition of SiO_2, K_2O, Na_2O, S, L.O.I., (ii) removal of MgO, and (iii) relatively inert behavior of Al_2O_3, TiO_2, MnO, Fe_2O_3. CaO is variably mobile, slightly gained in the chlorite-calcite and sericite-chlorite zones but depleted in the pyrite-sericite zone. Concnetrations of the trace elements are variable in the different alteration types, but a notable increase in Au, As, Ba, Sr, Rb, V, and Ni in the intensively altered rocks is verified. Investigation of the REE behavior reveals a little modification of their distribution pattern with hydrothermal alteration. Heavy REE are more or less unchanged, whereas light REE are significantly mobile in all alteration types.

New geochemical data provide evidence for progressive silicification, sericitization, and sulfidation as a function of gold mineralization. A proposed model for the hydrothermal alteration system for the Betam deposit includes fluctuation in pH and redox state (f_{O2}), mainly during the wall-rock sulfidation. This might have destabilized gold complexes and lowered gold solubility in solution, hence contributed at least partly in gold deposition in the study area. A decrease in the whole rock $\delta^{18}O$ values from un-altered country metasediments to the distal, intermediate and proximal alteration zones, respectively, might be attributed to rock interaction with an isotopically lighter fluid. In addition, sulfur isotope data of pyrite-arsenopyrite pairs in the mineralized quartz veins and adjacent wall-rock along with the calculated $\delta^{34}S_{\Sigma S}$ values for the ore fluids suggest derivation form non-homogenous (mixed magmatic and metamorphic) fluids.

Chapter 8 - This paper discusses the recent and dramatic rationalization of key sectors of South Africa's once powerful mining industry and the effects on former mining towns. Whilst older coalfields have been replaced by new areas of production, the same is not true for gold. A key challenge for mine towns facing job loss and mine closure is how to respond through appropriate local actions which can diversify local economies and create jobs. The paper draws on the experience of different South African centres in this regard.

Chapter 9 - Phytochelatins (PCs) are a group of small, metal-binding peptides that are biosynthesized by higher plants, some fungi and algae in the response to heavy metal exposure. One actual research topic focuses on better understanding the global effect that all elements present in natural environments exert on the PCs production by plants.

In this work, PCs levels were evaluated in the wild plants, chronically exposed to low or moderate levels of heavy metals. The quantification of total PCs in plant extracts was carried out by HPLC with fluorimetric detection, after derivatization of free –SH groups with monobromobimane. Additionally, the distribution of metals in molecular mass (MM) fractions of these same extracts was studied by size exclusion chromatography with on-line UV and ICP-MS detection. All samples were collected in Guanajuato city (Mexico), which has long been an important silver and gold mining area. Among different metals reported in Guanajuato soils, lead, cadmium, copper and silver were selected in this study, because of their capability to induce phytochelatins in plants. The common plants from this region were analyzed, namely: *Ricinus communis* (castor bean), *Tithonia diversifolia* (Mexican sunflower) and *Opuntia ficus* (nopal). The analytical approach involved the ICP-MS analysis of total

elements in soil, soil fractions and wild plants and also the evaluation of relationships between PCs, metal levels found in plants/soil and different soil parameters.

In the analysis of plants, PC-2, PC-3 and PC-4 were detected in nopal, PC-2 in castor bean, while in Mexican flower no phytochelatins were found. In further development, the extracts of soil humic substances were obtained and the distribution of metals in molecular mass (MM) fractions was studied by size exclusion chromatography with on-line UV and ICP-MS detection. The soil humic substances (HS) were also assessed.

In search of possible relationship between the parameters measured, the statistical analysis of correlation was performed. The results obtained indicate that the binding of metals to soil HS contributes in lowering their uptake by castor bean plant. On the other hand, the soils collected at nopal roots presented low HS levels and no correlation with metals in plant was found. The results obtained in the sequential extraction of soils and the abundance of sulfide minerals in Guanajuato indicate that the sulfide bound metals were the primary forms of Pb, Cu and Cd in soil adjacent to nopal roots. Owing to their generally poor solubility, rizosphere processes should be important in mobilizing metals and their uptake by nopal.

Our results provide further evidence on the role of environmental conditions in the accumulation of heavy metals in relation to PCs production in different plant genotypes. In particular, multi-elemental approach is necessary in studies on PCs induction in actual field situations, where plants (or other organisms) are exposed to a variety of metals and metalloids.

In: Gold Mining: Formation and Resource Estimation ISBN: 978-1-60741-096-6
Editors: M. D. Corral, J. L. Earle

Chapter 1

UNDERSTANDING FORMATION MECHANISMS OF GOLD DEPOSITS BY MEANS OF COMPUTATIONAL GEOSCIENCE METHODOLOGY

Chongbin Zhao
Computational Geosciences Research Centre,
Central South University, Changsha 410083, China

ABSTRACT

The prerequisite condition of gold mining is to find where gold deposits are located within the upper crust of the Earth. Since the existing gold deposits that are found through surface exploration technology will be completely mined in the foreseeable future, it is imperative to explore for new concealed giant gold deposits under the cover of the Earth surface. This requires that new predictive exploration methods be developed for understanding the fundamental mechanisms that control ore body formation and mineralization within the upper crust of the Earth. Towards this end, the computational geoscience methodology has been developed for investigating ore forming mechanisms over the past decade. The main purpose of this chapter is to present a modern mineralization theory that is not only associated with the advanced computational geoscience methodology, but also can be used to explore the potential mineral precipitation patterns in hydrothermal systems within the upper crust of the Earth. The central part of the modern mineralization theory is to consider the interaction between pore-fluid flow, heat transfer, mass transport and chemical reactions that take place within the upper crust of the Earth in a comprehensive manner. For a chemically equilibrium system, the approximate form (i.e. the rock alteration index and the improved rock alteration index) of the mineralization rate concept can be used to predict the mineral precipitation patterns in hydrothermal systems. But for a chemically non-equilibrium system, the detailed interaction between solute advection, solute diffusion/dispersion and chemical kinetics needs to be considered to determine potential mineral precipitation patterns in hydrothermal systems within the upper crust of the Earth. Several examples are given to demonstrate how the modern mineralization theory is used for predicting mineral precipitation patterns in hydrothermal systems.

Keywords: Formation mechanism, gold deposits, mineral precipitation patterns, computational geoscience methodology.

1. INTRODUCTION

Standard practice in traditional mineral exploration industry is to analyse data in two dimensions using geological maps and cross-sections, and to identify targets principally by experience and empirical methods. Although this kind of practice achieved significant success in finding gold deposits of some indicators on the Earth surface in the past, it has met a serious challenge in finding concealed gold deposits under the cover of the Earth surface in recent years. On the other hand, both a significant rise in living standards and a global growth in human population, particularly in China and India, are fuelling a dramatic increase in demand for natural minerals throughout the world. Since traditional exploration methods of empirical nature are commonly invalid in finding concealed giant ore deposits under the cover of the Earth surface, many of major existing gold deposits are not only depleting or experiencing declining grades, but also the rate of new discoveries has been significantly declined in the last few decades. The serious problem that we are confronting is that, if new deposits are not found and developed, there will be a long-term decline in the size and financial contribution of minerals industry within the whole world. As a result, the contradiction between minerals demand and supply may become so serious that the living standards of mankind must be degraded.

To find concealed giant ore deposits under the cover of the Earth surface, it is necessary to develop scientific and predictive methods, in which the controlling physical and chemical processes associated with ore body formation and mineralization occurring in the deep Earth can be considered effectively and efficiently. Towards this direction, the framework of a new scientific discipline, known as computational geoscience, has been established in recent years (Zhao et al. 2008a, 2009). Since computational geoscience is established through applying a combination of mathematics, physics, chemistry and advanced computer algorithms in the well-developed computational science to solve geoscience problems, it is obviously of multi-disciplinary nature crossing many fields of science. For this reason, the computational geoscience methodology is a comprehensive research methodology, which is formed by combining field observation, theoretical analysis, computational simulation and field validation. The primary aim of using the computational geoscience methodology is to investigate dynamic processes and mechanisms of observed geological phenomena, rather than to describe the observed geological phenomena themselves. The major physical and chemical processes, which are commonly considered in the computational simulation of ore forming systems within the upper crust of the Earth, are the material deformation process, pore-fluid flow process, heat transfer process, mass transport process and chemical reaction process (Garven and Freeze 1984, Yeh and Tripathi 1991, Steefel and Lasaga 1994, Raffensperger and Garven 1995, Zhao et al. 1997, Schafer et al. 1998, Zhao et al. 1998a, Xu et al. 1999, Zhao et al. 2000a-b, 2001a-b, Schaubs and Zhao 2002, Zhao et al. 2002-2005, 2006a-b, 2008a-f). These processes are often fully coupled in a nonlinear, multi-scale manner. Thus, we must not only develop modelling capabilities to simulate each of the above

processes, but also we have to develop modelling capabilities to simulate the forward and backward interactions amongst them in a seamless and parallel manner.

Using the computational geoscience methodology, we need to establish the following three kinds of models for a typical mineralization problem: a conceptual model, a mathematical model and a computational simulation model. In terms of establishing a conceptual model, the following five questions need to be answered (Hobbs et al. 2000, Schaubs and Zhao 2002, Gow et al. 2002, Ord et al. 2002, Sorjonen-Ward et al. 2002): (1) What is the architecture of the complete mineral system? (2) What is the geological history of the system with an emphasis on timing, pressure and temperature history? (3) What processes were responsible for driving pore-fluid flow? (4) What were the physical and chemical processes involved with (and signatures of) the pore-fluids responsible for mineralization? (5) What were the processes involved in the precipitation and development of minerals and alteration at the site of mineralization? The answers to these five questions are fundamental to the construction of realistic conceptual models of ore body generation and to supply detail of geometrical size, material distributions, physical and chemical processes, initial and boundary conditions for these models. In terms of establishing a mathematical model, three fundamental scientific principles, namely the conservation laws of mass, momentum and energy, as well as the related physical and chemical theorems are commonly used to describe the controlling processes associated with ore body formation and mineralization within the upper crust of the Earth. As a result, a set of partial differential equations are obtained from the derivation of the mathematical model. Using numerical discretization methods such as the finite element method, the finite difference method, the boundary element method and so forth, a computational simulation model consisting of a set of algebraic equations can be established from the derived mathematical model. After this set of algebraic equations is solved, numerical solutions of approximate nature can be obtained for the considered mineralization problem. Since numerical methods produce approximate solutions for ore body formation and mineralization problems, computational simulation models work well but only if they are good ones and their limitations are appropriately appreciated. For example, the numerical solution reliability of a mineralization problem is strongly dependent on the algorithm convergence, algorithm stability, mesh shape, time-step and other factors. To ensure the accuracy and reliability of computational simulation results for a mineralization problem, the above-mentioned factors need to be carefully considered in the process of establishing computational simulation models. A newly-developed computer program needs to be verified through the corresponding benchmark problem before it is used to solve any real mineralization problems. Otherwise, the reliability of the computational simulation solution obtained from the newly-developed computer program cannot be guaranteed.

Since a mineralizing system within the upper crust of the Earth is commonly regarded as a complex science system with multi-scale and multi-process characteristics, it is still very difficult to simultaneously simulate the whole mineralizing system, from a particle (i.e. mineral) scale to a crustal scale, in one computational model. Nevertheless, it is possible to separately simulate mineral precipitation patterns within a mineralizing system using a series of computational models of different scales. This allows only some key factors to be considered for each of the computational models. By integrating all the mineral precipitation patterns obtained from a series of computational models of different scales, it is possible to understand the formation mechanisms behind mineralizing systems. For this reason, several generic mineralization problems of different scales are considered in this investigation.

2. CONTROLLING PROCESSES ASSOCIATED WITH ORE BODY FORMATION AND MINERALIZATION WITHIN THE UPPER CRUST OF THE EARTH

From the scientific point of view, a mineralization problem within the upper crust of the Earth may involve the following physical and chemical processes: material deformation, pore-fluid flow, heat transfer, mass transport and chemical reactions. Since the time scale of a mechanical deformation process is much small than that of any other processes, material deformation due to tectonic actions can be decoupled from other key controlling processes associated with ore body formation and mineralization within the upper crust of the Earth. For example, it takes only a minute for an earthquake wave to travel a few thousands of kilometers within the Earth's crust, but it takes about a few tens of million years for a thermal source to conduct heat from the bottom to the top of a 10*km* thick crust. For this reason, the upper crust of the Earth can be treated as an undeformable porous medium, at least from the ore body and mineralization point of view. Although mechanical processes can be decoupled from many of other key controlling processes associated with ore body formation and mineralization, they can produce porosity and flow channels, which are essential for ore body formation and mineralization to take place within the upper crust of the Earth. This means that before running a computational model for solving a mineralization problem, a mechanical deformation problem needs to be firstly solved to determine the porosity distribution and flow channels. Regarding the mechanical deformation of crustal materials, there are two different approaches available. One approach is based on the concept of continuum mechanics, while the other approach is based on the concept of discontinuity mechanics. Both the finite element method and the finite difference method belong to the continuum mechanics approach, whereas the particle simulation method belongs to the discontinuity mechanics approach.

Compared with the finite element method (Zienkiewicz 1977, Lewis and Schrefler 1998) and the finite difference method (Zhao et al. 1994), the particle simulation method is more suitable for simulating porosity generation arising from spontaneous crack initiation within brittle crustal rocks (Zhao et al. 2006c, 2007a-c, 2008g). In the particle simulation method, Newton's second law is used to describe the motion of each particle, while a linear function is often used to describe the force-displacement relationship at a contact between two particles. If the normal force at a contact is greater than the corresponding normal bond strength, then a tensile crack is generated at this contact. Similarly, if the tangential force at a contact is greater than the corresponding shear bond strength, then a shear crack is generated at this contact. Since the particle simulation method can be used to simulate micro-structural elements of materials, it can produce numerical solutions to scientific and engineering problems where the macroscopic constitutive laws of materials are not available. In addition, the particle simulation method can be also used, in the continuum mechanics sense, to represent continuum materials through the separation of part of a computational domain, this enables the particle simulation method to be used for dealing with the coupled problem between continuum mechanics and discontinuity mechanics. With the relatively inexpensive high performance hardware rapidly becoming available, it is possible to consider coupled systems of particles consisting of millions and most recently billions of particles. Combined with recent algorithmic developments, the particle simulation method has become a powerful

tool for solving a diversity of scientific and engineering problems, ranging from powder technology, ceramics, design of composite materials, rock blasting, demolition, blast impact and a great number of applications in geological, civil, mechanical, naval and environmental engineering (Cundall and Strack 1979, Bardet and Proubet 1992, Saltzer and Pollard 1992, Donze et al. 1994, 1996, Scott 1996, Itasca Consulting Group, inc. 1999, Camborde et al. 2000, Iwashita and Oda 2000, Cundall 2001, Burbidge and Braun 2002, Finch et al. 2004, Cleary 2004, Klerck et al. 2004, McBride et al. 2004, Owen et al. 2004, Potyondy and Cundall 2004, Schubert et al. 2005, Zhao et al. 2006c, 2007a-c). The major advantage in using the particle simulation method is that since there is no mesh in the particle simulation method and the interaction between particles is explicitly expressed by contact forces and displacements, crack generation in brittle crustal materials can be modeled in a much easier and explicit manner. For this reason, the particle simulation method has been successfully used to deal with the numerical simulation of spontaneous crack generation problems in large-scale geological systems (Zhao et al. 2007a-c, 2008g).

For the mathematical modelling of pore-fluid flow, heat transfer and reactive mass transport processes at a crustal scale, Darcy's law is used to describe pore-fluid flow in fluid-saturated porous rocks, while Fourier's law and Fick's law are used to describe the heat transfer process and mass (chemical species) transport process respectively. In addition, the Oberbeck-Boussinesq approximation is employed to describe a change in pore-fluid density arising from a change in pore-fluid temperature. Using these scientific laws, the corresponding governing equations for steady-state (i.e. a state to represent the long-term response of a system) pore-fluid flow, heat transfer and reactive mass (chemical species) transport in two-dimensional fluid-saturated porous rocks can be expressed as follows:

$$\frac{\partial u}{\partial x}+\frac{\partial v}{\partial y}=0, \tag{1}$$

$$u=\frac{K_x}{\mu}(-\frac{\partial P}{\partial x}+\rho_f g_x), \tag{2}$$

$$v=\frac{K_y}{\mu}(-\frac{\partial P}{\partial y}+\rho_f g_y), \tag{3}$$

$$\rho_{f0}c_p(u\frac{\partial T}{\partial x}+v\frac{\partial T}{\partial y})=\lambda_{ex}\frac{\partial^2 T}{\partial x^2}+\lambda_{ey}\frac{\partial^2 T}{\partial y^2}, \tag{4}$$

$$u\frac{\partial C_k}{\partial x}+v\frac{\partial C_k}{\partial y}=D_{e0}(\frac{\partial^2 C_k}{\partial x^2}+\frac{\partial^2 C_k}{\partial y^2})+\phi R_k, \qquad (k=1, 2, \ldots n), \tag{5}$$

$$\rho_f=\rho_{f0}[1-\beta_T(T-T_0)], \tag{6}$$

$$\lambda_{ex} = \phi\lambda_{fx} + (1-\phi)\lambda_{sx}, \qquad \lambda_{ey} = \phi\lambda_{fy} + (1-\phi)\lambda_{sy}, \tag{7}$$

$$D_{e0} = \phi D_0, \tag{8}$$

where u and v are the velocity components of the pore-fluid in the x and y directions respectively; P and T are pore-fluid pressure and temperature; C_k is the concentration of chemical species k; ρ_{f0} and T_0 are the reference density of the pore-fluid and the reference temperature of the porous rock; μ and c_p are the dynamic viscosity and specific heat of the pore-fluid; λ_{fx} and λ_{sx} are the thermal conductivities of the pore-fluid and rock mass in the x direction; λ_{fy} and λ_{sy} are the thermal conductivities of the pore-fluid and rock mass in the y direction; ϕ and β_T are the porosity of the porous rock and the thermal volume expansion coefficient of the pore-fluid; D_0 is the diffusivity of the chemical species; K_x and K_y are the permeabilities of the porous rock in the x and y directions respectively; g_x and g_y are the gravity acceleration components in the x and y directions; n is the total number of chemical species in the system; R_k is a source/sink term for chemical species k due to the relevant chemical reactions in the considered mineralization system.

3. Understanding Some Typical Kinds of Dynamic Mechanisms of Ore Body Formation and Mineralization Using the Computational Geoscience Methodology

Although a real mineralization system within the crust of the Earth is a complicated and complex science system, it is possible to find the major factors and processes that control ore body formation and mineralization within the real mineralization system. In essence, ore body formation is a consequence of mineral dissolution, transportation, precipitation and enrichment within the upper crust of the Earth. No matter how complicated and complex a mineralization system is, the mass of a mineral must be conserved within the mineralization system. This means that for a given type of mineralization system, only a few key factors and processes may control ore body formation and mineralization within the mineralization system. In this regard, simplified generic models can be used to investigate the critical factors involved not only in setting an ore body at a particular location and but also in controlling the size and grade for a given type of mineralization system. From a geological point of view, there is a tendency to attempt to incorporate all known geological detail in computational models from the very beginning. If all the factors are considered in a computational model, it is very difficult to discovery the critical factors and processes that really control ore body formation and mineralization within the ore forming system. The preferred approach is to start as simply, but as realistically, as possible and then progressively add more detail as an understanding of the ore forming processes is developed. In many circumstances, a simple generic model may enable a lot of the critical issues to be defined and investigated. One

important aspect of this generic model approach is that it enables much progress to be made in understanding the formation mechanisms of ore deposits with a reasonably low level of data thus speeding the investigative process and cutting the computational cost. For such reasons, three different kinds of generic models are used to investigate the key factors and their effects on mineralization patterns in hydrothermal systems within the upper crust of the Earth.

3.1. General Patterns of Ore Body Formation and Mineralization Associated with Convective Pore-fluid Flow within Hydrothermal Systems

In this situation, Equation (1) is used to describe the mass conservation of pore-fluid; whereas Equations (2) and (3) are used to describe the momentum conservation of pore-fluid. Since heat can be transferred either by conduction in solid or by advection in pore-fluid, Equation (4) is used to describe the energy conservation of the porous rock system. For simplicity, only one typical aqueous mineral is considered in the mineralization system. This allows the reactive mass transport equation (i.e. Equation (5)) can be expressed in the following manner:

$$u\frac{\partial C_1}{\partial x}+v\frac{\partial C_1}{\partial y}=D_{e0}\left(\frac{\partial^2 C_1}{\partial x^2}+\frac{\partial^2 C_1}{\partial y^2}\right)+\phi R_1, \tag{9}$$

where C_1 is the concentration of the aqueous mineral; R_1 is the source/sink term due to the relevant chemical reactions in the system. Other quantities are of the same meanings as defined previously.

If the chemical solution is near equilibrium and the reacting mineral constitutes only a small fraction of the whole matrix in a porous medium, the source/sink term due to chemical reactions can be approximately expressed as follows (Phillips 1991, Zhao et al. 1998a):

$$R_1=\gamma(C_{1e}-C_1), \tag{10}$$

where γ is the reaction rate of dimension $1/t$; C_{1e} is the equilibrium concentration of the mineral.

It is noted that for a given aqueous mineral, R_1 being greater than zero means a source term for the aqueous mineral, while R_1 being smaller than zero means a sink term for the aqueous mineral, from the reactive mass transport of view. In the former case, the solid mineral in the porous rock is dissolved into the pore-fluid, whereas in the latter case, the aqueous mineral is precipitated into the pores of the porous rock. This indicates that from the reactive mass transport equation, the mineral dissolution or precipitation rate R_1 can be evaluated for a (near) chemically equilibrium system as follows:

$$\phi R_1 = u\frac{\partial C_{1e}}{\partial x} + v\frac{\partial C_{1e}}{\partial y} - D_{e0}\left(\frac{\partial^2 C_{1e}}{\partial x^2} + \frac{\partial^2 C_{1e}}{\partial y^2}\right). \tag{11}$$

For ore body formation problems, the diffusion term on the right hand side of Equation (11) is usually much smaller than the advection term (Phillips 1991). In this case, the mineral dissolution/precipitation rate, which forms the core part of the modern mineralization theory (Zhao et al. 1998a, 2002), can be approximated by the following equation:

$$\phi R_1 \approx u\frac{\partial C_{1e}}{\partial x} + v\frac{\partial C_{1e}}{\partial y} = \frac{\partial C_{1e}}{\partial T}\left(u\frac{\partial T}{\partial x} + v\frac{\partial T}{\partial y}\right) + \frac{\partial C_{1e}}{\partial P}\left(u\frac{\partial P}{\partial x} + v\frac{\partial P}{\partial y}\right). \tag{12}$$

For temperature gradient driven convective flows, the term $u\frac{\partial P}{\partial x} + v\frac{\partial P}{\partial y}$ is usually small, so that the sign of ϕR_1 is determined by the term of $u\frac{\partial T}{\partial x} + v\frac{\partial T}{\partial y}$, provided the partial derivative of C_{1e} with respect to T is positive definite in the temperature range considered. For this reason, the term of $u\frac{\partial T}{\partial x} + v\frac{\partial T}{\partial y}$ is called the rock alteration index (Phillips 1991) or *RAI* for short. Using vector definitions for both the pore-fluid velocity and the temperature gradient, *RAI* can be expressed in the following form:

$$RAI = u\frac{\partial T}{\partial x} + v\frac{\partial T}{\partial y} = \vec{u} \bullet \nabla T, \tag{13}$$

where

$$\vec{u} = u\vec{i} + v\vec{j} \text{ and } \nabla T = \frac{\partial T}{\partial x}\vec{i} + \frac{\partial T}{\partial y}\vec{j}.$$

Dimensionless variables and governing equations are always preferred in the study of problems involving multiple scales and multiple processes. The main advantages in using dimensionless variables and governing equations are as follows: (1) Solutions for dimensionless variables describe the behaviour of a family of problems rather than that of a particular problem. This makes the solutions more generally applicable. (2) Dimensionless variables can be used to measure the relative importance of various terms in governing equations, so that the dominant physical phenomenon can be identified for the problem. This provides a clear focus for the effective and efficient modelling of the problem. (3) Dimensionless equations can result in a significant reduction in the large differences between orders of magnitude for some terms in the corresponding dimensional equations. This generally makes the numerical solution more accurate and stable. For these reasons, the

following dimensionless variables are used to derive the corresponding dimensionless governing equations:

$$x^* = \frac{x}{H}, \quad y^* = \frac{y}{H}, \quad T^* = \frac{T - T_0}{\Delta T}, \tag{14}$$

$$u^* = \frac{H\rho_{f0}c_p}{\lambda_{e0}}u, \quad v^* = \frac{H\rho_{f0}c_p}{\lambda_{e0}}v, \quad P^* = \frac{K_h\rho_{f0}c_p}{\mu\lambda_{e0}}(P - P_0), \tag{15}$$

$$K_x^* = \frac{K_x}{K_h}, \quad K_y^* = \frac{K_y}{K_h}, \quad \lambda_{ex}^* = \frac{\lambda_{ex}}{\lambda_{e0}}, \quad \lambda_{ey}^* = \frac{\lambda_{ey}}{\lambda_{e0}}, \tag{16}$$

where x^* and y^* are the dimensionless coordinates; u^* and v^* are the dimensionless velocity components in the x^* and y^* directions respectively; P^* and T^* are the dimensionless excess pressure and temperature; K_h is a reference medium permeability coefficient in the horizontal direction; λ_{e0} is a reference thermal conductivity coefficient of the porous rock; $\Delta T = T_{bottom} - T_0$ is the temperature difference between the bottom and top boundaries of the porous rock; H is a reference length and P_0 is the static pore-fluid pressure.

Substituting the above dimensionless variables into Equations (1) to (4) yields the following dimensionless governing equations:

$$\frac{\partial u^*}{\partial x^*} + \frac{\partial v^*}{\partial y^*} = 0, \tag{17}$$

$$u^* = K_x^*\left(-\frac{\partial P^*}{\partial x^*} + RaT^*e_1\right), \tag{18}$$

$$v^* = K_y^*\left(-\frac{\partial P^*}{\partial y^*} + RaT^*e_2\right), \tag{19}$$

$$u^*\frac{\partial T^*}{\partial x^*} + v^*\frac{\partial T^*}{\partial y^*} = \lambda_{ex}^*\frac{\partial^2 T^*}{\partial x^{*2}} + \lambda_{ey}^*\frac{\partial^2 T^*}{\partial y^{*2}}, \tag{20}$$

where $\boldsymbol{e}$ is a unit vector and $\boldsymbol{e} = e_1\vec{i} + e_2\vec{j}$ for a two-dimensional problem; Ra is the Rayleigh number of the hydrothermal system.

$$Ra = \frac{(\rho_{f0} c_p)\rho_{f0} g\beta \Delta T K_h H}{\mu \lambda_{e0}}. \tag{21}$$

Based on the related dimensionless quantities, the dimensionless form of the *RAI* can be defined as follows:

$$RAI^* = u^* \frac{\partial T^*}{\partial x^*} + v^* \frac{\partial T^*}{\partial y^*} = \vec{u}^* \bullet \nabla T^*. \tag{22}$$

It is obvious that for $\frac{\partial C_{1e}}{\partial T} > 0$, $RAI^* > 0$ implies mineral dissolution; whereas $RAI^* < 0$ implies mineral precipitation. As a result, the value of RAI^* can be used as an approximate indicator to investigate the potential mineral precipitation patterns in hydrothermal systems within the upper crust of the Earth (Zhao et al. 1998a). To demonstrate this point, three basins of different shapes are considered in this section. As shown in Figure 1, the first basin is a trapezoidal basin. The ratios of the top width to height and the bottom width to height are 2 and 1 respectively. This basin is discretized into 2304 four-node quadrilateral elements. The second basin is a vertical compartment with an upper folded surface, consisting of two layers of different permeabilities. The ratio of the permeabilities is 10 between the lower and the upper layers. The total dimensionless height is 1.2 and the top layer has a dimensionless thickness of 0.2. The second basin is modelled by 2784 four-node quadrilateral elements. The third basin is a tilted compartment with folded surfaces top and bottom, composed of three layers. The permeability of the middle layer is 10 times that of both the top and the bottom layers. In addition, the dimensionless thicknesses for the top layer, middle layer and bottom layer are 0.2, 1 and 0.2 respectively. This basin is discretized into 3264 four-node quadrilateral elements. The permeability in the horizontal direction is assumed to be three times that in the vertical direction for all three basins. Except for free flow on the top surface, impermeable boundary conditions are applied to other three boundaries. In addition, two different constant temperatures are applied to both the top and the bottom boundaries respectively, whereas insulated boundary conditions are applied to the two lateral boundaries of the corresponding computational model.

Figure 2 shows the corresponding results for the dimensionless rock alteration index distributions, which are used to display the general precipitation/dissolution patterns of minerals within the three different sedimentary basins. In this figure, red and blue indicate the highest mineral dissolution and precipitation regions respectively. Since clockwise convective cells are formed in both the first computational model (i.e. the model for the trapezoidal basin) and the second computational model (i.e. the model for the compartment with upper folded surface), the mineral precipitation regions are located in the upper left regions of these two computational models. In these mineral precipitation regions, the aqueous mineral of an equilibrium concentration is transported from a high temperature region into a low temperature region. If the equilibrium concentration of a mineral decreases as the decrease of temperature, then the aqueous mineral transported from the high temperature region must be precipitated when it enters the low temperature region. Clearly, the general precipitation

patterns associated with ore body formation and mineralization are also different for these three different basins, indicating that basin shapes may have an important influence on the locations and tonnages of ore deposits within the upper crust of the Earth.

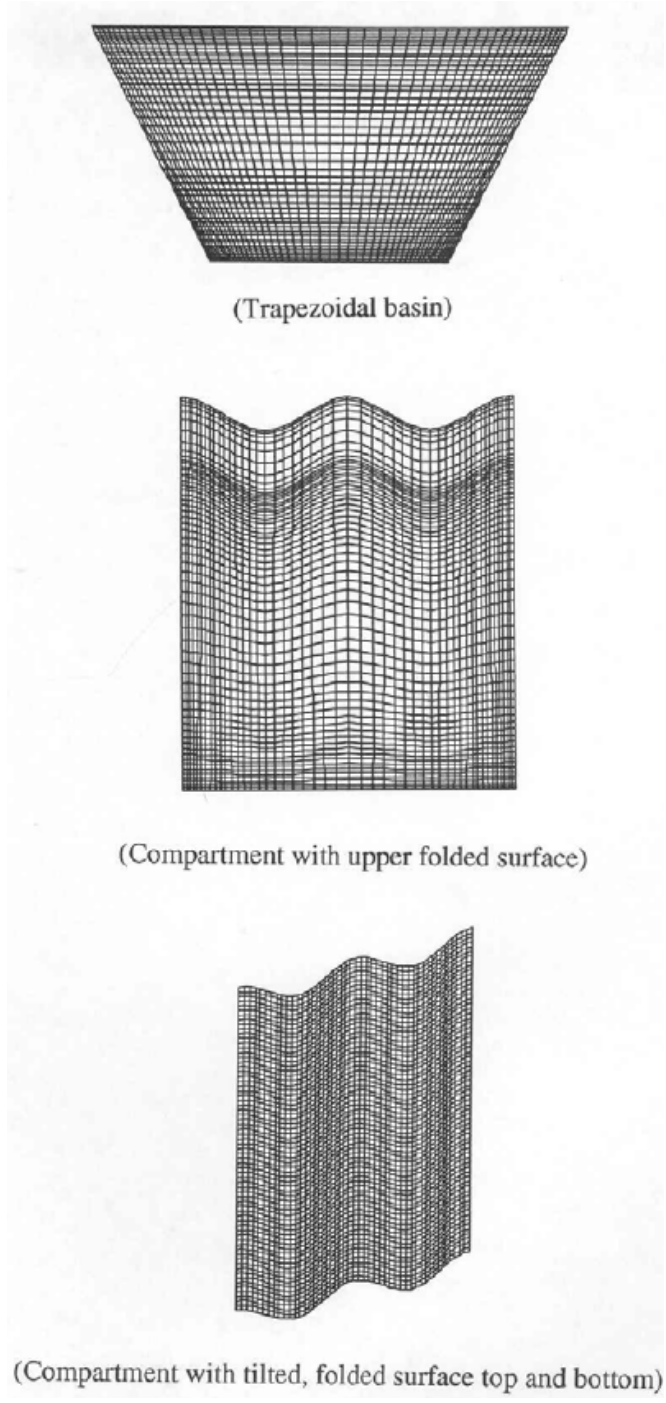

Figure 1. Finite element meshes for three different geological domains.

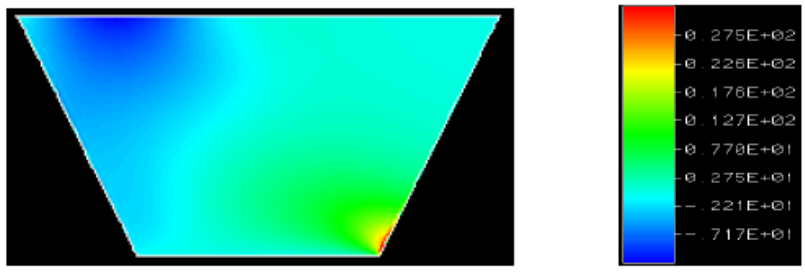

(Trapezoidal basin, *Ra*=80)

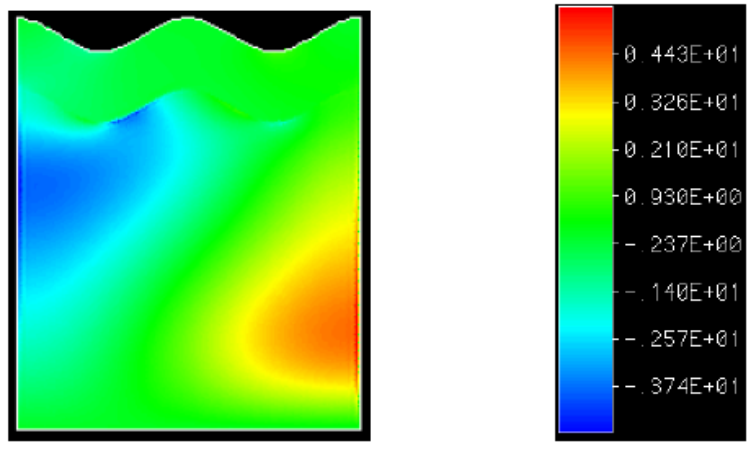

(Compartment with upper folded surface, *Ra*=100)

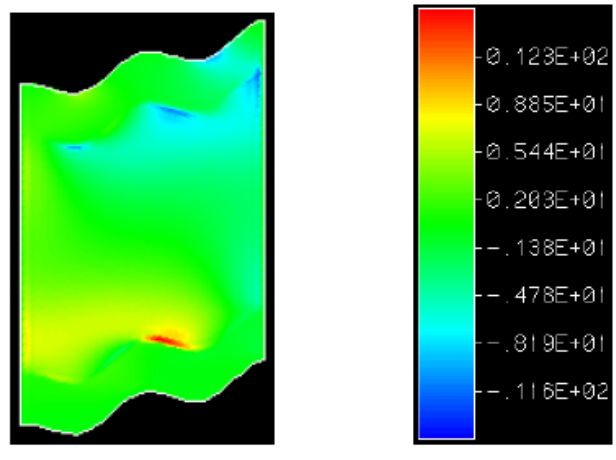

(Compartment with tilted, folded surface top and bottom, *Ra*=200)

Figure 2. Dimensionless rock alteration index distributions for three different geological compartments.

3.2. General Patterns of Gold Mineralization Associated with Convective Pore-fluid Flow within Layered Hydrothermal Systems

In the previous section, it has demonstrated that once the pore-fluid velocity and temperature distributions within a hydrothermal system are computed by the finite element method, the rock alteration index (*RAI*) (Phillips 1991, Zhao et al. 1998a) can be used to evaluate the most probable precipitation and dissolution regions of minerals in the system. If one is interested in predicting the precipitation and dissolution region of a specific mineral (e.g. gold) in a hydrothermal system, then the temperature and/or pressure dependent nature of the equilibrium concentration of the mineral should be taken into account. This leads to the improved rock alteration index (*IRAI*) for predicting the precipitation and dissolution region of a specifically-concerned mineral in any hydrothermal systems within the upper crust of the Earth (Zhao et al. 2000b).

From the scientific principles used in previous studies (Phillips 1991, Zhao et al. 1998a), the improved rock alteration index (*IRAI*) can be defined as follows:

$$IRAI = \frac{\partial C_e}{\partial T}\left(u\frac{\partial T}{\partial x} + v\frac{\partial T}{\partial y}\right) = \frac{\partial C_e}{\partial T}(\vec{u} \bullet \nabla T), \tag{23}$$

where C_e is the equilibrium concentration of the concerned mineral in a hydrothermal system.

Note that the difference between the rock alteration index and the improved rock alteration index is the inclusion of the term, $\frac{\partial C_e}{\partial T}$, in Equation (23). This means that the improved rock alteration index is mineral dependent because different minerals may have different equilibrium concentrations for the same temperature and/or pressure. For this reason, dimensional quantities, instead of dimensionless quantities, are often used to compute the improved rock alteration index (*IRAI*).

For a pyrite-pyrrhotite buffer (Shenberger and Barnes 1989), the equilibrium concentration of gold at temperature between $0^o C$ and $350^o C$ can be expressed in a piecewise manner as follows:

$$\log C^e_{Au} = 0.0369T - 7.1845 \qquad (0 \le T < 50^o C),$$

$$\log C^e_{Au} = 0.03T - 6.84 \qquad (50^o C \le T < 100^o C),$$

$$\log C^e_{Au} = 0.0248T - 6.32 \qquad (100^o C \le T < 150^o C),$$

$$\log C^e_{Au} = 0.0208T - 5.72 \qquad (150^o C \le T < 200^o C),$$

$$\log C^e_{Au} = 0.0144T - 4.44 \qquad (200^o C \le T < 250^o C),$$

$$\log C_{Au}^{e} = 0.0096T - 3.24 \qquad (250^{o}C \le T < 300^{o}C),$$

$$\log C_{Au}^{e} = 0.0036T - 1.44 \qquad (300^{o}C \le T \le 350^{o}C), \qquad (24)$$

where C_{Au}^{e} is the equilibrium concentration of gold.

Figure 3 shows the variation of gold (Au) equilibrium concentration with temperature under the pyrite-pyrrhotite buffer condition, while Figure 4 shows the distribution of the differentiation of gold (Au) equilibrium concentration with respect to temperature under the same pyrite-pyrrhotite buffer condition. It is observed that the solubility of gold in the pyrite-pyrrhotite buffer is essentially identical to zero below $150^{o}C$ and increases gradually from $150^{o}C$ to $350^{o}C$. More importantly, the differentiation of gold equilibrium concentration with respect to temperature may vary significantly from $150^{o}C$ to $350^{o}C$. This clearly indicates that using the improved rock alteration index may predict more accurately the precipitation and dissolution regions of gold in a hydrothermal system. For this reason, the improved rock alteration index is used to predict the possible regions of gold mineralization in this section.

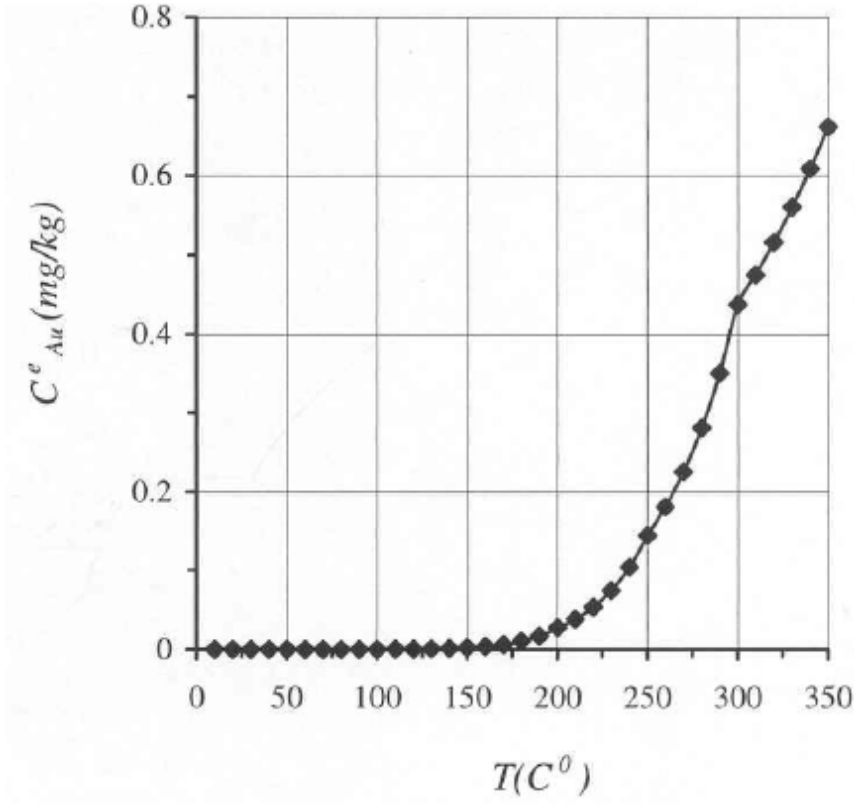

Figure 3. Variation of Au equilibrium concentration with temperature (Pyrite-Pyrrhotite buffer).

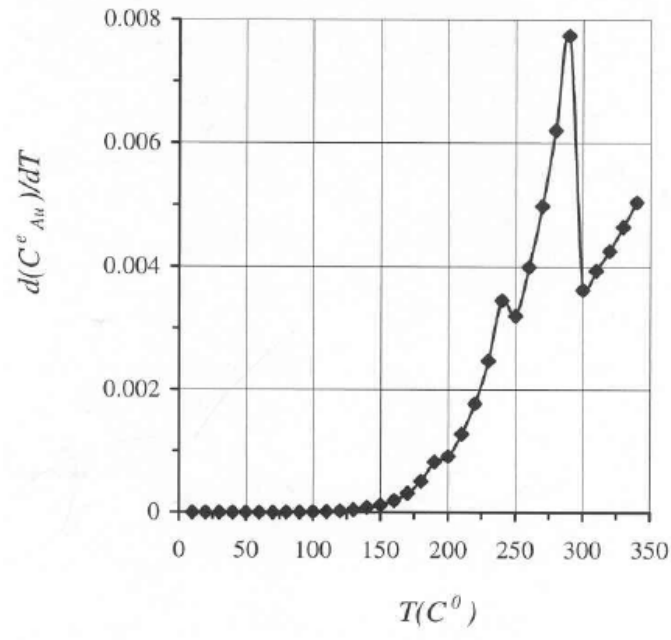

Figure 4. Distribution of the differentiation of Au equilibrium concentration with respect to temperature (Pyrite-Pyrrhotite buffer).

To achieve the above purposes, the finite element method associated with the progressive asymptotic approach procedure (Zhao et al. 1997) is used. As shown in Figure 5, a computational domain of two layers is discretized into 2500 quadrilateral elements with 2601 nodes in total. The length of the computational domain is 10*km*; while the thickness of each layer in the computational domain is 5*km*. The following parameters are used in the computation. For the pore-fluid, dynamic viscosity is $10^{-3} N \cdot s / m^2$; reference density is $1000 kg / m^3$; volumetric thermal expansion coefficient is $2.07 \times 10^{-4} (1/^0 C)$; specific heat is $4185 J / (kg \cdot ^0 C)$; thermal conductivity coefficient is $0.6 W / (m \cdot ^0 C)$. For the porous matrix, porosity is assumed to be 0.1 for both layers; permeability is $10^{-14} m^2$ for the upper layer; thermal conductivity coefficient is $3.35 W / (m \cdot ^0 C)$; the excess pressure at the top of the layered system is assumed to be zero. The temperature at the top surface of the layered system is $25^o C$. The conductive heat flux and the vertical pore-fluid velocity at the bottom of the layered system are $0.06 W / m^2$ and $1.7 \times 10^{-11} m / s$ respectively. From a physical point of view, the conductive heat flux of $0.06 W / m^2$ at the bottom of the layered system is approximately equivalent to applying an average vertical temperature gradient of $20^o C / km$ to the whole layered system if the upward throughflow is small. In order to examine the permeability effects of the lower layer on the convective pore-fluid flow, heat transfer and gold mineralization in the layered system, two permeabilities, namely $K^L = 10^{-17} m^2$ and $K^L = 10^{-16} m^2$, are used for the lower layer in the corresponding computations.

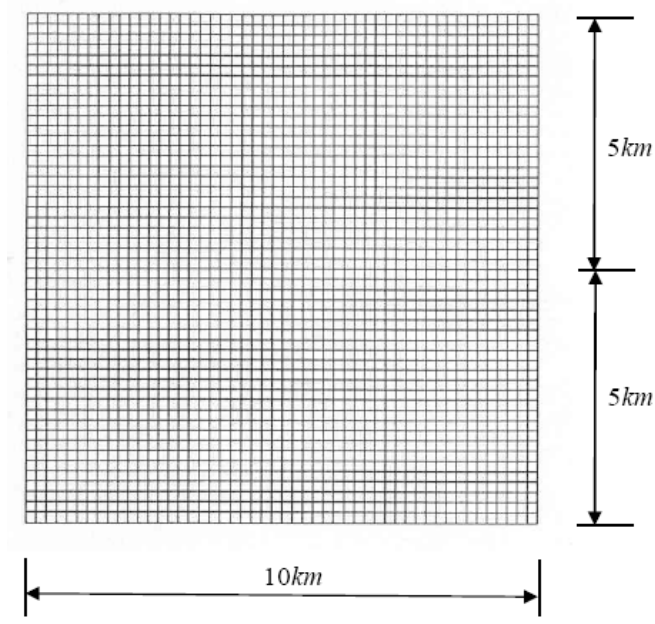

Figure 5. Finite element mesh for a layered hydrothermal system.

Figure 6 shows the pore-fluid velocity distributions in the layered hydrothermal system with upward throughflow due to two different permeabilities in the lower layer, while Figure 7 shows the corresponding stream function distributions in the layered hydrothermal system. Clearly, the convective pore-fluid flow driven by the temperature gradient occurs in the layered hydrothermal system. In the case of $K^L = 10^{-17} m^2$, the initial pore-fluid pressure gradient in the lower layer prior to heating the system is identical to the lithostatic pressure gradient, whereas the initial pore-fluid pressure gradient in the upper layer prior to heating the system is between the hydrostatic and lithostatic pressure gradients (Zhao et al. 1998b). However, in the case of $K^L = 10^{-16} m^2$, the initial pore-fluid pressure gradient in both the upper and the lower layers prior to heating the system is between the hydrostatic and lithostatic pressure gradients, even though the initial pore-fluid pressure gradient in the lower layer is greater than that in the upper layer. This indicates that no matter what value the initial pore-fluid pressure gradient in the layered system might be, the convective pore-fluid flow driven by the temperature gradient in a layered hydrothermal system can occur as long as the system is hot enough. Also, it can be observed that although the maximum values of the pore-fluid velocity are of the same order of magnitude for the two cases of different permeabilities in the lower layer, the patterns of the pore-fluid flow are significantly different. In the case of $K^L = 10^{-17} m^2$, the convective pore-fluid flow is dominated by one major convection cell, but in the case of $K^L = 10^{-16} m^2$, there are two major convection cells to dominate the pore-fluid flow. As expected, the convective pore-fluid flow driven by the temperature gradient has resulted in the localization of the temperature distribution in the layered hydrothermal system. This localization can be seen from the results shown in Figure 8.

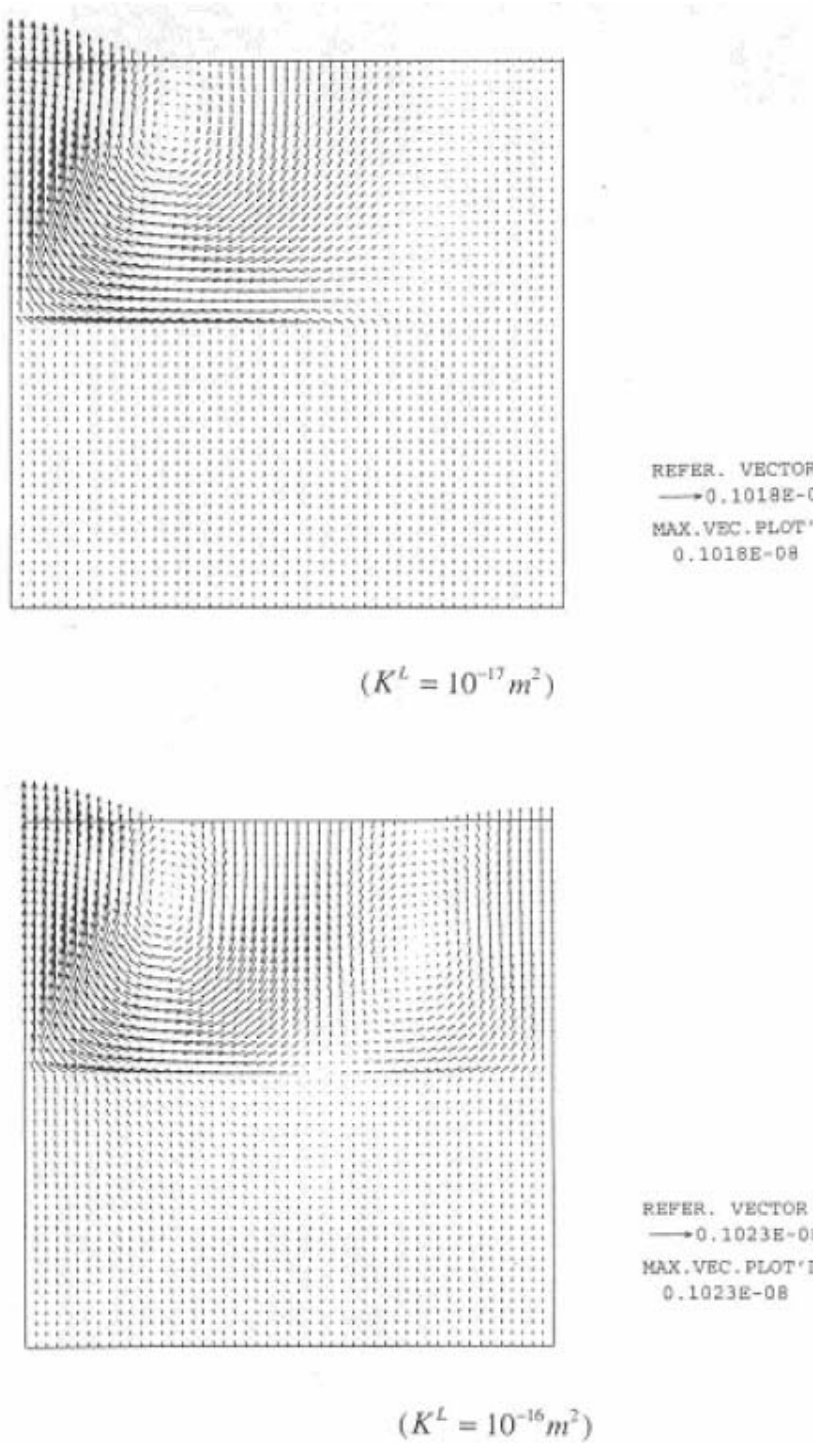

Figure 6. Pore-fluid velocity distributions in the layered hydrothermal system.

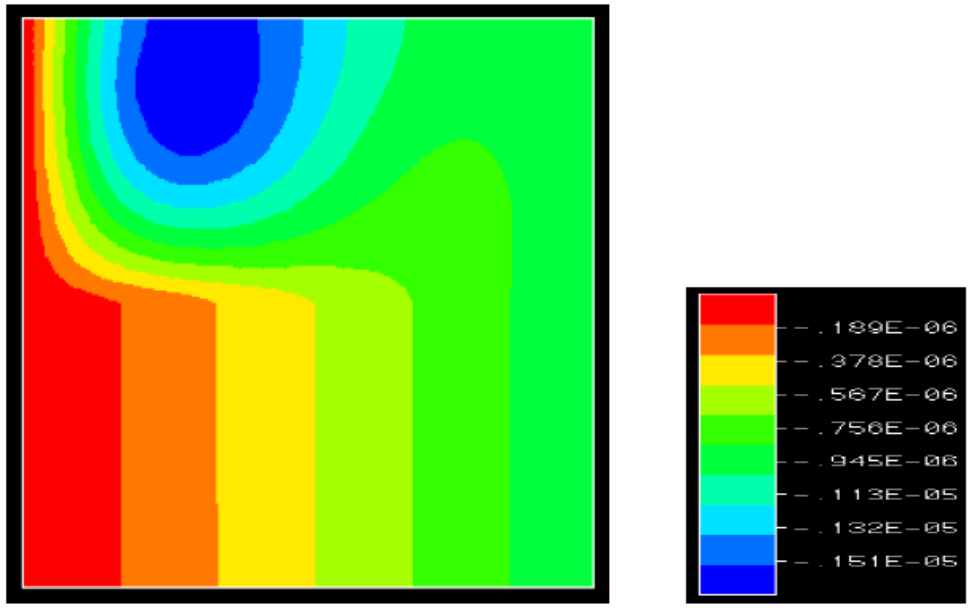

$(K^L = 10^{-17} m^2)$

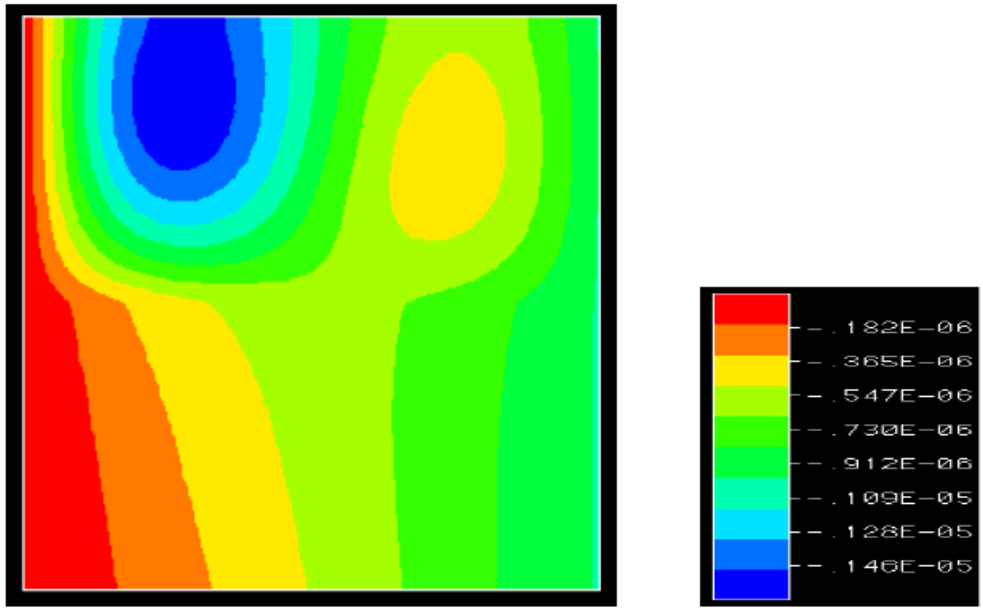

$(K^L = 10^{-16} m^2)$

Figure 7. Stream function distributions in the layered hydrothermal system.

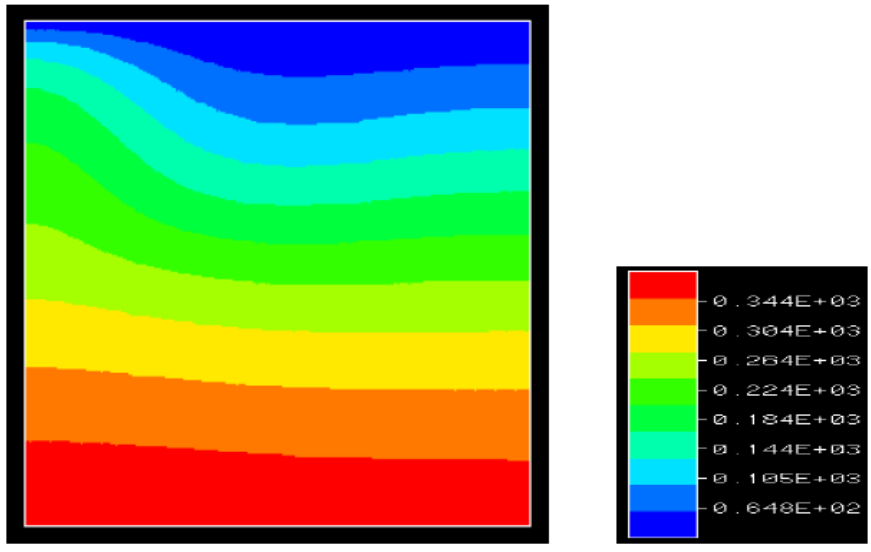

$(K^L = 10^{-17} m^2)$

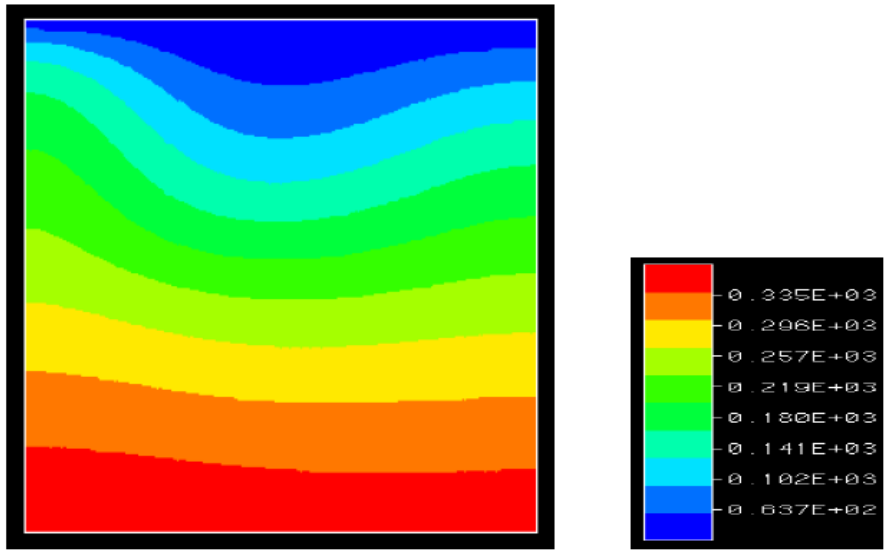

$(K^L = 10^{-16} m^2)$

Figure 8. Temperature distributions in the layered hydrothermal system.

Figure 9 shows the improved rock alteration index (*IRAI*) distributions in the layered hydrothermal system with upward throughflow due to two different permeabilities in the lower layer. In this figure, blue and red indicate the highest precipitation and dissolution regions of gold in the layered hydrothermal system. It is clear that in the upper layer of the system, the precipitation regions of gold are very similar for the two cases of different permeabilities in the lower layer, even though the dissolution regions of gold are remarkably

different for the two cases. In the lower layer of the system, the precipitation regions of gold are significantly different for the two cases of different permeabilities in the lower layer. This indicates that the relative ratio of the permeability of the upper layer to that of the lower layer may affect the gold mineralization in the layered hydrothermal system with upward throughflow. Since the highly localized, high grade regions of gold can be predicted in layered hydrothermal systems, it has been demonstrated that the proposed improved rock alteration index is useful for predicting the regions of gold mineralization in layered hydrothermal systems with upward throughflow.

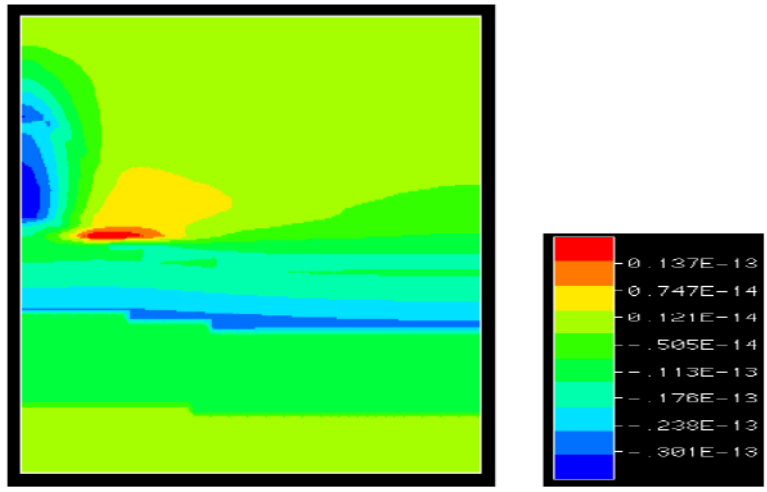

$(K^L = 10^{-17} m^2)$

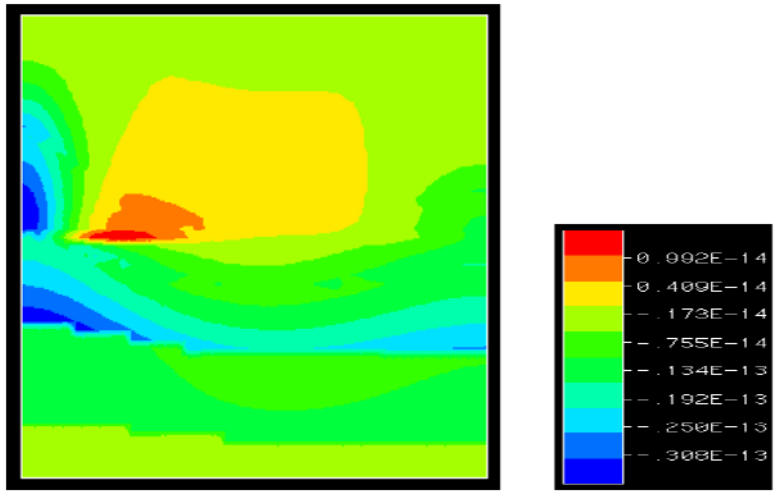

$(K^L = 10^{-16} m^2)$

Figure 9. Improved rock alteration index distributions in the layered hydrothermal system.

3.3. General Patterns of Ore Body Formation and Mineralization Associated with Focusing and Mixing of Pore-fluids within Two-dimensional Geological Fault Zones

For the purpose of investigating the transient process of ore body formation and mineralization associated with focusing and mixing of pore-fluids within two-dimensional geological fault zones, a time term needs to be considered in the reactive mass transport equation (Zhao et al. 2007d). Thus, Equation (5) can be rewritten in the following form:

$$\phi \frac{\partial C_k}{\partial t} + u \frac{\partial C_k}{\partial x} + v \frac{\partial C_k}{\partial y} = D_{e0}\left(\frac{\partial^2 C_k}{\partial x^2} + \frac{\partial^2 C_k}{\partial y^2}\right) + \phi R_k, \quad (k=1, 2, \ldots n). \tag{25}$$

Without loss of generality and simplicity, the following chemical reaction is considered to investigate the effect of solute advection, diffusion/dispersion and chemical kinetics on chemical reaction patterns within two-dimensional geological fault zones.

$$A + B \underset{k_b}{\overset{k_f}{\Leftrightarrow}} AB, \tag{26}$$

where A and B are two chemical reactants; AB is the chemical product due to this reaction; k_f and k_b are the forward and backward reaction rates, the faster of which is defined as the controlling reaction rate of this reaction.

From the chemical reaction point of view, the general chemical reaction source/sink terms due to the redox chemical reaction expressed by Equation (26), and included in the reaction-transport equation (i.e. Equation (25)), can be written as follows:

$$R_A = -k_f r^{n_f - 1} C_A C_B + k_b r^{n_b - 1} C_{AB}, \tag{27}$$

$$R_B = -k_f r^{n_f - 1} C_A C_B + k_b r^{n_b - 1} C_{AB}, \tag{28}$$

$$R_{AB} = k_f r^{n_f - 1} C_A C_B - k_b r^{n_b - 1} C_{AB}, \tag{29}$$

where C_A, C_B and C_{AB} are the concentrations of chemical species A, B and AB; R_A, R_B and R_{AB} are the chemical reaction source/sink terms associated with chemical species A, B and AB; n_f and n_b are the orders of the forward and backward reactions respectively; r is a quantity with a numerical value of one and units of the reciprocal of the chemical species concentration to balance the unit of the reaction source/sink terms due to different orders of chemical reactions. For the redox reaction expressed by Equation (26), the forward reaction is of the second order, while the backward reaction is of the first order. Since a redox system allows chemical reactions to proceed in both the product and the reactant directions, the

orders of the forward reaction (i.e. the chemical reaction proceeding towards the product) and backward reaction (i.e. the chemical reaction proceeding towards the reactant) can be determined from the related chemical kinetics.

In a theoretical study carried out previously (Zhao et al. 2007d), it has been demonstrated that for a permeable vertical fault zone and for a given solute diffusion/dispersion coefficient, there exist three possible types of chemical reaction patterns, depending on both the flow rate and the chemical reaction rate. The first type of chemical reaction pattern is dominated by solute diffusion and dispersion, so that minerals are precipitated at the lower tip of a vertical fault zone and as a thin sliver within the fault zone (i.e. Type 1 mineral precipitation pattern). The second type of chemical reaction pattern is dominated by solute advection, so that minerals are precipitated at or above the upper tip of the fault zone. For the third type of chemical reaction pattern, advection and diffusion/dispersion play similar roles in the reactive mass transport system, so that minerals are precipitated as wide mineralization within the fault zone. The related theoretical analysis also indicated that there exist both an optimal flow rate and an optimal chemical reaction rate, such that chemical equilibrium due to the focusing and mixing of two pore-fluids may be attained within the fault zone (i.e. Type 3 mineral precipitation pattern). However, for rapid and parallel flows, such as those resulting from a lithostatic pressure gradient, it is difficult for a chemical reaction to reach equilibrium within the fault zone, if the two pore-fluids are not well mixed before entering the fault zone (i.e. Type 2 mineral precipitation pattern).

To investigate three possible types of chemical reaction patterns arising from the effects of solute advection, diffusion/dispersion and chemical kinetics within two-dimensional geological fault zones, a generic model is considered to simulate a vertical permeable fault zone within the upper crust of the Earth. As shown in Figure 10, the length of the vertical fault zone is $5km$, with an aspect ratio of 20, meaning that the width of the fault zone is $250m$. The porosities of the fault zone and the surrounding rock are 0.35 and 0.1 respectively. The surrounding rock is assumed to have a permeability of $10^{-16}m^2$, while the permeability of the fault zone is 43 times that of the surrounding rock.

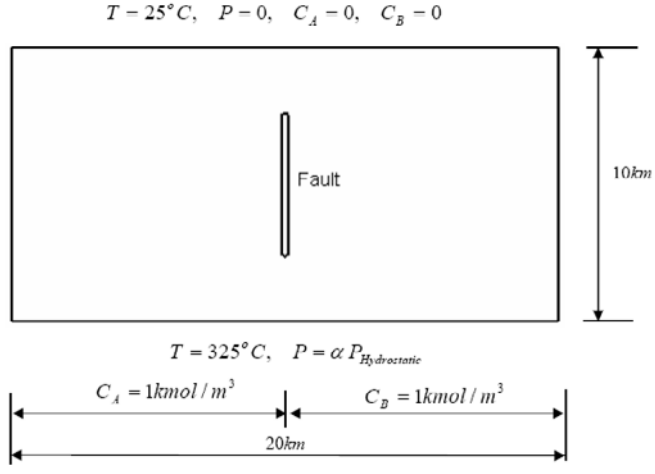

Figure 10. Geometry and boundary conditions of the generic model.

The top temperature is fixed at 25^oC and the geothermal gradient is $30^oC/km$, meaning that the temperature at the bottom is fixed at 325^oC. Two chemical reactants, whose concentrations are $1kmol/m^3$, are injected into the left half and right half bottom boundary respectively, while the concentrations of the two reactants and product are assumed to be zero initially at the top boundary of the computational model. The dispersion/diffusivity of both chemical species is $3\times10^{-10}m^2/s$ for the first two cases, where Types 1 and 2 mineral precipitation patterns take place within the reactive mass transport system. Through changing the value of α, different pore-fluid pressure can be simulated on the bottom boundary of the computational model.

For the pore-fluid, dynamic viscosity is $10^{-3}N\cdot s/m^2$; reference density is $1000kg/m^3$; volumetric thermal expansion coefficient is $2.1\times10^{-4}(1/^oC)$; specific heat is $4184J/(kg\cdot^oC)$; thermal conductivity coefficient is $0.59W/(m\cdot^oC)$. For the porous matrix, thermal conductivity coefficient is $2.9W/(m\cdot^oC)$; specific heat is $878J/(kg\cdot^oC)$; reference rock density is $2600kg/m^3$; the controlling chemical reaction rate of the reactive transport system is assumed to be $10^{-11}(1/s)$ for the first two cases associated with Types 1 and 2 mineral precipitation patterns within the reactive mass transport system. In order to appropriately simulate pore-fluid focusing and chemical reactions within the fault zone, a fine mesh is used to simulate the fault zone, while a mesh gradation scheme is employed to simulate the surrounding rock by gradually changing the mesh size away from the outline of the fault zone within the computational model. As a result, the whole computational domain is simulated by 306,417 three-node triangle elements.

Two different pore-fluid pressure gradients are considered to control the vertical pore-fluid velocity within the surrounding rock during the numerical simulation. To simulate the fast flow rate associated with Type 2 mineral precipitation pattern, the pore-fluid pressure gradient is assumed to be a lithostatic pressure gradient, which results in a vertical flow rate of $1.7\times10^{-9}m/s$ within the surrounding rock. This pressure gradient is used because it is considered to be near the highest reasonable pore-fluid pressure gradient likely to be encountered in nature. On the other hand, in order to simulate the slow flow rate associated with Types 1 and 3 mineral precipitation patterns, the excess pore-fluid pressure gradient is assumed to be one percent of a lithostatic pressure gradient minus a hydrostatic one, which results in a vertical flow rate of $1.7\times10^{-11}m/s$ within the surrounding rock. It is known that for pore-fluid pressure gradient dominated flow, the flow pattern around a permeable fault zone is dependent only on the contrast in permeability between the fault zone and the surrounding rocks, the geometry of the fault zone and the inflow direction relative to the axis of the fault zone (Phillips 1991, Zhao et al. 1999), but is independent of the pressure gradient along the fault zone. This means that although the pore-fluid pressure gradient is different in the three simulations, the streamline pattern within and around the fault zone must be identical for all the three cases, as demonstrated by the related numerical result shown in Figure 11. In all the three cases, pore-fluid flow converges into the fault zone at the lower end and diverges out of the fault zone at the upper end (Phillips 1991, Zhao et al. 1999).

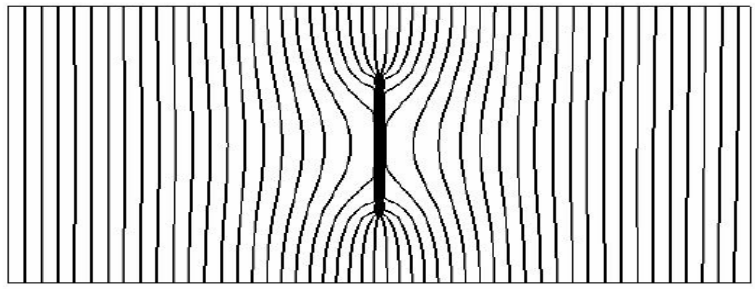

Figure 11. Streamline pattern of the generic model.

Figure 12 shows the concentration distributions of the two chemical reactants and the corresponding chemical product associated with Type 1 mineralization pattern at two time instants of t=500,000 and t=800,000 years. The distribution of the concentration of the chemical product comprises a lenticular shape within the fault zone. This coincides with what is expected from the theoretical analysis (Zhao et al. 2007d). For a fault zone of width 250m, the theoretical value of the optimal chemical reaction rate is $4.8\times10^{-15}(1/s)$ so that chemical equilibrium can be attained within the whole width of the fault zone (Zhao et al. 2007d). Since the optimal chemical reaction rate is much smaller than the controlling chemical reaction rate used in the computational simulation, the thickness of the chemical equilibrium within the fault zone is much smaller than the width of the fault zone itself. The theoretical estimate of the thickness of chemical equilibrium within the fault zone is 10.95m for a controlling chemical reaction rate of $10^{-11}(1/s)$. Since the theoretical thickness of chemical equilibrium within the fault zone is smaller than the thickness of the fault zone, the maximum concentration distribution of the chemical product comprises a very thin membrane, so that mineral precipitation comprises a thin lenticular shape within the fault zone and starts just at the lower tip of the fault zone. This is the fundamental characteristic of the first type of chemical reaction pattern.

Figure 13 shows the concentration distributions of the two chemical reactants and the corresponding chemical product associated with Type 2 mineralization pattern at two time instants of t=5000 and t=8000 years. Both chemical reactants are transported into the computational domain from the left half and right half of the base of the model. Due to pore-fluid flow focusing, both chemical reactants are transported much faster within the fault zone than in the surrounding rock. There is a strong interaction between solute advection, diffusion/dispersion and the controlling chemical reaction rate. Although both chemical reactants are transported into the fault zone, the mixing of the two pore-fluids carrying them is controlled by solute diffusion and dispersion. In the case of a non-equilibrium chemical reaction characterized by the chemical reaction rate of $k_R=10^{-11}(1/s)$, the theoretical chemical equilibrium length due to solute diffusion/dispersion is 5.48m, while the theoretical chemical equilibrium length due to solute advection is 8630m in the direction of the fault axis (Zhao et al. 2007d). Thus, the chemical equilibrium length due to solute advection is greater than the length of the fault zone itself, so that the chemical product distribution within the fault zone is controlled by solute advection. Because the chemical equilibrium length due to solute advection is greater than the total length of the fault zone plus its exit region (i.e. 5000m plus 2500m), chemical equilibrium cannot be reached within the height of the model,

indicating that the two pore-fluids cannot mix to produce an extensive mixing region due to the fast advection of them within the fault zone. This indicates that chemical equilibrium cannot be attained within the fault zone, implying geologically that mineral precipitation cannot take place within a permeable vertical fault zone for the chemical reaction considered. This is the fundamental characteristic of the second type of chemical reaction pattern considered in this investigation.

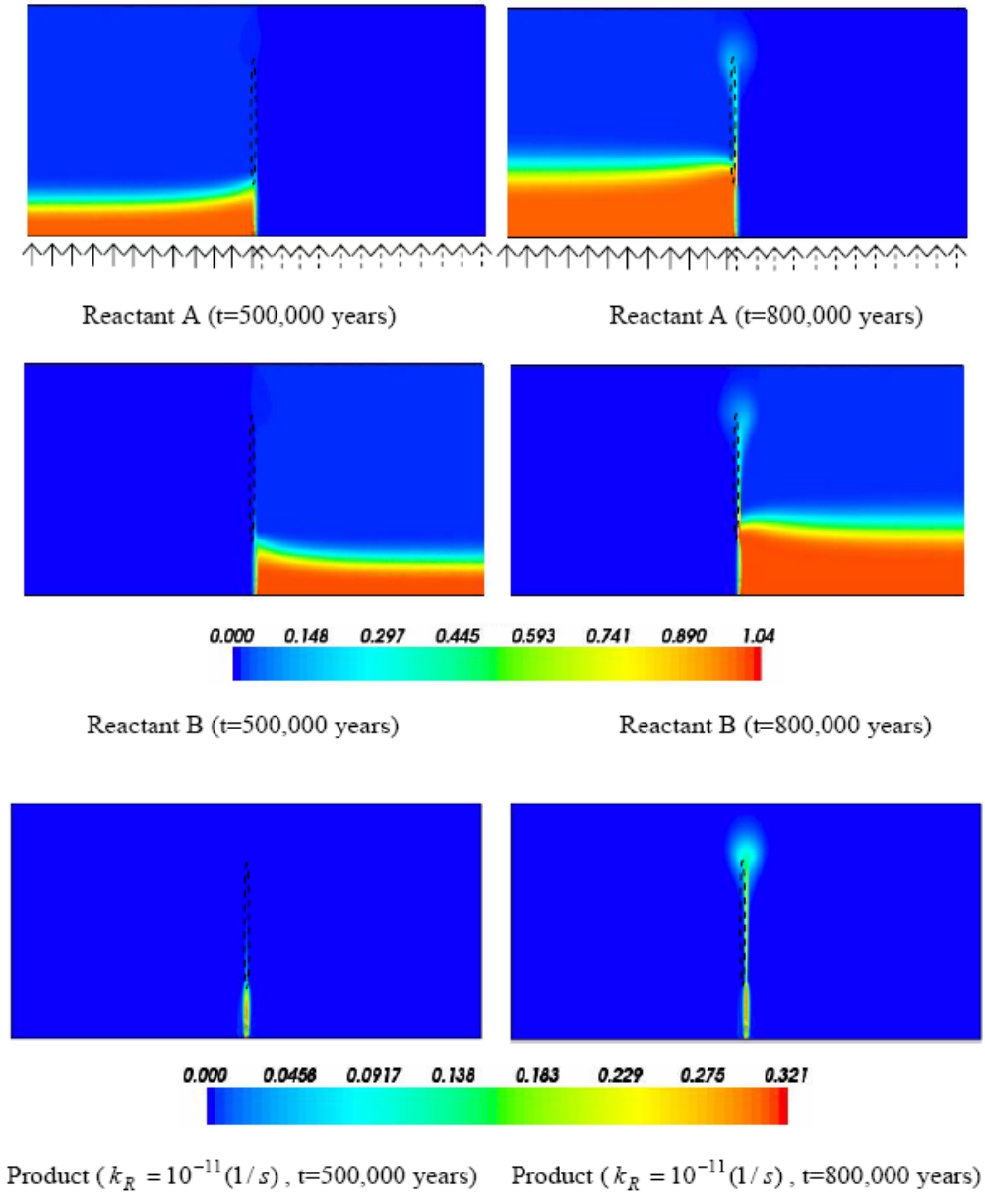

Figure 12. Concentration distributions of the chemical reactants and product at two different time instants (Type 1 mineral precipitation pattern).

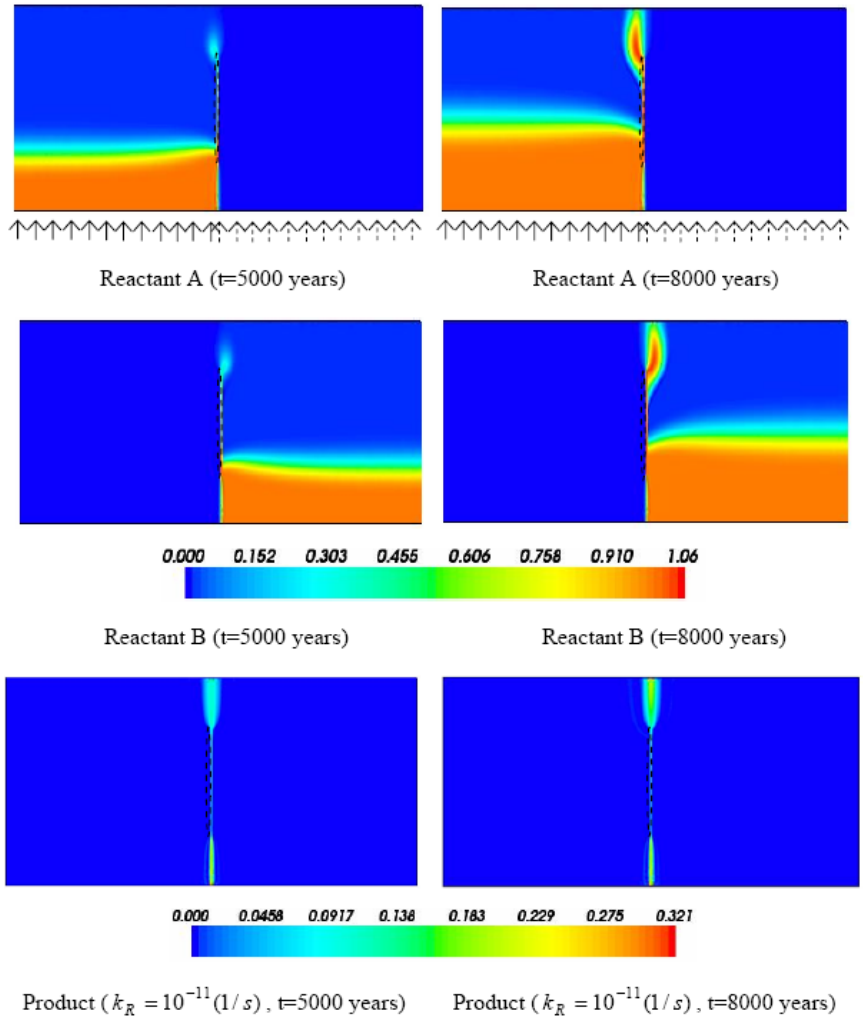

Figure 13. Concentration distributions of the chemical reactants and product at two different time instants (Type 2 mineral precipitation pattern).

Figure 14 shows concentration distributions of the two chemical reactants and the corresponding chemical product associated with Type 3 mineralization pattern at two time instants of t=500,000 and t=800,000 years. In order to enable the starting position of chemical equilibrium to be close to the lower tip of the vertical fault zone, the background pore-fluid pressure gradient within the surrounding rock is one percent of the lithostatic pressure gradient minus the hydrostatic gradient. Due to flow focusing, the maximum vertical flow velocity within the fault zone is about $4.68\times10^{-10}\,m/s$ in this particular situation. As the optimal chemical reaction rate is directly proportional to the solute diffusion/dispersion coefficient, it is desirable to select the value of a solute diffusion/dispersion coefficient as large as possible, so that the total CPU time in the simulation can be significantly reduced (Zhao et al. 2007d). For this reason, the solute diffusion/dispersion coefficient is assumed to be $3\times10^{-8}\,m^2/s$ in the numerical simulation. If the thickness of chemical equilibrium in the lateral direction of the fault zone is 80m, then the theoretical estimate of the optimal

chemical reaction rate is about $1.9\times10^{-11}(1/s)$, as can be calculated from the previously presented theory (Zhao et al. 2007d). As expected, the numerical simulation results (shown in Figure 14) clearly indicate that the maximum concentration distribution of the chemical product has a considerable thickness within the fault zone. This agrees well with what is predicted from the previous theoretical analysis (Zhao et al. 2007d). Due to the low pore-fluid velocity, a chemical equilibrium zone is also generated in the flow convergent region just in front of the fault zone. It is noted that this chemical equilibrium zone is almost separated from the chemical equilibrium zone within the fault zone. This phenomenon results from the distribution of pore-fluid velocity vectors arising from pore-fluid flow focusing just outside and within the fault zone. The geological implication of Type 3 mineral precipitation pattern is that if a mineral precipitation pattern of a certain thickness and length within a permeable vertical fault zone is observed, then it is possible to estimate both the optimal flow rate and the optimal chemical reaction rate during the formation of this precipitation pattern. On the other hand, if the flow rate and chemical reaction rate are known, then it is possible to estimate the width of the potential mineral precipitation pattern within a permeable vertical fault zone.

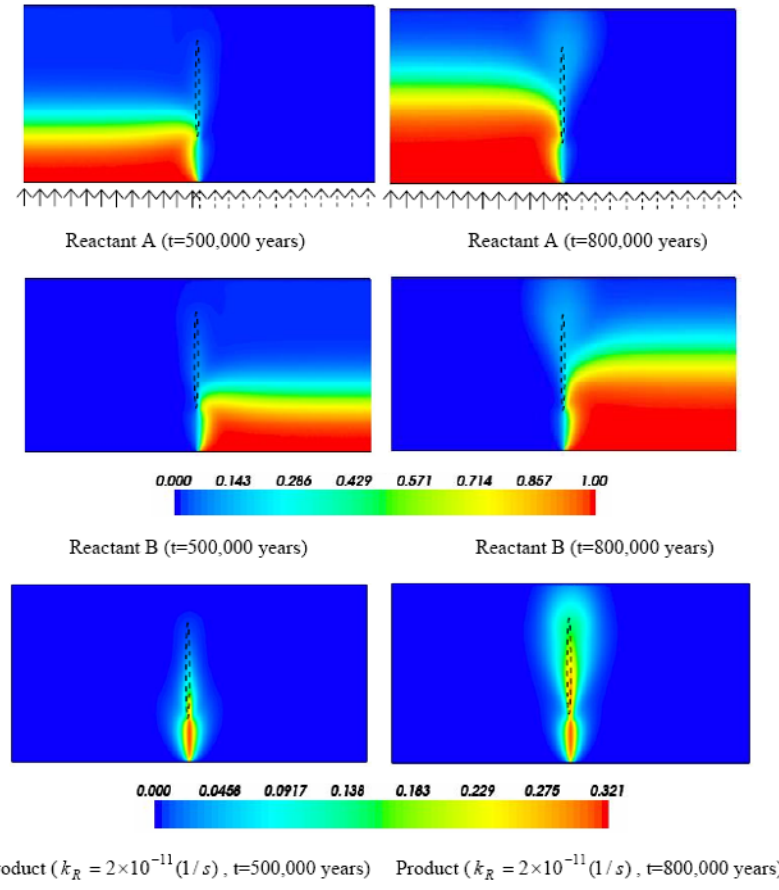

Figure 14. Concentration distributions of the chemical reactants and product at two different time instants (Type 3 mineral precipitation pattern).

4. CONCLUSIONS

A mineralizing system within the upper crust of the Earth is commonly regarded as a complex science system with multi-scale and multi-process characteristics. For such a system, it is still very difficult to simultaneously simulate the whole mineralizing system, from a particle (i.e. mineral) scale to a crustal scale, in one computational model. However, it is useful to separately simulate mineral precipitation patterns within a mineralizing system using a series of computational models of different scales. This allows only some key factors to be considered for each of the computational models. By integrating all the mineral precipitation patterns obtained from a series of computational models of different scales, it is possible to understand the formation mechanisms behind the mineralizing system.

Unlike the empirical and descriptive methods, which are traditionally used for minerals exploration, the computational geoscience methodology provides a scientific and predictive way to understand the predominant physical and chemical processes that control ore body formation and mineralization within the upper crust of the Earth. Since both the theoretical analysis and the computational simulation are two key elements of the computational geoscience methodology, it becomes possible to predict ore deposits in a quantitative manner, rather than just in a qualitative manner.

The core part of the modern mineralization theory is to evaluate, either analytically or computationally, the mineral precipitation/dissolution rate, which is usually a function of both space and time and can be used to predict potential mineral precipitation patterns within a mineralizing system. For the purpose of understanding general precipitation patterns of minerals in a chemically equilibrium mineralizing system or a near chemically equilibrium mineralizing system, the rock alteration index (*RAI*) can be approximately used for predicting the potential precipitation/dissolution regions of any minerals in hydrothermal systems within the upper crust of the Earth. However, in order to understand the general patterns of gold precipitation in a chemically equilibrium state or a near chemically equilibrium system, the improved rock alteration index (*IRAI*) needs to be used for predicting the potential precipitation regions within the upper crust of the Earth.

For a chemically non-equilibrium mineralizing system, the interaction between solute advection, solute diffusion/dispersion and chemical kinetics plays an important role in controlling the general precipitation patterns of minerals within the upper crust of the Earth. Owing to this interaction, there are three fundamental types of mineral precipitation patterns, namely the diffusion-dominated precipitation pattern, the advection-dominated precipitation pattern and both the diffusion and advection equally-dominated precipitation pattern. In particular, for a given chemically non-equilibrium mineralizing system within a permeable fault zone, there is an optimal flow rate that enables the mineral just to be precipitated within the permeable fault zone.

ACKNOWLEDGMENTS

This work is financially supported by the Natural Science Foundation of China (Grant No: 10872219). The author is also very grateful to the Central South University for financial support during writing this chapter of the book.

REFERENCES

Bardet, J. P. and Proubet, J. (1992). The structure of shear bands in idealized granular materials, *Applied Mechanics Review*, 45, 118-122.

Burbidge, D. R. and Braun, J. (2002). Numerical models of the evolution of accretionary wedges and fold-and-thrust belts using the distinct-element method, *Geophysical Journal International*, 148, 542-561.

Camborde, F., Mariotti, C. and Donze, F. V. (2000). Numerical study of rock and concrete behavior by distinct element modeling, *Computers and Geotechnics*, 27, 225-247.

Cleary, P. W. (2004). Large scale industrial DEM modeling, *Engineering Computations*, 21, 169-204.

Cundall, P. A. and Strack, O. D. L. (1979). A discrete numerical model for granular assemblies, *Geotechnique*, 29, 47-65.

Cundall, P. A. (2001). A discontinuous future for numerical modelling in geomechanics?, *Proceedings of the Institution of Civil Engineers: Geotechnical Engineering*, 149, 41-47.

Donze, F., Mora, P. And Magnier, S. A. (1994). Numerical simulation of faults and shear zones, *Geophysical Journal International*, 116, 46-52.

Donze, F., Magnier, S. A. and Bouchez, J. (1996). Numerical modeling of a highly explosive source in an elastic-brittle rock mass, *Journal Geophysical Research*, 101, 3103-3112.

Finch, E., Hardy, S. and Gawthorpe, R. (2004). Discrete element modeling of extensional fault-propagation folding above rigid basement fault blocks, *Basin Research*, 16, 489-506.

Garven, G. and Freeze, R. A. (1984). Theoretical analysis of the role of groundwater flow in the genesis of stratabound ore deposits: Mathematical and numerical model, *American Journal of Science*, 284, 1085-1124.

Gow, P., Upton, P., Zhao, C. and Hill, K. (2002). Copper-Gold mineralization in the New Guinea: Numerical modeling of collision, fluid flow and intrusion-related hydrothermal systems, *Australian Journal of Earth Sciences*, 49, 753-771.

Hobbs, B. E., Zhang, Y., Ord, A. and Zhao, C. (2000). Application of coupled deformation, fluid flow, thermal and chemical modelling to predictive mineral exploration, *Journal of Geochemical Exploration*, 69, 505-509.

Itasca Consulting Group, Inc. (1999). *Particle Flow Code in Two Dimensions (PFC2D)*, Minneapolis, Minnesota, USA.

Iwashita, K. and Oda, M. (2000). Micro-deformation mechanism of shear banding process based on modified distinct element method, *Powder Technology*, 109, 192-205.

Klerck, P. A., Sellers, E. J. and Owen, D. R. J. (2004). Discrete fracture in quasi-brittle materials under compressive and tensile stress states, *Computer Methods in Applied Mechanics and Engineering*, 193, 3035-3056.

Lewis R. W. and Schrefler B. A. (1998). *The Finite Element Method in the Static and Dynamic Deformation and Consolidation of Porous Media*, John Wiley & Sons, New York.

McBride, A. Govender, I., Powell, M. and Cloete, T. (2004). Contributions to the experimental validation of the discrete element method applied to tumbling mills, *Engineering Computations*, 21, 119-136.

Ord, A., Hobbs, B. E., Zhang, Y., Broadbent, G. C., Brown, M., Willetts, G., Sorjonen-Ward, P., Walshe, J. and Zhao, C. (2002). Geodynamic modelling of the Century deposit, Mt Isa Province, Queensland, *Australian Journal of Earth Sciences*, 49, 1011-1039.

Owen, D. R. J., Feng, Y. T., de Souza Neto, E. A., Cottrell, M. G., Wang, F., Andrade Pires, F. M. and Yu, J. (2004). The modelling of multi-fracturing solids and particular media, *International Journal for Numerical Methods in Engineering*, 60, 317-339.

Phillips, O. M. (1991). *Flow and Reactions in Permeable Rocks*, Cambridge University Press, Cambridge.

Potyondy, D. O. and Cundall, P. A. (2004). A bonded-particle model for rock, *International Journal of Rock Mechanics and Mining Science*, 41, 1329-1364.

Raffensperger, J. P. and Garven, G. (1995). The formation of unconformity-type uranium ore deposits: Coupled hydrochemical modeling, *American Journal of Science*, 295, 639-696.

Saltzer, S. D. and Pollard, D. D. (1992). Distinct element modeling of structures formed in sedimentary overburden by extensional reactivation of basement normal faults, *Tectonics*, 11, 165-174.

Schafer, D., Schafer, W. and Kinzelbach, W. (1998). Simulation of reactive processes related to biodegradation in aquifers: 1. Structure of the three-dimensional reactive transport model, *Journal of Contaminant Hydrology*, 31, 167-186.

Schaubs, P. and Zhao, C. (2002). Numerical modelling of gold-deposit formation in the Bendigo-Ballarat zone, Victoria, *Australian Journal of Earth Sciences*, 49, 1077-1096.

Schubert, W., Khanal, M. and Tomas, J. (2005). Impact crushing of particle-particle compounds: experiment and simulation, *International Journal of Mineral Processing*, 75, 41-52.

Scott, D. R. (1996). Seismicity and stress rotation in a granular model of the brittle crust, *Nature*, 381, 592-595.

Shenberger, D. M. and Barnes, H. L. (1989). Solubility of gold in aqueous sulfide solutions from 150 to 350^{o}C, *Geochimica et Cosmochimica Acta*, 53, 269-278.

Sorjonen-Ward, P., Zhang, Y. and Zhao, C. (2002). Numerical modelling of orogenic processes and mineralization in the southeastern part of the Yilgarn Craton, Western Australia, *Australian Journal of Earth Sciences*, 49, 935-964.

Steefel, C. I. and Lasaga, A. C. (1994). A coupled model for transport of multiple chemical species and kinetic precipitation/dissolution reactions with application to reactive flow in single phase hydrothermal systems, *American Journal of Science*, 294, 529-592.

Xu, T. F., Samper, J. Ayora, C., Manzano, M. and Custodio, E. (1999). Modelling of non-isothermal multi-component reactive transport in field scale porous media flow systems, *Journal of Hydrology*, 214, 144-164.

Yeh, G. T. and Tripathi, V. S. (1991). A model for simulating transport of reactive multispecies components: Model development and demonstration, *Water Resources Research*, 27, 3075-3094.

Zhao, C., Xu, T. P. and Valliappan, S. (1994). Numerical modelling of mass transport problems in porous media: A review, *Computers and Structures*, 53, 849-860.

Zhao, C., Mühlhaus, H. B. and Hobbs, B. E. (1997). Finite element analysis of steady-state natural convection problems in fluid-saturated porous media heated from below, *International Journal for Numerical and Analytical Methods in Geomechanics*, 21, 863-881.

Zhao, C., Hobbs, B. E. and Mühlhaus, H. B. (1998a). Finite element modelling of temperature gradient driven rock alteration and mineralization in porous rock masses, *Computer Methods in Applied Mechanics and Engineering,* 165, 175-187.

Zhao, C., Hobbs, B. E. and Mühlhaus, H. B. (1998b). Analysis of pore-fluid pressure gradient and effective vertical-stress gradient distribution in layered hydrodynamic systems, *Geophysical Journal International*, 134, 519-526.

Zhao, C., Hobbs, B. E., Mühlhaus, H. B. and Ord, A. (1999). Finite element analysis of flow patterns near geological lenses in hydrodynamic and hydrothermal systems, *Geophysical Journal International*, 138, 146-158.

Zhao, C., Hobbs, B. E., Mühlhaus, H. B., Ord, A. and Lin, G. (2000a). Numerical modelling of double diffusion driven reactive flow transport in deformable fluid-saturated porous media with particular consideration of temperature-dependent chemical reaction rates, *Engineering Computations*, 17, 367-385.

Zhao, C., Hobbs, B. E. and Mühlhaus, H. B. (2000b). Finite element analysis of heat transfer and mineralization in layered hydrothermal systems with upward throughflow, *Computer Methods in Applied Mechanics and Engineering*, 186, 49-64.

Zhao, C., Hobbs, B. E., Walshe, J.L., Mühlhaus, H. B. and Ord, A. (2001a). Finite element modelling of fluid-rock interaction problems in pore-fluid saturated hydrothermal/sedimentary basins, *Computer Methods in Applied Mechanics and Engineering*, 190, 2277-2293.

Zhao, C., Lin, G., Hobbs, B. E., Mühlhaus, H. B., Ord, A. and Wang, Y. (2001b). Finite element modelling of heat transfer through permeable cracks in hydrothermal systems with upward throughflow, *Engineering Computations*, 18, 996-1011.

Zhao, C., Lin, G., Hobbs, B. E., Wang, Y., Mühlhaus, H. B. and Ord, A. (2002). Finite element modelling of reactive fluids mixing and mineralization in pore-fluid saturated hydrothermal/sedimentary basins, *Engineering Computations*, 19, 364-387.

Zhao, C., Lin, G., Hobbs, B. E., Ord, A., Wang, Y. and Mühlhaus, H. B. (2003). Effects of hot intrusions on pore-fluid flow and heat transfer in fluid-saturated rocks, *Computer Methods in Applied Mechanics and Engineering*, 192, 2007-2030.

Zhao, C., Hobbs, B. E., Ord, A., Peng, S., Mühlhaus, H. B. and Liu, L. (2004). Theoretical investigation of convective instability in inclined and fluid-saturated three-dimensional fault zones, *Tectonophysics*, 387, 47-64.

Zhao, C., Hobbs, B. E., Ord, A., Peng, S., Mühlhaus, H. B. and Liu, L. (2005). Numerical modelling of chemical effects of magma solidification problems in porous rocks, *International Journal for Numerical Methods in Engineering*, 64, 709-728.

Zhao, C., Hobbs, B. E., Hornby, P., Ord, A. and Peng, S. (2006a). Numerical modelling of fluids mixing, heat transfer and non-equilibrium redox chemical reactions in fluid-saturated porous rocks, *International Journal for Numerical Methods in Engineering*, 66, 1061-1078.

Zhao, C., Hobbs, B. E., Ord, A., Kühn, M., Mühlhaus, H. B. and Peng, S. (2006b). Numerical simulation of double-diffusion driven convective flow and rock alteration in three-dimensional fluid-saturated geological fault zones, *Computer Methods in Applied Mechanics and Engineering*, 195, 2816-2840.

Zhao, C., Nishiyama, T. and Murakami, A. (2006c). Numerical modelling of spontaneous crack generation in brittle materials using the particle simulation method, *Engineering Computations*, 23, 566-584.

Zhao, C., Hobbs, B. E., Ord, A., Hornby, P., Peng, S. and Liu, L. (2007a). Particle simulation of spontaneous crack generation problems in large-scale quasi-static systems, *International Journal for Numerical Methods in Engineering*, 69, 2302-2329.

Zhao, C., Hobbs, B. E., Ord, A., Peng, S. and Liu, L. (2007b). An upscale theory of particle simulation for two-dimensional quasi-static problems, *International Journal for Numerical Methods in Engineering*, 72, 397-421.

Zhao, C., Hobbs, B. E., Ord, A., Robert, P. A., Hornby, P. and Peng, S. (2007c). Phenomenological modeling of crack generation in brittle crustal rocks using the particle simulation method, *Journal of Structural Geology*, 29, 1034-1048.

Zhao, C., Hobbs, B. E., Ord, A., Hornby, P., Peng, S. and Liu, L. (2007d). Mineral precipitation associated with vertical fault zones: The interaction of solute advection, diffusion and chemical kinetics, *Geofluids*, 7, 3-18.

Zhao, C., Hobbs, B. E. and Ord, A. (2008a). Investigating dynamic mechanisms of geological phenomena using methodology of computational geosciences: an example of equal-distant mineralization in a fault, *Science in China Series D: Earth Sciences*, 51, 947-954.

Zhao, C., Hobbs, B. E., Ord, A., Hornby, P., Mühlhaus, H. B. and Peng, S. (2008b). Theoretical and numerical analyses of pore-fluid-flow focused heat transfer around geological faults and large cracks, *Computers and Geotechnics*, 35, 357-371.

Zhao, C., Peng, S., Liu, L., Hobbs, B. E., and Ord. A. (2008c). Potential mechanisms of pore-fluid movement from the continental lithospheric mantle into the upper continental crust, *Journal of Central South University of Technology*, 15, 81-88.

Zhao, C., Hobbs, B. E., Hornby, P., Ord, A., Peng, S. and Liu, L. (2008d). Theoretical and numerical analyses of chemical-dissolution front instability in fluid-saturated porous rocks, *International Journal for Numerical and Analytical Methods in Geomech*anics, 32, 1107-1130.

Zhao, C., Hobbs, B. E., Ord, A., Hornby, P. and Peng, S. (2008e). Effect of reactive surface areas associated with different particle shapes on chemical-dissolution front instability in fluid-saturated porous rocks, *Transport in Porous Media*, 73, 75-94.

Zhao, C., Hobbs, B. E., Ord, A., Hornby, P. and Peng, S. (2008f). Morphological evolution of three-dimensional chemical dissolution front in fluid-saturated porous media: A numerical simulation approach, *Geofluids*, 8, 113-127.

Zhao, C., Hobbs, B. E., Ord, A. and Peng, S. (2008g). Particle simulation of spontaneous crack generation associated with the laccolithic type of magma intrusion processes, *International Journal for Numerical Methods in Engineering*, 75, 1172-1193.

Zhao, C., Hobbs, B. E. and Ord, A. (2009). *Fundamentals of Computational Geoscience*, Springer, Berlin.

Zienkiewicz, O. C. (1977). *The Finite Element Method*, McGraw-Hill, London.

In: Gold Mining: Formation and Resource Estimation ISBN: 978-1-60741-096-6
Editors: M. D. Corral, J. L. Earle

Chapter 2

AN OUTLOOK OF GIS APPLICATIONS IN MINERAL RESOURCE ESTIMATION

Wei Zhou*

Department of Geology and Geological Engineering,
Colorado School of Mines
1516 Illinois St. Golden, CO 80401

ABSTRACT

Miners, geologists, and engineers have been solving problems related to geo-spatial data for generations. A major task of mineral exploration consists of mapping the bedrock and surficial geology using traditional field methods, geochemical analysis, geophysical exploration, and aero-photo interpretations. Integration of field survey data and other pertinent information for the purpose of mineral resource estimation can be a time-consuming task. However since the development of Geographic Information Systems (GIS) technology in 1962, most of these tasks can now be accomplished in a more time-efficient manner. With the increasing popularity and functional development of GIS in recent years, many mining companies started using GIS as the preferred tool for mine planning, analysis, and management. The commodities market, environmental regulations and government policies pushed companies to further streamline their operations and become more competitive and cost effective. Moreover, the state and federal agencies involved in the mine permitting process are adopting the GIS format as the standard for communicating spatial data.

This paper presents a case study of GIS application in gold resource estimation. It is a synthesis of a series of previously published works. GIS technology has been applied to compile, integrate, analyze and visualize the offshore marine placer gold deposits at Nome, Alaska. With the help of GIS, information on placer gold deposits can be updated, queried, visualized, and analyzed much more effectively than before. Various geostatastical interpolation methods, such as Inverse Distance Weighted (IDW), Ordinary Kriging (OK), Ordinary Kriging with lognormal transformation (OK-log), Simple Kriging (SK) and Indicator Kriging (IK), were studied and compared to strike for an optimum approach of resource estimation. Ore body boundaries and the resource

* email: wzhou@mines.edu

estimation at various cutoff grades at any given domain can be calculated interactively. In addition, a web-based GIS was developed to facilitate remote users to access the data. The GIS architecture developed in this project was designed for general usage and can be adapted to mineral resource estimation in other study areas.

INTRODUCTION

The development of Geographic Information Systems (GIS) technology in 1962 provided a powerful time-efficient and cost-effective technique for miners, geologists, and engineers who have been solving problems related to geo-spatial data in traditional way for generations. A GIS is a computer system capable of assembling, storing, management, analyzing, and displaying geographically referenced data, i.e. geo-spatial data identified according to their locations (USGS, 2007). Practitioners also regard the total GIS as including operating personnel and the data that go into the system. With the ever evolving functionalities of GIS in recent decades, many mining companies started using GIS as the preferred tool for mine planning, analysis, and management. This might be also because the commodities market, environmental regulations and government policies force mining companies become more competitive and cost effective as well as the state and federal agencies involved in the mine permitting process are adopting the GIS format as the standard for communicating geo-spatial data (Bonham-Carter, 1994; Price 2001).

Economic geologists use various types of datasets to search for new economic deposits. Data collected range from geologic maps, remote sensing images, and geophysical images to databases. GIS is an ideal platform to bring various data together and deliver meaningful information. GIS now can also be used to integrate recent survey data with block models or mine design data from other mining software packages such as GeoSoft, Vulcan, MineSight, SURPAC Range, or Mining Visualization System (MVS) (ESRI, 2006).

A review of the literature on the GIS applications in mining industry, especially literature reviews on new developments and applications of GIS collected in GEOBASE, GeoRef geosciences database, and on websites, are conducted. From the literature, one can summarize that GIS have become an essential tool in mining industry for mine planning, analysis and management. These applications include:

1). Pre-production phase of a mine

a Site selection
b Land ownership
c Mineral claims
d Exploration management

2). Applications of GIS to the production phase of a mine

a Environmental Quality Monitoring
b Facilities Management
c Volume Computations
d Emergency management and industrial security

e Transport routes

3). Applications of GIS to the post-production phase of a mine

a Reclamation, Vegetation Characterization
b Slope-Aspect Characterization
c Volume Computations
d Visualization

4). GIS –based analysis method for technical research in field of mineral and mining

a Resources estimation
b Environmental impact assessment

The literatures cited next are not intending to be a complete bibliography list; rather it gives examples of the GIS applications in mining industry. An example given by ESRI (ESRI, 2006) is the GIS application in building a virtual 3D GIS model for Mayflower Gold Mine in southwest Montana. A 3D GIS database was created based on digitizing all of the historic mining and geological exploration data using ArcGIS with 3D Analyst extension (figure 1).

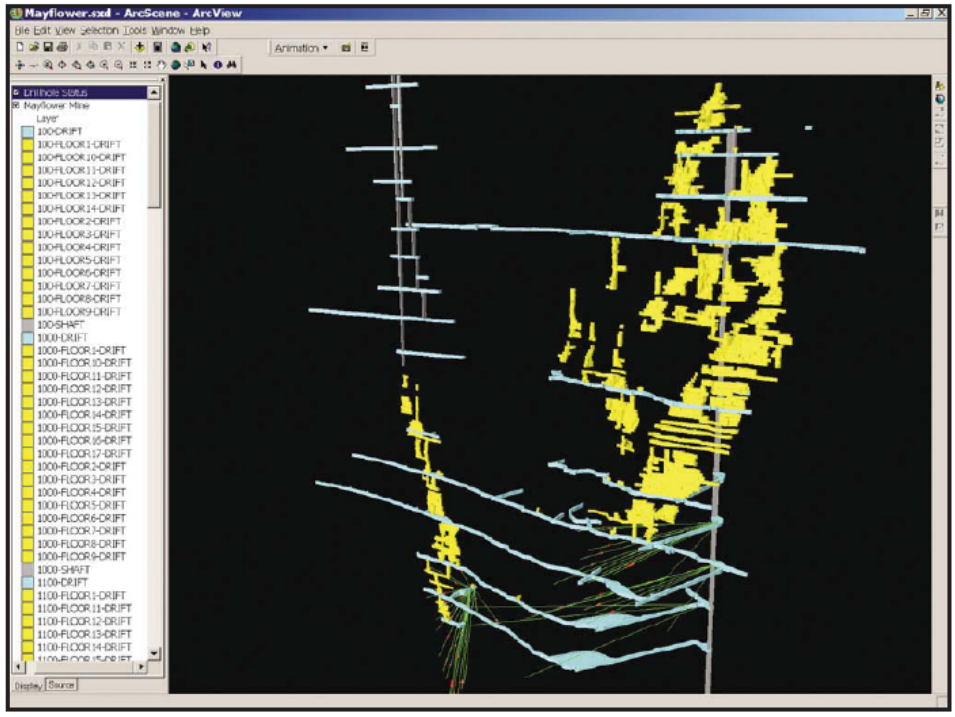

Figure 1. The Mayflower Mine complex visualized in 3D with ArcView and the 3D Analyst extension. This view is to the southeast and shows the heavily mined western ore body (right) and the narrow eastern ore body (left). (ESRI, 2006).

Hammond (2002) demonstrated an example of GIS application in a underground mining. This study focused on four areas: land ownership and mineral claims, exploration management, production, and mine safety. It combined the techniques of CAD (Computer Aided Design), GIS, and mining software to conduct the study. GIS facilitated the optimal siting and querying of service installations relative to production centers to meet the production parameters. The siting of refuge chambers relative to production centers was optimized and areas of potential safety concern were identified through proximity analysis in GIS. The same approach applied to finding the shortest route to emergency exits and preparation of maps to facilitate the prompt evacuation of mine personnel.

Berry and Pistocchi (2003) showed an application of GIS, together with multi-criteria analysis for supporting decision making, in the environmental impact assessment of open-pit quarries. Six main effects of open-pit quarrying activities on the environment were analyzed and integrated in GIS, i.e. noise, dust, air blasting, ground vibration, visual impacts, and landscape ecological disturbance. The environmental impact assessment case study hereby presented has been performed using the following:

1. In order to define the effects of quarrying activities, a set of descriptive- predictive models based on GIS analysis tools were constructed, prediction map were generated respectively.
2. In order to assign each pixel an impact score, a set of 'impact laws' were assumed based on judgment for each effect separately.
3. For evaluating and combining the impacts, the weights of relative importance to the various elementary impacts based on pairwise comparison technique were assigned.

This is a complex case study of GIS application in environmental impact assessment. In my opinion, all of processes of this case study can be integrated and fulfilled using ArcGIS and its programming tool – VBA and ArcObject.

Dillon and Blackwell (2003) discussed in general about GIS application in surface mining development. Starting from the exploration database, this paper describes how a GIS can be used for the development of mining plans based on topography, geology and mineralization information stored in a relational database.

The Application of GIS to Bauxite Mining in Jamaica (Almarales–Hamm, et al., undated) is an example of GIS applications supported by satellite imagery and orthorectified aerial photography to manage, analyze, and display data on tonnage, ore quality, location, and ownership. A customized 3D modeling and mine planning system using ArcGIS and its extensions provide tools that assist in the decision making process and reserve management.

Despite wide acceptance in other industries reliant on spatial information, GIS remains an under-utilized tool, especially real 3D tool in the mining industry. As an ideal tool to handling of spatially referenced data, GIS make it a powerful tool for use in exploration data management, mining planning, remediation decision making and environmental impact assessment.

A CASE STUDY OF GIS APPLICATION IN GOLD MINING

In this section, a case study of GIS application on placer gold resource estimation in Nome, Alaska is presents. This is a synthesis of previously published works by the faculty members and graduate students at the University of Alaska Fairbanks during the late 1990s and 2000s (Huang et al. 2001; Chen et al. 2003; Chen et al. 2005; Li et al. 2005; Luo et al. 2005; Zhou et al. 2007). The author was part of the research team, who was a faculty member at the Department of Mining and Geological Engineering at the University of Alaska Fairbanks (UAF) before she joined Colorado School of Mines in January 2008.

GIS has been applied to analyze the offshore marine placer gold deposits at Nome, Alaska. Two geodatabases, namely Integrated Geodatabase (IG) and Regularized 2.5D Geodatabase (R2.5DG) were created in this study. The IG served as a data container to manage various geological data, such as borehole, bedrock geology, surficial geology, and geochemical data. The R2.5DG was generated based on the IG and was used for gold resource estimate. Other features of this GIS infrastructure include data updating, query, analyzing, visualizing, and solid volume calculation. The gold resource estimation at various cutoff grades can be calculated interactively. A geostatistical study was carried out for optimizing the resource estimation approach. In addition, a web-based GIS (http://uaf-db.uaf.edu/website/) was developed to facilitate remote users to access and visualizing the offshore marine placer data.

The presentation of this case study will start with data collection, and then followed by methodology, database development, resource estimation and geostatistical analysis, web-based GIS, and will end with summaries.

Data Collection

Data sources for this study include private sectors of mining and mineral exploration, published literatures, unpublished reports, maps and open file reports from government agencies, documents from recording offices, and information through the Internet. During the summers of 1986 and 1987, WestGold Exploration Mining Company, Limited Partnership (WestGold) carried out 3400 line km of high-resolution seismic surveys of the lease area. Seismic data were interpreted to provide facies interfaces and thicknesses, allowing faulting to be identified and profiles to be drawn. Simultaneous side scan sonar surveys, with a 3-mm penetration, were used to map sediment type on the seafloor. From 1987 through 1989, WestGold completed 2530 holes and collected 57 bulk samples. Each hole was drilled in one-meter increments. The sediment from each one-meter interval was collected and stored, a brief sediment description was recorded and the gold content was assayed (Bronston, 1989).

Data files from 3468 drill holes in the offshore area at Nome were reformatted and complied. These file types are the principal sources of information for this project (Huang et al., 2001). Most drill hole logs record lithology, gold concentration value, and penetration blow count. Blow count data, the number of blows needed to drive each barrel through a sample length of 30 cm, provides sediment hardness information. A geologic key describes lithologic types intercepted. Gold concentration values are tabulated in oz/m^3 and oz/yd^3, along with “normalized” and “intensity” values. Normalized value is the relative gold

concentration as compared with a reference gold concentration. Intensity value shows normalized gold values (from 0 to 45) as 9 even intervals with intensity 9 signifying highest gold concentration.

The research team at UAF then re-compiled and integrated the information to better understand the geologic characteristics, geochemical and geophysical signatures, borehole data, economic considerations, oceanographic factors, submarine topography, and potential environmental impacts (Zhou et al. 2007).

Geology of Nome Area

Because of the extent and richness of the Nome gold resources, the area was studied extensively, and geological, geophysical, and geochemical characteristics of offshore gold deposits were well documented in the published literature. Various aspects of geology of the Nome placer deposits onshore and offshore have been described by Nelson and Hopkins (1972), and Bronston (1990).

There are 22 metasedimentary, metavolcanic, and metaplutonic bedrock units in the area. The Nome Group is a series of four lithostratigraphic units that are locally deformed by low-angle thrust faults. The Nome Group consists of the following four sub-units (Bundtzen et al., 1994):

- a basal, complexly deformed quartz-rich pelitic schist,
- a unit of mafic and pelitic schists and marble,
- a mafic-dominated schist assemblage, and
- a dirty marble (Bundtzen et al., 1994).

The bedrock topography (Pleistocene-Pliocene contact) was interpreted from high resolution seismic survey (Bronston, 1990). Extensive faulting in the Precambrian basement rock displaced the Pliocene sediments, producing an asymmetrical, concave trough synform, which plunges to the south. The east-west trending fault, which is named the “basin boundary fault” (Bronston, 1990), delineates the northern extent of the synform. Numerous smaller faults strike northeast and northwest at various angles to the basin boundary fault (figure 2)

Nome, Alaska is located on the southern coastline of the Seward Peninsula, on the northern coast of Norton Sound, which is a part of the northeastern Bering Sea (64°30′14″N, 165°23′58″W). Gold is abundant offshore (Koschmann and Bergendahl, 1968; Garnett, 2000) at Nome because fluvial and glacial processes transported gold from gold-enriched bedrock in the uplands into the marine environment where it was further concentrated by wave and current action. The USGS and USBM have summarized much of the geology of the area (Nelson and Hopkins, 1972; and Tagg and Greene 1973).

The lithologies of offshore sediments in the Nome area include arenites and gravels composed of red granite and quartz monzonite (Howkins, 1992). Fine-grained marine sediments deeply bury offshore bedrock east of Nome. Offshore bedrock is just below the sea bottom to the west. Figure 3 shows a lithologic map of the offshore sediments.

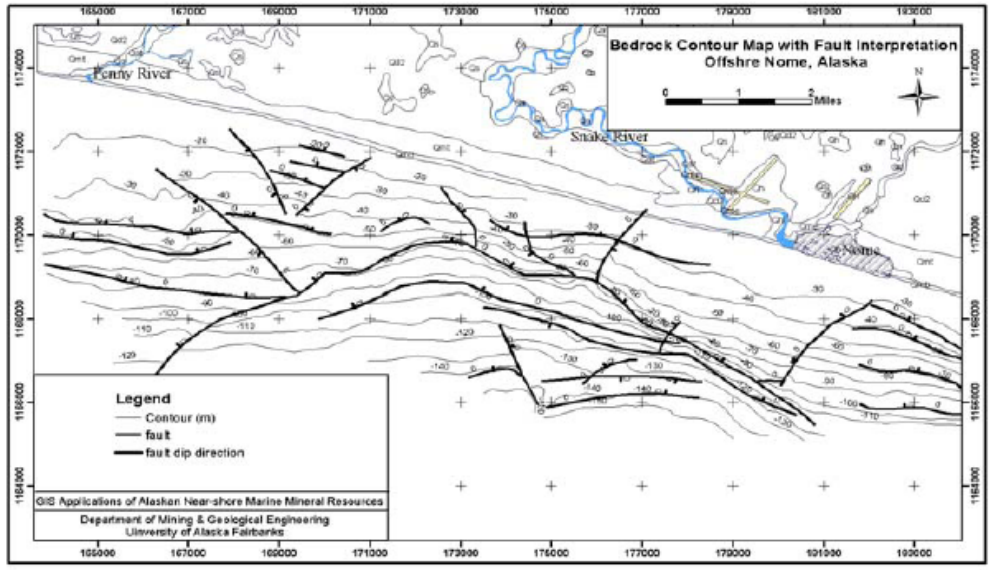

Figure 2. Bedrock Contour Maps with Fault Interpretation Offshore Nome (Bronston, 1990).

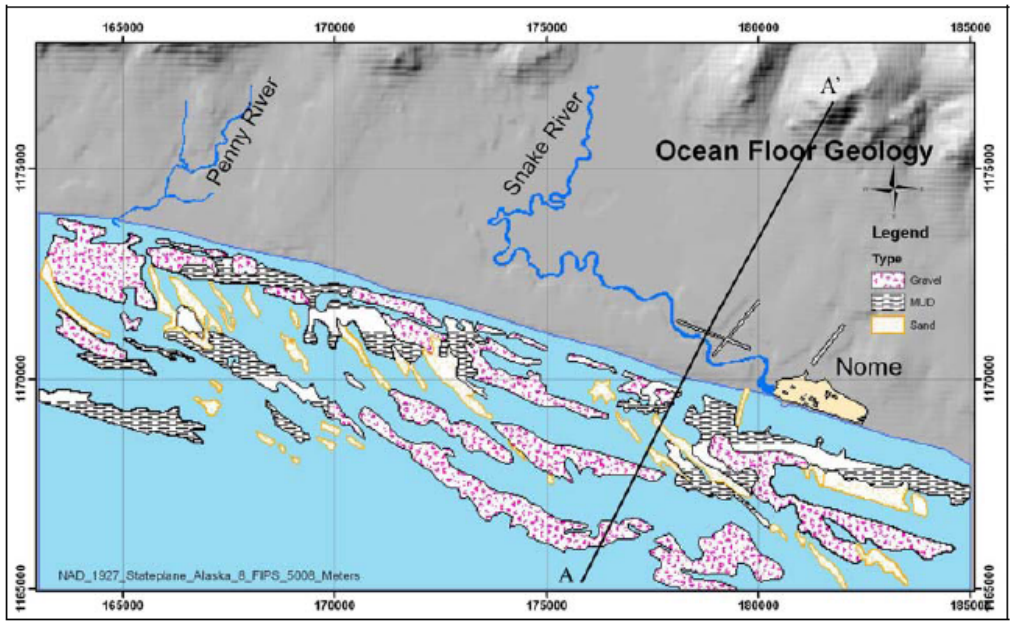

Figure 3. Lithologic map of the ocean floor off the coast of Nome (surficial geology digitized from Howkins, 1992).

Glaciations

Moraine deposits from glacier activity covers most of the area (figure 4), the most extensive of which is a surface drift sheet deposited during the Nome River glaciation period of the middle Pleistocene (Bundtzen et al., 1994). Subsequent periods (Stewart River, Salmon

Lake, and Mount Osborn glaciations) were less extensive and restricted to higher elevations and mountain valleys (Howkins, 1992).

According to Nelson and Hopkins (1972) glaciers have advanced past the present Nome coast at least twice (the early Pleistocene, and Illinoisan glaciations). These glacial activities resulted in the emergent beach deposits in the Nome area being a major source of placer gold by eroding and concentrating gold from bedrock.

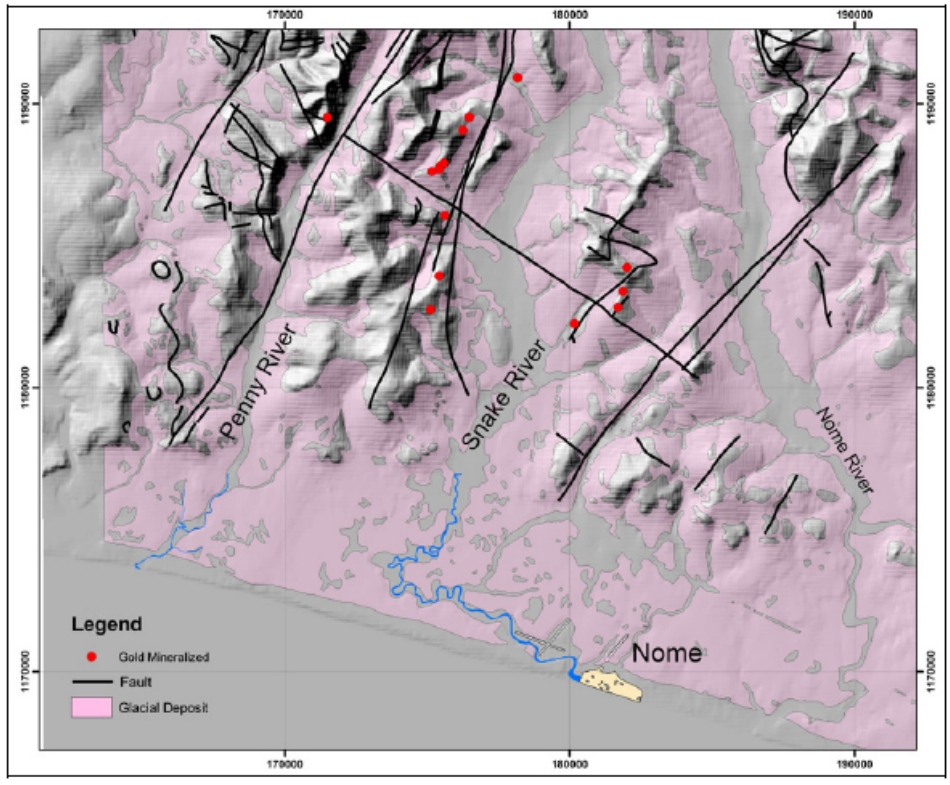

Figure 4. Distribution of glacial deposit in Nome (Bundtzen et al., 1994**).**

Economic Geology

Gold in the Nome area was sourced originally from gold-polymetallic-quartz-carbonate veins, stratiform, massive sulfide-barite deposits associated with felsic metavolcanic schist and metafelsite centers, massive sulfide-iron deposits hosted in carbonate-dominated terranes of uncertain origin, and heavy mineral placer deposits (Boyle, 1979). These materials were transported via streams and glaciers to a coastal environment, and subsequently concentrated in the marine and near-marine environments.

The formation of offshore gold deposits at Nome might be divided in three stages. During the first stages, lean gold gravels were deposited along the margins of the Bering Sea as stream deltas and fans. The next stage involved the coastal uplift. After uplift, the new beach was subjected to erosion by ocean wave, and gold-rich gravels became more concentrated. The final stage dealt with the idea that glaciation could lead to concentration of gold, as is seen in Nome. As glaciers moved, gold segregated from the sediments carried by glaciers due

to its high density. According to the concentration processes in these three stages, other placers in areas of heavy glaciation, especially valleys covered in glacial sediment may prove to be worthwhile exploration targets (Boyle, 1979).

Geodatabase Development

Data collected were compiled, integrated, and organized into two databases, named as IG and R2.5DG. Database is defined as one or more structured sets of persistent data, managed and stored as a unit and generally associated with software to update and query the data (Litton, 1987; Navathe and Elmasri, 2002; Date, 2003). A geodatabase in GIS includes data about the spatial locations and shapes of geographic features recorded as points, lines, areas, pixels, grid cells, or TINs, as well as their attributes. A geodatabase is a collection of geographic datasets for use by ArcGIS (ESRI, 2004a).

The IG was used to store all data that possibly could be collected for this project, which include borehole, bedrock geology, surficial geology, and geochemical data. The IG is capable of data management and information query. In order to estimate total resource of the placer gold in the Nome area, a database that facilitates volume calculation was needed. Therefore, another geodatabase known as R2.5DG was created. The two geodatabases are linked and related (cross-referenced) to each other through common attributes. Figure 5 shows the flowchart of the conceptual GIS architecture of this project. Detailed descriptions of the IG and R2.5DG are presented next.

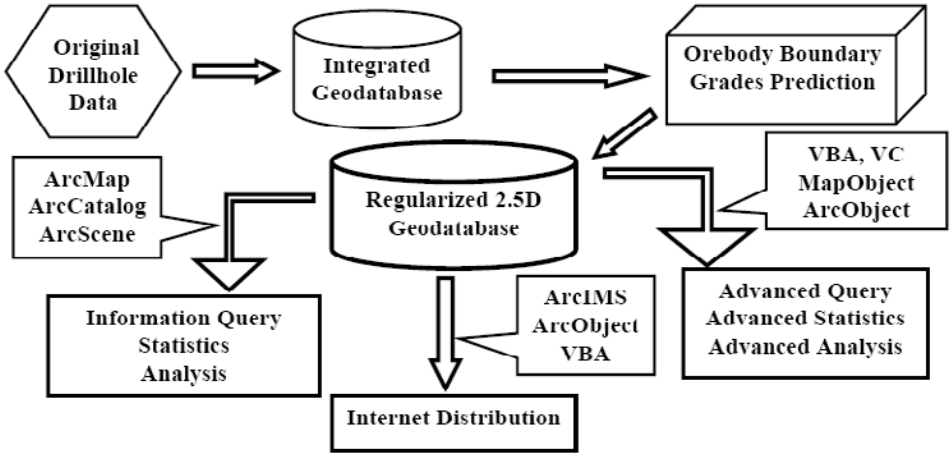

Figure 5. Conceptual GIS architecture of the project (Zhou et al., 2007).

All of the spatial data layers and non-spatial tables collected are stored in the IG. Table 1 lists the feature classes stored in the IG.

Table 1. List of Feature Classes in Integrated Geodatabase (Zhou et al. 2007)

Feature Class	Feature Type	Description
DH_location	Table	Drill hole location info
DH_segmentinfo	Table	Borehole segment attributes
DH_sliceinfo	Table	Layered orebody information
GeoDH_sliceinfo	Point	Layered orebody information
Lith_slice_Poly	Polygon	Layered lithology
OnshoreGeo	Polygon	Onshore geology
OffshoreGeo	Polygon	Ocean floor geology
Structure	Polygon	Offshore sediment structure elements
Permitblk	Polygon	Exploration permit blocks
Rivers	Polygon	Rivers, town and roads of Nome
Studyarea	Polygon	Study area boundary

The IG was created using the functions in Microsoft (MS) Access, ArcMap, and ArcCatolog. The IG is capable of displaying 3D surfaces using ArcGIS extensions, such as 3D Analyst, Geostatistics Analyst, and Spatial Analyst. However, it does not have the capability for solid three-dimensional analyses and cannot yield information on volume calculation and resource estimation. In order to be able to perform resource estimation, a quasi-3D geodatabase, known as Regularized 2.5 Dimensional Geodatabase (R2.5DG), was created by subdividing the study area into cells. The R2.5G is able to define orebody boundaries, perform grade extrapolation, and estimate the resource at any given spatial domain.

Within approximately 40.43 km^2 of the entire study area, a total of 3468 drill holes spaced from 50 to 120 meters apart, are distributed irregularly. To develop the regularized geodatabase, the area was divided into 10m by 10m grids, forming 404319 spatial records with one record for each cell. The finer the grid is and the more precise the result is. On the other hand, it would need more storage on the computer and take longer time to perform ore resource estimation. For the purpose of this project, a 10m by 10 m grid is sufficient for the precision and yet time efficient to perform ore resource estimation (Zhou et al. 2007).

Nome Offshore Gold Resource Analysis

There are many built-in functions in ArcGIS for mineral resource analysis. Some functions in the ArcGIS have been adapted and customized to query, analyze, and visualize the data, and to provide useful information for potential developers and general public.

Information Query

The geodatabases constructed supports the storage and analysis of geo-referenced data. The relational database management system (RDBMS) allows flexible data extraction, called a "query", with a single criterion or multiple criteria, based on Structured Query Language (SQL). Figure 6 shows the procedure of a customized query tool which allows the user to conduct a multi-variable query by drawing a polygon with a mouse. Pop-up windows for the polygon area will show information on selected information of drill holes, resource estimation, as well as statistical information within the selected area.

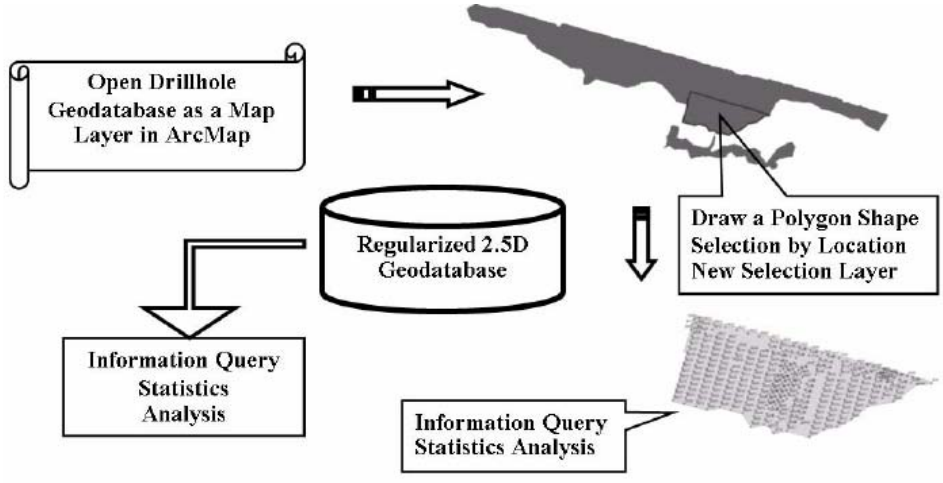

Figure 6. Procedure of information query on gold resource within a selected polygon area (Zhou et al. 2007).

Data Visualization

Visualization is the presentation of data in graphic format. Graphics provide the most intuitive representation of the data, while a detailed numerical table is useful for in-depth analysis.

The 3D drill hole plots with orebody boundaries (figure 7) can be created using ArcScene, an application program of ArcGIS package. Vertical cross-sectional orebody profiles can be created by using 3D Analyst (figure 8) along any defined polyline for each grid layer, based on parameters, such as gold grade, gold deposit thickness, sea floor elevation and others. Such profiles provide useful information for mining operation design. For example, it is often necessary to compare the distribution of an orebody with the distribution and characteristics of bedrock and types of sediment along vertical cross-sectional profiles.

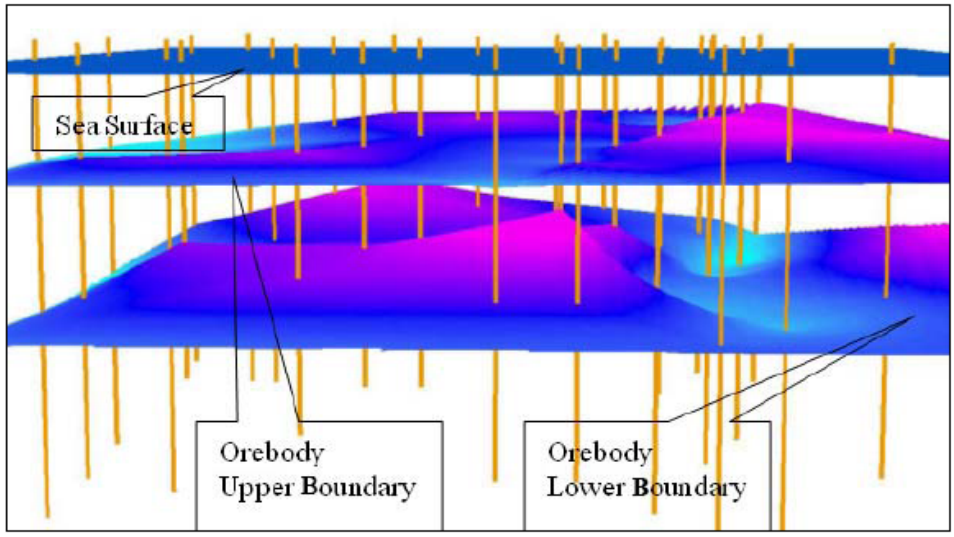

Figure 7. 3D visualization of drill holes and orebody boundaries (Zhou et al. 2007).

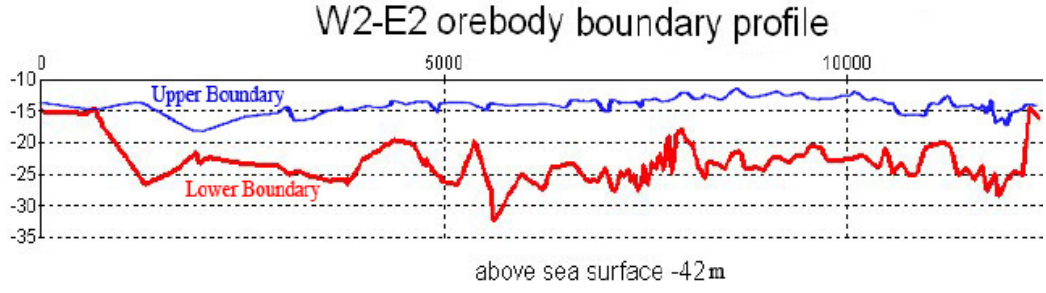

Figure 8. Vertical cross-sectional profiles of ore body boundaries (Zhou et al. 2007).

Sediment Data Analysis

The sediment type of each sample segment of drill hole was examined in the laboratory and recorded in original drill hole log. Nine sediment types were classified. Table 2 lists the criteria for sediment classification and code assignments.

Based on the depositional environment, Howkins (1992) divided the sediment facies of Nome offshore to five major facies groups – diamict, gravel, sand, mud and peculiar facies. To determine the horizontal and vertical distribution of sediments, layered lithology Thiessen polygon feature classes (Lith_slice_Poly) were created from layered lithology point feature classes (DH_sliceinfo) using ArcInfo and stored into the IG. A series of layered sediment distribution maps were then created using ArcGIS at various levels below sea surface level (-8, -12, -16, -20, -24, -28m) and below sea floor level (-1, -4, -8, -12m) to illustrate the changes in the sediment with depth. The distribution of sediments is highly comparable, comparing the ocean floor geology map (figure 3) with sediment distribution map at 1 meter below the sea floor (figure 9), which was generated from drill hole data in this study.

Table 2. Primary Sediment Type Classification (Howkins, 1992)

Number Code	Text Code	Description
1	MUD	Mud; silt and clay any mixture, may contain a trace of sand but no more than 5%.
2	SAM	Sandy mud; silt/clay coating sand grains, may be cohesive.
3	SAN	Sand; clean sand may have a trace of silt/clay, not enough to coat the grains, no more than 5%.
4	SAG	Sand and gravel; mixture of sand and gravel, may have a trace of silt/clay in the water but not enough to coat the grains, friable.
5	SWD	Slightly washed diamict; silt/clay, sand and gravel. Silt/clay enough to coat the grains. The mixture is moderately cohesive but will crumble (forms a crumbly ball).
6	DIA	Diamict; silt/clay, sand and gravel. Enough silt/clay to forma cohesive matrix (for a firm ball).
7	CRD	Clay rich diamict; silt/clay with 10% to 20% sand and pebbles. Appears to be a mud with rock fragments within its matrix (sticky and cohesive).
8	WAD	Washed diamict; sand, gravel, silt and clay, silt/clay enough to coat the grains, but doesn't give it cohesion (can't form a ball).
9	BER	Bedrock; angular fresh rock chips of one rock type, associated with high blow counts and little penetration.

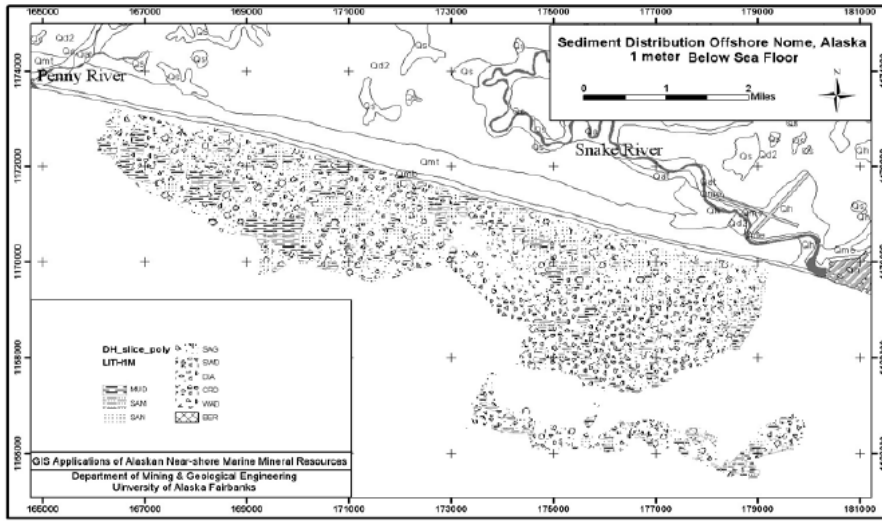

Figure 9. Sediment distribution map (1 meter below sea floor).

Gold Distribution with Sediment Type

The proportions of gold mineralization of each sediment type vary from 5% to 70%. Over 70% of samples of bedrock are mineralized. The high percentage mineralization of bedrock is in part due to the fact that the sample locations are at the interface of bedrock and diamict, where the particulates of gold have a higher chance to deposit right during transport. For other eight sediment types besides bedrock, from finer sediments (MUD, SAN) to coarser sediments (DIA, WAD), the percentages of mineralization decreases from 37.5% to 5%. This

indicates that ocean invasion and the erosion of gold-bearing glacial debris are one reason for gold dissemination (figure 10).

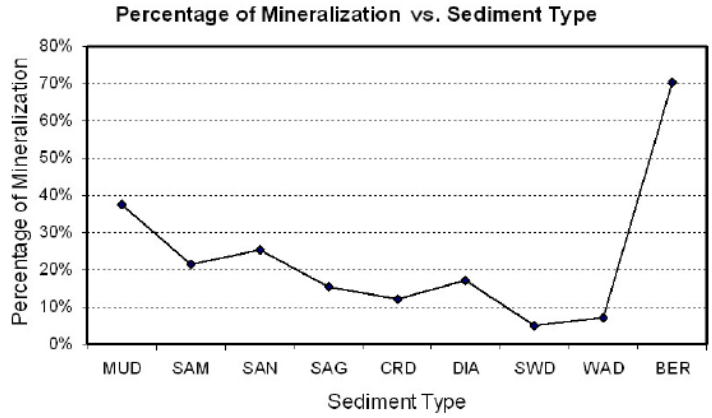

Figure 10. Percentage of Mineralization at Various Sediment Types (Chen et al. 2005).

The average gold contents of each sediment type are calculated with non-mineralized samples included. The results can be divided to two groups: The coarser grain sediments, i.e. SAG, CRD, DIA, SWD, WAD, have higher gold contents ranging from 220 to 309 mg/m³, and the finer grain sediments, i.e. MUD, SAM and SAN, have lower gold contents ranging from 119 to 154 mg/m³. The higher average gold content in diamict facies and gravel facies indicates that glacial sediments are origin of the gold.

Gravel facies, composed of SAG, which is the indicator of fluvial channel including outwash plains, beach, marine surface lag, and other high energy sedimentary environments, logically have the highest average gold content (309mg/m³), and also have a relatively higher proportion of mineralization (15.5%) among the coarse sediment group. Gravel facies sediments account for approximately 44% of the total gold resource in the sediment (figures 11).

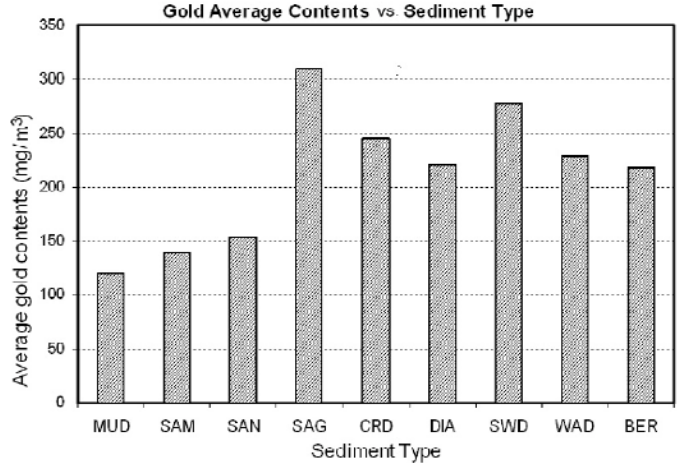

Figure 11. Gold Average Contents at Various Sediment Types (Chen et al. 2005).

Spatial Gold Distribution

Based on the gold grade attribute in layered orebody feature class (GeoDH_sliceinfo) stored in Integrated Geodatabase, using the interpolation tools in ArcGIS Geostatistics Analyst or 3D Analyst extension, a series of layered gold distribution maps (raster and contour) are generated at various sea surface levels (-18, -20, -22, -24, -26, -28 ,-30, and -42 m) and sea floor levels (-2, -4, -6, -8, -10, -12, and -14 m). Inverse Distance Weighted (IDW) interpolation and Indicator Kriging (IK) were used for generating the gold concentration surfaces. An influence neighborhood radius of 600 m and an inverse power of 2 were used in the IDW method.

Figure 12 shows under sea floor 2m gold distribution contour map. In this example, the gold distribution contour ranges from 200 to 8400 mg/m^3.

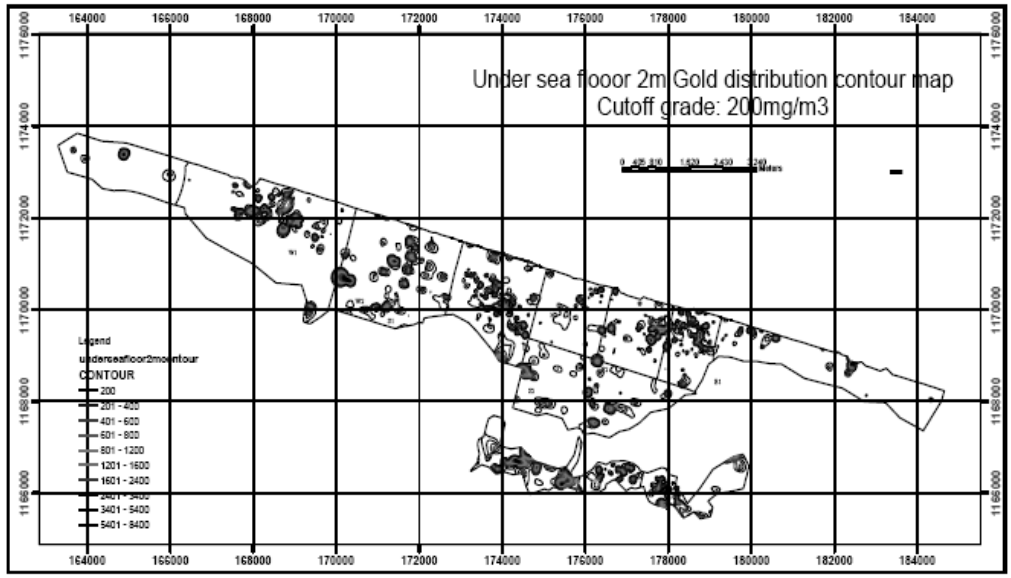

Figure 12. Gold distribution at 2m under sea floor (Zhou et al. 2007).

The offshore area of anomalous gold mineralization is oriented more or less parallel to the coast over an east-west distance of about 25km. Gold mineralization occurs at each block throughout the study area at the 200mg/m^3 cutoff grade. Based on the gold distribution, the study area is divided into twenty-seven sub-areas (figure 13) at the 200mg/m^3 cutoff grade. Six out of the twenty-seven orebodies, i.e. Red1, King1, Silver2, Humpy2, Tomc2 and Coho1, exceed 3 tons of gold resource, comprising more than 70% of the total resource. With an increased cutoff grade, the areas of anomalous gold mineralization shrink sharply. At the 600mg/m^3 cutoff grade and above, only 4 specific zones are particularly anomalous, i.e. Red1, King1, Tomc2 and Coho1.

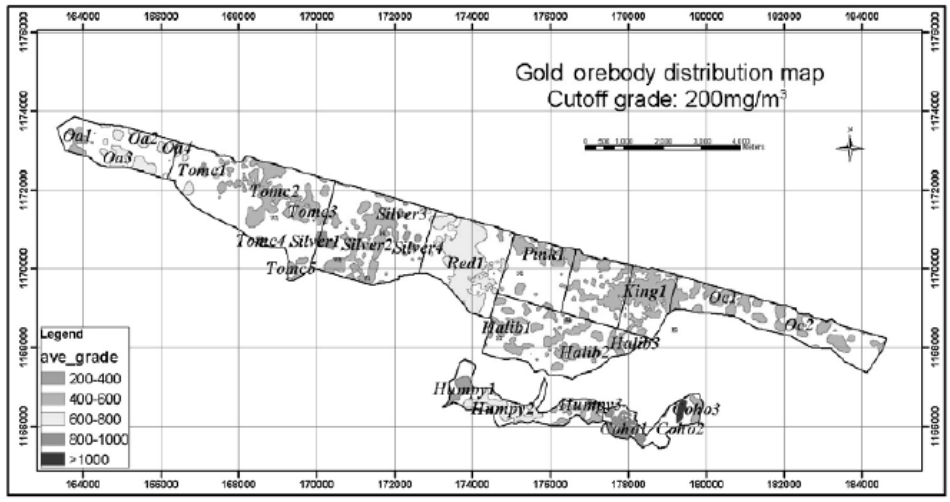

Figure 13. Gold deposit distribution map (cutoff grade: 200mg/m³).

Resource Estimation

Resource estimation is an important component of the mineral resource management. All gold resource calculation problems must deal with estimating two inter-related items: the grade and the associated volume. This grade could be the economic cut-off grade or the average grade within a pre-specified volume. The volume of ore can be estimated based on orebody boundary.

The first step for resource calculation is to determine orebody thickness and average gold grade for every borehole. Calculation of average gold grade for each borehole based on various cut-off grades is a time-consuming task. Since orebody boundaries are different at various cutoff grades, their associated thickness and average grade also are different. The calculations are performed repetitively in MS Access using SQL language, based on segment records stored in the borehole segment information table in the Integrated Geodatabase. The calculated average grades and thicknesses of various layers form the layered orebody information table.

The second step is to create a point layer and grid coverage and add them in the 2.5D Geodatabase. The point layer is used to store the layered orebody grades and thicknesses. In this layer, the entire study area is divided into 10m×10m grids, and each point feature object in the center of a cell represents this cell and all of the grades and thickness are stored in this point object. The entire study area is approximately 40.4319 km^2. The Regularized 2.5D Geodatabase contains 404319 spatial point records, each point record representing one 10×10m-grid cell.

The third step is to determine the thickness for each cell created during the second step. The attribute data in GeoDH_sliceinfo layer is utilized to build orebody boundaries. To determine the orebody thickness of each regularized cell, two orebody boundaries are generated based on the levels of the orebody's beginning depth and the ending depth, respectively. The orebody boundaries are interpolated using the Natural Neighbor method, which is an interpolation method that estimates the value of a cell using weighted values of

the input data points that are their natural neighbors, determined by creating a triangulation of the input points. The Natural Neighbor tool in ArcGIS can efficiently handle large numbers of input points. Other interpolators may have difficulty with large point datasets (ESRI, 2004b).

The next step is to interpolate the gold content for each regularized cell. Five interpolation methods are investigated and compared. IDW and IK were selected for interpolating the gold concentration contour maps (Li et al. 2005). The procedure of geostatistical analysis will be described in the next section.

The last step is to estimate the gold resource within the study area. After the thickness (T) and average grade (G) for each cell are obtained, one new column (G_ T) can be created to store $G_i \times T_i$. For any selected polygon area, $\sum(G_i \times T_i)$ and $\sum T_i$ can be obtained by using the "statistics" tool in ArcMap

The gold resource within a selected a polygon area is estimated by the following equation:

$$R = \sum(G_i \times T_i) \times 10 \times 10 \tag{1}$$

where G_i is grade value of each cell above cutoff grade.

T_i is thickness of each cell.

The average grade (G_{ave}) within a polygon area is given by:

$$G_{ave} = \frac{1}{\sum T_i} \sum(G_i \times T_i) \tag{2}$$

Table 3 gives total resource estimates at different cutoff grades within the entire study area. Both the actual and normalized gold values are calculated and stored in the IG. Depending on the cutoff grade, the total amount of gold resource ranges from 113,767oz (with a cutoff grade of 1000 mg/m^3) to 2,309,664 oz (with a cutoff grade of 0 mg/m^3). The average grade ranges from 0.233 g/m3 (with a cutoff grade of 0 mg/m^3) to 1.929 g/m^3 (with a cutoff grade of 1000 mg/m^3).

Table 3. Resource Estimations at Different Cutoff Grades (Zhou et al. 2007)

Cut-off Grade (mg/m³)	Orebody Area (m²)	Average Thickness (m)	Average Grade (mg/ m³)	Ore Volume (m³)	Resource (Kg)	Resource (Oz)
0	40429800	7.63	0.233	308325290	71840	2309664
200	18060600	4.86	0.554	87737850	48607	1562718
500	2438900	5.28	1.047	12886388	13492	433772
800	740400	5.33	1.441	3948949	5690	182949
1000	404600	4.53	1.929	1834422	3539	113767

Geostatistical Analysis

During the geostatistical analysis, five geostatistical approaches that built-in in ArcGIS are evaluated and compared. These geostatistical approaches include Inverse Distance Weighted (IDW), Ordinary Kriging (OK), Ordinary Kriging with lognormal transformation (OK-log), Simple Kriging (SK) and Indicator Kriging (IK). Cross-validation is used to examine the accuracy of the five approaches. It is determined that the OK and SK algorithms are not suitable for this dataset because of the difficulty of fitting the semivariogram model despite their lower RMSE (Root-mean-square error) and the higher RMSS (Root-mean-square Standardized). The OK-log algorithm does not provide satisfactory prediction either, because it places too much weight on the role of extreme values resulting in overestimation and extremely high RMSE. Reserve estimation of each blocks is conducted using each of the interpolation methods and compared with the reserve calculated using the conventional polygon method. The IWD and IK algorithm seem to provide estimations more agreeable with the conventional polygon method. The geostatistical analysis will be briefly described next. Detailed information about this geostatistcial study can be found in Li et al. (2005).

Data Characterization

Statistical characterization of the dataset revealed that the dataset is near lognormal distribution, high positive skewed, and apparently anisotropy. In addition, there exist a small number of outliers that affect the reserve estimation. These characteristics make the development of an interpolation model for the gold deposit very challenging.

The histogram and statistical summary of 449 average gold grades are shown in figure 14. As can be seen, the high positive skewness (3.37) indicates most of the values are in the low range and few extreme values on the high side exist in the data.

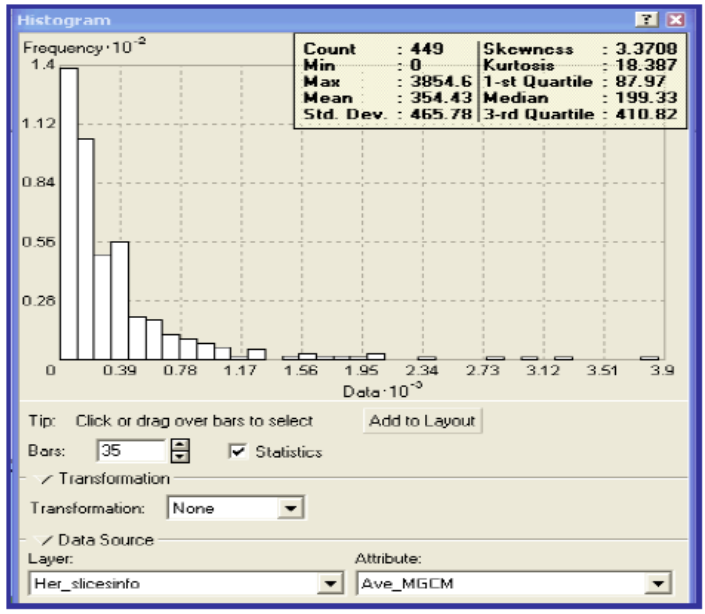

Figure 14. Histogram Chart of Dataset of Herring Block (Li et al. 2005).

Figure 14 also reveals that the data has an approximately lognormal distribution. OK and SK are first considered to be applied to this data set. OK can be applied without any transformation while SK can only be applied with lognormal transformation.

The analysis also reveals that the dataset is directional or anisotropy. An initial analysis indicates that the directions of maximum and minimum variation (geometric anisotropy) to be 68° and 158° approximately (figure 15). It is essential to take this anisotropy into consideration when applying a spatial interpolation model.

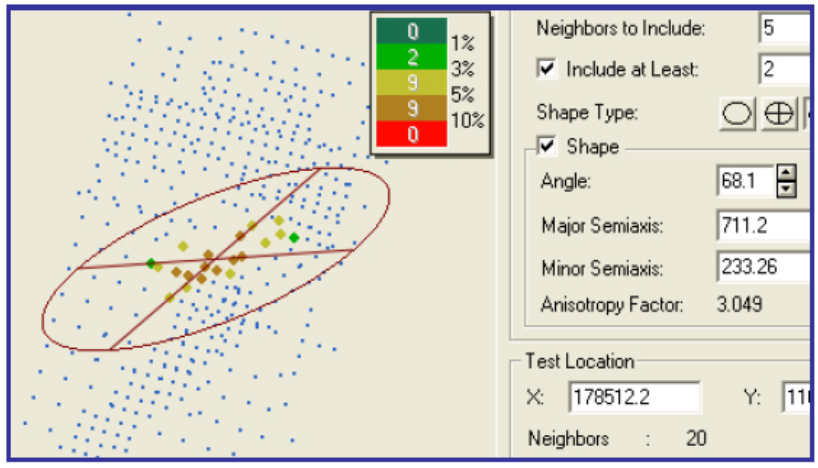

Figure 15. Anisotropy of the population of Herring Block (Li et al. 2005).

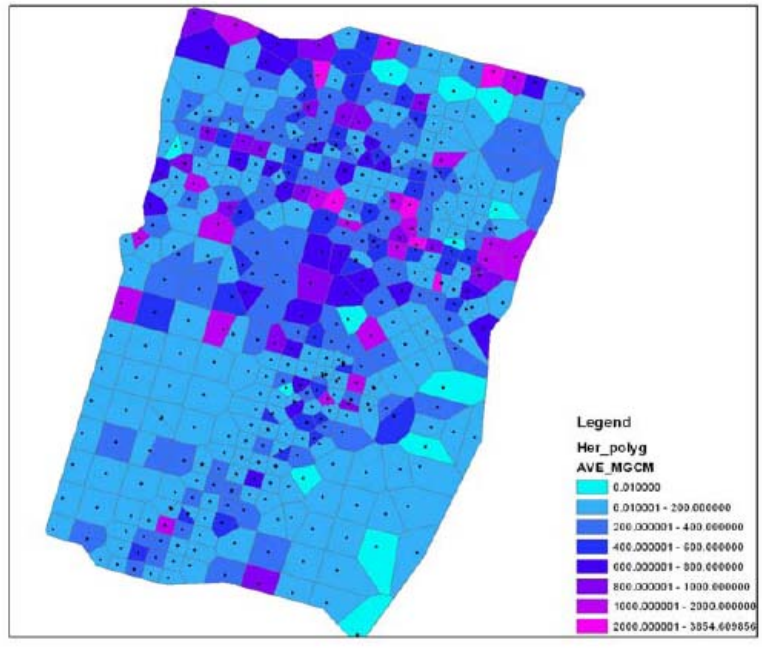

Figure 16. Thiessen polygon of drill hole grade distribution (Li et al. 2005).

A number of attempts are made applying regression techniques such as the simple regression and the Co-Kriging methods to investigate the correlations between the gold grade and the orebody depth from the sea floor and from the sea level. Weak correlation between gold concentration and the depth, however, are found.

Thiessen polygons file are generated from drill holes data to investigate the pattern of gold distribution and calculate the reserve using the Thiessen polygon method (figure 16). The analysis indicates that although the drill holes in Herring block are relatively even distributed, the gold grades fluctuate significantly in the horizontal direction.

Outliers

Dealing with extreme values is a frequently encountered practical issue, especially in the case of placer gold deposit. In this study, a small number of extreme values control significant proportion of the reserve estimation (Only 6% of the drillholes' average grades is greater than 1000mg/m3.). The variogram is sensitive to strong positive skewness, because a few exceptionally high values contribute to significant squared difference.

Three methods have been employed to deal with this issue in practices: (1) Remove the extreme values, based on certain probabilistic criteria and empirical, geological judgment. It is, however, not suitable to remove extreme values when the data carry valuable structural information. (2) Transform the data by taking logarithm or by other smoothing function. (3) Apply Indicator Kriging, which provides an alternative approach to model the spatial distribution of positively skewed populations and has the potential to overcome the limitations with other modeling techniques.

The approach of Indicator Kriging is to divide the dataset into 2 or more datasets using threshold values, and to quantify the probability that the value at unknown location is greater or less than a threshold level. After interpolating each dataset respectively, the final prediction value at unknown location is calculated by integrating the predicted value of each dataset with it probability.

Interpolation Approaches

Five interpolation methods, i.e. IDW, OK, Ok-log, SK and IK, are applied to generate a continuous gold concentration surface based on the bore hole data.

IDW is one of the many methods to perform interpolation of scattered spatial data. A neighborhood about the point to be interpolated is selected and a weighted average is calculated of the observed values within this neighborhood. The weighting factors of observed points are a function of the distance between the observed points to the interpolated point, the closer the distance the bigger the weights. The interpolating function is constructed as a linear combination of the observed values v_i at point x multiplied with weight functions w_i (Fisher et al., 1987):

$$f(x) = \sum_{i=1}^{n} v_i w_i(x) \tag{3}$$

where the weight factors $w_i (i = 1,2...,n)$ are constructed by normalizing each inverse distance:

$$w_i(x) = d_i^{-\lambda_i}(x) \Big/ \sum_{j=1}^{n} d_j^{-\lambda_j}(x) \quad (4)$$

where $d_i(x)$ is the Euclidean distance from point x to node x_i, and λ_i is the exponential power of weight. Each weight function w_i is inversely proportional to the distance from the point x_i where the value v_i is prescribed. The sum of the proportional factors $w_i(i = 1,2...,n)$ should equal to one.

The possible redundancy between samples depends not simply on the distance but also on the spatial continuity. Kriging methods, which use a customized statistical distance rather than a geometric distance to de-cluster the available sample data, are linear estimation that develops optimal weights to be applied to each sample in the vicinity of the block being estimated. They are based on the best linear unbiased estimation, which minimizes the mean error and the variance of the errors. They depend on the statistical model employed and the following mathematical formula.

$$Z(s) = \mu(s) + \varepsilon(s) \quad (5)$$

where Z(s) is the value of interest, μ(s) is the deterministic trend and ε(s) is auto correlated errors.

The variable s indicates the location which is the spatial coordinates in ArcGIS. Based on different assumptions of the error term, ε(s), there are several different Kriging methods, such as Ordinary Kriging, Simple Kriging, Universal Kriging, Indicator Kriging, Cokriging and others. All of them are built-in in ArcGIS Geostatistical Analyst extension.

Interpolations Assessment

Cross validation is used for assessing different Kriging methods. The Mean Standardized prediction Errors (MSE) and the Root Mean Square Error (RMSE) are shown in table 4.

The RMSE for estimates made using OK-log is the highest whereas for others they are almost the same. The OK-log algorithm will not provide satisfactory prediction either, because it places too much weight on the role of extreme values resulting in overestimation and extremely high RMSE. It is determined that the OK and SK algorithms not suitable for this dataset because of the difficulty of fitting the semivariogram model despite their lower RMSE and the higher RMSS.

Table 4. Comparison of prediction errors (Herring block)

Interpolation Method	RMSE	MSE
IDW	455.1	0.0714
Ordinary Kriging	452.7	-0.000218
Ordinary Kriging (Log)	718.6	0.0568
Simple Kriging	450.5	-0.003029
Indicator Kriging	452.9	0.067

Notes: RMSE: Root mean square error.

Comparison of Ore Tonnage

The reserves of Herring block are calculated using the five interpolation methods. The tonnages of gold for Herring block at various cut-off grades shown in table 5 and figure 17. The tonnage estimated by OK-log is excluded in this table since its extremely high RMSE and the tonnages almost double than those of other interpolation methods. For this reason, it is unsuitable for this dataset. For comparison, the reserve using the Thiessen polygons method is also calculated.

Table 5. Tonnages of gold of Herring Block with various cut-off grades (Herring block)

Interpolation Methods	Tonnage (Kg) of gold at various cut-off grade (mg/m³)							
	0	200	400	600	800	1000	1200	1400
IK	5380	4761	2974	424				
IDW	5209	4482	2696	1336	749	438	294	200
OK	5353	4737	2869	710	124	2		
SK	5427	4993	2548	516				
Polygon	4999	4146	2999	2460	1868	1246	1079	923

At lower cut-off grade from 0 mg/m³ to 400 mg/m³, the tonnages estimated using various interpolation methods has significant difference (figure 17), and the difference rapidly increases at higher cut-off grade. Polygon method gets the higher tonnages at all cut-off grade levels up to 1400 mg/m³ and IDW has the second highest estimation. Krigings (OK, SK, IK) have no estimation above the cut-off grade of 800 mg/m³ due to the smoothing effect.

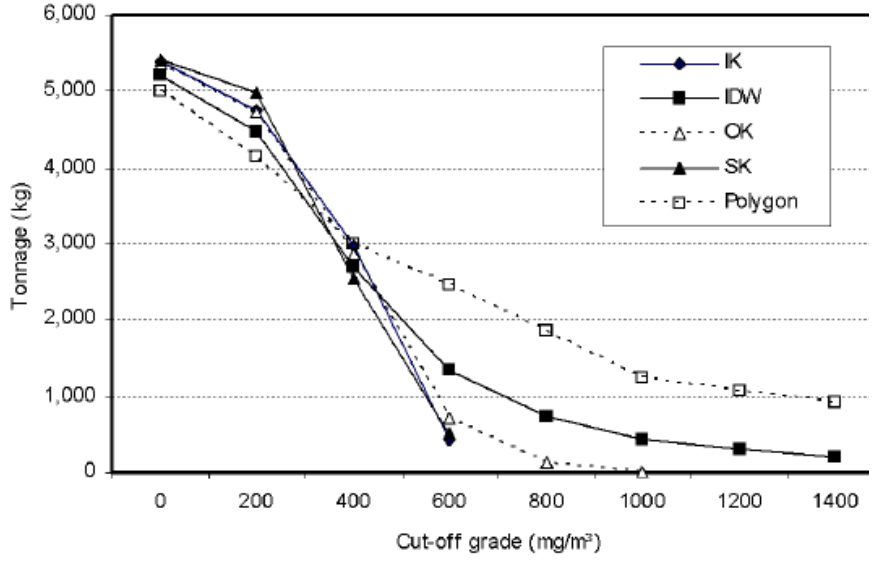

Figure 17. Tonnages of gold with various cut-off grades (Herring block) (Li et al. 2005).

The reserves of each block are estimated using the different interpolation methods. The results are shown in table 6 and figure 18. In general, there is a common trend for reserves estimated using various interpolation in each block, i.e., the reserves estimated by OK-log are

the highest, the Polygon are the lowest, and the others (IK, IDW, OK, and SK) are in middle range.

Figure 19 shows the trend of total reserves in the study area estimated using the five interpolation methods and the polygon method. The reserve estimated by OK-log is approximately twice as high as the others and SK has the second highest estimation. The polygon method has the lowest. The estimations by the other three methods (IK, IDW, and OK) have little difference.

Table 6. Tonnages (Kg) of gold of Blocks for various interpolation Methods

Block	Ok(log)	IK	IDW	OK	SK	Polygon
Herring	11672	5380	5194	5345	5415	4999
Halibut	9738	8901	8701	8737	8817	8357
Humpy_coho	14556	10776	10246	10190	10854	9869
Pink_King	12320	8978	8835	8852	10378	7882
Red	13870	10450	11332	10377	11173	9704
Silver	10386	10443	10326	10472	10539	9935
Tomcod_OA	14468	10615	10722	9422	11904	7581
OtherC	7554	5231	5015	5182	5648	3802
Total	94567	70778	70374	68578	74730	62131

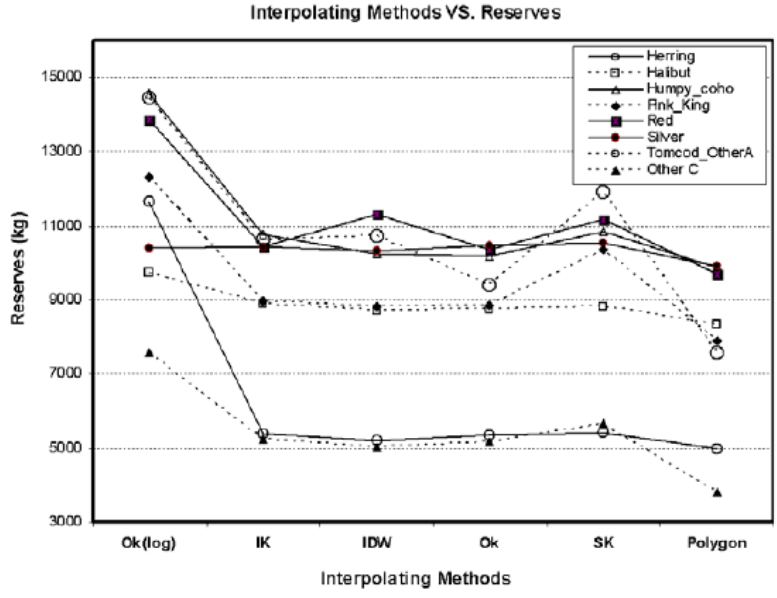

Figure 18. Tonnages of gold of blocks for various interpolation Methods (Li et al. 2005).

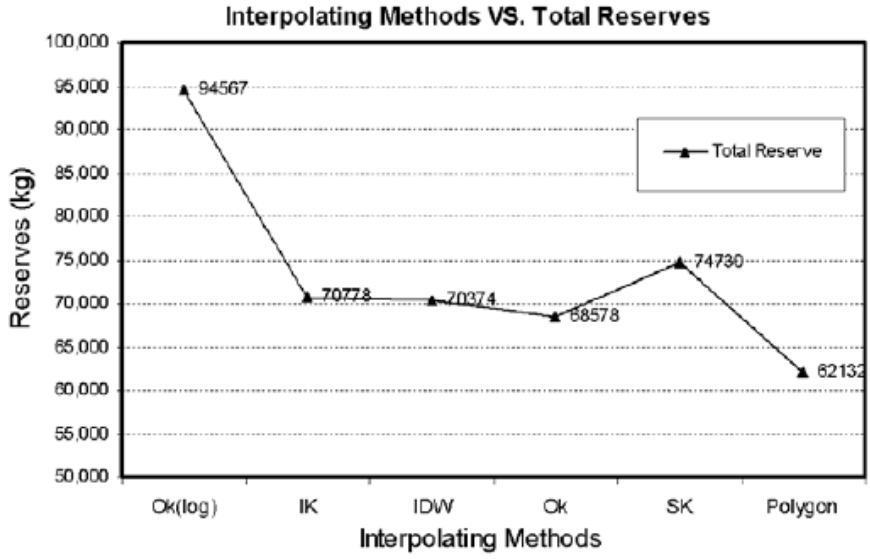

Figure 19. Total tonnages of gold for various interpolation Methods (Li et al. 2005).

Web-Based GIS

In order to facilitate information dissemination, a web-based GIS (http://uaf-db.uaf.edu/website/) was developed for this project using ArcIMS, an application program of ArcGIS package. A detailed description about the web GIS of the project can be found in Luo et al. (2005).

Software

ArcIMS is one of the application softwares for distributing mapping and GIS data and services on the Web. ArcIMS runs in a distributed environment and consists of both client and server components (ESRI, 2004c). The ArcIMS HTML Viewer and ArcIMS Java™ Viewers are client-side components. The ArcIMS Spatial Server, ArcIMS Application Server, ArcIMS Application Server Connectors, and ArcIMS Manager are server-side components (figure 20).

A client requests information from the server. The server processes the request and sends the requested information back to the client. The client then presents the information it receives. The complete architecture also includes an operating system, a Web server, a servlet engine, and client-side Web browsers.

Web Server

The basic function of a Web server is to receive requests from the Web browser and respond with a document from the server to the Web browser. The application server handles the load distribution of incoming requests. The application connector translates user's requests into ArcXML format and translates ArcIMS spatial server responds into HTML before returning back to the Web server. The ArcIMS monitor is used to track the state of the ArcIMS spatial server.

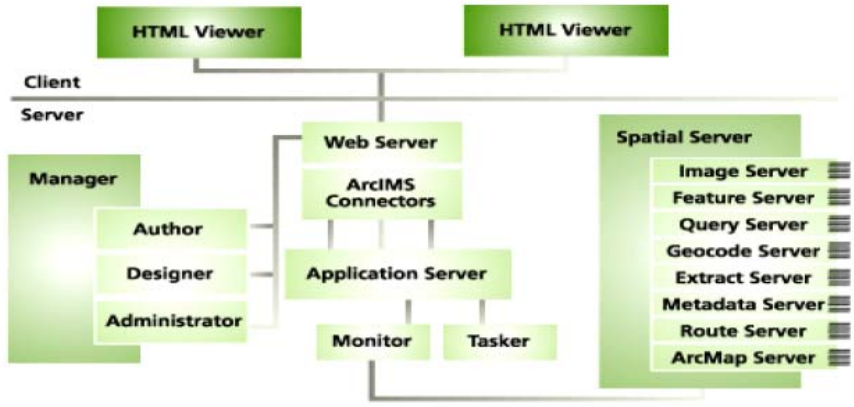

Figure 20. ArcIMS Components (ESRI, 2004c).

Clients Viewers

Three client viewers are included with ArcIMS: the ArcIMS HTML Viewer, the ArcIMS Java Custom Viewer, and the ArcIMS Java Standard Viewer. When users access the Web site, they will see a map inside the viewer you selected, which is embedded in the Web site. The viewer determines the look and functionality of the Web site. Using the tool bars in the viewer, users can: pan and zoom the map extent; query spatial and attribute data; create buffers around features; measure distances on the map; locate addresses; add MapNotes and EditNotes and Add data form local and Internet sources (ESRI, 2004c).

ArcIMS Manager

ArcIMS Manager is a Web-based application that supports the three main tasks we perform in ArcIMS—map authoring, Web site design, and site administration. These tasks can also be completed using the three independent ArcIMS applications—ArcIMS Author, ArcIMS Administrator, and ArcIMS Designer. The ArcIMS author is used to generate map configuration files, which are written in ArcXML and are the input to ArcIMS services. ArcIMS designer is used to design Web pages, including the WebPages layout, available toolbox, and functionality of the Webpages. The ArcIMS administrator is used to publish and administer services, including adding, starting and stopping and deleting services, or add and remove spatial and virtual servers.

Website of Nome Offshore Mineral Resource Management and Utilization

This Nome mineral resource website was designed to provide public and other users with easy access to Nome Offshore gold exploration and resource information. To achieve this goal, an interactive mapping application was created that allows users to search for gold exploring areas, borehole distribution, gold concentration, and approximately gold reserve at users interested districts, and to bring up maps, tables, query information about the offshore goldmine.

Clients can enter the Nome Mineral Resource website search for above-mentioned information by map layers. Freely zoom, pan, extent whole map layers, get identify results of active map layer, obtain the querying or searching results, using the AcrIMS tools on the ArcIMS WebPages. The different ArcIMS Viewers are shown in figures 21 and 22.

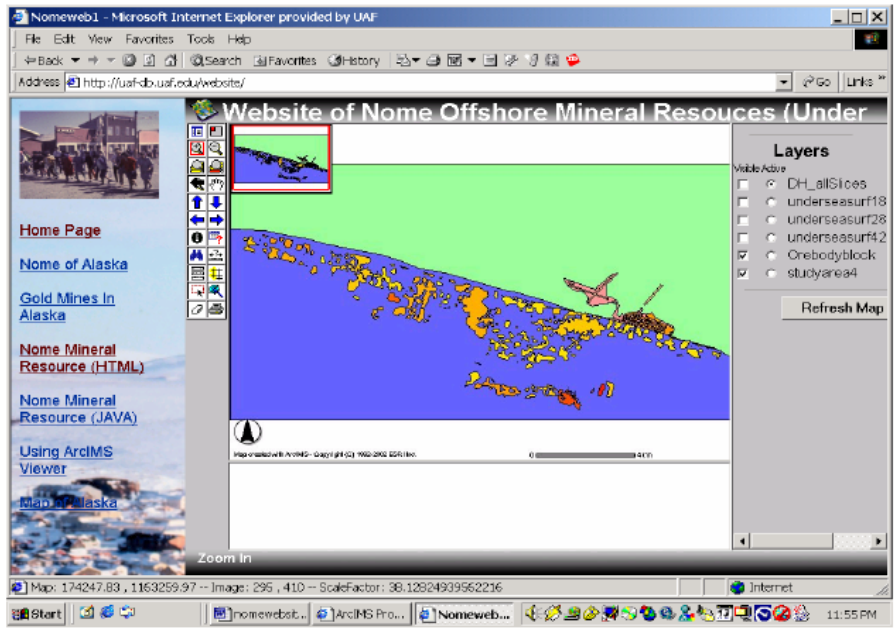

Figure 21. ArcIMS HTML Viewer.

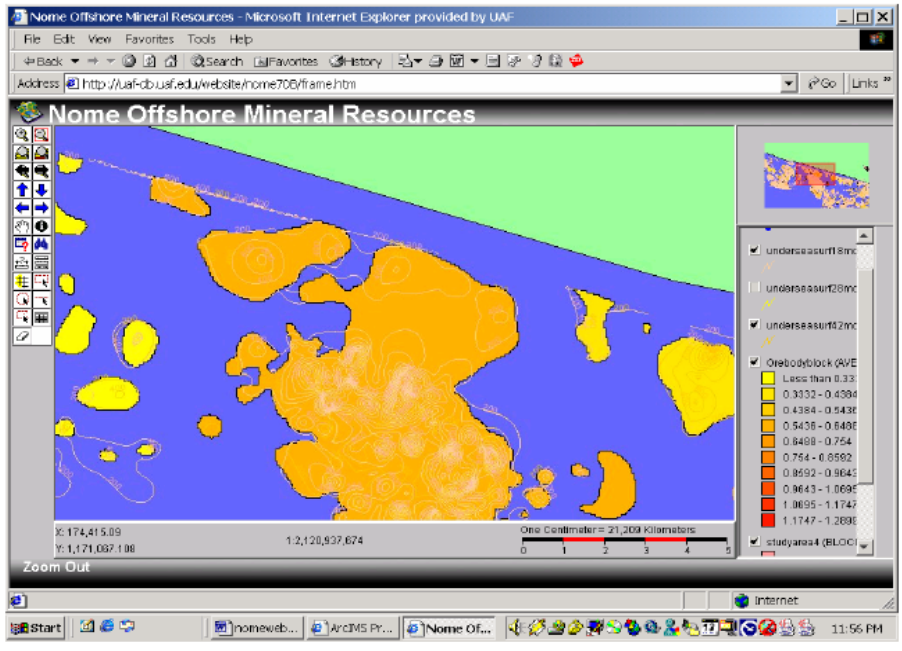

Figure 22. ArcIMS Java custom Viewer.

The following mineral resource information is available over this website:

1. General information about Nome offshore mineral resource exploration and unitization.
2. Publication and related information about mining and mineral resources in Nome, Alsaka.
3. The offshore area gold exploration information including exploration districts, boreholes logs, samples and geological profiles.
4. Mineral resource prediction results using geostatistic methods including average gold grades, average gold reserve, cut-off gold reserve, and gold concentration contours for different plane section at certain depth.

CONCLUSIONS

Based on literature review, GIS applications in mining, especially in gold mining, can be summaries into four categories, including in mining planning, in mining production, in mining reclamation, and in mining technical researches.

A case study that applied GIS for resource estimation of the offshore placer gold resources near Nome, Alaska was presented. Two databases were developed during this research, namely the IG and the R2.5DG. The IG is a data container which could be used for date management and information query, and the R2.5DG is capable of handling volume calculation, and resource estimation. A customized resource approach was built around this project, which can be used to estimate gold resources at different cutoff grades and different spatial domains in a time-efficient way. The geostatistical analysis in this case study has revealed that gold concentration dataset collected from the Nome offshore deposit are near lognormal distribution, positive skewed, directional, and has outliers. Inverse Distance Weighted (IDW), Ordinary Kriging (OK), Ordinary Kriging with lognormal transformation (OK-log), Simple Kriging (SK) and Indicator Kriging (IK) were assessed and compared with each other in the study. Cross-validation technique is employed to examine the accuracy of the five approaches. It is determined that the IWD and IK algorithm seem to provide estimations more agreeable with the conventional polygon method. A web-based GIS has been developed for this case study. This Web-based GIS provides government agency, and general public with a vast amount of information about Nome offshore mineral resource.

ACKNOWLEDGEMENT

The Nome placer gold GIS project was funded by authors the MMS (Minerals Management Services, U.S. Department of the Interior).

REFERENCES

Articles in Journals

Berry P.; Pistocchi A., A multicriterial geographical approach for the environmental impact assessment of open-pit quarries*, International Journal of Surface Mining, Reclamation and Environment.* 17, No.4 (2003) pp. 213-226

Bronston, M.A., Offshore placer drilling technology - A case study from Nome, Alaska: *Mining Engineering,* v. 42, No. 1, 1989, pp. 26-31.

Dillon U.; Blackwell G., The use of a geographic information system for open pit mine development, *CIM Bulletin.* 96, No.1069 (2003) pp. 119-121

Hammond, Anthony D., GIS applications in underground mining, *Mining Engineering,* 54, No. 9 (2002) pp. 27-30

Zhou, W.; Chen, G.; Li, H.; Luo, H.; Huang, S. L., GIS Application in Mineral Resource Analysis – A Case Study of Offshore Marine Placer Gold at Nome, Alaska*, Computers and Geosciences,* 33 (2007), pp. 773–788.

Books

Bonham-Carter, G.F., 1994, Geographic Information Systems for geoscientists: Modelling with GIS, Pergamon Press, Oxford, 398 p.

Date, C. J., 2003, An Introduction to Database Systems, 8th edition, Addison Wesley 1024p.

Fisher, N. I., Lewis, T., and Embleton, B. J. J., 1987, Statistical analysis of spherical Data, Cambridge University Press, 329p.

Litton, G., 1987, Introduction to Database Management: A Practical Approach, William C Brown Pub, 532p.

Navathe, S. B. and Elmasri, R., 2002, Fundamentals of Database Systems, 3rd Edition, Addison Wesley Longman, 1000p.

Edited Books

Garnett, R.H.T., Marine placer gold, with particular reference to Nome, Alaska. In: David S. Cronan (ed), Handbook of Marine Mineral Deposits, CRC Press, 2000, pp.67 – 101.

Reports and Theses

Boyle, R. W., The Geochemistry of Gold and its Deposits, Geological Survey Bulletin 280, Geological Survey of Canada, 1979, 584p.

Bronston, MA, A view of sea-floor mapping priorities in Alaska from the mining industry: C1052, US Geological Survey Reports on Alaska Released in 1991, 1990, pp.86-91.

Bundtzen, T. K., Reger, R. D., Laird, G. M., Pinney, C. S., Clautice K. H., Liss S. A., & Cruse, G. R., "Progress_Report on the Geology and Mineral Resources of the Nome

Mining District,", Division of Geological & Geophysical Surveys, Public-Data File 94-39, 1994

Chen, G.; Huang, S; Zhou, W., GIS Applications to Alaskan Near-shore Marine Mineral Resources, Stage II: Enhancement of Web Site; Improvement of GIS Structure; Predictive Model Development; and New Site Identification and Study, an unpublished report to Minerals Management Services, U.S. Department of the Interior by University of Alaska Fairbanks, 2003, 45 p.

Chen, G.; Zhou, W.; Huang, S; Li, H.; Luo, F., GIS Applications to Alaskan Near-shore Marine Mineral Resources (Phase III), an unpublished report to Minerals Management Services, U.S. Department of the Interior by University of Alaska Fairbanks, 2005, 159 p.

Howkins, C. A., A Model for Shallow Marine Placer Depositions: Based on the Marine Gold Placers at Nome, Alaska, University of Toronto, Master's Thesis, 1992, 188p.

Huang, S.; Chen, G.; Maybrier, S.; Brennan, K. L.,GIS Applications to Alaskan Near-Shore Marine Mineral Resources, an unpublished report to Minerals Management Services, U.S. Department of the Interior by University of Alaska Fairbanks, 2001, 280 p.

Koschmann, A. H., and Bergendahl, M. H., 1968, "Principal gold-producing areas of the United States," *Geological Survey Professional Paper* 610.

Li, H., Resource Estimation and Analysis for Offshore Placer Deposit using GIS Technology, Master's Thesis, University of Alaska Fairbanks, 2004, 154p.

Nelson, C. H. and Hopkins, D. M., Sedimentary Processes and Distribution of Particulate Gold in the Northern Bering Sea, *Geological Survey Professional Paper* 689, 1972

Price, M.J., 2001, "Geographic Information Systems and Industrial Minerals", preprint 01-116, Society of Mining Engineers

Tagg, A. R., and Greene, H. G., 1973, High-resolution seismic survey of an offshore area near Nome, AK: Geological Survey Professional Paper 759-A.

Conference Symposiums

Li, H. H. Luo, G. Chen, W. Zhou and S. Huang, Visualized Geostatistical Analysis of Nome Offshore Gold Placer Deposit Using ArcGIS - A Case Study, the Proceedings of 2005 Society for Mining, Metallurgy, and Exploration (SME) Annual Meeting, February 28 - March 2, Salt Lake City, Utah, 2005

Luo, H., H. Li, G. Chen, W. Zhou and S. Huang, Application of Web GIS for Nome Alaska Offshore Mineral Resource Management and Utilization, the Proceedings of 2005 Society for Mining, Metallurgy, and Exploration (SME) Annual Meeting, February 28 - March 2, Salt Lake City, Utah, 2005

Electronic Media

USGS, Geographic Information Systems, February 22, 2007, URL: http://erg.usgs.gov/isb/pubs/gis_poster/

ESRI, GIS Best Practices for Mining, August 2006, URL: http://www.esri.com/industries/mining/business/literature.html

Almarales–Hamm, D.; Campos, G. D.; Murray, B. and Russell, N., The Application of GIS to Bauxite Mining in Jamaica, Undated, URL: http://www.esri.com/mapmuseum/mapbook_gallery/volume19/mining7.html

ESRI (Environmental Systems Research Institute, Inc.), Building A Geodatabase, ESRI Digital Book, 2004a, 382p.

ESRI (Environmental Systems Research Institute, Inc.), Using Spatial Analyst, ESRI Digital Book, 2004b, 232p.

ESRI (Environmental Systems Research Institute, Inc.), Getting Started With ArcIMS 9, ESRI digital book, 2004c, 66p.

In: Gold Mining: Formation and Resource Estimation ISBN: 978-1-60741-096-6
Editors: M. D. Corral, J. L. Earle

Chapter 3

THE INFLUENCE OF GOLD MINING INDUSTRY ON THE POLLUTION OF ROŞIA MONTANĂ DISTRICT

Anca-Iulia Stoica, Raluca-Mariana Florea and George-Emil Baiulescu
Department of Analytical Chemistry, Faculty of Chemistry,
University of Bucharest, 4-12 Regina Elisabeta Blvd.,
030018, Bucharest-3, Romania

ABSTRACT

Gold mining from Roşia Montană is located in the Apuseni Mountains, in the west-central part of Romania and can be traced back to approximately 106 a.d. at the beginning of the Roman occupation of Dacia. In the medieval times the sporadic mining activity was mentioned, but accelerated in the XVIII-XIXth centuries. In the last 60 years underground and open surface mining activities were conducted, but presently, due to some Romanian governmental budget constraints, the state-owned mining company develops activities only at a small scale.

The study of Roşia Montană ecosystem was based on zinc, cadmium, lead, copper and manganese concentration determination in the streams, rivers and drinking water. Also, the concentration of gold from two medicinal plants, *Equisetum arvense* and *Achillea millefolium* collected from this region and from the other one was determined. It was observed that the concentrations of heavy metals were above the limits accepted by the Romanian Standard. One of the main pollution source is the solid rock (waste) deposited by the river sides. Acid Rock Drainage (ARD) is a naturally occurring process caused when water and air come into the contact with rocks containing sulphide minerals. Naturally occurring bacteria bring about acidification which in turn leaches heavy metals from rocks. The acid water produced can disturb the aquatic life and contaminate dinking water supplies.

It is well known from literature, that *Equisetum arvense* is a gold bioaccumulator and it is used as a prospector for its ores. The medicinal plants collected from Roşia Montană district presented a higher concentration of gold than the plants from other regions. From the results obtained it was observed that Roşia Montană District is an ecosystem impacted by the mining industry.

INTRODUCTION

Roşia Montană is located in south part of Apuseni Mountains, in west side of Romania. The area is recognized as a historical mining site, named the Golden Quadrilateral and spread over approximately 550 square kilometers. There gold and silver ores were extracted.

The start of mining activity is mentioned on beginning of Roman Empire occupation in Dacia. The earliest data of Roşia Montana, equivalent of the village of Alburnus Maior, are the roman waxed plates dated 131 – 166 A.D. The Middle-Ages in Roşia Montană was characterized by sporadic mining activity. During the AUSTRO-HUNGARIAN Empire domination, the XVIII-XIXth centuries, the gold and silver mining was accelerated and a chain of artificial lakes was constructed to supply the necessary water for processing the ores. After First World War the extraction was reduced significantly, and underground mining was stopped in 1985. In 1970 an open pit mine was started in Cetate Mountain to recover the rest of ore remained from the previous exploitations [1]. This pit removed 120 meters from the superior part of the Cetate Mountain and produced about 400 000 tones of ore/year. The grinded ore was concentrated by conventional flotation. The concentrate was then transported to Zlatna, south-east of Roşia Montană, for melting and the liquid effluents were discharged untreated into Abrud river.

Due to the processing steps that include discharging of possible contaminated waters and storage of solid rock waste on the ground this study aims to characterize the status of three selected rivers (Roşia River, Corna River and Abrud River) washing the area and a local source of potable water, from the point of view of contamination with heavy metals. Twelve samples collection points were established to monitorize the heavy metals concentration for one year with 2 months frequency. Monitoring results presented in this study are for samples collected starting with April 2004. The elements determined were: copper, cadmium, zinc, lead and manganese. The results indicate high heavy metals concentration above the legally established limits for this type of surface waters, respectively for potable water. The surface waters in the area were not investigated in the last 15 years until 2000 when a new excavation project was brought into discussion and monitoring was performed to draw up an environmental impact evaluation report. These data were not published during the performance of our study.

In 2006 we continue the study of this area, collecting samples from two medicinal plants, *Equisetum arvense* and *Achillea millefolium,* to determine the gold and other metals (silver, tellurium, chromium, cobalt, lithium) indicated to be presend due to geology of the location, including some heavy metals (zinc and copper). To conclude about the capacity of *Equisetum arvense* (common name: horsetail) to concentrate the gold we determined this element from 2 samples of *Equisetum arvense* with different origin then Roşia Montană.

STUDY AREA DESCRIPTION

Topography

Roşia Montană is located in south part of Apuseni Mountains, north of Meridional Carpathian Mountains and west of Transylvanian plateau. The area has a hilly character, with

valleys and peaks of altitude starting from 500 meters in west part of mining excavation area along Abrud and Arieş Valley to altitude of 1200 meters in east [2].

The Roşia Montană locality is situated on 81 kilometers NW from Alba Iulia Municipality, 50 kilometers NE from Brad town, 15 kilometers SE from Câmpeni town, 10 kilometers NE from Abrud town, 150 kilometers from Turda town and 135 kilometers from Cluj-Napoca city. The villages included in Roşia Montană locality are: Dăroaia, Coasta Henții, Curături, Gura-Roşia, Cărpiniş, Soal, Vîrtop, Gîrda-Bărbuleşti, Iacobeşti, Bălmoşeşti, Țarina, Blideşti, Corna, Bunta and Roşia Montană [1].

The surface water courses are radiating from the highest peaks, located on east side of mining excavation, and flows to west and north in Abrud and Arieş Rivers. The village of Roşia Montană is divided in two parts by the river Roşia flowing to west and collecting all drained waters from peaks situated from east to west. The southern line of peaks is washed by rivers collected in Săliştei and Corna Valleys [3].

The lowest altitude is Roşia Valley, 577 m, and the highest, peak Curmătura, 1256 m. This variation of altitude and hardness of the rocks was favorable for erosion and an interesting relief appeared, the material eroded being transported and stored into the Abrud and Arieş Valleys.

The relief characteristics are determined by the diversity of geological forms present in the area. Volcanic relief is predominant with wide plateaus of andesite lava in North, South and East. Sedimentary formation has generated relief forms as hills, with smooth or abrupt braes, especially in areas close to valleys or rivers [2].

The crests from the mining area are rounded in profile with rock forms occasionally. The fields are suitable for pasturage.

Climate

The area climate is classified as temperate continental climate with powerful topographic influences. The winters are cold with snows and lasting between 4 to 6 months. The rainfalls are recorded with a maximum during summer time. Annual average temperature is 6 – 8 $^{\circ}$C, and average temperature of extreme months are -4 $^{\circ}$C (January) and +15 $^{\circ}$C (July). This lower temperature is delaying the vegetation development with 2 – 4 weeks comparing with planes from inferior Arieş Valley and from Mureş Valley. Average depth of frost is 0.5 to 1.0 m [1].

Relative humidity of the air is approximately 77 % for the entire period of time, with maximum of humidity recorded in September 1988, 93 %. During one year the lowest relative humidity was recorded in August (average of 72 %) and highest in December (84 %).

The distribution of nebulosity, related to relative humidity, recorded high levels in December and low levels in August.

The highest levels of precipitations are recorded in June – July and the lowest in February – March. An exception was observed for August 1989 with a maximum of 203.5 mm recorded. A relative interchange of humid period with dry period during the year was observed. The snow covers totally the ground from October to March, sometimes (few exceptions – during the cold winters) to April. The period with most abundant snows is January-February. Annual average precipitations are between 800 and 1000 mm/year.

Wind parameters recorded on 6 m high from the ground are: multi-annual average frequency on 8 directions (FMM in %) and monthly averages of wind speed (m/s). Reported

at a 10 years period the dominant multi-annual average frequencies are from SW – main direction, NE and W. Approximately direction SW-NE of the Roşia Valley is determinant for wind main direction. The calmest periods are February, June and September. The average wind speed for 10 years period is between 2.3 and 4.2 m/s, on SW dominant direction, but also from W, E and NE [4].

Geology

The petrographyc studies revealed that the host rock in the mining area is a porphyritic felsic volcanic formed of phenocrysts of feldspar, hornblende, biotite and quartz found in a finer grained volcanic matrix. A strong alternation was recorded that impiede to determine the K-feldspar to plagioclase ratio however at least some of the primary feldspars were K-feldspar; the host is therefore either a dacite or a rhyolite.

For other lithologies present a section of hydrothermal breccias with clasts of the felsic volcanic, a sandstone, and in some cases fragments of earlier adularia veining were observed.

The mineral relationship shows an evolutioning sequence for this hydrothermal system. Alteration and deposition in samples from that zone was intense [5].

Stage I alteration and deposition: Adularia ± quartz ± rutile ± sulphides, mostly pyrite. The wallrock alteration is as follows: feldspars → adularia, groundmass → quartz + adularia, and mafics → sulphides, rutile and quartz. Deposition of these phases conducted to adularia – quartz stockwork zones, deposited banded quartz – adularia – pyrite veines in fractures, and locally generated hydrothermal breccias with comminuted altered wallrock fragments re-cemented in a matrix of microcrystalline quartz, adularia and sulphides (pyrite >> chalcopyrite) [6].

Stage II alteration and deposition: stage I minerals are altered to illite, illitic clays, quartz and sulphides. Fractures assigned to this event are filled by illite – quartz - sulphides. This fracturing created stockworks of veins, sheeted zones of microfractures. At this stage, hydrothermal breccias with illite altered clasts of the wallrock volcanic and sediments typically set in a matrix of microcrystalline to chalcedonic quartz with minor illite/illitic clay and sulphides were created. Also the open spaces in stage I veins were filled by stage II minerals. Post brecciation fractures were filled in by quartz – illite and sulphides. Late in stage II a generation of Iron– carbonates that hosts base metal sulphides, silver sulphosalts and locally gold also occurs. Pyrite is the earliest sulphide associated with the illite. This is overgrown later by pale sphalerites, chalcopyrite, galena, and silver phases, including freibergite > polybasite-pearcite > argentite and possible argento-pyrite. Stage II is the main mineralization event and it is associated with illite and/or carbonates in veins, but more commonly fills in open spaces in earlier veins and veinlets. Gold is coarse and free as overgrowths of older quartz, is included within carbonates, or is bound as inclusions in, or intergrowths with, silver phases. Gold is also rarely included in late pyrite, and is suspected to be present in submicroscopic inclusions in argento-pyrite or, arsean – pyrite.

Stage III alteration and deposition: smectite – kaolinite → limonites – jarosite – chalcocite and covellite. This is the latest overprint. The lack of crystallinity of the phases conducts to the ideea that could be supergene in origin. The possibility that some of the smectite and kaolinite might be late hypogene related to the collapse and steam-dominated stage of decay cannot be ruled out. At least one gold grain observed was of supergene origin

associated with limonites at the site of a former pyrite grain. This confirms that at least locally, the deposit is supergene enriched [6].

According with the alteration and mineralization sequence describe above, it is likely that the system was a high level low sulphidation epithermal system exposed at the upper middle reservoir levels. Stage I probably occurred when temperatures were around 250-260^{o} C from fluids that were dilute brines traveling in a host rock with high vertical permeability by virtue of its fracturing, and high lateral permeability along the margins of the flows. Local boiling occurred and created local hydrothermal breccias.

The cooling of the fluid and mixing with local groundwaters represents Stage II. This cooling/mixing created a weak acid fluid at around 220-240 $^{\circ}$C and which was out of equilibrium with the Stage I alteration. The result was overprinting and replacement of Stage I minerals by illites and quartz. Continued cooling and mixing with condensate fluids during drawdown of the system was the probable mechanism of base metals silver and gold deposition. The presence of hydrothermal breccias reflected that there must have been local boiling as the system self-sealed during the decay cycle. It is possible that this boiling generated the late stage adularia founded in some areas [6].

The gold and silver deposition occurred towards the end of this decay cycle, as the petrographic work has shown and that the main mineralizing event was late during the decay cycle of the system. The gold is free and coarse as well as finer grained and bound within other sulphides. The paragenetic situation of the gold corroborates observation that better gold grades were found in quartz-carbonate zones and why gold grades were higher in zones where the quartz was observed to be microcrystalline and was associated with clays.

Hydrogeology and Hydrology

Arieş River is the most important water source of Apuseni Mountains, with ¾ of its total effluents formed in the mining area of Roşia Montană. This river, 164 km long, is the principal affluent of Mureş River. The climate characteristic for mountain area, with rich precipitation level and moderate temperatures sustains the stable hydrological conditions.

Artificial lakes are numerous in Roşia Montană area. Long time mining excavations determined that water courses in Roşia Montană to became inferior category waters due to sterile rock, discharges from industrial activities, farms and homes. Water pollution can be trace back to medieval times, according with historical records [7].

Abrud River is the most important affluent from right of Arieş River. Abrud tributaries are: Selişte a River, Corna River, Roşia River, Vâtop River. Multi-annual average debit, upstream of Abrud town is 1.47 m^3/s and downstream 2.10 m^3/s. Along the valley small area of depression can be observed, especially on confluence with affluents, where alluviums are formed. Roşia or Foaieş River starts at Tarina tarn, Big tarn and Brazi tarn and along the valley collects mine waters that gives him an yellow-red color due to the iron oxides. The minimum debit recorded for Roşia is 10 L/m and the maximum debit is 300 L/m, with a pH between 3 and 4. The valleys are narrow with abrupt banks. The debit is not constant and some valleys are complete dry during summer [7].

In Roşia Montană area the phreatic water systems are characterized by artificial channels or paths from 2000 years old, varying permeability but generally low compared with

geological complex and flowing direction of phreatic water from east to west with a local distortion due to mining activity.

This water is originating from rain waters and can percolate few hundreds of meters through unsaturated layers to reach the phreatic surface estimated to be on 680 meters above sea level, in Roşia Montană paleo-volcanic complex. There is on horizontal component with an average debit of 30 L/s evacuated from Roman gallery situated at 850 m above sea level on north part of Roşia Montană and another one with an average debit of 7 L/s from 714 gallery on Roşia Montană entrance [5].

Two spring lines, radiating from Roşia Montană are characteristic for these valleys. Very frequently those are seasonal, with low debit and usually used to supply one home or for animal feeding.

HISTORY OF MINING IN ROSIA MONTANA AREA

Roşia Montană is the oldest mining settlement in Romania established by documents maintained, with historical value (about 1,870 years old). Wax tablets discovered in the galleries of Roşia Montană represent a great discovery and an important record about Roman Law. On tablet no. XVlll, dated February 6, 131 AD, appears the first mention of the name Alburnus Maior, the ancient name of Roşia Montană as the place where first the Dacians and later the Romans extracted gold. The Roman emperor conquered Dacia in 106 AD for the riches of those mountains. The mining works in Roşia Montană are older than the Rome building according with ^{14}C analysis performed by German mining museum in Bochum.

After conquer of Dacia, the financial situation of Roman Empire was solved. The emperor start building numerous edifices as the Columnar being the most important roman art monument finished in 113, water pipe – Traiana Aqua. Ancient historian mentions incredible sums to describe the riches obtained from Dacia. Ioannes Lydus, a writer from VI century, that used the missing book of Traian physician (Criton), was corrected by the French historian J. Carcopino and the quantities are still impressive: 165.000 kilograms of gold and 331.000 kilograms of silver. No archeological significant traces to prove the pre-roman mining activity were found but it is likely that the gold was extracted before roman occupation because the Romans were aware of the gold and silver ores in the area. The mines were administrated by an Emperor's special assigned clerk and a developed managing system was in place. The mining administration was located in Zlatna (Ampelum – the roman name) but the center of mining extraction was in Alburnus Maior, were a mining village was developed. The date when the Romans stopped the gold extraction is uncertain [8].

In 1786 – 1855 periods, 25 wooden plates covered with wax and containing writing in cursive Latin were found here. The plates represents selling- buying contracts, the "bill" for some services, loan, prices and spending list, groceries list for a party.

The mining methods were the same used in other parts of Roman world. The easiest way to extract the gold was to crash in iron or stone vessels the gravel with gold, milling it with mill stones rotated by slaves, animals or water and then washing it on inclined wooden boards with small ditches were gold veins stopped. After this the sieving was the next operation and melting in clay pots. Another method was to obtain pits were after the rock has heated water or vinegar was poured and the stone cracked. After this the stones were washed and sieved.

The best method was to form horizontal galleries sustained by wood pillars that after the hill was penetrate were removed and the galleries fowled down one at the time [8].

The arheological descoveries in Roşia Montană mining area are very important and should be protected. One of these is an ancient mausoleum, a double circular grave monument that was discovered in the Hop – Gauri area of Roşia Montană. The monument dates back to Roman Empiere ocupation in Dacia times. It is unique discovered in Romania and so well preserved. The mausoleam was preserved on-site through a special program but his state in the futre could be unclear because the mausoleum is located between a sterile dump and an open pitand a future mining project could provoqe damage to this monument preserved in the area.

Another discovery is a hydraulic wheel found at the start of the 20th century in the Păru-Carpeni area of Roşia Montană that was used to drain water from the underground antique. In the area the Roman galleries can be visited.

RESULTS AND DISCUSION

Understanding the sources, interactions and effects of pollution it is essential for controlling pollutants in a safe environment. Very small quantities or traces of metal ions are required for normal growth and metabolism, for example, copper, iron, nickel, and zinc. Metal ions produce physiological poisoning by becoming attached or adsorbed on the cellular enzymes, causing inhibition of enzymatic control of respiration, photosynthesis and growth [9]. Heavy metals can be very harmful for an ecosystem. One of the most significant problems is that heavy metals are more dangerous than organic compounds, because there are not biodegradable and have a cumulative effect.

Heavy metals present in the waste from mining and metallurgical activities are often dispersed in environment by wind and water. The extent and degree of heavy metals contamination in the vicinity of mines may vary depending of geochemical characteristics, the mineralization of tailings, physical-chemical conditions and the process used to extract metals. Pollutant cadmium in water may arise from industrial discharges and mining wastes [10].

Cadmium is very similar with zinc, and these two metals frequently are present in some ores together. The effects of acute cadmium poisoning in humans are very serious, high blood pressure, kidney damage, and damage of red blood cells. Some physiological action of cadmium is due to its chemical similarity to zinc and may replace zinc in some enzymes, producing a disturbance of enzyme stereostructure and impairing its catalytic activity [11]. Inorganic lead can be present in environmental samples due to industrial and mining sources, and also due to gasoline which is a major source of atmospheric and terrestrial lead. Acute lead poisoning in humans may cause severe dysfunction of the kidney, reproductive system, liver, brain, and central nervous system leading to sickness or death. Lead poisoning from environmental exposure is thought to have caused mental retard for many children [12].

The most important step in environmental analysis is the sampling, because the sample can be modified or destroyed due to non-correct sampling systems, loss of sample compounds, contamination and sample decomposition.

Usually, it is necessary that the time between sample collection and analysis, to be as short as possible. In some cases the analysis must be performed in few minutes after sample collection. Others, such as the determination of temperature, must be done on the body of water itself. Within a few minutes after collection, water pH may change, dissolved gases (oxygen, carbon dioxide, hydrogen sulfide, chlorine) may be lost, or other gases (oxygen, carbon dioxide) may be absorbed from the atmosphere, also oxidation-reduction reactions may cause substantial errors in analysis [9].

This chapter presents results obtained in a research theme divided in two areas of interest. First part of the study performed in Roşia Montană mining area is concentrated on establishing the status of surface natural waters impacted by mining excavation and processing activities. The second part presents data about the accumulation of gold and other toxic metals (copper, zinc) by horsetail (Equisetum arvense) in comparison with milfoil (Achillea millefolium) collected from the same mining and ore processing area.

The stream studied is 20 km long with a variable width of 50–500 cm. Twelve water samples were collected in the view to determine the heavy metals concentration, four from the Corna River, five from Roşia River, and three from the Abrud River (Picture 1).

The samples were collected in polypropylene containers. The waters were filtered and refrigerated before analysis, which was made within 24 h after collection. The research was based on field work consisting of visual observation of the area, informal interviews, measurements of the distance between the samples sites, and sample collection [13, 14].

Usually the total metal load in rivers from mining areas is transported included in particulate phase, depending on chemical and physical characteristics of the environment and on metal behavior against geochemical conditions of the area under discussion. An exception can be admitted for rivers affected by acid mine drainage where the most important fraction of the metal load is discharged from the mine sites in solution or in association with colloids. The waters in Roşia Montană have an acid character (pH average value of 3 – 4) and Acid Rock Drainage (ARD) occurred due to high content of sulphide minerals in the area. The metals determined on water samples collected from the area represents only the metal load in solution, considered to be representative to describe the status of surface waters.

Modern analytical techniques as inductively coupled plasma atomic emission spectrometry (ICP-AES) and graphite furnace - atomic absorption spectrometry (GFAAS) were used to determine the concentration of heavy metals from Roşia Montană ecosystem. Heavy metals from water samples were determined by inductively coupled plasma atomic emission spectrometry (ICP-AES). The instrument used, a SPECTROFLAME-P (SPECTROAnalytical Instruments, Germany), has the following characteristics: argon was of spectral purity (99.998%), cooling flow rate 12 L min^{-1}, auxiliary flow rate 0.8 L min^{-1}, nebulizer flow rate 1 L min^{-1}, and consumption rate of the liquid sample was about 2 mL min^{-1}.

The instrument has 30 fixed spectral channels that can simultaneously be monitored by the three polychromators and allows for background correction, application of internal standard method and other facilities [15, 16].

Picture 1. Map of the collection sites.

The rivers considered in this chapter are Corna River, Roşia River and Abrud River. Corna River and Roşia River are flowing into the Abrud River.

Four samples were collected from the Corna River: sample1 - Corna spring, sample 2 - Corna (village), sample 3 - Bunta (small village), and sample 4 - Gura Cornei (before Corna River flows into Abrud River). The mining processing waters flow in Roşia Montană River. Five samples were collected from this river: sample 7 - Roşia Montană spring, sample 8 - Roşia Montană (small stream in the open pit area), sample 9 - Blideşti (small village, with submerged old mining machines), sample 10 - Ignăteşti (one of the rock processing areas), and sample 11 - Iacobeşti (before Roşia Montană River flows into Abrud River).

Waters of another mining area, Zlatna, where processing of copper continues, flow in Abrud River, before Corna River. The distance between Zlatna and Corna River confluence is about 40 km. From the Abrud River three samples were collected: sample 5 - Abrud (small town, downstream the Corna River confluence), sample 6 - Abrud exit, and sample 12 - Gura Roşiei (downstream of Roşia Montană River confluence).

The sample site data and samples visual characterization are presented in table 1. The visual aspect was maintained for every sample during the period under discussion.

Table 2 presents the concentrations for each sample site in May 2005. Increased concentrations of metal ions are observed for samples 1, 5, 8, 9, 10 and 11. For sample 5, in Abrud town, the concentration can be explained by domestic waste waters that are discharged into Abrud River and other waste materials deposited on the river bed. As mentioned earlier, samples 8, 9, 10 and 11 were collected from the area where intense mining activity has

developed along the river course. Presently, the mining activity was reduced, but the solid rock (waste) deposited by the river side remained the main pollution source.

Table 1. The water characteristics at the sampling sites

Sample	Sample name - description	River bed width (m)	Depth in the sampling point (m)	Appearance
1	Corna spring	0.50	0.30	Dark-red with suspensions
2	Corna	2.00	0.75	Clear, light-red
3	Bunta	1.50	0.80	Water with a good clearance
4	Gura Cornei	3.00	0.45	Muddy, contains alluvium
5	Abrud city	12.00	1.00	Muddy with suspensions, a lot of domestic wastes deposited near the bank
6	Abrud	11.50	1.00	Muddy with suspensions
7	Roşia Spring	1.00	0.30	Light-red, few suspensions
8	Roşia Montană	2.50	0.45	Rust colored, with suspensions
9	Blindeşti	2.00	0.50	Rust colored, a little muddy
10	Ignăteşti	2.50	0.40	After collection point some equipments in water
11	Gura Roşiei	2.00	0.40	Light-red
12	Gura Roşiei (the last part)	9.00	0.90	Muddy, alluvium matter
13	Drinking water	underground spring	-	Clear

Table 2. Experimental data from samples collected in may 2005 [17]

Element	Cd	Cu	Mn	Pb	Zn
Sample	*mg/L*	*mg/L*	*mg/L*	*mg/L*	*mg/L*
1	0.110	0.080	320.700	0.540	18.590
2	< LOD	< LOD	17.460	0.010	0.730
3	0.010	0.010	4.980	0.010	< LOD
4	0.010	< LOD	3.640	0.010	< LOD
5	0.010	< LOD	0.900	0.010	0.040
6	0.010	< LOD	0.500	0.010	0.010
7	0.010	0.030	1.740	0.030	0.080
8	0.010	0.210	9.310	0.020	1.310
9	0.030	0.570	34.560	0.060	5.710
10	0.050	0.490	30.350	0.060	5.420
11	0.030	0.380	22.890	0.010	3.940
12	0.020	< LOD	2.800	0.020	0.160
Drinking water	0.004	0.001	0.024	0.007	0.001

LOD-limit of detection.

In May 2005, a sample of drinking water from the mining area was also collected. The water flows from an underground spring, but the concentrations of heavy metals indicate that the spring washes some ore deposits. In table 3 the data imposed by the National Standard Committee of Romania are compared with the experimental data obtained in this study (STAS 4706 – 88) [18]. The potable water sample is compared also to standard imposed values for surface waters category.

Table 3. Metal concentration in surface waters: reference and determined data

Elements	SR mg/L	Drinking water	Experimental data mg/L					
			maximum			minimum		
			November 2004	*February 2005*	*May 2005*	*November 2004*	*February 2005*	*May 2005*
Cadmium	0.003	0.004	0.150	0.170	0.110	<LOD	<LOD	<LOD
Copper	0.005	<LOD	1.330	1.350	0.570	<LOD	<LOD	<LOD
Lead	0.050	0.007	0.250	0.230	0.540	0.010	0.010	0.010
Manganese	0.300	0.024	141.200	223.200	320.700	0.110	0.080	0.500
Zinc	0.030	0.001	8.750	15.550	18.590	0.010	0.010	0.010

SR-Romanian Standard, LOD-Limit of Detection.

By comparing those data it is possible to have an idea about the pollution degree at a local level. It can be observed that in some location sites the concentration of these heavy metals were very high. The samples in which the concentrations are very high were collected from Roşia River, where the area was intensely affected by mining activity. As a result of this research the actual situation of the most important rivers from Roşia Montană area can be established.

Variation of heavy metals concentration in environment departments depends on climatic conditions (temperature, precipitation, wind, etc.), pH, some interactions and reactions between these heavy metals and another compounds present in the environment. For example, between the concentration of cadmium from a river water and the concentration of the same element in sediments is established an equilibrium due to temperature, evaporation, and flow characteristics [19, 20].

pH has an important role concerning the presence/absence of some metal ions such aluminum, iron, cadmium, zinc and lead and the decreasing of pH produce disappearance of some species (i.e. fish species) or appearance of new mutagenic species. The concentration of cadmium, zinc and lead in waters can be high due to increasing of acidity and if these ions are present in soluble state become very dangerous for organisms. Lead and cadmium can displace calcium from bones and these become brittle; lead, cadmium and chromium can be concentrate in the liver and kidneys and cause malfunctioning of these organs. The nervous system is attacked even by the smallest concentration of lead and copper and the effects vary from brain damage to damage of the peripheral nerves causing problems of muscular coordination and poor eyesight [17].

Specific toxic effects in human vary according to the ion type, multi–ion combinations, tissue concentrations, the frequency of dosage, and the age of each persons. The water samples were collected during one year with approximately 2 months frequency, between April 2004 and May 2005.

To measure how well the data obtained follow a particular distribution it was used the Anderson-Darling statistic (figures 1-5). This was applied only for metals concentration determined in sample collection site number 10 – Ignăteşti, located after mine excavation and primary processing of ores area. For this statistic, the better the distribution fits the data, the smaller this statistic will be. This statistic can help to test whether a sample of data comes from a population with a specified distribution. The determinations were performed using Minitab 15 application. Information obtained is: the data follow or not a specified distribution.

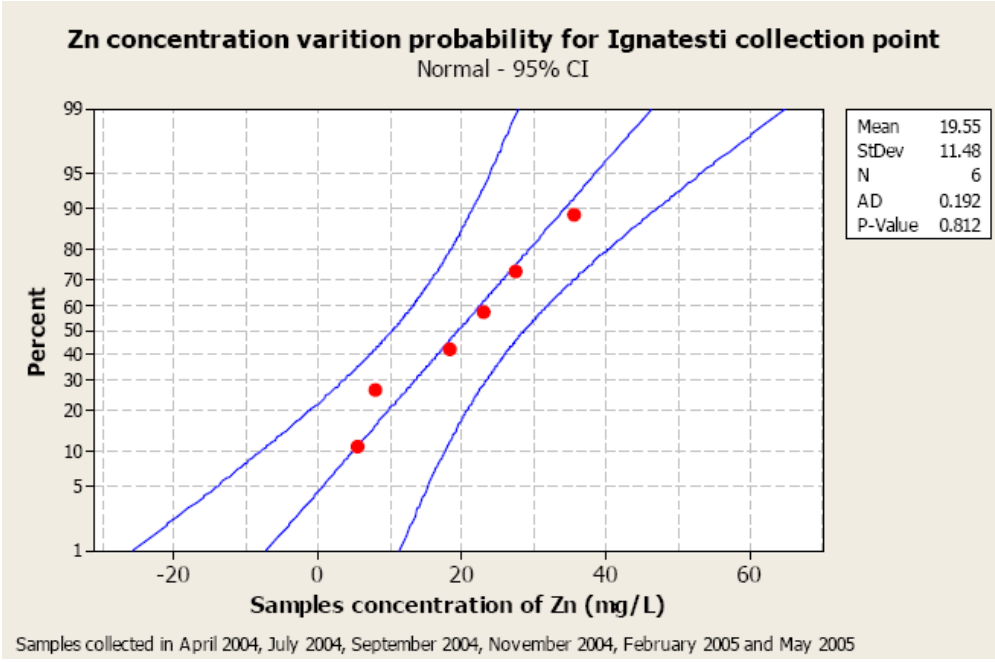

Figure 1. The probability of Zn concentration variation in Ignăteşti collection point (sample No. 10 – close to processing area).

N represents the number of samples considered. If the p-value (when available) for the Anderson-Darling test is lower than the chosen significance level (usually 0.05 or 0.10), conclude that the data do not follow the specified distribution. Minitab also displays approximate 95% confidence intervals (curved blue lines) for the fitted distribution. These confidence intervals are point-wise, meaning that they are calculated separately for each point on the fitted distribution without controlling for family-wise error. Usually, points outside the confidence intervals occur in the tails. In the lower half of the plot, points to the right of the confidence band indicate that there are fewer data in the left tail than one would expect based on the fitted distribution.

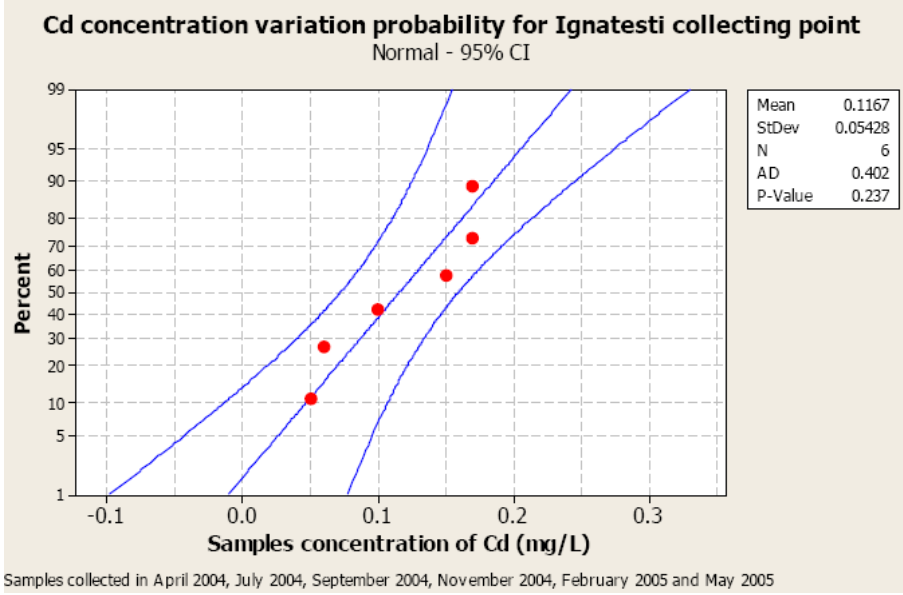

Figure 2. The probability of Cd concentration variation in Ignăteşti collection point (sample No. 10 – close to processing area).

Ignăteşti collection point is situated on Roşia River. The water from Roşia River has a yellow-orange color and an acid pH, and the most important source of pollution consists in mine waters, which are discharged into this river, increasing the concentration of cadmium and lead.

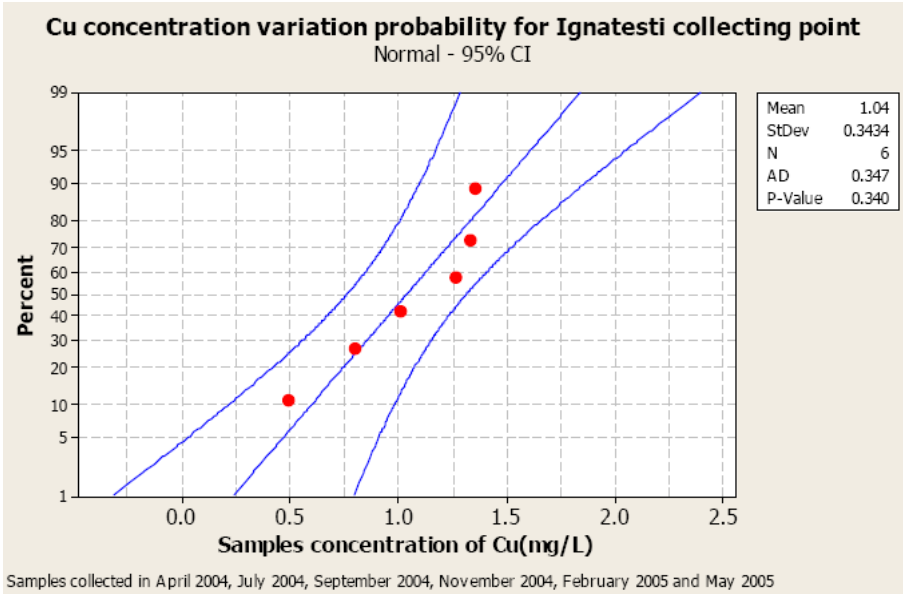

Figure 3. The probability of Cu concentration variation in Ignăteşti collection point (sample No. 10 – close to processing area).

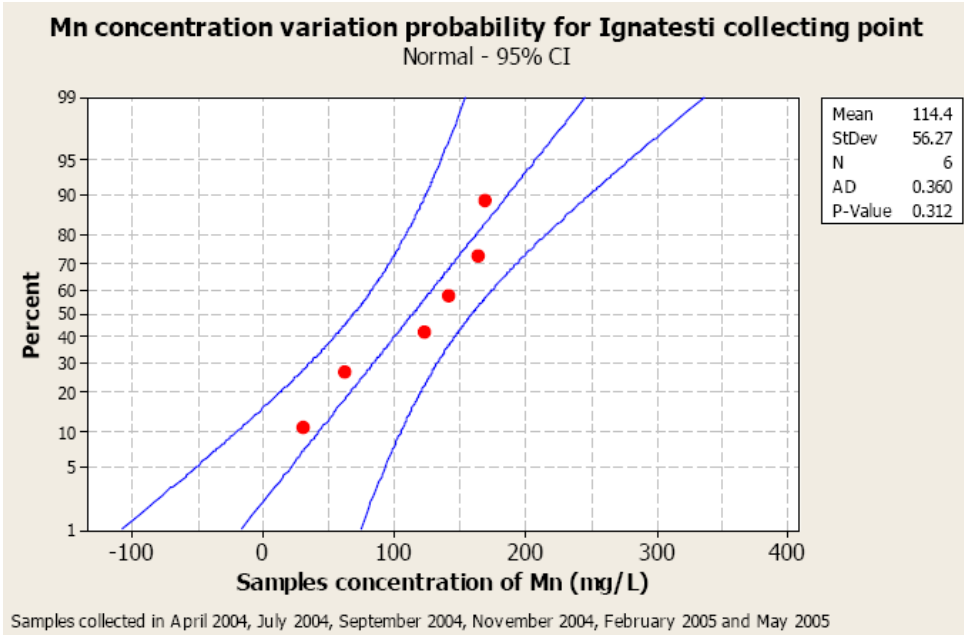

Figure 4. The probability of Mn concentration variation in Ignăteşti collection point (sample No. 10 – close to processing area).

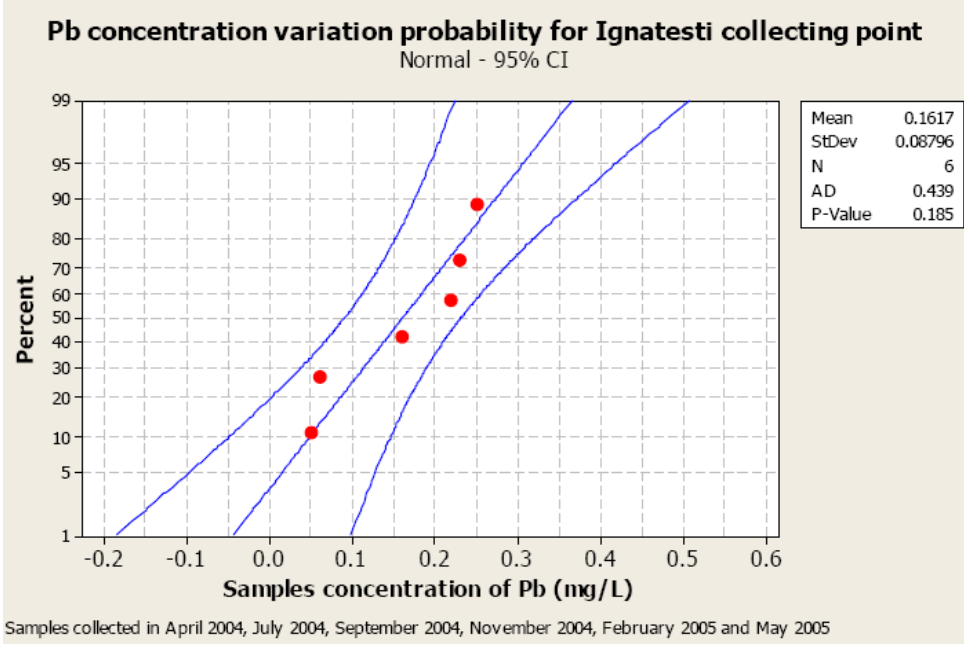

Figure 5. The probability of Pb concentration variation in Ignăteşti collection point (sample No. 10 – close to processing area).

The Abrud River is the most important collector of the surface water from mining site Bucium and Roşia Montană. The pH of these waters is weakly acid, and the concentration of

heavy metals is higher than maximum admitted concentration. The variation pattern does not describe a linear decreasing of the concentration with distance from the main heavy metal source, due to geometry of the river bed and possible to high concentration of Fe and Mn found in water samples. Fe and Mn could be involved in metal retention by sequestration in oxyhydroxides [21].

The mining activity from the past in the Roşia Montană ecosystem had as result the contamination with heavy metals, which are soluble due to water acidity (as a result between sulphides and environmental conditions).

The type of drainage, metal and sulphides rich discharged from tailing areas can continue for decade after mining closure.

River tailings deposition consist on mine waste and tailings materials which are transported from a mining district and deposited by natural process at a variable distance from the origin.

The contaminants can be introduced in the ecosystem by different human activities, such as waste disposal, storage and transportation of commercial materials, mining activities, agricultural operations, and other activities. The evolution in time of heavy metal concentrations were plotted for 3 sample collection sites: Ignăteşti, Blideşti and Roşia Montană (figures 6-10).

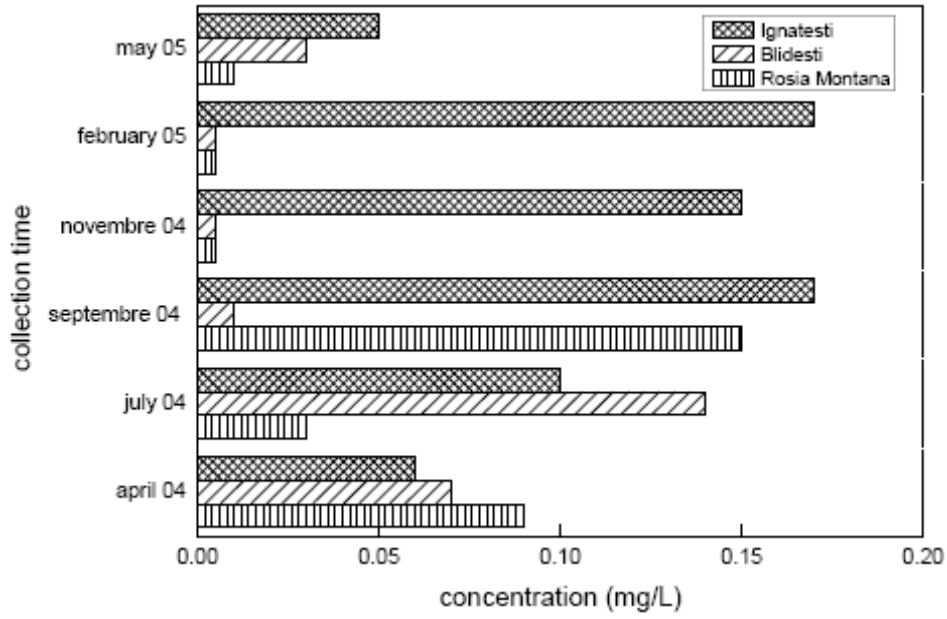

Figure 6. Variation of cadmium concetration for one year on Roşia River.

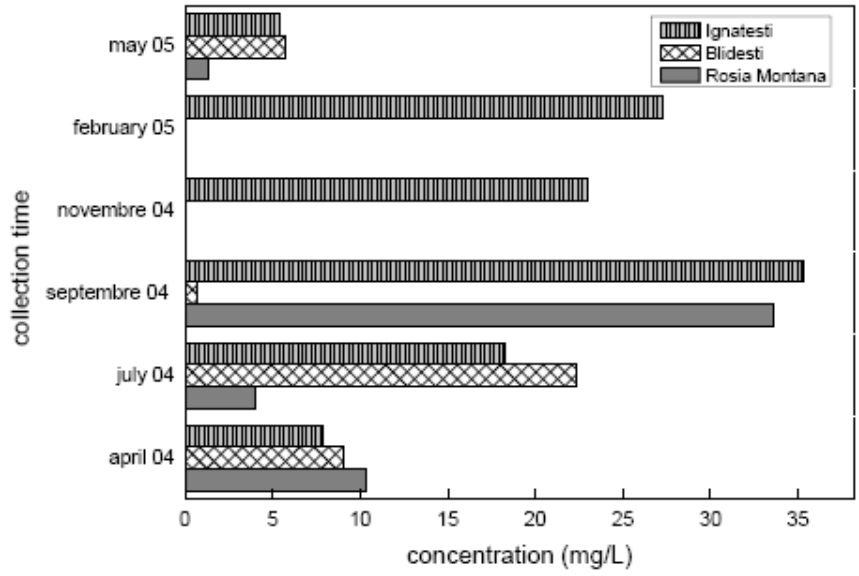

Figure 7. Variation of zinc concentration for one year on Roşia River.

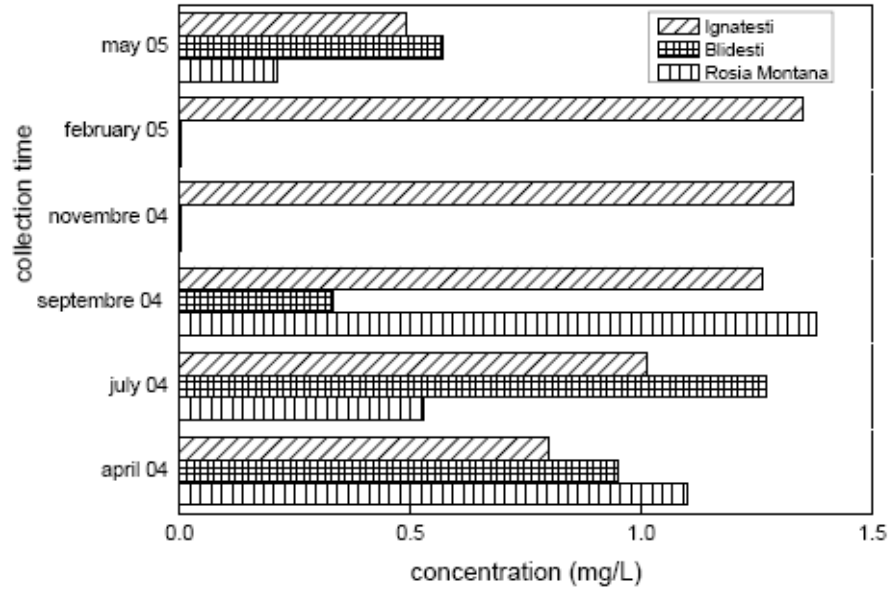

Figure 8. Variation of copper concentration for one year on Roşia River.

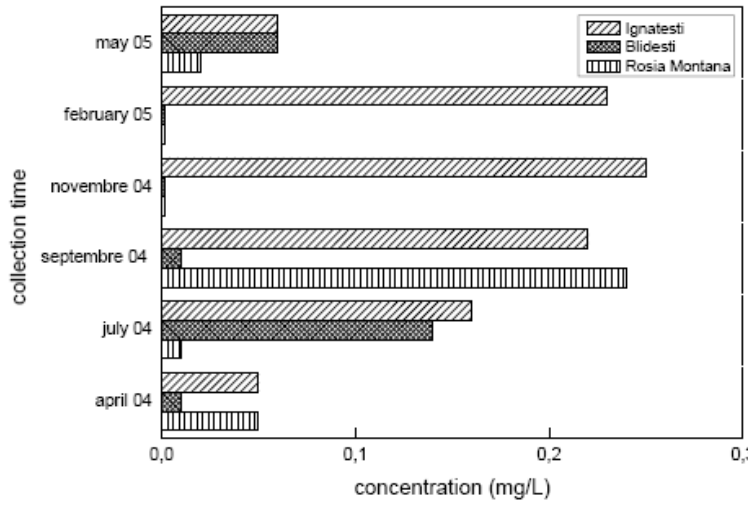

Figure 9. Variation of lead concentration for one year on Roşia River.

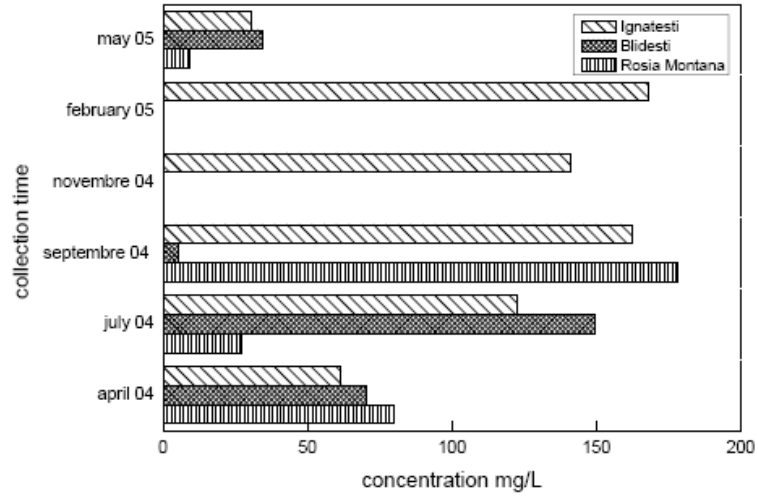

Figure 10. Variation of manganese concentration for one year on Roşia River.

Rainwater, particularly acid rain, overexposed surface mines, and mine tailings produce highly mineralized runoff frequently referred to as *acid mine drainage.* This runoff can percolate into the ground and degrade the quality of groundwater. In addition, water seepage through underground mines can leach toxic metals from exposed ores and raw materials and introduce them to groundwater. Oxidation and leaching connected with coal mining produce high iron and sulfate concentrations and low pH in groundwater [22]. Loading from tailings and waste rock areas depends on the mineralogy of the extracted ore. The metal content of the drainage water strongly depends on pH, which control the solubility and the mobility of metal ions. Copper is in general strongly bound to mineral surfaces for a wide pH range, while zinc is more mobile in natural waters, especially in acid environments [23, 24].

To be able to observe the variation of cadmium, copper, lead, manganese and zinc concentrations over one year, the concentration of these elements from April 2004 were plotted as a function of the concentration for the same elements from May 2005 (figures 11-15).

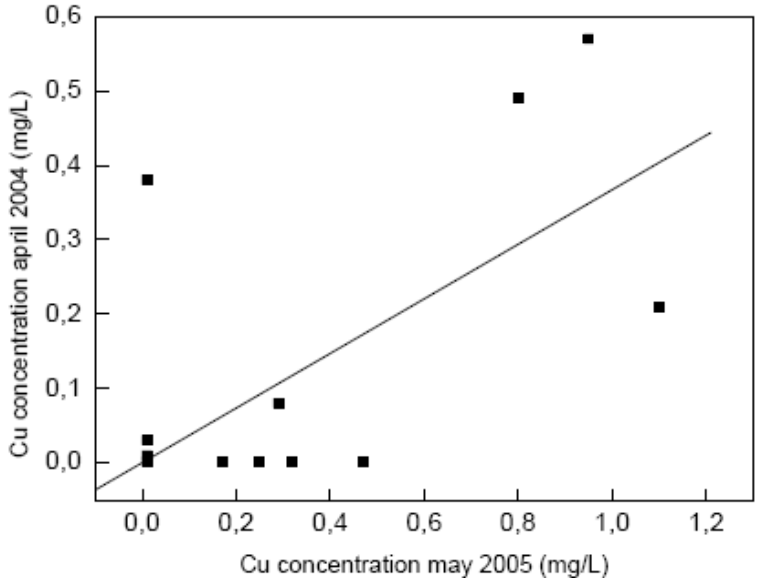

Figure 11. Copper concentration variation during April 2004 versus May 2005.

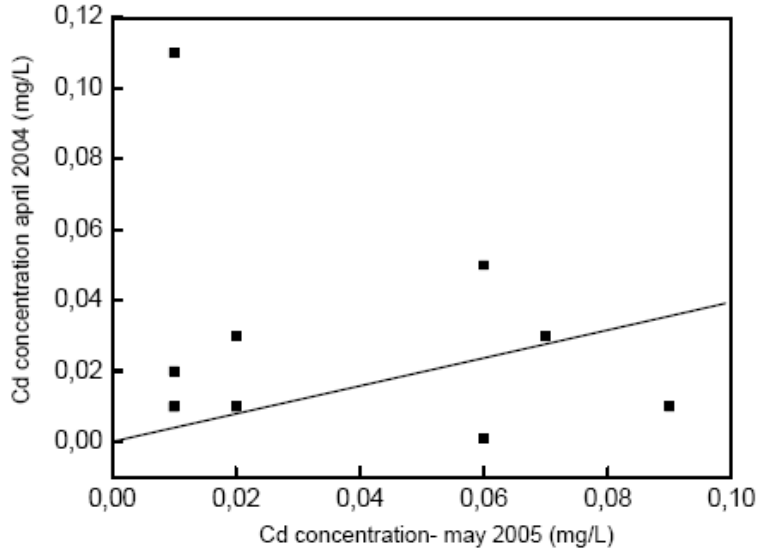

Figure 12. Cadmium concentration variation during April 2004 versus May 2005.

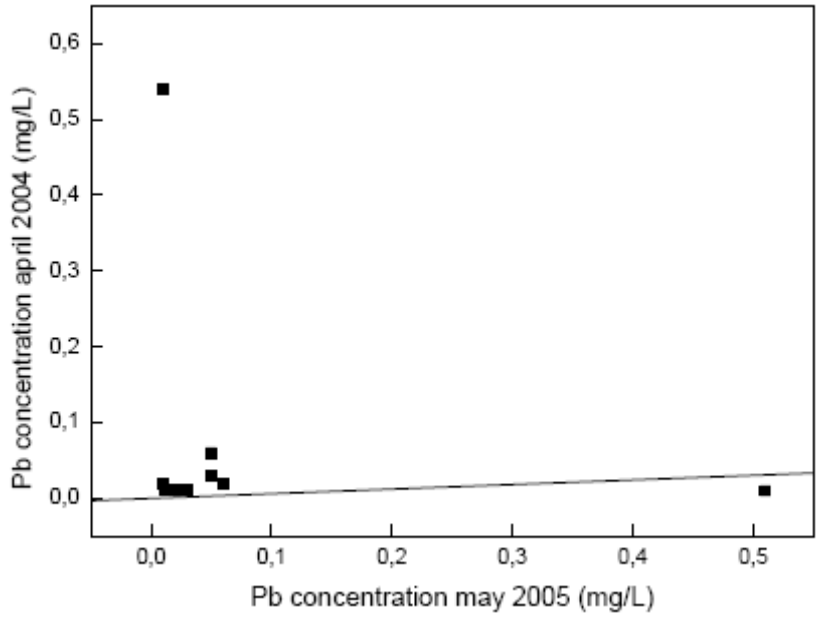

Figure 13. Lead concentration variation during April 2004 versus May 2005.

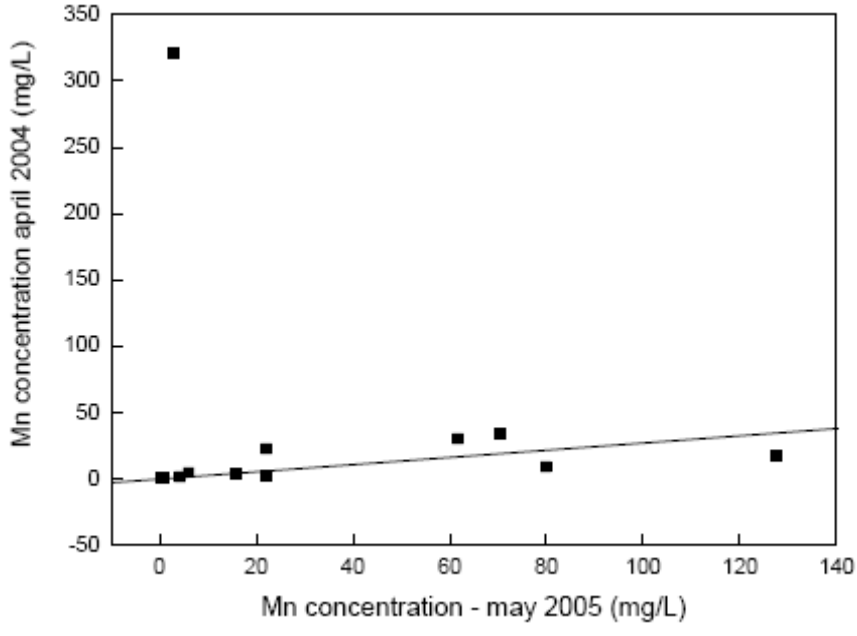

Figure 14. Manganese concentration variation during April 2004 versus May 2005

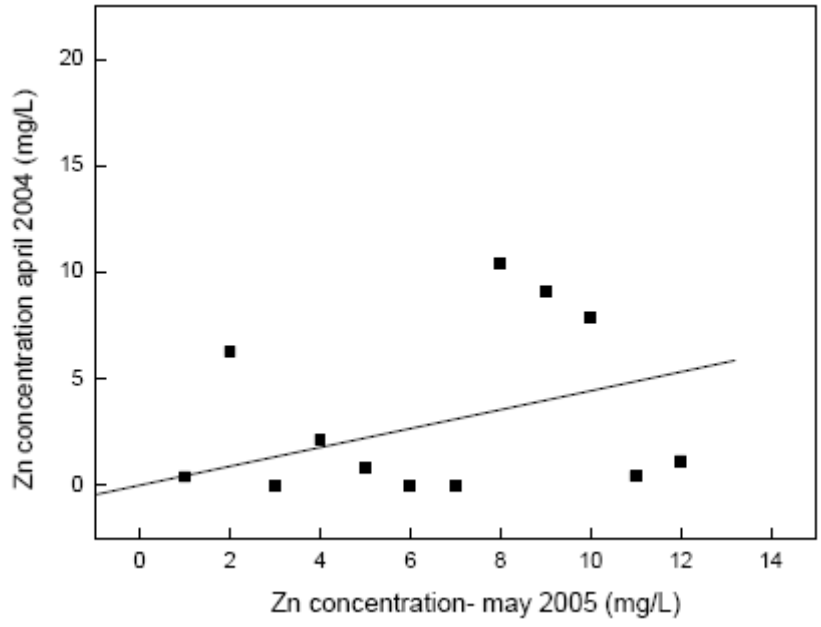

Figure 15. Zinc concentration variation during April 2004 versus May 2005.

From these figures on can observe that only for copper the concentrations decrease after one year for the most of the collected samples. In the case of lead, cadmium and manganese the concentrations do not decrease after one year (exception only for one or two collection sites). For zinc it was observed that for approximately 50% of location sites the concentrations decrease after one year.

One of the most important environmental problems is represented by side-products of mineral refining consisting in waste *tailings.* By the nature of the mineral processing operations employed, tailings are usually finely divided and then subjected to chemical weathering processes. Heavy metals associated with metal ores can be leached from tailings, producing water runoff contaminated with cadmium, lead, and other pollutants. Large quantities of cyanide solution can be used to extract low levels of gold from ore, producing obvious toxicological hazards.

Environmental problems resulting from exploitation of extractive resources - including disturbance of land, air pollution from dust and smelter emissions, and water pollution from disrupted aquifers are aggravated by the fact that the general trend in mining involves utilization of less rich ore. In both cases, past or present mining activities represent a current source of pollution for atmosphere, geosphere and hydrosphere within an ecosystem [25, 26]. The extent and degree of heavy metal contamination around mines may vary depending on geochemical characteristics, the mineralization of tailing, physical-chemical conditions and the processes used to extract metals [22]. The pollution with heavy metals represents an important risk for human health and environment. The most important is the form in which a metal exists in environment; it can be transformed from one form into another or it can exist in different form simultaneously. If it is known the speciation of metals it is possible to predict the possible forms in which it can be retained in soil, sediment, water or plants.

The gold concentration in ores of Roşia Montană is diminished and a new extraction project involves more efficient method for this low concentration, meaning leaching processes based on cyanide properties. This method is very aggressive for environment and also an open pit extraction method will be required. Hundreds of square kilometers of forest will disappear.

Using two vegetal prospectors we aimed to emphasize the need for a more environmental friendly solution for gold extraction in this area, demonstrating that the plants in the area contains already important quantities of toxic metals, as an indicator of ecosystem status.

The plants selected were horsetail (*Equisetum arvense*) and milfoil (*Achillea millefolium*). Nine samples were collected and analyzed for gold and other associated metals close to Corna River and Abrud River surface water courses that are the main water courses in the area collecting an important part of industrial waters, pluvial waters and mine residual waters [27, 28]. Also for a comparative study other two samples of commercial horsetail, with known origin were analyzed (plants collected from Bucharest area, 600 km to Roşia Montană– one sample, and plants collected from Ramnicu Valcea area, 450 km to Roşia Montană).

The samples were collected, for horsetail in April and September 2006 and for milfoil in September 2006 (table 4). The plants, commercial horsetail analyzed for comparison, were acquired in April 2006 having a known origin. The sample collection points were the same for both plants and the maximum distance between the species was of 45 cm. The plants collection points are: Corna spring (Picture 2), Bunta (small village), and Abrud exit (small town, down stream the Corna River confluence with Abrud River).

This study is based on the characterization of horsetail and milfoil samples from Roşia Montană, a gold mining area in Romania, by determining the gold and other metals concentrations in these species. The gold concentrations found were significant, but also high concentrations of toxic elements as copper and zinc were determined.

For plants the sample preparation was as following: the plants were cut off in small pieces and dehydrated at 101 ± 2 $^{\circ}$C, until constant mass. 0.5000 g/sample of dried plant were weighted in sterile containers. Open air digestion method was applied using nitric acid solution 65 % and hydrogen peroxide solution with thermo treatment. De-ionized water was added up to 10 mL. The solution was centrifuged and the elements of interest were determined by graphite furnace - atomic absorption spectrometry. The instrument used was a SPECTRAA 880 Varian (characteristics: double spot, wavelength 185 – 900 nm, background correction deuterium lamp for 185 – 425 nm for 2.5 abs.) with atomization furnace graphite tube GTA 100 Varian (40 – 3000 $^{\circ}$C, with one degree steps and automatic control of two working gases and cooling water). The maximum quantity of sample injected is of 100 μL, with 0.2 μL precision, using automatic sample dispenser PSD Varian. The nitrogen was generated in the laboratory using a Nitrox – Dominik Hunter generator of 99.999 % gas purity with a debit of 3 L/min [29]. The de-ionized water was obtained using Maxima USF Elga equipment, with a debit of 2 L/min and electrical resistance of 18.2 MΩ. All substances used are of spectrometric purity.

The mechanism of gold absorption is similar with the one for tellurium. High concentration of copper was also determined in samples collected from Roşia Montană and extremely higher for those acquired from the market. All samples were prepared and analyzed in the same working conditions [30]. The concentrations of zinc determined for both species are extremely high and caused by the extensive exploitation in the area. The ores mined in

Roşia Montană have important quantities of copper, zinc, manganese and lead, elements transferred in surface waters that act as transport ways from the source to surrounding areas up to 25 km [17].

The area Roşia Montană can be considered a polluted area with heavy metals, and the degree of pollution is reflected in the quantities accumulated in the plants collected from this area.

Picture 2. *Equisetum arvense* in Corna spring area, September 2006.

Table 4. Plant samples identification

SAMPLE	SAMPLE DESCRIPTION
1	*Equisetum arvense,* commerce, indicated origin: Bucharest
2	*Equisetum arvense,* commerce, indicated origin: Râmnicu Vâlcea
3	*Equisetum arvense*, collected from Roşia Montană area: Corna Spring, April 2006
4	*Equisetum arvense*, collected from Roşia Montană area: Bunta, April 2006
5	*Equisetum arvense*, collected from Roşia Montană area: Abrud exit, April 2006
6	*Equisetum arvense*, collected from Roşia Montană area: Corna Spring, September 2006
7	*Equisetum arvense*, collected from Roşia Montană area: Bunta, September 2006
8	*Equisetum arvense*, collected from Roşia Montană area: Abrud exit, September 2006
9	*Achillea millefolium,* collected from Roşia Montană area: Corna Spring, September 2006
10	*Achillea millefolium,* collected from Roşia Montană area: Bunta, September 2006
11	*Achillea millefolium,* collected from Roşia Montană area: Abrud exit, September 2006

Horsetail is widely distributed throughout the temperate climate zones of the northern hemisphere, including Asia, North America, and Europe. Horsetail is a unique plant with two distinctive types of stems. One variety of stem grows early in spring and looks like asparagus, except for its brown colour and the spore-containing cones on top. The mature form of the herb, appearing in summer, has branched, thin, green, sterile stems and looks very much like a feathery tail. Horsetail is the sole descendant of the giant fernlike plants that covered the earth some 200 million years ago. Horsetail is very rich in silica acid and silicates, which provides approximately 2-3% elemental silicon. Potassium, aluminium, and manganese along with fifteen different types of bioflavonoids are also found in the herb. The presence of these bioflavonoids is believed to cause the diuretic action, while the silicon content is said to exert a connective tissue-strengthening and anti-arthritic action. Some experts have suggested that the element silicon is a vital component for bone and cartilage formations. Horsetail can absorb gold dissolved in water better than most plants, up to 4 ounces per ton of fresh stalks [31].

Table 5. Determination of gold and other associated elements (g/tone of dried plant) in fertile stems of horsetail (*Equisetum arvense*) from Roşia Montană area and in two samples of horsetail purchased from the market

Sample	1		2		3		4		5	
		% RSD		*% RSD*		*% RSD*		*% RSD*		*% RSD*
Au	9.800	0.50	6.060	0.30	16.600	0.10	14.400	1.20	19.840	0.10
Li	0.050	9.90	1.020	3.20	0.760	9.10	1.240	5.80	0.820	7.40
Ag	0.140	4.50	0.110	8.70	0.420	9.20	0.220	3.20	0.110	0.00
Te	9.810	1.20	7.160	7.10	3.290	4.80	20.200	0.30	1.820	2.50
Cu	108.300	2.80	157.600	4.20	2.970	1.90	8.010	1.60	0.730	0.20
Cr	0.022	0.50	0.078	7.10	2.670	0.80	17.340	2.90	0.800	2.80

RSD-Relative Standard Deviation.

Table 6. Comparative study of gold, telur and zinc accumulation in sterile stems of horsetail (*Equisetum arvense*) and milfoil (*Achillea millefolium*) from Roşia Montană area

Sample	Au g/t (dried plant)	RSD %	Te g/t (dried plant)	RSD %	Zn g/t (dried plant)	RSD %
6	11.73	6.00	4.19	0.00	187.80	6.70
7	10.20	1.90	2.49	2.80	425.40	1.60
8	9.90	3.10	3.06	4.60	525.60	5.30
9	3.05	2.70	1.15	2.50	117.00	2.90
10	3.68	3.20	1.13	0.00	109.20	0.30
11	4.14	3.10	1.27	0.20	120.60	0.20

RSD-Relative Standard Deviation.

Higher quantities of gold are obtained for the samples collected from the Roşia Montană compared with the concentrations determined for samples acquired from the market (tables 5-6). To be sure about the selectivity of horsetail for gold, lithium, silver, tellurium, copper, chromium were determined in the same samples. Sample 1 was collected from an area were

mining waste were not stored [27, 28]. The highest gold concentration was obtained for the sample collected in the area of mining waste storage, were due to naturally occurred acidity the gold could be transferred into solution [17].

Table 7. Report of gold to tellurium (Au/Te) for concentration determined from infertile stems of horsetail (*Equisetum arvense*) and milfoil (*Achillea millefolium*) from Roşia Montană area

Sample	Au :Te (concentrations determined on the same sample)	
	Equisetum arvense	*Achillea millefolium*
Corna Spring_september	2.79	2.65
Bunta_september	4.09	3.25
Abrud exit_september	3.23	3.25

Usually, plants have the own mechanism to protect them from the stress induced by heavy metals. The most important fact is that the heavy metals are channeled into the food, animals and finally humans by plants.

For samples obtained from the market, the horsetail is originated one sample from Râmnicu Vâlcea, south part of Romania, and the other sample near Bucharest. The gold concentrations are significant but lower then the concentrations obtained for samples collected in Roşia Montană. For the samples with lower gold concentration the concentration of tellurium is significant. The mechanism of gold absorption is similar with the one for tellurium. Also high concentration of copper was determined in samples collected from Roşia Montană and extremely higher for those acquired from the market. All samples were prepared and analyzed in the same working conditions [30].

In September together with sterile stems of horsetail we collected milfoil. All parts of the plants were included in analysed sample.

The 100 or so species of milfoil are herbaceous perennials, most with fragrant lacy foliage and small daisy-like flower heads borne in rounded corymbs. Commonly known as yarrow, this has leaves that are greyish green, aromatic, and very finely dissected, like soft dainty ferns. The plant forms dense spreading mats of lacy leaves from rhizomes that creep beneath the ground surface. Common yarrow is a cosmopolitan weed originally native to Europe and western Asia. Today it grows in temperate regions worldwide. In Europe, yarrow is a ubiquitous weed in hedgerows pastures and fields, and seldom allowed near respectable gardens.

In table 6 the gold, tellurium and zinc concentrations determined for horsetail in September are compared with the data obtained for milfoil collected in the same field trip. The gold and tellurium were determined to probe the selectivity of horsetail for gold and also to determine if the gold absorption mechanism is connected with tellurium absorption mechanism. Studing the results presented in table 6 we can observe that the ratio of gold and tellurium concentrations is similar for the two species collected from the same sample collecting point, and presented in table 7. The same conditions of soil, same composition and same climate characteristics determine the absorption of gold and tellurium in the same ratio for two different species.

CONCLUSIONS

This study was based on water samples characterization from three rivers in Roşia Montană District, a gold mining area in Romania. Determining the concentration of heavy metals enabled the conclusion that Roşia Montană District is an ecosystem impacted by the mining industry.

As shown in table 3 the maximum admitted concentration has exceeded by over 1,000 times. To re-establish equilibrium in this ecosystem, mining activities must be stopped or pollution controls must be established. While these water courses are not used for industrial purposes or for human consumption, they do flow into the Mureş River, an important water supply for industry.

Five elements, cadmium, copper, lead, manganese and zinc which are considered to be the most toxic metallic elements from geological point of view in Roşia Montană area were determined comparatively.

The equilibrium of an ecosystem can be easily disturbed by modifying any biotic or non-biotic characteristic. Due to mining activity in this area, the forests were destroyed, especially beech, this type of tree it is present only in isolated zone, as a relic of ancient forests. The missing of some vegetal species, i.e. beech, can produce very important damage of soil stability and also on ecosystem trophyc chain.

The running waters drain the mining waters and that can produce a missing of ichthyologic fauna from some valleys. In this area the pollution was observed from the Middle Age. After the researches on can conclude that the Roşia Montană ecosystem were partially destroyed due to mining exploitation. Though these rivers are not used for domestic activities in this area, can be produced some direct or accidental intoxication in the case of human and in the case of domestic animals. The vegetation from area is disturbed. The artificial lakes from Aries river reservoir in Metaliferi Mountains are common in Roşia Montană area. Some of these lakes were built in XIXth century, as banks for gold-mine exploitation. The water rivers from Roşia Montană are characterize as inferior category water as a result of water became from ancient mines, as a results of wastes drain from mine, domestic wastes and industrial activities. The waters which are drain from mine's wastes are acid due to the natural process.

Presently, the heavy metals concentration (cadmium, copper, lead, manganese and zinc) in Roşia Montană area are under the limits accepted by Romanian Standard. In some cases the difference is more than 1000 times than the maximum accepted concentration.

The area Roşia Montană can be considered a polluted area with heavy metals, and the degree of pollution is reflected in the quantities accumulated in the plants collected from this area.

REFERENCE

[1] Sântimbreanu, A., *Muzeul Mineritului din Roşia Montană*, Ed. Sport – Turism, Bucharest, RO, 1989; pp 12-27.

[2] Balintoni, I. *Ro .J. Tect. & Reg. Geol.* 1994, *75*, pp 51- 57.

[3] Maliszewska, W. *Environ Pollut* 1985, *37*, pp 195- 199.

[4] Technical university of Bucharest 2006. Environmental impact evaluation report: Initial meteorological study [E-pdf]. www.rmgc.ro

[5] Ianovici V., *Geologia Munţilor Apuseni*, Ed. Academiei RSR, Bucharest, RO, 1976, pp 36-42

[6] Leary, S., O'Connor, G.O., Minut, A., Tamas, C., Manske, S., and Howie, K., 2004: *The Roşia MontanăOre Deposit*, Chapter 6 in Au-Ag-telluride Deposits of the Golden Quadrilateral, Apuseni Mountains, Romania, N.J. Cook and C.L. Ciobanu, Eds. Guidebookof the International Field Workshop of IGCP Project 486, IAGOD Guidebook Series 12.

[7] Bleahu, M., Ghiţulescu, T.P., Savu, M., *The Structure of The Apuseni Mountains*. Carp. Balk. Geol. Assoc. XII Congr., Guide to Excursion B3, Institute of Geology and Geophysics, Bucharest, RO, 1981, pp 23-25.

[8] Marinescu I., "Alburnus Maior" - centru antic minier – Introducere, Roşia Montană, prezent şi viitor. Notă de probleme sociale şi de mediu" 2004. www.alburnulmaior.ro

[9] Stoica, A.I., Lochmüller, C.H., Baiulescu, G.E. *Environmental Analytical Chemistry – Concepts* , Ars Docendi, Bucharest, RO, 2004, pp 10-15.

[10] Pichard, J. A., Bisson, M., Diderich C., Houeix M., Hulot, C., Lacroix, G. Lefèvre, J.P Lévêcue. S., Magaut, H., Morin A. et Pépin G., *Fiche de donnees toxicologiques et environnementales des substances chimiques, Cadmium et ses derives*, INERIS, FR, 2004, pp 87-96.

[11] Pichard, J. A., Diderich, R., Houeix, N., Hulot, C., Lacroix, G., Lefèvre, J.P., Lévêcue, S., Magaut H. et Morin, A., *Fiche de donnees toxicologiques et environnementales des substances chimiques, Zinc et ses derives*, INERIS, FR, 2003, pp 65-78.

[12] Pichard, J. A., Bisson, M., Hulot, C., Lefèvre, J.P., Magaut, H., Oberson-Geneste D., Morin, A. et Pépin, G., *Fiche de donnees toxicologiques et environnementales des substances chimiques, Plomb et ses derives*, INERIS, FR, 2002, pp 57-65.

[13] Stoica, A.I., Baiulescu, G.E. and Abould-Enein, H.Y. *Toxicol. & Environm. Chem.* 2000*, 77*, pp 143-150.

[14] Suess J. M., *Examination of Water for Pollution Control*, *Volume **1**, Sampling, Data Analysis and Laboratory Equipment*, Pergamon Press, Vol. 1, 1982, pp 34-38.

[15] Manahan S. E., *Environmental Chemistry*, 5th edn., Lewis Publishers, Michigan, 1991

[16] Conway R.A., *Environmental risk analysis for chemicals*, Krieger Publishing Company, Florida, 1993.

[17] Florea, R.M., Stoica, A.I., Baiulescu, G. E., Capota, P., *Environ. Geol*., 2005, 48, pp 1132 – 1137.

[18] Comitetul National pentru Stiinta si Tehnologie, Institutul Român de Standardizare, STAS 4706 – 88, 1988.

[19] Mamdouh S. M., Mohamed I. E., Manal M. E., *Chem. and Ecol*. 2007, 23, pp. 201-216.

[20] Qingyun F., Jiang H., Hongxi X., Changwei L., Ying L., Ying S., Lili S., *Environ. Geol.* 2007, 53, pp.239-251.
[21] Taylor, M. P., *J. Geochem. Explor.* 2007, 92, pp. 55-72.
[22] Miller J. R., *J. Geochem. Explor.* 1997, 56, pp.101-118.
[23] Willscher S., Pohle C., Sitte J., Werner P., *J. Geochem. Explor.* 2007, 92, pp. 177-185.
[24] Martinez-Sanchez M. J., Navarro M.C., Perez-Sirvent C., Marimon J., Vidal J., Garcia-Lorenzo M.C., Bech J., *J. Geochem. Explor.* 2008, 96, pp.171-182.
[25] Navarro M.C., Perez-Sirvent C., Martinez-Sanchez M. J., Vidal J., Tovar, P. J., Bech J., *J. Geochem. Explor.* 2008, 96, pp.183-193.
[26] Heikkinen P. M., Raisanen M. L., *J. Geochem. Explor.* 2008, 97, pp. 1-20.
[27] Nkongolo K. K., Vaillancourt A., Dobrzeniecka S., Mehes M., Beckett P., *Bull. Environ. Contam. Toxicol.* 2008, 80, pp. 107-111.
[28] Wierzbicka M. H., Przedpelska E., Ruzik R., Ouerdan L., Polec – Pawlak K., Jarosz M., Szpunar J., SzakielA., *Protoplasma,* 2007, 231, pp. 99-111.
[29] Sato, H., Ueda, J., *Anal. Sci.* 200, 16, pp. 1089 – 1090.
[30] Ekinci Dogan, C., Turhan, K., Akcin, G., Aslan, A., *Ann. Chim. (Rome)*, 2006, 96, pp. 229-237.
[31] Weiss, R.F., *Herbal Medicine*, AB Arcanum, Sweden, 1998.

In: Gold Mining: Formation and Resource Estimation ISBN: 978-1-60741-096-6
Editors: M. D. Corral, J. L. Earle

Chapter 4

ECONOMIC EVALUATION OF GOLD MINING PROJECTS: FROM STATIC DISCOUNTED CASH FLOW TO REAL OPTIONS

***Sabry A. Abdel Sabour*[1] *and Graham Wood*[2]**

[1] Department of Mining and Materials Engineering, McGill University, FDA Building, 3450 University Street, Montreal, Quebec, H3A 2A7, Canada.

[2] AMEC Americas Ltd., 111 Dunsmuir Street, Vancouver, British Columbia, V6B 5W3 Canada.

ABSTRACT

Economic evaluation of gold mining projects is a key input to the go/not-to-go decision. This is usually carried out by developing a cash-flow model projecting future revenues, capital and operating costs and other cash flow items. Based on these cash inflows and outflows, net annual cash flows throughout project lifetime are generated and measures of project merit, such as payback period (PB), discounted cash flow internal rate of return (IRR) and net present value (NPV), are estimated. In such conventional economic analysis, annual revenues are estimated assuming that future gold prices and gold production are known with certainty. If the analysis requires dealing with a foreign currency, the conventional practice is to assume certainly-known future exchange rates. In most cases, flat gold prices and exchange rates are applied throughout project life time. As with market variables, future amounts of gold production are assumed to be known with certainty.

In reality, both the market and geological variables are highly uncertain. Given this fact, it is possible that future conditions will be different from what is expected at project start-up time. In this case, management is expected to respond to the new information by revising original operating plans. The important shortcoming of conventional economic evaluation methods, based on static discounted cash flow analysis, is that they ignore this management flexibility to alter or revise production decisions in the future based on the new information. In some cases, the additional value of such management flexibility

[1] E-mail: sabry.abdelhafezabdelsabour@mcgill.ca

[2] Tel: (604) 664-3597, E-mail: graham.wood@amec.com

could be a large proportion of project value and can have a significant impact on the decision-making process.

In contrast to static evaluation methods, the real options valuation (ROV) approach can incorporate the dynamic nature of future operating policy into current value estimates of gold mining projects. In this respect, management flexibility to revise original production plans in the future according to the new information is integrated into the financial evaluation model. This article aims to explore the differences between conventional static economic evaluation methods and the modern ROV technique. A comparison between the two evaluation approaches is provided through a case study of a gold mining project.

Keywords: Gold mining; Economic evaluation; Discounted cash flow; Real options valuation.

INTRODUCTION

The purpose of economic evaluation of a gold mining project is to estimate its net economic worth which is the basis for mergers, acquisitions, resources allocation and investment decision making, among others. Economic measures of merit that have historically been used in the mining business include payback (PB) period, discounted cash flow techniques such as internal rate of return (IRR) and net present value (NPV). Economic evaluation of mining projects using these measures of merit requires estimating future costs to be incurred and future revenues to be generated from mining operations throughout project lifetime. However, as explained by Davis (1996), future costs can be estimated within a narrow confidence band because they do not usually vary significantly from engineering estimates. The real problem for evaluators is forecasting future revenues which are highly uncertain due to the volatility of metal prices. The level of volatility indicates how future prices can deviate from the current expectations (Brunetti and Gilbert, 1995). It reflects the fact that unforeseen economic conditions may cause unexpected variations in commodity prices. Achireko and Ansong (2000) explained that the main cause of metal price volatility is the unpredictable shifts in the balance of supply and demand.

Uncertainty about future metal markets is one of the major sources of risk affecting mining project viability. Figure 1 shows, for example, the average monthly market prices of gold over the period 1990-2008 in current US dollars. It is obvious that these prices are highly volatile and do not keep a constant trend, which makes it speculative to define deterministic forecasts for future gold prices. Therefore, it is difficult for mine evaluators to have precise forecasts for future prices of gold over the mine life. However, under this uncertain environment, mining companies usually base mine project evaluations on long-term expectations of metal prices. The actual behaviour of these metal prices in markets can be better or worse than expected. Such deviations can result in an actual mine value, based on the actual market realizations, that is significantly higher or lower than that estimated based on metal price expectations. In monetary terms, this may cause a multi-million dollar loss due either to the foregone extra profits that could be gained during the periods of favourable market conditions or to the net realized capital losses as a result of the unexpected weak market.

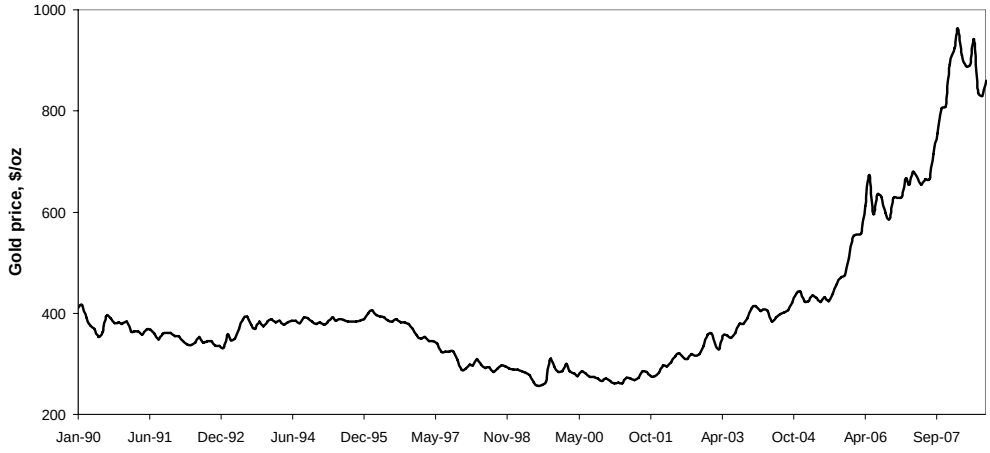

Figure 1. Average monthly market prices of gold, 1990-2008.

As an alternative to the classical NPV method, real options valuation (ROV) has gained popularity since the mid 1980's as a promising technique for valuing mining investments. It provides a framework for analyzing the optimal timing of project development and the optimal management of the mine after starting production. The ROV has been increasingly investigated over the past two decades as an efficient alternative to the traditional discounted cash flow analysis due to its ability to deal with the uncertainty of future outcomes and to incorporate the value of future management actions in response to uncertainty resolutions.

This article provides a brief overview and compares the conventional discounted cash flow and the ROV techniques. A case study of a gold mining project will be provided to illustrate how the valuation results of both the conventional and the modern techniques could be different. The focus in this work will be on uncertainty over gold prices. Other sources of uncertainty related to geology and technical risk will not be considered here.

Conventional Evaluation Techniques

Conventional project merit measures such as PB period, IRR and NPV are estimated by projecting cash inflows and outflows throughout project lifetime. Cash inflows consist of annual revenue projections for the mine. Cash outflows such as capital and operating costs, royalties and income taxes are subtracted from the inflows to arrive at the yearly net cash flow projections. Cash flows are assumed to occur at discrete time points, usually at the end or the beginning of each year.

PB period can be defined as the time required for the project to repay its capital investments and is usually calculated from the start of production. Projects or investment proposals with shorter PB periods are preferred over those with longer PB periods. Although PB period is widely used in the mining industry as a merit measure for comparing alternatives and mutually exclusive projects, its usefulness is limited by the fact that it does not consider cash flows beyond the payback period.

Differently from PB period, IRR, also known as discounted cash flow rate of return (DCFROR), considers all life of mine cash flows. IRR is defined as the interest rate at which

the project will break-even assuming that cash flows will be re-invested at that rate. An IRR greater than a company-objective rate indicates a good project while an IRR less than a target one indicates that the project is less attractive. Although IRR is more efficient than the PB period, some practical problems arise when net cash flows change sign many times throughout project lifetime.

NPV is probably the most common technique for evaluating mining investments. To estimate the NPV for a mining project, annual net cash flow (NCF) projections are discounted back to the project valuation date using an appropriate discount rate. The discount rate appropriate to a specific project will depend on many factors, including the type of commodity; and the level of project risks, such as market risk, technical risk and political risk, among others. The discounted, present values of the net cash flows are summed to arrive at the project's NPV. For more details about conventional mining projects evaluation methods see for example Wells (1978), Gentry and O'Neil (1984), Taylor (1986), Smith (1997), Torries (1998) and Hustrulid and Kuchta (2006). Since it is the most popular among conventional economic evaluation techniques used in the mining business, the focus in this article will be on the NPV method.

From the previous discussion, two major problems can be seen to be limiting the usefulness of the NPV method. First, the NPV applies a single discount rate to discount future net cash flows to the present time. This implies that all cash flow components have the same level of risk. It is clear that this assumption is not accurate since costs are not as risky as revenues and even metal prices do not exhibit the same risk profile. The second problem associated with the conventional NPV is the fact that it does not consider metal price uncertainty and the management responses to the resolution of that uncertainty. The NPV assumes that future metal prices are known with certainty and all production decisions are made upfront. Therefore, the conventional NPV does not consider the management flexibility to change or alter decisions in the future in response to falling/rising metal prices. Examples of management flexibility include, for example: delay of development plans, expansions, contractions, temporarily shutting down and abandonment of mining operations. In a world of highly volatile metal prices, this management flexibility may have a great impact on the value of mining projects. As explained by Keswani and Shakleton (2006), the management flexibility to take some future actions in response to new information can considerably increase the value of a project. More definitely, Moyen et al. (1996) demonstrated that for high cost mines, the value of management flexibility can equal the static net present value of the mine that was calculated without taking into account the operating flexibility. The failure of the conventional NPV method to capture the value of real options embedded in mining investments may mislead the decision-making process and result in rejecting good investment opportunities.

Real Options Valuation

The ROV has been increasingly used over the past two decades as an efficient alternative to traditional discounted cash flow analysis due to its ability to deal with the uncertainty of future outcomes. Research on options valuation started in 1973 when Black and Scholes (1973) proposed a model for valuing European-style options. Brennan and Schwartz (1985) extended the technique of options valuations to mining investments when they valued a

mining project with the management flexibility to temporarily shutdown and reopen or abandon the mine depending on the output price level and volatility. Since that date, the research on applying ROV to mining investments has taken several directions. McDonald and Siegel (1986), Trigeorgis (1990), Mardones (1993), Frimpong and Whiting (1997) Abdel Sabour (1999; 2001) analyzed the management flexibility to defer investments and to temporarily close or abandon an active project. Sagi (2000) extended the ROV further to handle cutoff grade problems. Cortazar and Casassus (1998) proposed a ROV model to value the management flexibility to expand mine capacity. Samis and Poulin (1998), Kamrad and Ernst (2001) and Samis et al. (2001) discussed incorporating the non-homogeneity of mineral deposits into the ROV. Recent applications of the ROV to real-life mining projects include Lemelin et al. (2006; 2007).

It is worthwhile, before proceeding to the rest of the article, to give a brief review of options valuation techniques. As mentioned above, a closed form solution for the value of an option can be determined using the Black and Scholes (1973) model if the option is European, the stock pays no dividend, and the stock price follows Brownian motion with constant interest rate and volatility. Since the real options embedded in mining investments are American-style with multiple sources of uncertainty, analytical solutions are not applicable and numerical techniques have to be applied for valuing these real options. These numerical techniques are finite difference, binomial lattice, and Monte Carlo simulation. As explained by Schwartz (1977) and Brennan and Schwartz (1977), in the finite difference method, the partial differential equation governing the value of an option is replaced by a system of difference equations that can be solved recursively from known boundaries. The lattice method (Cox et al., 1979) is simpler than the finite difference method and it assumes that the commodity price can go up or down at definite percentages and probabilities. The main shortcoming of both the finite difference and lattice methods is that they become impractical for valuing capital investments with multiple sources of uncertainty as in the cases of multi-metal mining projects or when having to deal with exchange rate uncertainty in addition to metal prices uncertainty. This is because, for both techniques, the level of complexity grows exponentially with the number of uncertain state variables (Barraquant and Martineau, 1995 and Grant et al. 1997). The Monte Carlo method (Boyle, 1977) is based on simulating a large number of price paths. Then the option payoffs throughout the simulated paths are determined by applying the optimal exercise policy and are discounted back to time 0. Option value is then approximated by averaging over the number of simulated price paths. Until recently there was a belief that the Monte Carlo method is applicable only to European-style options with known and fixed maturities since it is a forward induction technique. This belief that it could not handle the early exercise feature of American-style options started to change in 1993 when Tilley (1993) proposed an extension for the Monte Carlo method to be able to value American-style options using the bundling algorithm. Following Tilley (1993), several algorithms have been proposed to overcome the limitations of Tilley's algorithm, and to provide more practical simulation procedures. For example, Barraquant and Martineau (1995) provided the stratified state approach to deal with the cases of multiple sources of uncertainty. Carriere (1996) proposed an algorithm that depends on estimating the conditional expectation using nonparametric regression. Broadi and Glasserman (1997) suggested a simulation algorithm that has some features of the lattice methods. Recently, Longstaff and Schwartz (2001) proposed the least-squares Monte Carlo (LSM) approach for valuing American-style securities which combines simulation with least-squares regressions. Abdel

Sabour and Poulin (2006) extended the LSM to valuing real capital investments under multiple uncertain market prices and provided a validation for its accuracy in valuing mining investments having compound options. Further extensions of the LSM were carried out by Dimitrakopolis and Abdel Sabour (2007) and Abdel Sabour and Dimitrakopolis (2008) incorporating geological uncertainty, in addition to market uncertainties, and providing applications to open pit mine planning.

In summary, although the first options valuation model has been developed more than three decades ago, some mining practitioners still doubt the applicability of real options valuation in the mining business. One reason for this could be the complex mathematics required to develop a real options valuation model which might be discouraging mining managers from applying the ROV in valuation studies. Second, many practitioners doubt if the real options approach can bring new insights or knowledge to the decision making process. However, it seems that the simulation-based real options valuation technique described above can provide a simple and efficient framework for valuing mining projects with the ROV. This technique can deal with the complexity of the mining industry and provides opportunities for the mining business to apply the ROV in regular strategic investment studies. The question that needs an answer now is why ROV? The next section aims to answer this question through a practical case study of a gold mining project.

VALUING A GOLD MINING PROJECT

In this section, a case study of an open-pit gold mine is provided. Financial analysis of the project will be carried out using both the conventional economic evaluation procedures based on the static NPV and the ROV. The aim is to investigate the difference between the two techniques and illustrate the significance of the new information that ROV can bring to decision makers. Table 1 lists the base case constants and assumptions used in both sets of evaluations. Table 2 provides an expected schedule of waste and ore production, grade, recovery, capital and operating costs. For the sake of the study, all analyses are performed on a before-tax basis.

Table 1. Base case parameters[3]

Discount rate	%	8.00
Gold price	$/oz	650
Insurance premium	%	0.20
Refining charge	$/oz	5.00
Pay factor	%	98.00
Transportation	$/oz	3.00
Closure Cost	$/t mined	0.10

[3] Base case metal prices and exchange rate are provided for explanation purposes only. These assumed figures do not necessarily reflect AMEC's or any other party's expectations.

Table 2. Mine production and cost data

Year	Waste	Ore	Au grade	Au recovery	Capital Costs	Operating Costs
	000's tonnes	000's tonnes	g/tonne	%	$ million	$ million
-2					40.00	
-1					35.00	
1	3,415	539	3.93	78	40.00	18.12
2	1,550	697	3.48	83	17.00	16.56
3	2,908	948	3.46	83	12.00	18.70
4	5,360	1,041	3.34	77	13.00	20.05
5	7,564	991	3.27	81	13.00	20.75
6	5,022	1,002	3.32	78	14.00	19.81
7	3,034	1,014	3.25	80	10.00	20.43
8	3,547	1,053	3.15	78	11.00	21.35
9	3,036	991	3.10	84	10.50	20.65
10	4,106	1,049	3.07	83	11.20	19.71
11	2,600	1,067	2.89	84	6.50	20.74
12	5,377	1,181	2.76	79	7.40	20.23
13	6,188	1,051	2.48	82	6.70	20.58
14	6,373	1,065	2.35	78	7.60	21.88
15	6,090	897	2.37	80	9.80	20.97
16	6,422	846	2.36	82	10.30	20.99
17	6,702	762	2.39	83	8.90	20.70
18	6,718	832	2.38	83	10.20	20.42
19	6,810	781	2.38	79	8.30	20.33
20	6,501	834	2.41	82	6.00	20.19

FINANCIAL ANALYSIS USING THE STATIC NPV TECHNIQUE

Financial analysis, using conventional NPV, starts with developing a spreadsheet financial model to estimate the net economic worth of the proposed mining project. This is carried out by estimating net future cash flows and discounting them back to the current time using an "appropriate" discount rate. This is usually followed up with sensitivity analysis and sometimes also with Monte Carlo simulation to give mine managers an idea regarding risk inherent to the investment. A simplified example of conventional cash flow models is shown in figure 2. Using the data in tables 1 and 2, the conventionally estimated NPV of the gold mine was $31.70 million.

Calendar year		2009	2010	2011	2012	2013	2014	2015	2016	2017	2018	2019	2020
Project year		1	2	3	4	5	6	7	8	9	10	11	12
Production year		-2	-1	1	2	3	4	5	6	7	8	9	10
Metal prices													
Gold	$/oz	650	650	650	650	650	650	650	650	650	650	650	650
Recovered metal value	$ million			34.57	41.88	56.57	55.92	54.62	53.96	55.33	54.27	53.73	56.14
Production costs													
Total	$ million			(18.12)	(16.56)	(18.70)	(20.05)	(20.75)	(19.81)	(20.43)	(21.35)	(20.65)	(19.71)
Smelter deductions													
Total	$ million			(1)	(1)	(1)	(1)	(1)	(1)	(1)	(1)	(1)	(1)
Refining charges													
Total	$ million	0.00	0.00	(0.26)	(0.32)	(0.43)	(0.42)	(0.41)	(0.41)	(0.42)	(0.41)	(0.41)	(0.42)
Freight	$ million			(0.17)	(0.20)	(0.27)	(0.27)	(0.26)	(0.26)	(0.26)	(0.26)	(0.26)	(0.27)
Marketing & other	$ million			0.00	0.00	0.00	0.00	0.00	0.00	0.00	0.00	0.00	0.00
Insurance charges	$ million			(0.07)	(0.08)	(0.11)	(0.11)	(0.11)	(0.10)	(0.11)	(0.11)	(0.10)	(0.11)
Total	$ million			(0.23)	(0.28)	(0.38)	(0.38)	(0.37)	(0.36)	(0.37)	(0.37)	(0.36)	(0.38)
Operating cash flow				15	24	36	34	32	32	33	31	31	35
Capital expenditure													
Total Capital Expenditure	$ million	(40)	(35)	(45)	(17)	(13)	(13)	(13)	(14)	(10)	(11)	(10)	(11)
Net project cash flow	$ million	(40)	(35)	(29)	7	23	21	19	19	23	20	21	24

Figure 2. A simplified conventional cash flow model.

As a part of the conventional economic evaluation procedure, sensitivity analysis is usually performed to investigate effects of changing project key variables on one or more of the measures of economic merit. This is carried out by changing one variable at a time while holding the others constant. Figure 3 shows an example of the sensitivity analysis. The graph depicts sensitivity of the project's NPV estimated at 8% discount rate to variations in gold price, capital cost, operating cost and gold price volatility. What can be inferred from the sensitivity analysis in figure 3 is that the NPV turns out to be negative if gold price is 8% less than that in the base case, or when either the capital or the operating costs are 18% higher than that of the base case. Also, what can be read from the graph is that project's NPV is more sensitive to changes in gold price than it is to changes in capital and operating costs. When comparing capital and operating costs, the project profitability is slightly more sensitive to changes in capital costs than operating costs. Although the sensitivity analysis may provide useful information, its impact on the strategic decision making process is limited. The conventional decision-making rule, which is "go ahead if NPV is positive", is still largely independent of the outcomes of sensitivity analysis. Another important conclusion that can be drawn from figure 3 is that the NPV estimates are independent of gold price volatility. This is inferred from the graph by the flat line representing project sensitivity to gold price uncertainty.

Differently from sensitivity analysis, a more advanced tool to investigate and quantify project risk is to run Monte Carlo simulation on one or more economic merit measures. Monte Carlo simulation allows for investigating the effects of all key variables simultaneously instead of one-by-one as in the conventional sensitivity analysis presented in figure 3. However, it is not regularly used in real-life mine project studies. In this article, the NPV calculated at 8% discount rate is simulated assuming, for simplicity and as per common practice, that gold prices, capital costs and operating costs follow symmetric triangular distributions. Based on these distributions, a large number of cash flow scenarios are generated and their corresponding NPV's were calculated at 8% discount rate. As shown in figure 4, since the distributions of input variables are assumed to be symmetrical with

correlation coefficients equal to zero, the expected NPV is approximately the same as the single value estimate of about $31.7 million. One of the advantages of Monte Carlo simulation over the conventional single value estimate is that it generates distributions for the possible NPV of the project. This gives a clear idea about project risk and allows for estimating confidence limits around the NPV. As shown in figure 4, the 10th and 90th percentiles (in $ million) are -58.96 and 122.41.

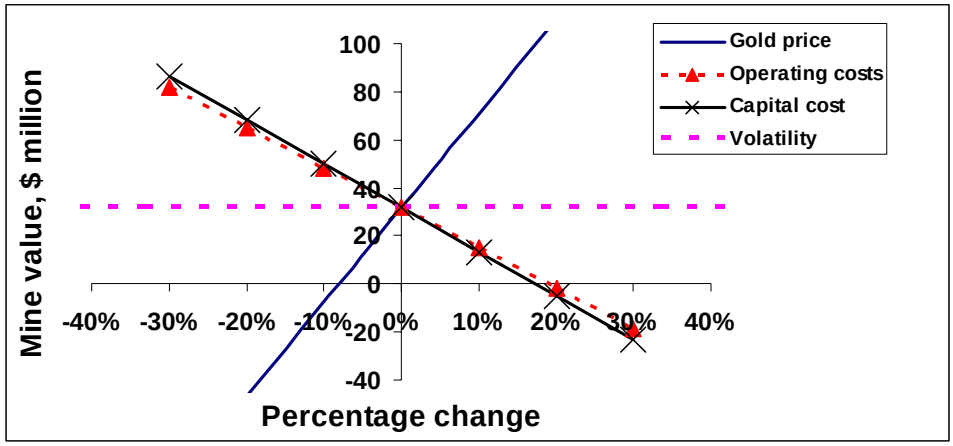

Figure 3. Sensitivity of the NPV to changes in key variables.

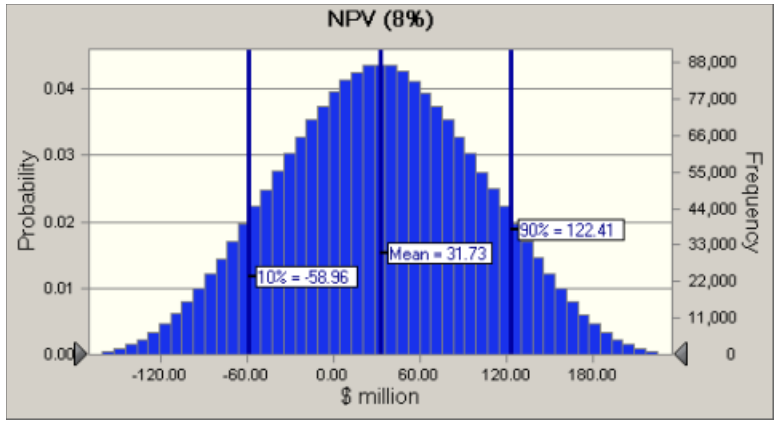

Figure 4. Monte Carlo simulation results.

Although Monte Carlo simulation gives more insight into the risk associated with the expected NPV, it does not contribute significantly to the strategic decision-making process. It uses the same assumption of the static, single-value, NPV method regarding management flexibility. Conventional simulation assumes that conditions remain constant and management will do nothing regarding future changes in metal prices, for instance. As shown in figure 4, simulation provides distribution for the possible NPV without any indication of how to manage the risk of having negative NPV's. Conventional financial analysis does not

include flexibility for management to take actions in order to avoid long-term, major, negative net cash flows.

FINANCIAL ANALYSIS USING ROV

The flexible valuation model in this article is based on Monte Carlo simulation and incorporates the flexibility to shutdown the mine early (the abandonment option) in response to falling gold prices. To keep things simple while illustrating the concept of operating flexibility, other complex operational flexibilities such as the flexibility to shutdown the mine temporarily and re-open or abandon it later will not be considered here. Interested readers can refer to Abdel Sabour and Poulin (2006) and Lemelin et al. (2006; 2007) for more details about the temporary closure/re-open option and also for applications to real life mining projects.

In ROV, it is assumed that mine management will have the chance to examine mine production policy at some regular time intervals, usually at the end of each year, and decide whether to go ahead with the next year's production plan or close the mine at this time. There will be a trade off between closing the mine in period t and paying the closure cost, or continuing production and wait until period t+1. The decision whether to close the mine early or continue until next period will depend, among other factors, on capital expenditures, metal prices and production costs in addition to the difference between the closure costs of periods t and t+1. A large number of paths (or sequences of values) are simulated for gold price and cash flows are evaluated for each path. Then, the valuation model internally determines the optimal choice at each period and revises cash flows accordingly.

To maintain simplicity and to be able to compare results of the static NPV to ROV, correlation between gold price and the stock market is ignored. As a result, there is no risk-discounting and the same discount rate of 8% used in conventional NPV analysis will also be used in the ROV. This is carried out by setting correlation coefficient to 0 in the ROV model. As explained in Abdel Sabour and Wood (2008), considering correlation between metal prices and stock market is straightforward and is easily carried out at no, or negligible, extra cost. However, over focusing on correlation and risk-discounting seems to be distracting readers and adds extra complexity to the understandability of ROV by mining practitioners. Rolling out correlation eliminates many of the apparent complexities and allows for focusing on the most significant issue which is the operating flexibility to modify decisions in the future.

As with the static NPV, to run the ROV model future prices need to be projected throughout project life. Then net cash flows are estimated based on future costs and revenues. This is approximately the same as the conventional NPV analysis presented above. The only new issue here is that uncertainty about market variables and management flexibility to respond to the resolutions of such uncertainty are integrated into the financial model. Modeling uncertainty about future metal prices is usually carried out using stochastic models such as the geometric Brownian motion and mean-reversion, for instance (see Dixit and Pindyck, 1994 and Schwartz 1997 for more details about stochastic processes for modeling metal prices). Conventional NPV valuations are usually based on deterministic future market, assuming perfect knowledge of future metal prices by defining what is called "long-term"

metal price expectations. As shown in figure 5, in conventional NPV, gold price throughout project life is assumed to be flat at $650/oz. To keep things simple and to focus only on the difference in mechanism between the static NPV and the ROV, the same assumption about future gold prices is used in the ROV model. In this respect, future prices of gold will be assumed to be flat at $650/oz. The only difference is that a gold price volatility of 15% is introduced. Therefore, while conventional NPV uses a flat, certain gold price of $650/oz throughout project life, ROV uses the simulated gold prices. As shown in figure 5, the average of those simulated prices is flat at $650/oz as with the static NPV but uncertainty is reflected by simulations.

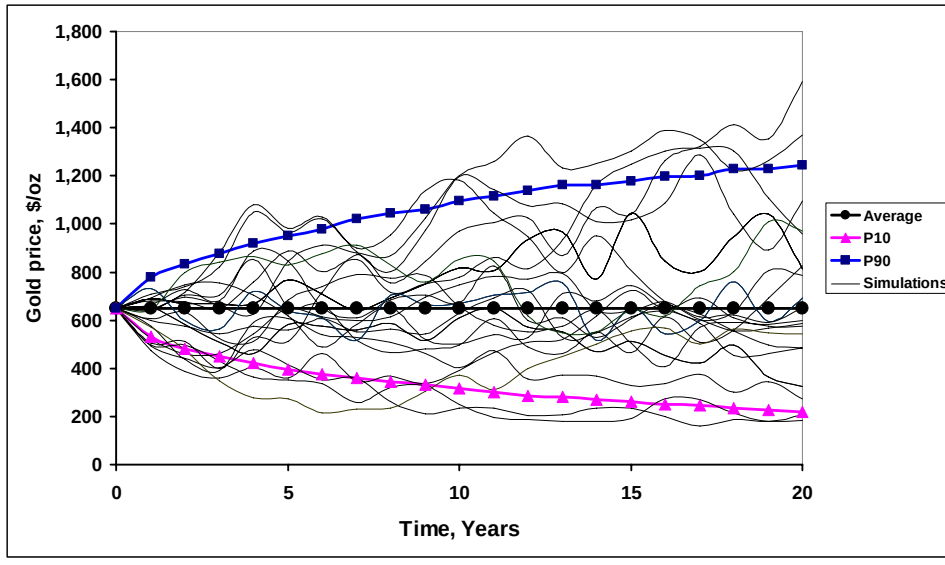

Figure 5. Gold price modeling.

For the sake of this study, 50,000 simulations of gold price have been produced at each year. As with the conventional NPV, all calculations were carried out on a before-tax basis. The expected mine value in this case has been found to be $52.8 million. This is about 67% higher than the conventional NPV estimate of $31.7 million. The difference between the two estimates represents solely the value of management flexibility to shutdown the mine early if the expected value of future mining operations is negative.

Figure 6 shows the sensitivity of mine value, estimated by the ROV, to changes in project key variables. It is obvious that there are significant differences between this graph and figure 3 that is based on the static NPV. Differently from figure 3, and based on the data of this case study, the mine value in figure 6 never goes below 0. As the gold price decreases, the mine value decreases but since management has the right to exercise the abandonment options, the mine value levels at approximately 0 if the initial gold price is 30% less than that in the base case. Also, when capital and operating costs increase the mine value decreases but remain positive even at 30% increase. The most important point here is that, in contrast to the NPV results in figure 3, the mine value estimated by the ROV is sensitive to variations in uncertainty level. As shown in figure 6, other parameters held constant, there is a direct relationship between level of uncertainty and the expected mine value.

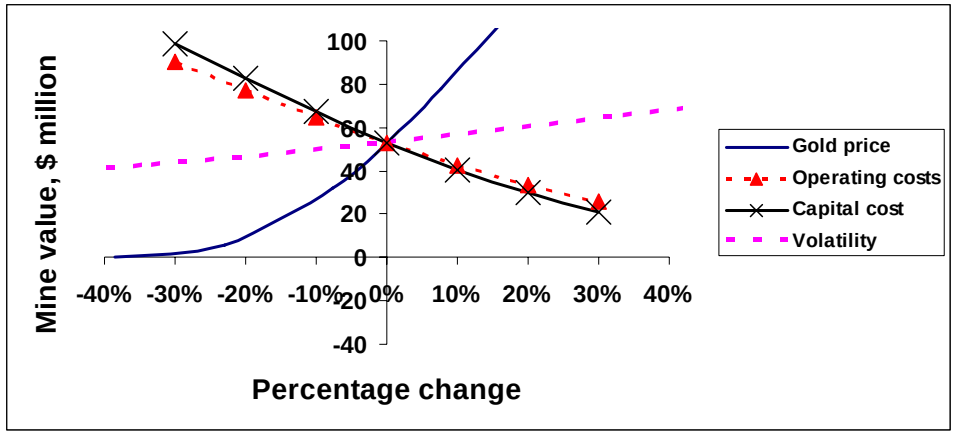

Figure 6. Sensitivity of the mine value estimated by ROV to changes in key variables.

ANALYSIS OF RESULTS

As shown above, mine value estimated by the ROV is significantly higher than that estimated by the conventional NPV[4]. Table 3 shows a comparison between the cash flows of the two techniques. As indicated from the table, life-of-mine gross revenue estimated by the NPV is greater than that of the ROV. This is mainly due to the fact that ROV considers the possibility that the mine will be closed early while the NPV does not consider such flexibility. The same can be said about operating costs, smelter deductions, refining and selling charges, capital expenditure and abandonment costs. However, since the early closure flexibility enables management to avoid major negative cash flows, the present value of NCF's estimated by ROV is higher than that estimated by the NPV. This is also depicted in figure 7 that shows the cumulative net cash flows of both techniques.

Table 3. Summary of Cash flows of the ROV and the NPV

Cash Flow ($ million)	ROV	NPV
Revenue	691.4	911.5
Operating costs	247.1	403.2
Smelter deductions	13.8	18.2
Refining charge, transportation, marketing	7.1	11.2
Insurance charge	1.3	1.8
Capital expenditure	210.5	308.4
Abandonment costs	6.9	11.8
Net cash flow	204.6	157.0
Discounted net cash flow (NPV @ 8% discount rate)	52.8	31.7

[4] For brevity, from now on, NPV will indicate the static conventional NPV and ROV will indicate flexibility-based valuation. Both use the discounted cash flow concept.

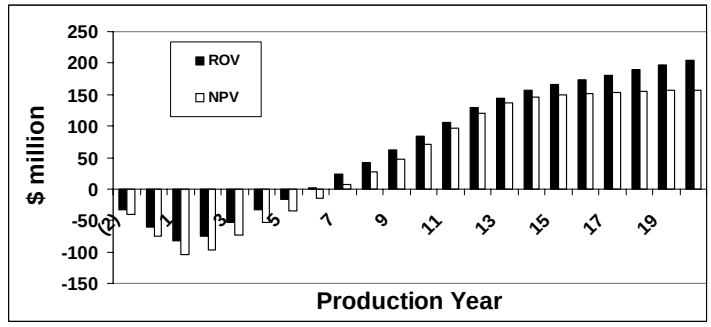

Figure 7. Cumulative net cash flows.

The decision to abandon the mine early will be taken based on prevailing metal prices and current and future capital and operating costs. As mentioned above, the reason why ROV produced a mine value that is greater than that of NPV is the integration of operating flexibility to early shutdown operations. This is indeed a fundamental difference between the two techniques. As illustrated in figure 8, the NPV assumes a 100% probability that the mine will be operating throughout its entire, predefined life regardless of what happens to cash flows. Whereas, with the ROV this probability declines as the mine matures due to increasing costs or decreasing revenues or both.

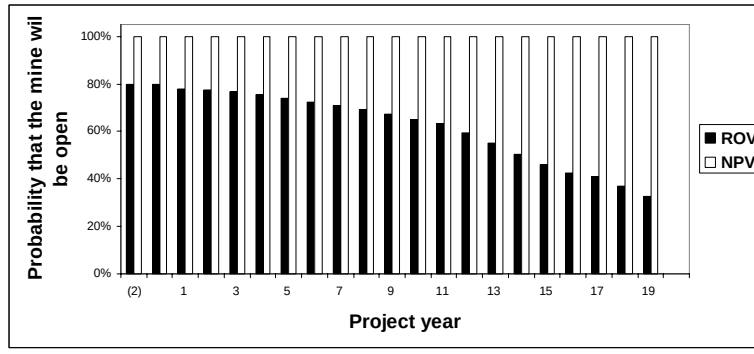

Figure 8. Probability that the mine will be operating.

An interesting question could be: what are the drivers for the differences in financial analysis between the ROV and the NPV? To answer this question, it is important to examine how the results are sensitive to two major variables. These two variables are the level of gold price and the uncertainty about market price of gold. It is worth noting here that to investigate the effect of one variable all other variables will be held constant.

To study the effect of gold price level, all calculations were replicated over the range of $400/oz to $1000/oz gold price at $100 intervals. The other variables such as volatility, mine production, operating and capital costs are the same as in the base case of tables 1 and 2. Figure 9 shows the probability that the mine will be open over the gold price range. As indicated in figure 9, the NPV-determined probability is independent of gold price level while that of the ROV is highly dependent on gold price. At low gold prices, the probability that the mine will remain open is small and it increases with increasing gold price level. As the gold price reaches a high level, the curve representing the ROV-based probability moves closer to

that of the NPV. Therefore, as shown in figure 10, the difference between the valuation results of both techniques, termed the value of flexibility, is high at low gold prices and diminishes as the gold price increases. That is because at high gold prices, the probability that the mine will be abandoned decreases, the probability that it will remain operating increases and the two techniques produce approximately the same value estimate. In such cases of relatively very high gold prices, the value of management flexibility to shutdown operations early is negligible, as shown in figure 10.

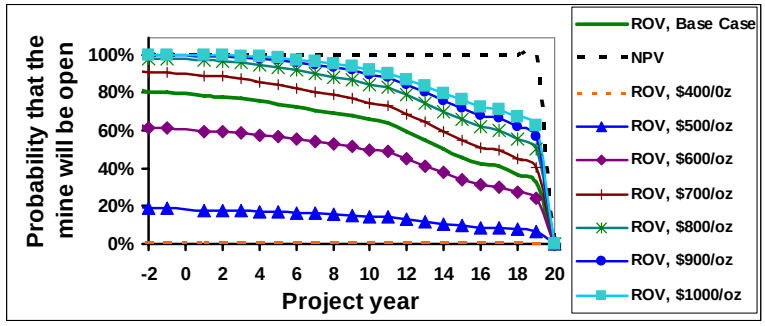

Figure 9. Probability that the mine will be operating at various gold prices.

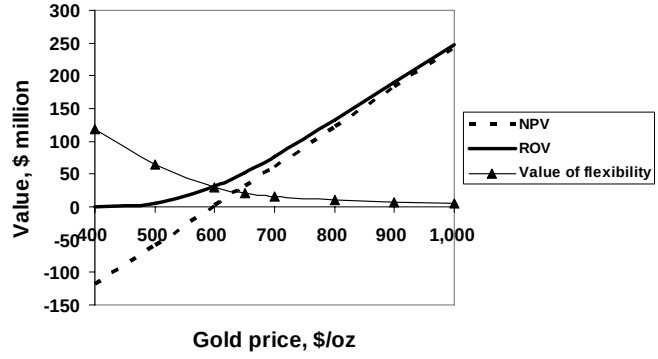

Figure 10. Value of flexibility at various gold prices.

Now, we will investigate the level of uncertainty and its effect on the financial results of both the ROV and the NPV. This is carried out by varying the standard deviation of gold price from 0 to 0.3 at 0.05 intervals. As shown in figure 11, at higher uncertainty levels, the difference between the valuation results of both techniques is large. As mentioned earlier, this difference represents the additional value of management flexibility to stop production in response to collapsing or falling gold price markets. As the uncertainty decreases investors become more certain about future gold prices and the difference between the two techniques decreases. If management is fully certain about future prices of gold, they will be able to make all decisions before starting production and the two techniques will produce exactly the same valuation results. In this case, the value of management flexibility to shutdown the mine in the future is zero, as depicted in figure 11. This is illustrated in figure 12 which shows the probability that the mine will be in production at different uncertainty levels. It is obvious that

as the uncertainty decreases, the ROV-based curve moves upward and becomes closer to the NPV-based one. When uncertainty is assumed to be completely negated, the two curves, corresponding to the two techniques, become identical.

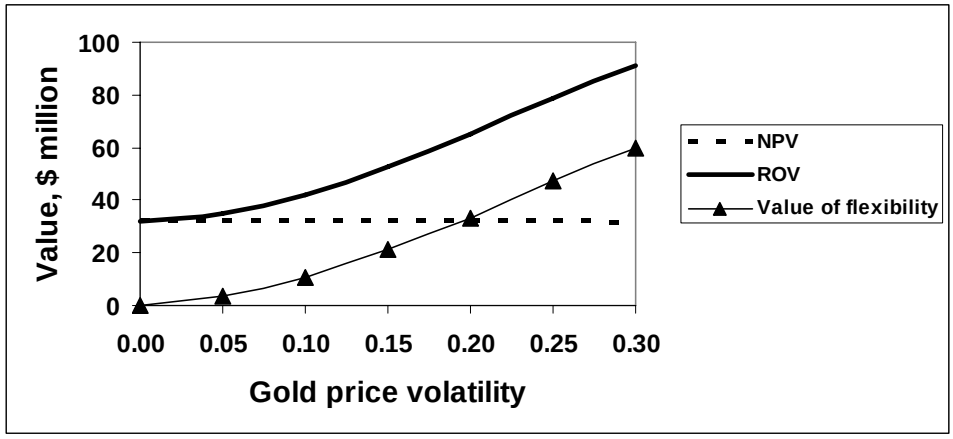

Figure 11. Value of flexibility at various uncertainty levels.

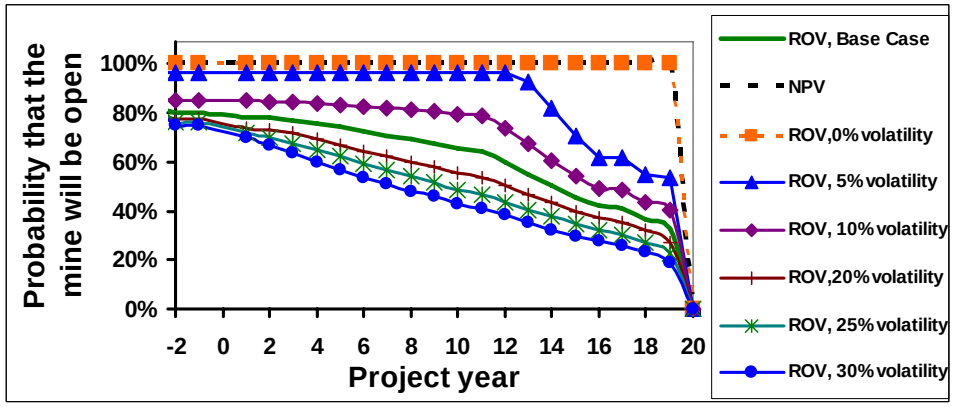

Figure 12. Probability that the mine will be open at various uncertainty levels.

The above discussion shows that gold price uncertainty is the major driver of differences in results between the NPV and the ROV. This conclusion can be strengthened by examining cumulative net cash flows (CNCF) generated by both techniques at various volatility levels, as shown in figure 13. It is clear, as noticed earlier, that at 0% volatility CNCF's of the two techniques are exactly the same. As the level of volatility increases, CNCF's estimated by the ROV become greater than those estimated by the NPV. The difference between the two sets of estimates depends on the uncertainty level (see the graphs corresponding to 5%, 10% ….etc in figure 13). As the level of gold price volatility reaches 30%, life-of-mine CNCF's of ROV become approximately double those of the NPV estimations.

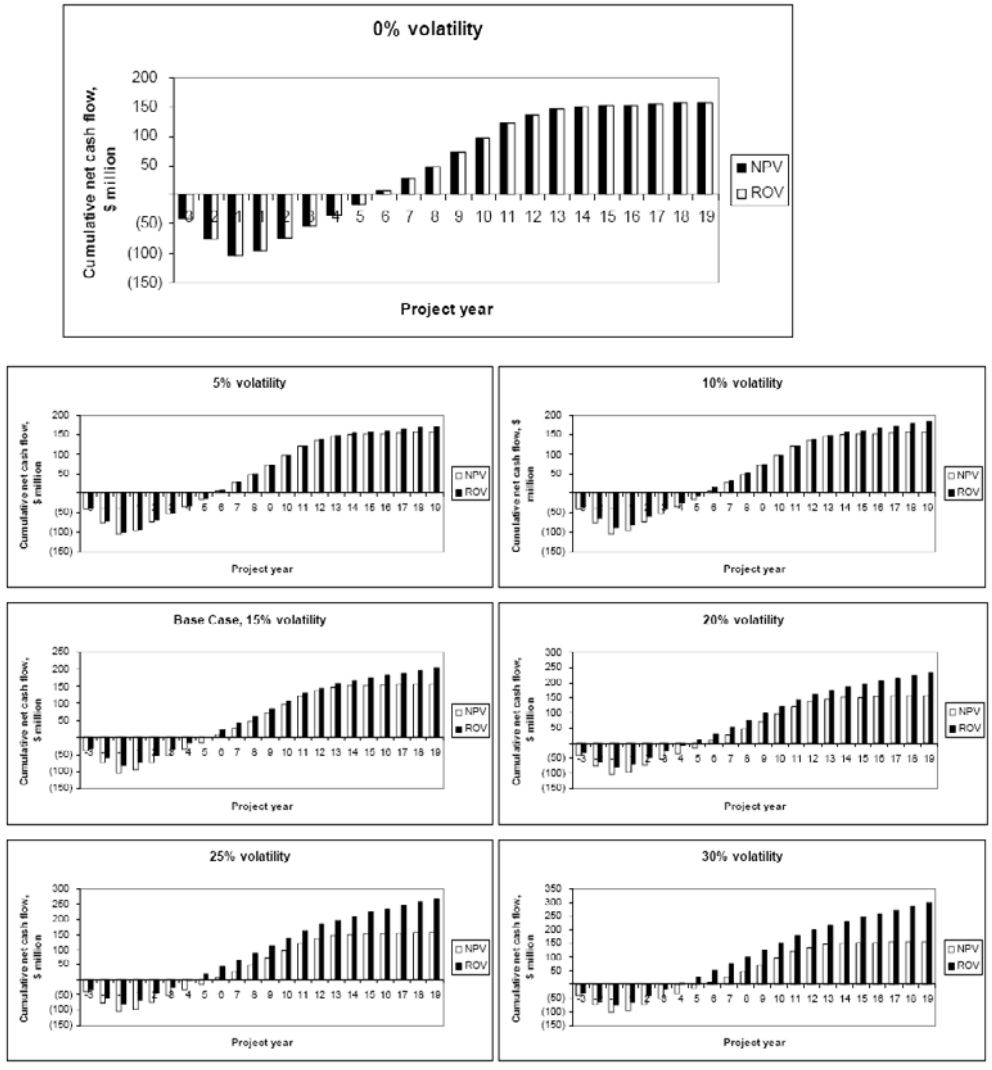

Figure 13. CNCF comparison at various uncertainty levels.

As shown above, the additional value of management flexibility could represent a significant component of the total value of the mining project. This depends, among other things, on the project profit margin and the level of uncertainty. In this respect, the ROV has the ability to reflect the relationship between uncertainty and project value in the valuation results, while the conventional NPV does not. Therefore, based on the discussion above, the NPV can be considered as a special case of ROV when the level of uncertainty about future cash flows is not significant. Since this is not the case for most mining investments, valuation results of the static NPV should be handled with caution.

CONCLUSION

Economic evaluation of gold mining projects is a key input to the decision-making process. This article presented an overview of the conventional and the modern economic evaluation techniques. A practical example of a gold mining project was provided to compare the valuation results of the NPV and the ROV. The results show that the difference between the two techniques could be significant especially for relatively marginal projects and/or when the price of the underlying commodity is highly uncertain. When the commodity price is fairly high, and/or its level of uncertainty is negligible, the two techniques may produce close valuation results.

The difference in valuation results between the ROV and the conventional NPV analysis is due to the difference in dealing with financial uncertainty and management responses to resolution of such uncertainty. The conventional NPV analysis assumes that production will continue as planned regardless of changes in future markets. In reality, various types of operational flexibility could be recognized in the mining business. These include: choice of investment timing, mine expansion, temporary shutdown/resumption of mining operations and early closure of the whole mining project, among others. In contrast to the conventional static NPV, ROV enables modeling financial risk associated with mining projects and integrating the value of management flexibility to take future actions in response to uncertainty resolutions. Therefore, as shown in this article, while the conventional NPV assumes that there is a 100% probability that the mine will be operating throughout its predetermined life, ROV results show probabilities that the mine could be closed early as a result of adverse financial conditions.

As it ignores real-life environments of mining businesses, that are filled with uncertainties and possibilities to revisit and revise production plans at any future time, the conventional NPV may produce inaccurate mine valuations. As shown in this study, the NPV tends to underestimate mining projects. This can mislead the decision-making process and result in rejection of good investment opportunities. As a promising, efficient alternative to the static NPV, ROV seems to be dealing properly with uncertainty and operational flexibility. With the simulation-based ROV models, mining businesses will be able to easily handle multiple sources of uncertainty and incorporate various types of operational flexibility into mining financial analysis.

REFERENCES

Abdel Sabour, S. A. (1999). Decision making with option pricing and dynamic programming: development and application. *Resources Policy,* 25 (4), 257-264.

Abdel Sabour, S. A. (2001). Dynamics of threshold prices for optimal switches: the case of mining. *Resources Policy,* 27 (3), 209-214.

Abdel Sabour, S.A. and Poulin, R. (2006) Valuing real capital investments using the least-squares Monte Carlo method. *The Engineering Economist,* 51(2), 141-160.

Abdel Sabour, S.A., and Dimitrakopoulos, R. (2008). Mine plan selection under uncertainty. Mining Technology: *IMM Transactions Section A,* in press, 12 p.

Abdel Sabour, S.A., and Wood, G. (2008). Modeling financial risk in open pit mine projects: Implications for strategic decision-making. Accepted in Strategic vs Tactical Approaches in Mining 2008, Laval University, Quebec City, September 28-October 01, 2008, 156-165.

Achireko, P.K., and Ansong, G. (2000). Stochastic model of mineral prices incorporating neural network and regression analysis. *Trans. Instn. Min. Metall.* (Sect. A: Min. technol.) 109(January-April), A49-A54.

Barraquand, J., and Martineau, D. (1995). Numerical valuation of high dimensional multivariate American securities. *Journal of Financial and Quantitative Analysis*, 30(3), 383-405.

Black, F., and Scholes, M. (1973). The pricing of options and corporate liabilities. *Journal of Political Economy,* 81(3), 637- 654.

Boyle, P. (1977). Options: A Monte Carlo approach. *Journal of Financial Economics,* 4(3), 323–338.

Brennan, M.J. and Schwartz, E.S. (1977). The valuation of American put options. *Journal of Finance,* 32(2), 449–462.

Brennan, M.J. and Schwartz, E.S. (1985). Evaluating natural resource investments. *Journal of Business,* 58(2), pp. 135-157.

Broadie, M., and Glasserman, P. (1997). Pricing American-style securities using simulation. *Journal of Economic Dynamics and Control,* 21(8/9), 1323-1352.

Brunetti, C., and Gilbert, C.L. (1995). Metal price volatility, 1972-95. *Resources Policy.* 21(4), 237-254.

Carriere, J. (1996). Valuation of the early-exercise price for options using simulations and nonparametric regression. *Insurance: Mathematics and Economics,* 19(1), 19-30.

Cortazar, G., and Casassus, J. (1998). Optimal timing of a mine expansion: implementing a real options model. *The quarterly Review of Economics and Finance,* 38(3), 755-769.

Cox, J.C., Ross, S.A. and Rubinstein, M. (1979). Option pricing: a simplified approach. *Journal of Financial Economics,* 7(3), 229-263.

Davis, G.A. (1996). Using commodity price projections in mineral project valuation. *Mining Engineering*. (April), 67-70.

Dimitrakopoulos, R.G. and Abdel Sabour, S.A. (2007). Evaluating mine plans under uncertainty: Can the real options make a difference?. *Resources Policy,* 32, 116-125.

Dixit, A.K. and Pindyck, R.S. (1994). Investment under Uncertainty. Princeton University Press, New Jersey.

Frimpong, S., and Whiting, J.M. (1997). Derivative mine valuation: strategic investment decisions in competitive markets. *Resources Policy,* 23(4), 163-171.

Gentry, DW and O'Neil, TJ. (1984). *Mine investment analysis,* AIME, New York, USA

Grant, D., Vora, G., and Weeks, D. (1997). Path-dependent options: extending the Monte Carlo simulation approach. *Management Science,* 43(11), 1589-1602.

Hustrulid, W, and Kuchta, M. (2006). Open pit mine planning & design, Taylor & Francis plc., London, UK

Kamrad, B., and Ernst, R. (2001) An economic model for evaluating mining and manufacturing ventures with output yield uncertainty. *Operations Research,* 49(5), 690-699.

Keswani, A. and M.B. Shackleton. (2006). How real option disinvestment flexibility augments project NPV. *European Journal of Operational Research,* 168(1), 240–252.

Lemelin, B., Abdel Sabour, S.A., and Poulin, R. (2006). Valuing Mine 2 at Raglan using real options. *International Journal of Mining, Reclamation and Environment,* Volume 20, Number 1, 46-56.

Lemelin, B., Abdel Sabour, S.A., and Poulin, R. (2007). A flexible mine production model based on stochastic price simulations: application at Raglan mine, Canada. Mining Technology: *IMM Transactions Section A,* Volume 116, Number 4, 158-166.

Longstaff, F.A. and E.S. Schwartz. (2001). Valuing American options by simulation: A simple least-squares approach. *The Review of Financial Studies,* Vol. 14, No. 1, 113–147.

Mardones, J.L. (1993). Option valuation of real assets: application to a copper mine with operating flexibility. *Resources Policy,* 19(1), 51-65.

McDonald, R., and Siegal, D. (1986). The value of waiting to invest. *The Quarterly Journal of Economics,* 101(4), 707-727.

Moyen, N., M. Slade, and R. Uppal. (1996). Valuing risk and flexibility: A comparison of methods. *Resources Policy,* 22(1/2), 63–74.

Sagi, J. (2000). The interaction between quality control and production. In: Innovation and Strategy, Flexibility, Natural Resources and Foreign Investment: New Developments and Applications in Real Options, edited by L. Trigeorgis, Oxford University Press.

Samis, M., and Poulin, R. (1998). Valuing management flexibility: a basis to compare the standard DCF and MAP frameworks. *CIM Bulletin*, 91(1019), 69-74.

Samis, M.R., Laughton, D. and Poulin, R. (2001). Valuing a multi-zone mine as a real asset portfolio-a modern asset pricing (real options) approach. Available online at: http://ssrn.com/abstract=280801 (October 8, 2001).

Schwartz, E. S. (1997). The stochastic behaviour of commodity prices: implications for valuation and hedging. *Journal of Finance,* 52(3), 923-973.

Schwartz, E.S. (1977). The valuation of warrants: implementing a new approach. *Journal of Financial Economics*, 4(1), 79-93.

Smith, L.D. (1997). A critical examination of the methods and factors affecting the selection of an optimum production rate. *CIM Bulletin,* February, 48–54.

Taylor, HK. (1986). Rates of working of mines-a simple rule of thumb. *Trans. Instn. Min Metall*. (Sec.A: Min. industry) October, A203–A204.

Tilley, J.A. (1993). Valuing American options in a path simulation model. *Transaction of the Society of Actuaries,* 45, 83-104.

Torries, T.F. (1998). Evaluating mineral projects: *Applications and misconceptions,* SME, USA

Trigeorgis, L. (1990). A real options application in natural resource investments. *Advances in Futures and Options Research,* 4, 153-164.

Wells, H.M. (1978). Optimization of mining engineering design in mineral valuation. *Mining Engineering, December,* 1676–1684.

In: Gold Mining: Formation and Resource Estimation ISBN: 978-1-60741-096-6
Editors: M. D. Corral, J. L. Earle

Chapter 5

GOLD MINING IN GHANA

Benony K. Kortatsi[1] and Thomas M. Akabzaa[2]
[1] CSIR-Water Research Institute, P. O. Box M32, Accra, Ghana
[2] Geology Department, University of Ghana, P. O. Box Legon

ABSTRACT

Ghana is a major player in the gold mining industry globally and in Africa in particular. The country is ranked 11th in the global league of gold producers and the second, only after South Africa, in Africa. Ghana's gold bearing rocks are confined to five parallel bands of metavolcanic and metasedimentary rocks locally called gold belts. The most dominant of these belts is the Ashanti belt, which accounts for nearly 80% of the gold mines and 90% of total annual gold output. Four main kinds of gold deposits exist in these gold-bearing corridors. These are placer or alluvial deposit, which occurs along stream courses draining these corridors, and quartz reef (free milling); extracted mainly by gravity concentration; sulphide ores and the oxidised sulphide ore; both of which are extracted by heap-leach methods. Non-sulphidic paleoplacer (free milling) ore occurs mainly in the Banket conglomerates of the Tarkwaian Formation. The premier valued gold is associated with well sorted and packed hematite rich conglomerates that occur in the thinner beds. The oxidised ores, associated mainly with the Birimian rock formation, occur in the weathered rocks and are derived from sulphides, principally arsenopyrite,and pyrites and their primary derivatives are the sulphide ores etc. Two main types of mining operations exist- large scale and artisanal mining. The artisanal miners exploit mainly placer or alluvial gold. The chemistry of gold ores, type of mining and processing technologies employed, present considerable challenges to water resources management in these mining area. Almost all surface water bodies within the mining areas are polluted and aquatic life in most of them is extremely low or non existent. Significant number of streams and shallow wells has disappeared due to over abstraction of groundwater for gold processing and dewatering of mines. Acid mine drainage is also a major concern. Though groundwater contamination is not a major concern in the mining areas due to impoverishment of the rocks of heavy metals, isolated cases of high arsenic, mercury, iron, manganese and aluminium concentrations in groundwater are of major concern for drinking water supply. Gold mining has also resulted in severe land degradation and major environmental concerns.

INTRODUCTION

Ghana is major of important auriferous zones within the Birimian Rock System of the West African Craton and the country's colonial name "Gold Coast" is derived from this legacy. Gold mining in Ghana dates back about 700 hundred years ago, long before Europeans arrived at the end of the 15th century. However, written records have restricted the period to 130 years (Marston et al., 1992). It has been estimated that Ghana provided two-thirds of Africa's gold production between the late fifteenth and middle nineteenth centuries (Quashie et al., 1981). Before the onset of the Second World War, 35 gold mining companies were active in Ghana.

Ghana is still a major gold producer. From 1931 to 2007, Ghana produced 63,798,830 ounces or1984.5 metric tonnes of gold. In 2007, Ghana's gold output reached historic record of 2,628,290 ounces or 81.92 metric tonnes, consisting of production from nine large scale mines and several formal and informal small scale and artisanal producers (Minerals Commission, 2008). Currently the country is the second and tenth producer of gold in Africa and the world respectively.

Ghana's rising gold production is bolstered by a combination of policy reforms and surging prices of the commodity. Ghana since 1983 has been implementing policy reforms with the adoption of more investor-friendly new mining laws and ancillary legislation, providing regulatory and administrative frameworks to govern the sector (Songsore et al., 1994). A number of investors responded favourably to these reforms resulting in significant increases in foreign direct investment and associated influx of mining capital, technology and skills and resulting in remarkable increases in mineral production in the country. The rise in gold price in recent years has also generated a lot of mining activity in the gold mining areas of Ghana by both large scale miners and small-scale (legal as well as illegal) miners in almost all areas of rich gold deposits. Currently, mining contributes to nearly 5% of the GDP of Ghana and minerals comprise 37% of total export earnings with gold accounting for approximately 90% of the total mineral exports and thus making gold the focal point of mining and minerals development.

FORMS OF GOLD OCCURRENCE; MINING AND PROCESSING METHODS

Gold deposits in Ghana occur in five generic forms: primary vein deposits with accessory sulphide, disseminated sulphide ores, oxidised sulphide ores, paleoplacer deposits and recent placer deposits. The major difference between the sulphide ores and quartz-vein ores with respect to their ore mineralogy are: the quartz-vein ore contain visible "free gold", where as the former carry gold largely as submicroscopic inclusions in sulphide. The primary gold vein deposits are usually considered to be either hydrothermal or igneous-metamorphic (Hastings, 1983). The disseminated sulphide ores generally have sulphide content less than 20% (Hirdes and Leube, 1989; Milese et al., 1991) and are usually made up of sulphides of especially arsenopyrite but including pyrite and pyrrhotite, chalcopyrite and bornite, allabandite, ullmanite, gerdorffite,coellite, marcasite, rotle/tinatite/leucoxene, and a little galena and

sphalerite. The gold occurs in mechanical combination with the sulphide minerals and can be separated by straking and/or roasting and cyanidation (Mireku-Gyimah & Suglo, 1993).

Oxidized ores are those which have been concentrated by chemical and mechanical weathering of gold-bearing reefs and often occur close to the surface in residual subsoil above the water-table. They are derived principally from arsenopyrite, realgar (AsS), opiment (As_2S_3) and other sulphides. The gold is free-milling and generally fine and extracted by cyanide heap-leaching. Paleoplacer gold, also free milling, where it occurs is confined to the Tarkwaian rocks. The paleoplacers often contain fragments of Birimian rocks, and are considered to be derivatives of the primary gold vein deposits from the Birimian (Kesse, 1985). The gold here is usually concentrated in the more mature and better sorted matrix-poor gravel horizons. Hight payloads associated with hematite rich conglomeratic thin beds in the so-called "Banket" quartzitic conglomerates near the base of the Tarkwaian system. These ores are typically extracted by crushing, milling and cyanidazation.

Recent placer or alluvial deposits are found throughout areas underlain by rocks of the Birimian Super Group. They occur in riverbed and flats, in old and recent valleys and terraces of streams draining primary and secondary gold deposits (Acquah, 1992). These deposits are exploited by medium scale dredge companies, formalized small scale miners and illegal miners. Extraction is by gravity concentration and amalgamation. The various mining and procession methods as applicable in Ghana are listed in table 1 .

Table 1. Mining and processing methods used in gold mines in Ghana

Company/Mining/Activity	Treatment method	Geological Formation
Small Scale Mining/Artisanal mining (Licensed and unlicensed)	panning/sluicing/ mercury amalgamation of gold	Recent material and near-surface quartz reefs in Birimian rocks
Dredging		Recent materials in ancient and modern river channels
Dunkwa Goldfields	Amalgamation of concentrated gold from alluvial/river bed by dredging	
Bonte Gold		
Open Cast		
Ashanti Goldfield (Obuasi)	Carbon-in-leach(CIL)/ cyanide-heap leach of oxide and sulphide ores	Birimian metavolcanics and metasediments
AshantiGoldfields (Iduapriem)	CIL/ cyanide-heap leach of oxide and sulphide ores and heap leaching of pale placer ore	Birimian metavolcanics and Tarkwaian conglomerates
Goldfields (Tarkwa)	Cyanide Heap leaching	Tarkwaian conglomerate
Goldfields (Damang)	CIL/Cyanide Heap leaching	Tarkwaian conglomerate, phyllite, sandstones and dolerite intrusions
Golden Star Resources (Bogoso/Prestea)	Straking/roasting/Heap cyanidation/heap leach/CIL/Carbon-in-pulp (CIP)/ Bioxidation	Meta-volcanics of the Birimian System
Golden Star Resources (Wassa)		
Golden Star Resources (Prestea Underground	Straking/roasting/Heap cyanidation	Meta-volcanics of the Birimian
Ashanti Goldfield (Obuasi)	CIL/Cyanide Heap leaching and Straking/roasting	Meta-volcanics and meta sediments of the Birimian
Central Africa Gold (Bibiani Mine)	CIL/Cyanide Heap leaching	Meta-sediments of the Birimian

GEOLOGICAL SETTING OF AURIFEROUS AREAS

Primary gold bearing rocks are confined to the Birimian Supper Group which denotes supracrustal rocks of the West African Craton, which stabilised around 2.0 billion years ago (Wright et al., 1985). These supracrustal rocks comprise thick sequences of metamorphosed sediments and volcanics called the Birimian System, and much smaller and scattered shallow water sediments called the Takwaian System (table 2). These rocks occur in parts of Ghana, Cote d'Ivoire, Burkina Faso, Guinea, Mali, Liberia and Niger dominating the eastern and northern portions of the craton and host all major gold mines in West Africa. Gold mineralization in the Birimian is essentially in the form of auriferous quartz veins of reefs and also as sulphide ore, while mineralisaiton in the Tarkwaian Formation is found in association with argillaceous sediments, blanket reefs or conglomerate beds, analogous to those of the Witwatersrand in South Africa.

Recent structural data suggest the Birimian rocks and the overlying Tarkwaian sediments were jointly deformed in a single progressive deformation event. This event resulted in extensive folding around a sub-horizontal gently plunging axis. The deformation appears more intense in the Birimian rocks than Tarkwaian rocks. According to Eisenlohr and Hirdes, (1992) regional metamorphism of these rocks does not exceed the greenschist facies. Because of its growing metallogenic potential, the Birimian Super Group has received considerable attention, particularly in the last two decades, as results of increased mineral exploration efforts in the West African region (Wright et al., 1985; Taylor et al., 1988; Leube et al., 1990; Eisenlohr and Hirdes, 1992).

THE BIRIMIAN

The Birimian System, dated around 2.2 to 2.3 Ga (Taylor et al., 1988; Melisi et al., 1992), was deposited on an Archean basement with unknown age. In traditional Ghanaian literature (Junner, 1935; Kesse 1985), the Birimian System consists of two distinct lithological associations generally referred to as the Lower and Upper Birimian, unconformably overlain by the Tarkwaian System and intruded by a variety of granitic suites.

The Birimian System accounts for more than 70 % of gold production in Ghana hosting all but two of all operating large scale gold mines in the country. According to Kesse (1985), vein and lode-type gold ores occur in five distinct forms: as auriferous quartz veins which cut the Birimian System; as veins and stockworks in granite porphyries which intrude the Birimian system; as sulphide ore which have been arisen through mineralisation of the country rocks in the Birimian system; as oxidised ores which have been concentrated by chemical and mechanical weathering of gold-bearing veins; as pegmatite dykes associated with the granitic rocks in the Birimian System.

The Lower Birimian is lithologically defined as a predominantly meta sedimentary unit consisting of argillaceous rocks, tuffs and greywacke. It exhibits foliation planes and has been extensively intruded by Cape Coast type or "G1" granitic batholiths. The Upper Birimian is dominated, however by meta-volcanics and pyroclastic rocks and intruded by Dixcove-type or "G2" granitic rocks (Kesse, 1985; Leube et al., 1990).

On the regional scale, there is no consensus on the stratigraphic positions of the two units of the Birimian and the associated Tarkwaian rocks. Francophone geologists consider what is termed Upper Birimian in Ghana as either older than or largely contemporaneous with the so-called Lower Birimian in Ghana (Wright et al., 1985; Eisenloiir and Hirdes, 1992). Recent workers on the Birimian System (Hirdes et al., 1992; Davis et al., 1994; and Sylvester and Attoh, 1992), albeit some differences, appear to broadly agree on the stratigraphy following the works of Leube et al. (1990). On the basis of isotopic and regional geological and structural studies, the Birimian is now interpreted to consist of NNE-SSW trending alternations of coeval parallel sequences of volcanic and sedimentary/volcanoclastic assemblages called "belts" and "basins", respectively. Both volcanic belts and sedimentary basins are intruded by early to late-kinematic granitoids (Taylor et al., 1988; Leube et al., 1990; Eisenlohr and Hirdes, 1992; Hirdes et al., 1992).

The belt rocks consist of basaltic flows, andesitic to dacitic pyroclastic rocks and lavas, volcanogenic turbidites and manganiferous chert that have been metamorphosed to greenschist facies and intruded by early kinematic granitoids. The basin rocks comprise fragmental felsic rocks, flysch-type turbidites metamorphosed to amphibolite facies rocks that are intruded by large concordant peraluminous granitoids (Sylvester and Attoh, 1996).

Generally, there is widespread manganiferous horizons found at various stratigraphic levels within the Birimian rocks. Bands of quartz-spessartite rock-gondite-and manganiferous phyllites occur towards the top of Upper Birimian, commonly associated with tuffs and silicified argillites and chert. Manganese rich horizons also occur at stratigraphically lower levels in the Upper Birimian and have been found in uppermost Lower Birimian as well. There is a spatial relationship between manganese and gold occurrences on a regional scale. Manganese is also predominantly bound to the flanks of volcanic belts. In addition to the Manganese and gold, the belt/basin transitional zones are characterised by the presence of other chemical sediments, namely chert, Fe-Ca-Mg carbonates, sulphides and rocks rich in elemental chemical constituents (Hirdes &Leube, 1989).

The rocks are generally characterized by isoclinals folds, with a steeply dipping foliation of 70 -90^{o} that is generally parallel to lithological layering. Fractures and faults are both parallel and perpendicular to the strike of foliation. Metamorphic grades range from greenshit to almandine-amphibolite facies in these rocks, which are also important sources of diamonds and manganese (Wright et al., 1985).

THE TARKWAIAN

The Tarkwaian System, aged 2,131-2,095 Ma, is made up of a sequence of clastic sedimentary rocks, which comprise sandstones, conglomerates and phyllites. It has spatial association with 'belt' rocks of the Birimian. The Tarkwaian currently host two active mines which account for about 30% of Ghana's gold output. It is regarded as detritus of Birimian rocks and granitoids that were uplifted and eroded in the Eburnean event (Eisenlohr and Hirdes, 1992). This assertion, supported by Kesse (1985) and Leube, et al., (1990), is due largely to the preponderance of volcanic and sedimentary pebble clasts in the conglomerates of the Tarkwaian which are reminiscent of Birimian rocks. The rocks are metamorphosed

paleo-sedimentary beds that lie unconformably on the Birimian and are comprised of the Kawere, Banket, Tarkwa phyllite and Huni series (figure 1).

The Kawere is made up of repeated sequence of polymictic, poorly-sorted matrix-supported conglomerates grading up through immature pebbly quartzites to cross-bedded feldspathic rocks, quartz and granitic material.

The Kawere is overlain by the Banket series which is the gold bearing strata in the Tarkwaian. It comprises three units:

i a conglomerate bed at its base known as the Basal or Main Reef, made up of beds of quartz-pebble conglomerates interbedded with quartzites.
ii the Middle Reef comprising a series of conglomerates and breccia and
iii an Upper Breccia series with cross bedded seams which occur throughout the series, particularly in the coarse members.

This is, in turn overlain by the Tarkwa phyllite consisting of a series of metamorphosed siltstones and mudstones. The Tarkwa phyllite is capped by the Huni series consisting of a sequence of parallel-laminated and cross-bedded, medium grained, feldspathic quarzites with intercalations of Dompim Phyllite.

Structurally, the Tarkwaian in most place has a synclinal structure defined by two deformation domains; a high strain southwestern domain and a low strain southeastern domain. The high strain domain has a penetrative NE trending foliation and a SW plunging lineation associated with the overturned SE verging steep structures and reverse faulting. On the other hand, the low strain domain has zones exhibiting gentler open folds with low bedding dips. In some places minor faulting alternate with zones of tighter folding with steeply NW-dipping to recumbent axial planes (Smith, 2001).

Table 2. Stratigraphy of the Birimian Supper Group

Formation/Series	Approximate Thickness (m)	Composite lithology
Quartz/pyrites/tourmaline veins Intrusive dolerite, felsite, porphyry and granitoids		
TARKWAIAN SYSTEM		
Huni Sandstone and Dompim Phyllite	1370	Sandstones, grits and fine-grained feldspathic quartzites with bands of phyllites.
Tarkwa Phyllites	120-400	Huni sandstone transitional beds and green and greenish grey chloritic and sericitic phyllites and schists. Chloritoid-magnetite-carbonate.
Banket Series	120-600	Tarkwa phyllite transitional beds and sandstones, quartzites, grits, breccias and conglomerates.
Kawere Group	250-700	Quartzites, grits and phyllites and conglomerates.
Angular		Unconformity
Birimian	4,500-8000	Meta-volcanics, volcaniclastics and sediments
After Junner et al., 1942)		

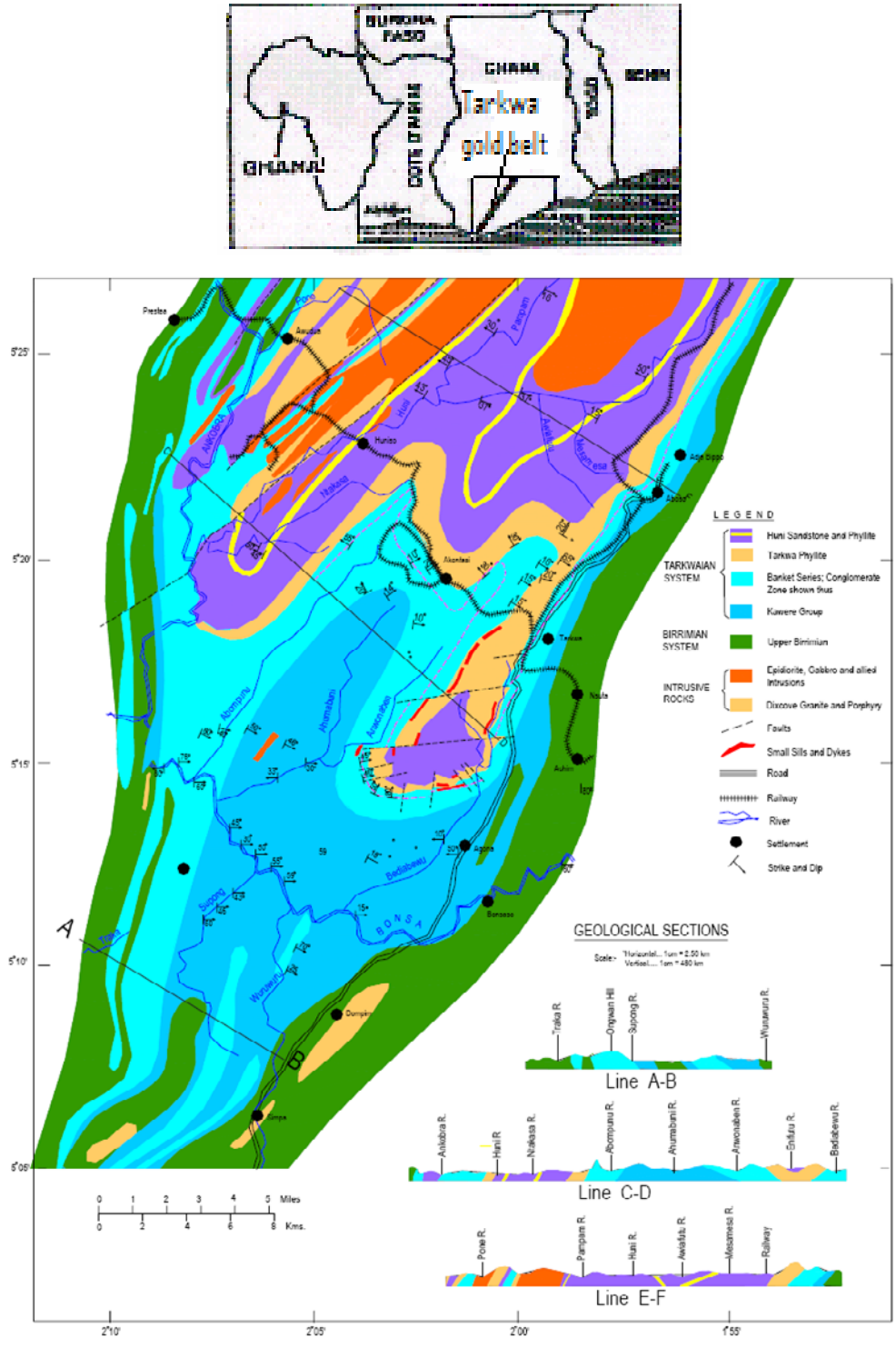

Figure 1. Geological map of the study area showing the Birimian and the Tarkwaian systems (After Junner et al., 1942).

ARTISANAL MINING

Artisanal mining comprised formalised small-scale mining and unregistered small scale (illegal) mining also known as galamsey operations. These groups operate in areas of the country occupied by Birimian and Tarkwaian rocks. They are largely in areas unoccupied by large scale miners, however, others encroach on properties of large scale mining companies. They exploit placer deposits along most of the rivers and streams draining the country's Birmian and Tarkwaian rocks, on crests of reefs and on detritus.

Panning is the dominant technique used by artisanal miners for extracting gold from placer ore using the density contrast between the gold and the gangue material. Usually the mined ore is placed in a large metal or plastic pan, combined with an adequate quantity of water, and agitated so that the gold particles, being of higher density than the other material, settle to the bottom of the pan (Figure 2). The lighter waste material such as sand, mud and gravel are then washed over the side of the pan, leaving the gold behind. The same principle may be employed on a larger scale by constructing a short sluice box, with barriers along the bottom to trap the heavier gold particles as water washes them and the other material along the box. This method better suits excavation with shovels or similar implements to feed ore into the device.

Figure 2: Small-scale (galamsey) operation at Aboso near Tarkwa

Mercury has played an important role in the processing of gold ores in Ghana. Gold processing using mercury involves a process known generally as amalgamation. The process involves dressing a sheet of metal with a thin layer or coat of liquid mercury. A mixture of powdered rock containing gold is passed over the plate. The particles of gold adhere to the

mercury on the plate to form the gold-mercury amalgam while the waste rock powder washes away. The mercury is then evaporated and the gold recovered. However, mercury amalgamation is inefficient and only approximately 60 percent of the gold in the ore can be recovered (Carlos et al, 1997). It is against this background that the more efficient cyanide leaching method is preferred by the major gold mining companies operating in Ghana. Nonetheless, because it requires little capital investment in equipment, mercury amalgamation is still widely used by the small-scale miners and the galamsey operators in Ghana particularly in the Tarkwa-Prestea area.

Major problems include destruction of arable land and virgin forest and pollution of surface water bodies, largely from mercury use. The miners use panning and sluicing techniques to win alluvial gold found in recent and unconsolidated sediments and reefs along the rivers.

In dredge mining, medium size companies employ dredging technology to mine alluvial gold in recent and unconsolidated sediments along three major rivers, mostly in gravel sections-the Offin River, Bonte River and the Birim River in the Ashanti, Western and Eastern Regions respectively. The ore treatment method involves the screening of the loose material to get rid of the coarse pebbles and gravity concentration in three stages by means of jugs (primary, secondary and tertiary). This is followed by amalgamation of the concentrated gold with mercury contained in a mercury-silver trap. The mines employed bulldozers, scrappers and front-end loaders to clear the topsoil. The overburden is then stripped by a caterpillar backhoe excavator. The stripped material is transported by dump trucks to mine-out areas behind the floating wash-plant for use in reclamation and restoration. The loose auriferous layer is excavated by caterpillar backhoe excavator, which feeds the material directly into a wash plant that floats on a pontoon. The loose material is screened to remove coarse pebbles and then undergoes gravity concentration in stages (primary, secondary and tertiary. This is followed by amalgamation of the gold. The oversize particles and the tailings from the various stages of screening and jigging on the wash plant are discharged.

ENVIRONMENTAL CHALLENGES OF MINING IN GHANA

In spite of its significant role on economic development of Ghana, mining has been causing some major environmental problems. The problems are even more exacerbated in the mining area due to the intensity of the mining activities as a result of increases in world gold price, lack of interest in farming and lack of alternative job opportunities in the area among others. These coupled with decades of total neglect in enforcing mining code and regulations and the upsurge of small-scale mining (mostly illegal miners) operations in almost all areas of rich gold deposits have resulted in the most widespread problems include land degradation, land instability, destruction of farm lands and contamination/pollution of water bodies particularly with mercury and other toxic trace metals. High levels of pollutants including toxic elements such as arsenic, lead, cadmium and mercury were reported in the Ankobra and the Pra Rivers whose drainage basins include the major mining areas of Ghana (WRRI, 1986) resulting in the demand for clean drinking water, being of primary concern in these gold mining area.

LAND DEGRADATION

Surface mining in Ghana involves land preparation. For instance, large tracks of land are cleared to make way for mining and construction of waste dumps and heap leach sites. In the process whole villages have been displaced and many farm lands have been destroyed. Also destroyed or bulldozed are many important trees species, thus depriving the environment of its flora and fauna (figure 3). Additionally, top soils are being removed from hills and entire slopes enhancing erosion and exposing the rock to the weather. These rocks contain sulphides, which are oxidized to generate acid drainage and often run off into streams and rivers or seep through permeable hill fronts to recharge aquifers.

Another major environmental problem similar to land degradation is land instability. The instability of the land is as a result of the blasting of gold bearing rocks using dynamites to loosen them for conveyance to crushers en route to heap leach site. In the process, shock (p or seismic) waves are generated in the earth that create instability in the earth within the vicinity of the blasts. The instability causes cracks in buildings in villages and towns within the sphere of influence of the seismic wave. Approximately 40% of buildings at both Bogoso and Prestea have developed mega cracks as a result of continuous blasting in the mines nearby. The blasting has not only caused cracks in buildings alone, but also in sanitation facilities such as septic tanks resulting in their leakages. Another associated problem with the blasting is heavy noise created by the dynamite as well as heavy vehicular presence. These vehicles are used for carting of rock materials to heap leach sites and waste -dumps. The noise these vehicles make is often a time deafening.

Figure 3. Large stretch of cleared land at Tarkwa in readiness for surface mining operation.

DEPLETION OF WATER BODIES

Mining requires a lot of water for processing and communities including the miners need good quality water for drinking and for other domestic uses. Realizing that most of the surface water resources are already polluted or presumed polluted by mining activities, groundwater water resources are heavily relied upon for both domestic use and for processing of gold in particular and minerals in general. However, the mining areas being crystalline have aquifers, which are limited in extent making groundwater resources in the mining areas are relatively scarce. Nonetheless, adequate groundwater has been obtained for domestic use.

However, due to over pumping of wells in the mines for mineral processing and dewatering, surface and groundwater levels have been depleted. Some streams which were hitherto perennial have become ephemeral; shallow wells dry up completely or drastically reduce in yield leading to very long queues at water points. Additionally, the migration of people to the mining areas have swelled up the population putting enormous pressure on the already overstressed infrastructure. Thus one can see very long queues of children and women at well points (figure 4).

Figure 4. Queue of children waiting patiently to fetch water at a borehole point.

POLLUTION OF WATER BODIES

Mining can influence the quality of water in four major ways. These include generation of acid mine drainage that can contaminate groundwater and making it unfit for drinking. A second source of influence of mining activities is the release of trace metals in unacceptable proportions into the water bodies thereby rendering the water supplies potentially dangerous

for potability. A third source of impact is groundwater salinisation. Deep mining may encounter stagnant and connate or fossil waters that may be of very high salinity that can contaminate fresh groundwater and make its potability doubtful. The fourth source of impact of mining on water resources is contamination from chemical agents used in the recovery of minerals such as gold. The chemical agents, even in minor concentrations, are often highly toxic to all sources of life (Carlos et al., 1997). Thus residues left over or a spill during usage may find their way into groundwater system and render the water physiologically dangerous.

ACID MINE DRAINAGE

Mineral compounds and metals generally exist in an oxygen free or anaerobic environment and in a reduced state below the ground surface. Mining, whether surface or underground, unearths these mineral or metal deposits and exposes them to the weather. Similarly, fresh rocks and minerals in anaerobic environment underground may be exposed to oxygen through the mineshaft and adits during mining. When exposed, sulphides particularly iron sulphides such as pyrite [FeS], chalcopyrite [$CuFeS_2$] and arsenopyrite [FeAsS]) react with water and oxygen to produce sulphuric acid (H_2SO_4) leading to the generation of acid mine drainage (Banks et al, 1997). Generation of acid mine drainage is not only limited to iron sulphides alone, but other metallic sulphides as well. The greatest amount of acid mine drainage, however, is generated by iron sulphides. Major minerals that are associated with the production of acid mine drainage (AMD) are presented in table 3. The drainage running off the mine site or sulphide rocks exposed by mining may flow into streams or infiltrate through subsurface materials into the groundwater system making the once-clean groundwater unfit for life.

Table 3: Major minerals associated with acid mine drainage (AMD) with those that occur in the mining areas in Ghana printed in italic

Mineral	Composition
Arsenopyrite	*FeS_2.FeAs, FeAsS*
Bornite	$CuFeS_4$
Bournonite	*$PbCuSbS_3$*
Chalcocite	Cu_2S
Chalcopyrite	*$CuFeS_2$*
Covellite	CuS
Galena	*PbS*
Millerite	NiS
Mobybdenite	MoS_2
Pyrite	*FeS_2*
Pyrrhhdite	$Fe_{11}S_{12}$
Sphalerite	*ZnS*
Tennalite	[(Cu, Fe, Zn,) As_4S)]

After Gray, 1997.

The overall process of pyrite oxidation that lead to acid mine drainage (AMD) may be described as in equation (1)

$$4\,FeS_{2(s)} + 15O_2 + 14H_2O = 4Fe(OH)_{3(s)} + 8SO_4^{2-} + 16H^+(aq) \quad (1)$$

Depending on the pH value, this reaction takes place in different ways (Iribar et al., 2000). The process of pyrite oxidation is mostly inorganic in a neutral pH environment, and the reaction in equation (1) often proceeds in two steps (Appelo and Postma 1999). Initially, the polysulphide is oxidised to sulphate by O_2 as in equation (2)

$$2FeS_{2(s)} + 7O_2 + 2H_2O = 2Fe^{2+} + 4SO_4^{2-} + 4H^+ \quad (2)$$

Pyrite + Oxygen + Water = Ferrous Iron + Sulphate + Proton (acid)
Subsequently, Fe^{2+} is partially oxidised to Fe^{3+} consuming protons

$$4Fe^{2+} + O_2 + 4H^+(aq) = 4\,Fe^{3+} + 2H_2O \quad (3)$$

Additional pyrite oxidation may take place where Fe^{3+} acts as an electron acceptor (equation 4) (Appelo and Postma 1999). Hydrolysis may also occur leading to the formation of amorphous $Fe(OH)_{3(s)}$ as in equation (5) (Banks et al., 1997). Both processes lead to the production of additional protons (acidity)

$$FeS_{2(s)} + 14Fe^{3+} + 8H_2O = 15Fe^{2+} + 2SO_4^{2-} + 16H^+ \quad (4)$$

$$Fe^{3+} + 3H_2O = Fe(OH)_{3(s)} + 3H^+ \quad (aq.) \quad (5)$$

Similar to the oxidation of pyrite, the oxidation of arsenopyrite by oxygen may be described by the well-known equation (6). This also leads to the production of protons.

$$4FeAsS + 13O_2 + 6H_2O = 4Fe^{2+} + 4AsO_4^{3-} + 4SO_4^{2-} + 12H^+(aq.) \quad (6)$$

Other sulphide minerals oxidise similarly to produce trace metals and sulphate. It is not all sulphide minerals that oxidise to produce protons or acidity by themselves. For example sphalerite (ZnS), as in equation (7), does not oxidise to produce protons or acidity. However, the subsequent hydrolysis as given in equation (8) does (Banks et al., 1997).

$$ZnS + 2O_2 = Zn^{2+} + SO_4^{2-} \quad (7)$$

$$Zn^{2+} + 2H_2O = Zn(OH)_2 + 2H^+ \quad (8)$$

Though several natural processes including weathering usually expose fresh sulphide rocks to the air and water (eg rain) and therefore chemical reactions can produce acid mine drainage even where there is no mining, mining dramatically accelerates the process of acid generation. This is because it breaks open the subsurface and exposes large volumes of fresh sulphide rocks to the atmosphere in a relatively short time. Furthermore, by crushing rocks for the extraction of gold the surface area of the rock is being increased and therefore the potential for acid generation is increased. Additionally, finely ground sulphide bearing

tailings left over from gold ore beneficiation processes can also be a major source of acid mine drainage.

In Ghana, though acid mine drainage is mainly associated with small streams in the vicinity of mine concession, pH values less than 4 are usually realized. Acid mine drainage is not a major problem with regards to groundwater in gold mining areas in Ghana because of the high acid neutralizing capacity (ANC) of aquifers in the mining areas. High acid neutralising capacity is either provided by the carbonate species or alluminosilicates within the geological formations. According to Grimvall et al. (1986), several natural neutralizing reactions will consume large quantities of hydrogen ions before any changes in pH can be observed. Carbonate weathering would normally give rise to pH >6; while silicate and alumino-silicate buffering would give rise to 5.0≤ pH ≤6.0. Similarly, cation exchange (exchange involving H^+, Na^+, Ca^{2+}. etc.) reactions would give 4.0≤ pH ≤5.0 while metal buffering (dissolution of metal hydroxides) would give pH >4.0 (Grimvall et al., 1986). Groundwater pH values in the mining areas in Ghana are generally within the range 5.6- 6.9. However a few isolated localities exist where the pH is below 5.

TRACE METAL POLLUTION

A second kind of impact of mining activities on water quality in a mining area in Ghana is pollution by toxic trace metals. Trace metals are dissolved metallic elements that occur or can be present in water bodies, often at concentrations well below 0.1 mg l^{-1}, but occasionally much higher (Freeze and Cherry, 1979). Prior to mining, trace metals are locked in rocks underground and are mostly in the reduced state (Carlos et al., 1997). During mining, the rocks are unearthed and the metals set free as wind blows over soil and returns to earth in rain or as dry fallout. Furthermore, the metals can be set free through the dissolution of rocks by CO_2 charged water or acid mine drainage and can spread through the environment particularly water bodies in dangerous concentrations that can have adverse impact on human health.

Statistical summary of chemical parameters determined in 148 groundwater samples from the studied area is presented in table 4. It can be seen from the table that the analytical results have not revealed the trace metal loadings initially anticipated of a mining area. The average chemical composition of the Birimian rocks from the Bogoso area is presented in table 5. Although, sulphide ores that form significant portion of the Birimian rocks are known to be associated with high trace metal concentration, the Birimian rocks ores are only low to medium in trace metal contents. Trace metals that occur in relatively high concentration in the rocks include aluminium, arsenic, barium, iron and manganese. Generally trace metal content of groundwater in the Tarkwaian area is low and may also be attributed to the fact that the rocks of the Tarkwaian formation (table 6) especially those containing the gold ores, are devoid of most trace metals (Marston et al., 1992). As a result, the trace metals concentrations in the boreholes and wells also follow the same trend. Only aluminium, arsenic, barium, iron, manganese, and nickel have concentrations significantly above the background values in a few of the boreholes and wells in the gold mining areas.

Aluminium (Al) is the third most common element in the earth's crust and is widely distributed in nature and is thus a constituent of all soils, plants and animal tissues (Monier-

Williams, 1935). The main pathways that aluminium generally enters water systems are industrial wastes, erosion, dissolution of minerals and soils, contamination from atmospheric dust and precipitation. The concentration of Al in water is controlled by the pH, the type and concentration of complexing agents that may be present, the oxidation state of the mineral components, and the redox potential of the system (WHO, 1984).

Table 4. Statistical summary of chemical parameters determined in 148 groundwater samples. Temp. in ^{o}C, pH in pH-units, EC in µS cm^{-1}, Ca to Al in mg l^{-1}, As to Zn in µg l^{-1}

	Detection limit	Min	Max	Mean	Median	STD	WHO (2004) Guideline limit
Temp		22.1	29.3	25.8	26.0	1.3	
pH		3.9	7.0	5.9	5.9	0.6	
Cond		37.3	956.0	168.2	124.0	139.3	
Ca	0.01	0.3	87.3	11.6	6.6	15.2	
Mg	0.01	0.1	77.1	5.2	3.6	8.9	
Na	0.1	2.2	71.3	12.8	10.8	8.4	200
K	0.01	0.0	19.2	1.6	0.8	2.5	
HCO3	0.1	0.1	258.0	67.0	51.5	55.7	
SO4	0.2	0.1	507.0	10.5	0.8	57.4	250
Cl	0.1	2.0	43.0	8.1	6.2	6.6	250
NO3	0.2	0.2	21.9	1.4	0.2	3.3	50
Si	0.1	3.6	39.4	17.0	14.0	9.7	
F	0.05	0.01	11.10	0.20	0.07	1.08	1.5
Fe $_{(total)}$	0.003	<0.003	16.800	1.276	0.233	2.529	0.3
Al	0.1	0.02	2.39	0.10	0.02	0.34	0.2
As	0.05	0.00	64.00	8.79	1.55	15.65	10
B	0.5	6.00	118.00	8.52	6.00	11.31	300
Ba	0.04	1.00	502.00	40.82	17.50	75.63	700
Cd	0.02	<0.02	7.2	0.1	0.02	0.2	3
Cr	0.2	<0.2	205.4	2.7	2.7	1.2	50
Cu	0.04	4.00	62.00	8.12	4.00	9.59	2000
Hg	0.05	<0.05	3.85	0.18	0.05	1.8	1
Mo	0.03	<0.03	4.6	0.1	0.03	0.1	70
Mn	0.02	1.00	1020.00	116.97	52.05	155.75	500
Ni	0.06	<0.06	746.1	9.8	7.28	10.3	20
Pb	0.03	0.56	167.5	2.2	1.33	3.2	10
Rb	0.01	<0.01	47.4	0.6	0.33	0.9	
Sb	0.025	<0.05	7.2	0.1	0.05	0.3	5
Se	0.5	<0.5	254.6	3.4	1	4.2	10
Sn	0.05	<0.05	4.1	<0.06	0.05	0.3	
Sr	0.1	4.00	546.00	116.41	63.00	123.89	
Th	0.02	<0.02	1.4	<0.02	0.02	0.	
U	0.01	<0.01	0.9	<0.01	0.01	0.07	
V	0.02	<0.02	0.88	0.33	0.18	0.26	
Zn	0.1	4.00	1500.00	47.28	12.00	151.91	3000

Table 5. Summary of analyses of metals in waste rocks from the Bogoso mines (Birimian rocks)

No	Ag	Al	As	Ba	Be	Ca	Cd	Co	Cr	Cu	Fe	K	Mg	Mn	Mo	Na	Ni	Pb	Sb	Se	Sn	Te	Zn
	Mg /g	Mg/g	Mg/g	µg/g	Mg/g	mg/g	µg/g	mg/g	µg/g	µg/g	mg/g	mg/g	mg/g	mg/g	µg/g	Mg/g	µg/g	µg/g	µg /g	µg/g	µg/g	µg/g	µg/g
MEAN	<0.5	74.8	1.2	516.1	1.6	5.8	1.1	20.1	105.0	126.0	46.9	20.0	10.3	1.2	<0.5	10.5	18.1	9.1	<70	<20	<20	<50	90.7
MEDIAN	<0.5	80.8	0.3	545.0	1.5	1.6	0.8	19.0	95.0	67.0	47.0	18.0	8.0	0.6	<0.5	8.5	0.1	8.0	<70	<20	<20	<50	88.5
MAXIMUM	<0.5	130.0	18.0	910.0	4.9	61.0	4.0	110.0	250.0	3410.0	140.0	61.0	71.0	26.0	<0.5	41.0	110.0	23.0	<70	<20	<20	<50	220.0
MINIMUM	<0.5	1.1	0.0	5.4	0.5	0.2	0.6	0.0	18.0	1.2	7.5	0.2	0.1	0.0	<0.5	0.3	0.0	1.0	<70	<20	<20	<50	13.0
MODE	<0.5	100.0	0.3	540.0	1.2	0.6	0.7	0.0	10.0	110.0	47.0	18.0	11.0	0.7	<0.5	8.5	0.1	6.0	<70	<20	<20	<50	110.0

Table 6. Partial ICP analyses of composite tailing samples from Abosso Mine (Tarkwaian rocks)

No	Al (ppm)	As (ppm)	Ba (ppm)	Ca (ppm)	Cr (ppm)	Cu (ppm)	Fe (%)	Mg (ppm)	Mn (ppm)	Ni (ppm)	Pb (ppm)	S (ppm)	Ti (ppm)	V (ppm)	Zn (ppm)
1	689	130	30	308	62	74	3.39	Bld	494	Bld	187	204	581	72	Bld
2	802	Bdl	47	520	74	44	4.01	209	666	Bld	Bld	517	677	87	Bld
3	583	Bdl	39	265	81	115	4.66	Bld	545	Bld	202	Bld	837	100	Bld
4	772	Bdl	48	480	54	58	3.21	198	530	116	310	198	557	67	85
5	523	Bdl	41	202	56	Bld	3.27	Bld	499	73	212	168	584	64	Bld
6	674	Bdl	46	613	51	Bld	3.31	192	632	68	Bld	Bld	575	67	50
7	820	Bdl	54	1050	64	44	3.54	344	771	Bld	Bld	430	571	72	79

Bdl=below detection limit for elements as follows (in ppm): As=100; Mg=100; Ni=60; Pb=200; S=160; Zn=40. The following elements were also reported as being below the indicated detection limits (in ppm): B=40; Be=0; Bi=200; Cd=20; Co=20; K=600; Li=12; Mo=10; Na=200; P=120 (except sample no 5, P=126) Sb=400; Se=400; Sn=40; Te=200; Zr=40. All analyses by INCO Ltd, Sudbury, Canada, of aqua regia digests.

In many gold mining areas in Ghana, Al ion concentration in groundwater is in the range 0.0-2.5 mg l^{-1} with a mean of 0.19 mg l^{-1}. As expected, the high Al concentrations are associated with boreholes with lower pH values. For instance, one borehole at Dumasi close to Bogoso with identification number 44-I-45-4 has the lowest mean pH value of 3.89 and the highest concentration of Al of 2.51 mg l^{-1}.

Similarly at Tamso in the vicinity of Tarkwa, a borehole (20-I-89-1) has a mean pH and Al ion concentration of 3.94 and 1.28 mg l^{-1} respectively. Figure 5. illustrates the temporal variation in Al ion concentration ingroundwater in the gold mining district of the Tarkwa-Prestea

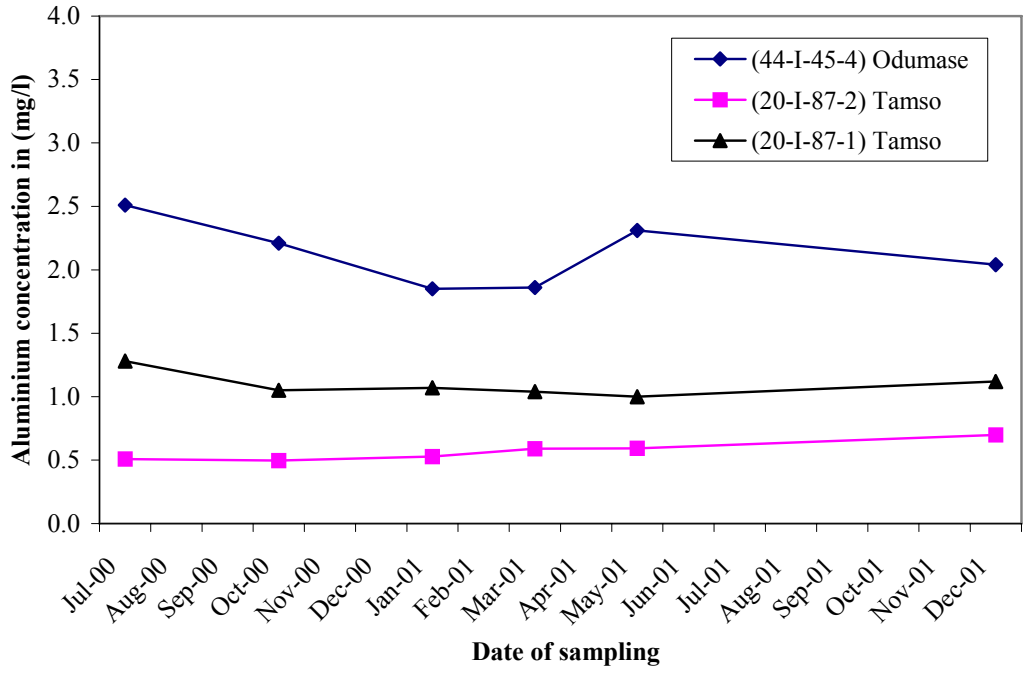

Figure 5: Temporal variation in Al^{3+} concentration in selected boreholes in the Tarkwa-Prestea area of Ghana.

Generally, aluminium (Al^{3+}) appears to have only little deleterious effect on humans. Nonetheless, aluminium toxicity has been associated with central nervous system disorders including Alzheimer's disease and dialysis dementia (Moskowitz et al., 1986). However, the greatest problem associated with the metal is the incidence of discolouration it produces in drinking water and its distribution systems that increases when aluminum concentration exceeds 0.2 mg l^{-1} in water and makes the water aesthetically unacceptable (WHO, 2004).

The aluminum concentration in groundwater within the Preastea areas of Ghana appears to pose major quality problem to borehole water supply since approximately 20% of the boreholes have Al^{3+} concentration exceeding the WHO (2004) maximum acceptable limit for water potability. Similarly, Smedley et al. (1995) observed that the Al^{3+} concentration exceeded the WHO (2004) guideline limit for potable water in 10% of the domestic wells around Obuasi, also a major gold mining area about 100 km to the north-east of the Tarkwa-Prestea area.

The primary sources of As contamination in the environment are metal smelting, chemical manufacturing, pesticide application and coal combustion (Diaz-Barringa et al., 1993; Lagerkvist and Zetterlund, 1994). Arsenic (As) occurs naturally in many types of rocks, especially shales, phosphorites, and sulphide ores that also contain iron, manganese, copper and lead. Nonetheless, the highest concentrations of arsenic is found in sulphide minerals particularly arsenopyrite (FeAsS), realgar (AsS) and orpiment (As_2S_3) (Hounslow, 1995). Therefore, terrain rich in sulphide minerals such as the Birimian rock area can have high concentration of arsenic (As) in both surface and ground waters as a result of sulphide oxidation and solution. For instance, Tseng et al. (1968) measured As concentration of 1.8 mg l^{-1} in water samples from artesian wells in sulphide-rich black shales from south-west Taiwan. Since sulphides oxidation can take place without mining, arsenic can enter the groundwater system irrespective of whether mining has taken place or not once oxidation and solution have taken place. However, since mining unearth large volumes of sulphide minerals, mining is thus responsible for arsenic in groundwater in mining areas than the natural oxidation process.

In Ghana, coal combustion and pesticide applications in the mining areas are very rare while chemical manufacturing is non-existent. Therefore, the moderate Arsenic levels as observed in the water are as a result of mining and/or smelting of sulphide ore. Consistent with the geology, high arsenic concentrations occur in groundwater mainly in areas underlain by Birimian rocks around Bogoso-Prestea area and Ashanti goldfields where the highest concentration of approximately 64 μg l^{-1} was measured. Groundwater in areas underlain by Tarkwaian rocks is almost devoid of arsenic. Generally, however, the concentration of As in the shallow groundwater is very low and varies from 0.0 mg l^{-1} to 0.064 mg l^{-1} with a mean value of 0.003 mg l^{-1}. Approximately 20% of the shallow (<100 m) wells and boreholes have arsenic concentration slightly in excess of the WHO (2004) guideline limit of 0.01 mg l^{-1} through out the mining areas of Ghana. These wells are mainly located in the neighbourhood of Bogoso in Birimian rocks.

On the contrary, some of the surface waters (creeks) draining or emanating from the waste rocks have relatively high levels of arsenic concentration (table 7).

The very low concentration of arsenic in the shallow groundwater in spite of the high presence of arsenopyrite in association with the gold ore suggests a level of co-precipitation of arsenic with ferric oxyhydroxide in the creeks before possible infiltration into the aquifer. Similar observations were made in the Ashanti goldfields area where As concentration in streams with concentration up to 350 μg l^{-1} far exceeded that of groundwater (highest concentration 64 μg l^{-1}). The explanation given was that it was not likely the stream water As was derived from the bedrock. Since the prevailing wind direction was towards the north, the high stream water values result from airborne pollution derived from the PTP chimney stack in Obuasi (Smedley et al., 1995). This again suggests the influence of mining on groundwater.

Table 7: Summary of chemical characteristics of surface water samples from the Bogoso mines in the Tarkwa –Prestea area

	Location	pH	EC.	Al	As	Ca	Co	Cu	Fe	Mg	Na	Ni	Zn	SO_4
			µS cm^{-1}	µg/l	µg/l	mg/l	µg/l	µg/l	mg/l	mg/l	mg/l	µg/l	µg/l	mg/l
T2	Stream draining tailings spill S dam	5.0	1310	35	13	13	168	5	37	16	189	9	32	622
C1	Chujah pit	7.0	750	28	8	63	15	3	0	66	11	67	59	412
C2	Seep into Chujah pit	5.6	150	12	18	3	64	4	19	7	7	134	116	44
C3	Chujah stage 3 Pit	3.4	220	3410	5	4	51	133	0	4	4	112	206	74
C4	Odumase Creek	6.5	90	68	13	7	1	8	1	5	11	4	41	-
C5	Nankafa East Pit	7.1	400	76	5	65	0	3	0	7	6	1	9	214
C6	Nankafa Creek	6.8	230	22	7	18	26	2	0	14	11	27	17	-
C7	Chujah 3 Pit	3.9	410	800	14	26	120	209	1	20	5	275	125	190
C8	Chujah 3 ‘Spring’	2.4	2900	42500	2730	81	1160	2720	277	75	9	1860	1080	1840
C9	Odumase h/w Pit	4.7	20	713	30	2	168	43	4	2	4	27	27	-
C10	Mansahaie pit	5.5	30	15	57	1	2	2	0	1	7	5	8	-
C11	Bogo Creek	6.4	160	39	175	8	1	15	6	4	12	4	35	-
C12	Mansi River	6.9	50	44	5	5	1	3	2	3	7	2	7	-
N1	Pond north of Marlu Dump (West)	7.3	430	24	104	39	0	36	0	29	4	3	4	173
N2	Pond north of Bogoso north dump	3.6	490	774	14	20	172	125	1	27	6	183	106	247
N3	Bogoso North Pit	2.9	730	7430	119	11	268	4320	7	10	5	441	111	236
N4	Marlu Pit	6.7	560	67	16	48	5	23	0	31	10	37	7	250
S1	Ablifa pit(small pond)	4.5	20	34	13	1	1	2	0	0	6	2	8	-
S2	Subri Creek	6.6	100	34	10	9	1	2	0	5	8	2	5	-

CONTAMINATION FROM CHEMICAL AGENTS USED IN GOLD RECOVERY

Certain chemical agents such as cyanide, sulphuric acid and mercury are essential for mineral recovery. However, when these agents are spilled or the residue left in the waste rock or mine sites, it can be leaked or leached into water resources in larger concentrations than required for the water to remain potable and thus contaminate water resources (figure 6). Consequently, the third kind of impact that mining can have on water quality is contamination from chemical agents used in mineral recovery and embellishment. These chemical agents are discussed in this section.

CYANIDE

Cyanide often occurs naturally in the environment, mostly in plants. However, in a gold mining environment such as the Tarkwa –Prestea area where cyanide heap leaching has become the main mode of gold extraction by major gold mining companies, any cyanide found in the environment can be attributed to gold mining .

In cyanide heap leaching, the ore is extracted and piled in heaps often some metres high. Occasionally, the ore is first crushed to smaller particles to increase the surface area thereby increasing the efficiency of the leaching process. The heap is then sprayed with a dilute sodium cyanide solution (approximately 250- 500 ppm sodium cyanide with pH between 10 and 11) through an irrigation system and allowed to trickle through it approximately at a rate of 6 l hr^{-1} m^{-2} of heap surface (Acquah, 1993). During percolation through the heap, gold particles in the heap are bonded with the solutions. The resulting fluid (pregnant solution) complex is allowed to drain down a synthetic liner to the bottom of the pad. The solution then flows over the liner to the perimeter of the heap where it is collected and pumped by pipe or drain to a lined retaining pond. Collection ponds and heap pads are usually lined with impermeable material (usually high density poly-ethylene (HDPE), plastic over clay, sometimes asphaltic concrete) designed to avoid the loss of pregnant solution and to prevent cyanide solution from escaping into groundwater or surface water.

Heap leach piles are usually constructed in separate lifts, or layers of ore. After most of the gold has been leached out of one lift, a new or fresh ore is placed on top of the old lift. The heap is again leached with solution. Each leaching cycle may take up to three months. After a sequence of leaching cycles, piles can tower as high as 90 metres. Some heaps sprawl over hundreds of acres.

Once the gold-bearing liquid is collected in the pregnant solution pond, it is pumped to a processing facility for recovery of the metal. Gold is recovered by running the pregnant solution over activated carbon materials that retain the gold-cyanide complex. The carbon is then washed with a highly alkaline cyanide solution to release the gold. The process continues by the addition of zinc to the wash solution, thereby initiating a chemical reaction that causes the gold to precipitate (to settle out of a solution) by gravity. The resulting impure gold is usually further purified by electrical refining and smelting.

The cyanide solution that is left over from processing is stored on outdoor ponds and then re-used on the heap in a subsequent leaching cycle. Fresh cyanide is added to this solution

before another round of leaching. Heap leaching requires large amounts of cheap sodium cyanide. Hundreds of millions of ponds are consumed each year by the mining industry.

Free cyanide (HCN plus CN^{-1}), which is a primary toxic agent has been heavily used in the major mining areas for the extraction of gold by the major gold mining companies. There have been major environmental problems. In October 2004, there was a spill of cyanide from the Bogosu Gold's new tailings dam, which drained into the Ajoo stream, the only stream left in the community (as the rest of the streams were considered dead as a result of disappearance due to mining). The deadly chemical killed fish, crabs and lobsters and polluted the stream, which is the main source of drinking water for the Dumasi community and its environs. There was a repeat spillage in July 2006. Thus cyanide spillage as result of mining has been a major environmental problem. The potential impact of cyanide on groundwater has not been measured. It has been known from groundwater monitoring data from a number of mining operations throughout the world that, generally, there is little or no impact of cyanide on groundwater quality due to the natural degradation process of cyanide. Furthermore, Smith and Smith and Mudder (1991) pointed out that when elevated cyanide concentrations in groundwater do occur, it is the result of seepage from wastes having higher cyanide levels than those typically found in gold mill effluents, where the attenuation capacity of the underlying material is overwhelmed.

Mercury in the environment does not only come naturally from the degassing of earth crust, but also from industrial activities such as cement manufacturing, mining and smelting as well as waste disposal (Voege, 1971; Wershaw, 1970; WHO, 1980). Mercury can enter the soil through direct application of mercury-containing fertilisers, lime and fungicides (Wershaw, 1970). The occurrence of mercury in water is due mainly to leaching from rocks and sometimes from release into water in the form of wastewater effluents from industrial plants that use mercury (Holden, 1972).

Figure 6. Surface water pollution at Dumasi.

In most surface waters, the most predominant species of mercury are mercuric hydroxide and chloride (WHO, 1984). Mercury is commonly used in batteries, thermometers, fungicides, antiseptics and dental fillings. Human exposure to mercury results mainly from eating food contaminated with mercury, usually fish or shellfish and from the mercury vapour released from dental fillings (Voege, 1971; WHO, 1984).

Mercury has played an important role in the processing of gold ores in Ghana. Gold processing using mercury involves a process known generally as amalgamation. The process involves dressing a sheet of metal with a thin layer or coat of liquid mercury. A mixture of powdered rock containing gold is passed over the plate. The particles of gold adhere to the mercury on the plate to form the gold-mercury amalgam while the waste rock powder washes away. The mercury is then evaporated and the gold recovered. However, mercury amalgamation is inefficient and only approximately 60 percent of the gold in the ore can be recovered (Carlos et al, 1997). It is against this background that the more efficient cyanide leaching method is preferred by the major gold mining companies operating in Ghana. Nonetheless, because it requires little capital investment in equipment, mercury amalgamation is still widely used by small-scale miners and galamsey operators .

The toxicity of mercury depends on its chemical form. The form of mercury found in fish and shellfish is organic or carbon-containing mercury. The form of mercury found in dental fillings is metallic mercury (Carlos et al, 1997). The form of mercury associated with rocks and with mining and smelting is inorganic or non-carbon-containing mercury. Inorganic mercury in the environment can be transformed to organic mercury by micro-organisms. The most common form of organic mercury, methyl mercury, can accumulate in some types of fish to high concentrations.

Human exposure to methyl mercury occurs when contaminated fish or shellfish are eaten (Carlos et al., 1997). Methyl mercury is more likely to cause nervous system toxicity than inorganic mercury (WHO, 1980).

Both short and long-term oral exposure to inorganic mercury salts can lead to kidney damage, including kidney failure. Oral ingestion of inorganic mercury is rapidly accumulated in the kidney and it is very irritating to the gastrointestinal tract and can cause nausea, vomiting, pain, ulceration and diarrhoea (WHO, 1980). Toxicity to the brain and nervous system has been reported following large doses of inorganic mercury taken medicinally (WHO, 1980).

In Ghana, the concentration of mercury (Hg) in the water resources particularly groundwater varies in the range 0.0-0.038 mg l^{-1}. However, mercury has not been detected in any of the rocks within Ghana, neither are there other industries in the area, apart from mining, that can release mercury in significant quantities to the environment. Further, the temporal variation in mercury (figure 7) portrays a trend whereby the concentrations of mercury in boreholes and wells are very high and in most cases more than ten fold above the WHO (2004) guideline limit of 0.001 mg l^{-1} for potable water during the rainy months (May-October) but virtually below detection limit during the dry season (November- April). In other words, mercury concentration in the groundwater is high in samples taken in July and October but below detection in samples taken from November to January. The samples taken in early May indicated only low mercury concentration in some wells. If the mercury were derived from the geological formation, one would expect more uniform and even distribution in its concentration at all times. However, it appears that the mercury concentrations in the wells are related to the recharge regimes of polluted surface water. This is likely to occur

during the wet season than in the dry season. The low concentration observed in the samples taken in May could be due to delayed recharge water reaching the aquifer. Consequently, the occurrence of mercury in the groundwater bodies could be largely due to contamination from surface sources, perhaps as a result of the indiscriminate use of mercury for gold processing by small scale miners.

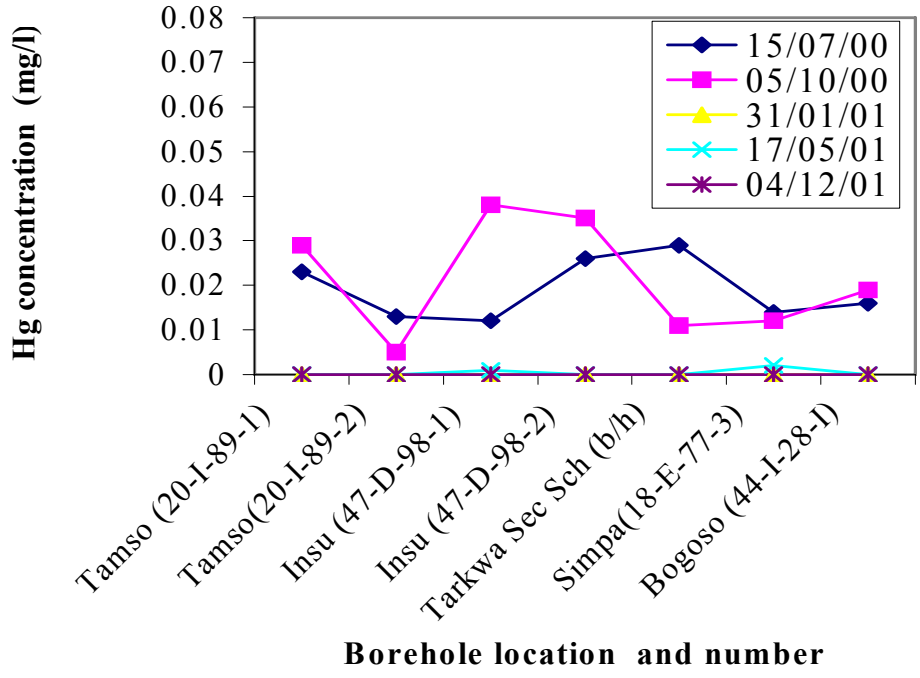

Figure 7. Temporal variation in Hg concentration in groundwater from Tarkwa –Prestea area.

CONCLUSION

In Ghana and almost the whole of West Africa, primary gold bearing rocks are confined to the Birimian Supper Group which denotes supracrustal rocks of the West African Craton. The supracrustal rocks comprise thick sequences of metamorphosed sediments and volcanics called the Birimian System, and much smaller and scattered shallow water sediments called the Takwaian System.

Gold deposits occur in five generic forms, which are primary vein deposits with accessory sulphide, disseminated sulphide ores, oxidised sulphide ores, paleoplacer deposits and recent placer deposits.

Mining is carried out by both large scale mining companies and Small Scale Mining/Artisanal mining companies. The Small Scale/Artisanal miners use mainly panning/sluicing/mercury amalgamation for gold extraction while the large mining companies use CIL/cyanide-heap leach of oxide and sulphide ores and heap leaching of pale placer ore or straking/roasting/heap cyanidation/heap leach/CIL/CIP/bioxidation.

Gold output in Ghana reached historic record of 2,628,290 ounces or 81.92 metric tonnes in 2007 and currently the country is the second and tenth producer of gold in Africa and the world respectively. Ghana's rising gold production is bolstered by a combination of policy reforms and surging prices of the commodity

Despite the economic gains, there are enormous environmental problems associated with the gold mining industry. These include land degradation, land instability, destruction of farm lands and contamination/pollution of water bodies particularly with mercury and other toxic trace metals.

REFERENCES

Acquah, P. C., 1992. Emerging Trends in gold ore processing and some related environmental issues in Ghana. *Regional Trends in African Geology*. Proceedings of the 9th International Geological Conference (Accra, 2nd to 7thNovember 1992) Geological Society of Africa.

Acquah, P. C., (1996). Natural Resources Management and Sustainable Development: The Case for Gold. In: Mining and Environment Research Network (MERN) Bulletin No.9: 39-44.

Appelo C.A. and Postma, D., (1999). Chemical analysis of Groundwater. Geochemistry, Groundwater and Pollution. AA Balkema/Rotterdam/Brookfield. p10-69

Banks, D., Younger, P. L., Arnesen, R. T., Iversen, E. R. and Banks, S. B. (1997). Mine-water chemistry: the good, the bad and the ugly. *Environmental Geology 32(3)*.

Carlos D., Da Rosa, J. D., Lyon, J. S., Udall, S. L., and Hocker, P. M., (1997). Golden Dreams, Poisoned Streams. *Mineral Policy Center. Washington. D. C*.

Diaz-Barriga, F., Santos, M. A., Mejia, J., Batres, L., Yanez, L., Carrizales, L., Vera E., Del Razo, L. M. and Cebrian, M. E.(1993). Arsenic, and cadmium exposure in children living near a smelter complex in San Luis Potosi, Mexico. *Environs. Res. 62, 242-250.*

Eisenlohr B.N. and Hirdes, W., 1992. The structural development of the early Proterozoic Birimian and Tarkwaian rocks of southwest Ghana, West Africa. *Journal of African Earth Sciences,* Vol. 14. No. 3*:* 331-325.

Freeze R.A., and Cherry J.A. 1979. Groundwater. Prentice hall Inc, New Jersey. p238-302

Grimvall, A., Cole, C. A., Allard, B., and Sanden, P. 1986. Quality trends of public water supplies in Sweden. Acid Precipitation and Human Health-Part 1. *Water Quality Bulletin* Volume 11, No. 1. 6-11 and 58.

Hastings, D. A. 1983. On the tectonics and metallogenesis of Ghana. Unpublished report. U. S. department of Interior, U.S.G.S. Eros Data center, Sioux Falls, South Dakota.

Hirdes, W., Davis, D.W. and Eisenlohr, B.N., (1992). Reassessment of Porterozoic graintoid ages in Ghana on the basis of U/Pb zircon and monazite dating. Precambiran Research*, 56:* 89-86.

Hirdes, W., and Leube, R. 1989. On gold mineralization of the Birimian Supergroup in Ghana/West Africa. Ghanaian-German Mineral Prospecting Project, *Geol. Surv. Dept*. Ghana; BGR, Hanover, Germany. 1989

Holden, A. V. 1972. Present levels of mercury in man and his environment. In: Mercury contamination in man and his in the environment. *Vienna, Internatioinal Atomic Energy Agency. Technical Report Series No. 137*

Hounslow, A. W. 1995. Water Quality Data Analysis and interpretation, *Lewis Publishers*, Boca Raton, New York.

Iribar, V., Izco, F., Tames, P., Antiguedad, L., and DA Silva, A., (2000). *J. of Environmental Geology*. 39 (7): 800-806

Junner, N. R., (1932). Geology of the Obuasi Goldfield. *Gold Coast. Gold Coast Geol. Surv. Mem. 2*. 71p.

Junner, N. R., (1935). Gold in the Gold Coast. *Gold Coast Geol. Surv. Memo.* 4. 5,30p.

Junner, N. R., Hirst, T. and Service. H. (1942). Tarkwa Goldfield. *Memoir No.6. Gold Coast Geological Survey.*

Kesse, G.O., (1985). The mineral and rock resources of Ghana. A.A. Balkema. Rotterdam, The Neitherlands, 618p.

Lagerkvist, B. J. and Zetterlund, B. (1994). Assessment of exposure to arsenic among smelter workers: a five year follow-up. *Am. J. Industr. Med*. 25, 477-4

Leube, A., Mauer, R., and Kesse O., (1990). The Early Proterozoic Birimian Supergroup of Ghana and Some Aspects of its Associated Gold Mineralisation. *Precambrian research, 46:* 139-165.

Marston, R. J., P. Woolrich and J. Kwesi. (1992). Closely associated stock work and Paleoplacer gold mineralisation in the early Proterozoic Tarkwaian System of Ghana. *Regional Trends in African Geology. Proceedings of the 9th International Geological Conference, Accra. 2nd-7th November 1992. Geological Society of Africa/ Geological Society of Ghana.*

Miliesi, J.P., Ledru P., Ankrah, P., Johan, V., Marcoux, E., and Vinchon Ch., (1991). The metallogenic relationship between Birimian and Tarkwaian gold deposits in Ghana. *Mineralium Deposita, 26,* 228-238.

Minerals Commission, 2008. Statistical summary of the Mining Sector in Ghana 2007.

Mireku-Gyimah D and Suglo S., (1993). The mining industry in Ghana. Trans. Instn Min, Metall. A59-67.

Monier-Williams, G. W. (1935). Aluminium in food. *London. Ministry of health (1935) Reports on Publish Health and Medical subjects*

Moskowitz, P. D., Coveney, E. A., Hamilton, L. D., Kaplan, E. and Medeiros, W. H. 1986. Identifying human population at risk from acid deposition mobilised materials in drinking water supplies: A preliminary Pilot study. Acid precipitation and Health –part 1 *Water Quality Bulletin 11*, *No 1*. 12-18 and 59.

Quashie, L. A. K., Pentsil, B. K., Kesse, G. O. and Thompson, P. T. A., (1981). Report of the Committee for Increased Gold Output in Ghana. Revised Edition. New York. DP/ UN/ GHA-78-003/ 3.

Smedley P. L., Ednunds W.M., West J.M., Gardner S.J. and Pelig-BA K. B. 1995. *Vulnerability of Shallow Groundwater Quality due to Natural Geochemical Environment. Health problems related to Groundwater in the Obuasi and Bolgatanga Areas, Ghana.* Report prepared for ODA under the ODA/BGS Technology Development and Research Programme, Project 92/5.

Smith, L. (2001) The geology of the Tarkwa mine resources, Gold Fields *78-054. US Environmental Protection Agency, Cincinnati.* 203p.

Smith and Mudder, 1991. Chemistry and Treatment of Cyanidation Wastes, Adrian Smith and Terry Mudder; Mining Journal Books Ltd., 1991

Songsore, J., Yankson, P.W.K., AND Tsikata, G.K., 1994. Mining and the Environmental: Towards a Win-Win strategy (A study of the Tarkwa – Aboso – Nsuta Mining complex in Ghana). June. 185p

Sylvester, J., and Attoh, K., 1992. Lithostratigraphy and Composition of 2.1 Ga Greenstone Belts of the West African Craton and Their Bearing on Crustal Evolution and the Archean- Proterozoic Boundary. *Journal of Geology, vol. 100:* 377-393.

Taylor, P.N., Moorbath, S., Leube, A. and Hirdes, W., 1988. Geochronology and crustal evolution of Early Proterozoic granite-greenstone terrains in Ghana/West Africa. *Abstract., International Conferenceon th Geology of Ghana with Special Emphasis on Gold Comm. 75th Anniversary of Ghana Geol. Surv. Dept., Accra.* p43-45.

Tseng, W. P., Chu, H. M., How, S. W., Fong, J. M., Lin, C. S. and Yeh, S. 1968. prevalence of skin cancer in endemic areas of chronic arsenicism in Taiwan. *J. Nat. Cancer Inst*., 40 453-463

Voege, F. A. 1971. Levels of mercury contamination in water and its boundaries. In: Proceedings of the symposium on mercury in man's environment, Ottawa, *Royal Society of Canada* p.107.

Water Resources Research Institute (WRRI). 1986. Effect of mining activities on River Ankoba and its tributaries. *Unpublished Water Resources Research Institute's Technical publication*.

Wershaw, R. L. 1970. Sources and behaviour of mercury in surface waters. *In: Mercury in the environment, Washington DC. US Geological Survey Professional paper No.713*

World Health Organisation (WHO), 1984. Guidelines for drinking water quality Volume 2. *Health criteria and other Supporting information. World Health Organization. Geneva, 1984.*

World Health Organisation (WHO), (2004). Guidelines for drinking water quality Final task group meeting. WHO Press/World Health Orga, Geneva.

Wright J.B., Hastings W.B., and Jones, H.R, 1985. Geology and Mineral resources of West Africa. George Allen and Unwin, London. p38- 50.

In: Gold Mining: Formation and Resource Estimation ISBN: 978-1-60741-096-6
Editors: M. D. Corral, J. L. Earle

Chapter 6

ENVIRONMENTAL IMPACT AND HEALTH RISK OF GOLD MINING IN GHANA

Alfred A. Duker
Kwame Nkrumah University of Science and Technology,
Kumasi, Ghana

ABSTRACT

Ghana has had a long history of gold production, and is known that in the 18th century gold was shipped by foreign trading ports (e.g., British, Dutch, Danish) from the Ashanti Region of the then Gold Coast. The Ashanti Region is a primary gold producing area; and in the former times the Ashanti goldfields was the source of the wealth of the Ashanti Kings. Today, the gold mining sector in Ghana is one of the most important and fast growing industries earning foreign exchange for the country. It exerts strong physical, socio-economic and cultural benefits on the nation and particularly on the local residents. Unfortunately, gold mining has caused arsenic contamination through the oxidation of sulphide minerals as well as diffuse contamination of mercury to be released into the environment. Consequently, vegetation has become degraded and giant plant species have been dwarfed. Foodcrops are also found to have high content of arsenic. Fruit trees and rootcrops now have longer maturity period and eventually low yields of agricultural products. The result is that malaria, cancer and non-cancer diseases, Buruli ulcer and other skin diseases are prevalent in these mining environments.

Keywords: Goldmining, arsenic, mercury, Buruli ulcer, environment, surface water.

INTRODUCTION

Goldmining dates as far back to the beginning of civilization. This kind of exploitation has increased till today, and it follows the trend of human needs in modern society. There are several ways of mining gold. They include the following:

Panning is an easy technique for searching for gold but not commercially viable when it comes to extraction from large deposits. Wide pans (constructed from metals or plastic) are

filled with sand and gravel that are suspected to contain gold. Water is added, shaken and the gold sorted out of the material.

Sluicing in which water was piped into successively narrow pipes leading to hoses with nozzles, which sprayed strong jets of water aimed at gravel faces to wash gold-bearing gravels. A sluice box is used to extract the gold. It was a long terraced wooden box over which gold bearing gravel was washed. Each step of the box had a lip that trapped the heavier gold and allowed the lighter material to be washed away. It was a technique used by most small scale mining companies.

Dredging in which badges known as dredges scooped gravel off river bottoms, separated the gold on board and dumped the waste rock.

Hardrock mining followed quartz veins rather than loose sediment, which contained gold. Open-pit mining or underground mining could be used.

In general there are two types of goldmining that are practiced. These are:

- Surface mining
- Underground mining

SURFACE MINING

This type may include quarries, open pits, strip contour mines and mounting top removal. This may involve the removal of several hectares to square kilometers of overburden materials and may subsequently lead to large open pits or quarry and extensive overburden piles.

UNDERGROUND MINING

This type is a complex operation that involves working beneath thick overburdens, which are connected to the outside by shafts and passageways. Consequently equipment used also range from simple to highly automated machinery. Extraction of materials require the use of highly-powered mining and hauling as well as skilled labour, especially in case of large scale mining as opposed to small scale mining.

SMALL SCALE MINING

In this case reference here is made to artisanal mining, which is undertaken by individuals or small groups of people. Small scale mining has its shortcomings in terms of the efficiency of its operations, the nature of its extractions, safety, health and environmental conditions (Aryee et al., 2003). Small scale mining applies manual processes, low technology and is conducted in small scale. They may operate with or without license. Those operating without a license are referred to in Ghana as ‘galamsey’. Because these illegal miners often pilfer from or operate on concessions of large scale mining companies they often have

confrontations with both state law enforcement agencies and security personnel of large scale mining companies.

In Ghana most small scale miners apply the following methods:

- Shallow alluvial mining
- Deep alluvial mining, and
- Hardrock mining

In *shallow alluvial mining* vegetation is cleared and excavation done until the gold-rich layer is reached. The mineralized material is removed and the gold recovered by sluicing technique. Galamsey miners generally use this method of mining.

The *deep alluvial mining* is normally applied to deep alluvial deposits found in some major river banks in Ghana. In this case excavation is done until the gold-bearing gravel horizon is reached (i.e., a depth of about 7-12 metres). Necessary precautions are taken to prevent the collapse of the pit. The gold-bearing gravel is removed and sluiced to obtain the gold.

The technique of *hardrock mining* is applied to gold-bearing reefs located either deep down the pit or to the surface. To intercept the reefs, holes are sunk and the reefs worked through these holes along the strike. Where possible, small scale miners use chisel and hammers to break the ore, otherwise explosives are used.

REGULATORY ENVIRONMENTAL PRACTICES

To ensure that environmental impacts are kept to the minimum, gold miners are required to obtain environmental permit from the Environmental Protection Agency (EPA) of Ghana. It is a precondition for the granting of a permit and a license. The EPA requires the proposed operational methods, the site plan of the area where the mining is to take place, the anticipated environmental impact and proposed mitigation measures as well as cost of reclamation (Aryee et al., 2003). District field officers at mine centres also work together with the EPA to ensure that environmental damage is kept to the minimum. Unfortunately galamsey operators cannot be controlled in respect of the regulatory environmental practices, and even when arrested by enforcement agencies fines imposed are often too small to deter them.

GOLD BOOM IN GHANA

Ghana has had a long history of gold production, and is known that in the 18th century gold was shipped by foreign trading ports (e.g., British, Dutch, Danish) from the Ashanti Region of the then Gold Coast. The Ashanti Region is a primary gold producing area; and in the former times the Ashanti goldfields was the source of the wealth of the Ashanti Kings. Gold, today, still plays a role in the customary practices of the traditional chieftaincy institution. Chiefs therefore keep an eye over goldmining within their lands whether it is small scale or large scale mining.

The surge in gold mining resulted in increased gold production which has established Ghana as the second largest gold producer in Africa after South Africa. The surge or the gold boom periods occurred first between 1902-1918, second in 1929-1943, third in 1949-1974 and fourth in 1985 to date (Dzibodi-Adjimah, 1996). Several mining companies are involved in the exploitation and are in various stages of rehabilitation, prospecting, exploration and development.

Today, the gold mining sector in Ghana is one of the most important and fast growing industries earning foreign exchange for the country. It exerts strong physical, socio-economic and cultural benefits on the nation and particularly on the local residents.

ENVIRONMENTAL IMPACTS OF MINING

Mining irrespective of the scale of operation has its negative impacts on the environment. The extent of the impacts depends on the method of operation. But these are reduced to the minimum due to supervision by environmental monitors. Illegal miners, however, by their way of operation, largely, clandestine cannot be monitored and held responsible for any environmental damage. The damage to the environment fall in the following areas: (i) air, (ii) vegetation and forest degradation, (iii) surface water, (iv) soil and foodcrops and (v) human health.

Air

Mining operations, especially the small scale miners, generate gaseous pollutants that are of the size that fall into the respirable dust range capable of causing respiratory diseases (Aryee et al., 2003). They also handle mercury (i.e., burning of gold amalgam) in poorly ventilated enclosures that could endanger their health for lack of protective clothing.

Long periods of mining without an arsenic scrubber has caused air-borne suspended As_2O_3 particles to settle on leaves and eventually washed onto the topsoil by rainwater. It is even suggested that high arsenic concentration levels in stream water could be attributed to such air-borne pollution derived from chimney stacks (Smedley et al. 1996).

Vegetation and Forest Degradation

Large piles of waste coupled with abandoned excavations, in many cases are left behind by miners. These go together with vast stretches of barren land or degraded forest. The pits that are left are filled with water, and become breeding grounds for mosquitoes.

The soil structure is disturbed when vegetation is removed for mining, thus the destruction of the top soil of the land. This does not only imply the destruction of agricultural land but also the susceptibility of the land to erosion.

The arsenic dispersion in the atmosphere due to the roasting of the ore without the use of an arsenic scrubber for a long time had caused degradation of vegetation and ‘dwarfing’ of giant plant species (Asiam, 1996). Fruit trees and rootcrops are found to have longer maturity

period and eventually low yields of agricultural products (Asiam, 1996). Tuffour (1997) noted that the effluent containing arsenic and cyanide from processing plants at Obuasi have been implicated in the blighting of trees in the Forest Reserves in that area, where residents also complain that wildlife is virtually non-existent in the reserves.

Surface Water

During sluicing and amalgamation processes, solid suspension and mercury are discharged into rivers and streams on which residents depend. Fishes in these streams are found to have high levels of mercury. In some cases, dredging and sluicing into surface waters have caused fishes to disappear in some rivers (Dzigbodi-Adjimah, 1996). Tailings that have also not been properly disposed of are mobilized by run-off into water bodies. This situation often leads to siltation and colouration of water bodies, consequently leading to flooding in these environments.

Goldmining also causes arsenic contamination through the oxidation of sulphide minerals, which are released into the environment. The arsenic contamination is also mobilized by rivers and streams and deposited on floodplains and agricultural soils. Furthermore, there have been accidental arsenic spillages into streams and overflow of tailings treatment sumps into settlement and farmlands.

Soils and Foodcrops

Studies have shown that soils in mining environments have been contaminated with arsenic (Amasa, 1975; Amonoo-Neizer and Amekor, 1994; Smedley et al., 1996; Asiam, 1996). In the event of flooding, rivers mobilize these contaminated soils into floodplains and nearby agricultural soils. Interestingly, farmers prefer to cultivate foodcrops on these floodplains. Foodcrops grown on arsenic-enriched soils also tend to take up arsenic (Sarkodie et al., 1997; Alam et al., 2003)

HUMAN HEALTH

Studies by Amasa (1975) showed that workers in goldmining at Obuasi, Ghana had high hair arsenic between 196 ppm to 1940 ppm. The average of hair arsenic in normal hair was found by Smith (1967) to be about 0.65 ppm. In a related study Ahmad et al. (2000) found galamsey workers in the Ashanti Region who had hair mercury levels as high as 1000 ppm. These were asked to seek medical advice.

The inhabitants of settlements near to minesites are not only exposed to arsenic dispersion in solution but also through airborne dispersion of arsenic (Hinwood et al., 2004; Kavanagh et al., 1997) some of which are inhaled. Amasa (1975), for example, reported of arsenic and sulphur poisoning 8 km north of Obuasi. The illegal miner or the galamsey generates a lot of dust. They, however, do not water down the rock surfaces to allow the dust

to settle down before restart of work. The result is that the galamsey contracts very early pneumoconiosis or silicosis (Lewis, 1997).

Residents in mining environments depend on surface water for drinking, cooking and other domestic uses. Even where potable water exists; it is mostly intermittent and therefore not available throughout the year. Unfortunately, these surface waters become contaminated due to mining activities. For example, surface water contamination in parts of the Ashanti Region of Ghana (i.e., Amansie West District) where artisanal activities are prevalent within the Offin River environment, arsenic concentration levels in water range between 0.22 mg/l and 2.92 mg/l. However, in the Oda River east of the Offin River where there is scarcely mining activities, water arsenic level range from 0.02 mg/l to 0.17 mg/l (Duker et al., 2005). The difference between the two environments points to exacerbation of this contamination due to mining operations.

Amasa found that arsenic levels in staple food in some parts of the mining area at Obuasi ranged between 1.89 ppm and 4.80 ppm. Sarkodie et al. (1997) also found the content of arsenic in some other staple foods in the same mining environment ranging between 0.10 ppm and 3.08 ppm. They further found that these concentrations followed the rainfall pattern and increased from January to a peak in September/ October when the rainfall was highest.

Obiri et al. (2006) studied the uptake of arsenic and other toxic metals by cassava, cocoyam and other tubercrops grown on contaminated soils in mining communities in the Western Region of Ghana. Their study evaluated human health risk from the eating of cassava, cocoyam and other staple foods and found that the risk of cancer and non-cancer related cases were high in several of the communities.

The ingestion of foodcrops from contaminated soils and water contaminated with arsenic implies defect in the immune system (Lantz et al., 1994; Gonseblatt et al., 1994). Stienstra et al. (2001) and Van der Werf et al. (1999) have also indicated that the down-regulation of the immune system is a risk factor for the development of Buruli ulcer (BU) disease.

Interestingly, incidences of BU in the Offin River environment have a range of 4- 53, whilst that on the Oda River is 1-4. The above situation, however, could further be enhanced by poverty (Asiedu and Etuaful, 1998) coupled with malnutrition in children in the area.

SUMMARY

Goldmining is a major contributor to the foreign exchange earnings of Ghana, but such exploitation needs to be ethical in order to minimize environmental damage. The activities, however, of the galamsey which cannot be controlled raises concern as to environmental damage, safety risks and health. Arsenic minerals are associated with gold ore and thus arsenic is dispersed in the environment especially through galamsey operations, causing water sources and agricultural soils on which the communities depend to be contaminated during rainfall and flooding.

The difference in the arsenic situation in the Offin and Oda River basins could be attributed to the mining operations. Similarly, it could be said that such mining activities might have contributed to the health situation in these environments. Health risk is high in the mining environments, which implies that health officials need to carefully monitor and assist such communities.

REFERENCES

Ahmad, K., Osae, E. K., Nyarko, B. J. B., Serfor- Armah, Y. 2000. Neutron activation analysis for some toxic elements in the hair of some "galamsee" workers In Ghana. *J Ghana Sci Assoc* 2 (1): 39-44.

Alam, M. G. M., Snow, E. T., Takana, A. 2003. Arsenic and heavy metal contamination of vegetables grown in Samta village, Bangladesh. *Sci Total Environ* 308, 83-96

Amasa, S. K. 1975. Arsenic pollution of Obuasi goldmine, town and surrounding countryside. *Environ Health Perspect* 12, 131-135.

Amonoo-Neizer, E. H. and Amekor, E. M. K. 1994. Determination of total arsenic of some food and cash crops, vegetation, cooked food, fish, meat, soil and water from Kumasi, Obuasi and their environs. *J Univ Sci Technol* 14:8-16.

Aryee, B. N. A., Ntibery, B. K., Atorkui, E. 2003. Trends in the small-scale mining of precious minerals in Ghana: a perspective on its environmental impact. *J Cleaner Prod* 11, 131-140.

Asiam, E. K. 1996. Environmental assessment of gold beneficiation: Arsenic audit and impact on the Obuasi environs. *Ghana Min J* 2 (1): 17-20.

Asiedu, K. and Etuaful, S. 1998. Socioeconomic implications of Buruli ulcer in Ghana: a three-year review. *Am J Trop Med Hyg* 59, 1015-1022.

Duker, A. A., Carranza, E. J. M., Hale, M. 2005. Spatial relationship between arsenic in drinking water and *Mycobacterium ulcerans* infection in the Amansie West district, Ghana. *Min Mag*, 69 (5): 707-717.

Dzibodi-Adjimah, K. 1996. Environmental concerns of Ghana's gold booms: Past, present and future. *Ghana Min J* 2 (1): 21-26.

Gonseblatt, M. E., Vega, L., Montero, R., Garcia-Vargas, G., Del Razo, L. M., Albores, A., Cebrian, M. E., Ostrosky-Wegman, P. 1994. Lymphocyte replicating ability in individuals exposed to arsenic via drinking water. *Mutat Res* 313, 293-299.

Hinwood, A. L., Sim, M. R., Jolley, D., de Klerk, N., Bastone, E. B., Gerostmoulos, J., Drummer, O. H. 2004. Exposure to inorganic arsenic in soil increases urinary inorganic arsenic concentrations of residents living in old mining areas. *Environ Geochem Health* 26, 27-36.

Kavanagh, P., Farago, M. E., Thornton, I., Goessler, W., Kuehnelt, D., Schlagenhaufen, C., Irgolic, K. J. 1997. Urinary arsenic species in Devon and Cornwall residents, UK. A pilot study. *Analyst* 123, 27-29.

Lantz, R. C., Parliman, G., Chen, G. J., Carter, D. E. 1994. Effect of arsenic exposure on alveolar macrophage function. I. Effect of soluble As (III) and As (V). *Environ Res* 67 (2): 183-195.

Lewis, G. T. 1997. Addressing the galamsey problem: The view from the Ghana Chamber of Mines. *National Symposium Proceedings- The Mining Industry and the Environment.* April 14-15, UST, Kumasi, pp. 53-68.

Obiri, S., Dodoo, D. K., Okai-Sam, F., Essumang, D. K., Adjololo-Gasokpoh, A. 2006. Cancer and non-cancer health risk from eating cassava grown in some mining communities in Ghana. *Environ Monit Assess* , 118 9103): 37-49.

Sarkodie, P. H., Nyama, D., Amonoo-Niezer, E. H. 1997. Speciation of arsenic in some biological samples from Obuasi and its surrounding villages. *National Symposium*

Proceedings- The Mining Industry and the Environment. April 14-15, UST, Kumasi, pp. 146-154.

Smedley, P. L., Edmunds, W. M., Pelig-Ba, K. B. 1996. Mobility of arsenic in groundwater in the Obuasi gold-mining area of Ghana: some implications for human health. In: Appleton, J. D., Fuge, R., McCall, G. J. H. (eds), *Environ Geochem Health.* Geological Society Special publication No. 113, pp. 163-181.

Smith, H. 1964. Interpretation of the arsenic content of human hair. *Forensic Sci Soc J* 4, 192.

Stiestra, Y., van der Graaf, W. T. A., te Meerman, G. J., The, T. H., de Leij, L. F., van der Werf, T. S. 2001. Susceptibility to development of *Mycobacterium ulcerans* disease: review of possible risk factors. *Trop Med Int Health* 6 (7): 554-562.

Tuffour, K. 1997. Mining degradation of forest land resources and rehabilitation. *National Symposium Proceedings- The Mining Industry and the Environment.* April 14-15, UST, Kumasi, pp. 43-48.

Van der Werf, T. S., van der Graaf, T. A., Tappero, J. W., Asiedu, K. 1999. *Mycobacterium ulcerans* infection. *The Lancet* 354, 1013-1018.

In: Gold Mining: Formation and Resource Estimation ISBN: 978-1-60741-096-6
Editors: M. D. Corral, J. L. Earle

Chapter 7

HYDROTHERMAL ALTERATION GEOCHEMISTRY OF THE BETAM GOLD DEPOSIT, SOUTH EASTERN DESERT, EGYPT: MASS-VOLUME-MINERALOGICAL CHANGES AND STABLE ISOTOPE SYSTEMATICS*

***Basem A. Zoheir*†[1] *and Nedal N. Qaoud*[2]**
[1]Department of Geology, Benha Faculty of Science, 13518 Benha, Egypt
[2]Department of Geology, Faculty of Science Al-Azhar University, Gaza

ABSTRACT

Although gold production is relatively minor from the Arabian–Nubian shield at present, extensive alluvial and lode fields along the western side of the Red Sea in Upper Egypt and northern Sudan were worked out by the ancient Egyptians for thousands of years. In the Eastern Desert of Egypt, numerous but small gold deposits are generally related to auriferous quartz veins commonly associated with brittle-ductile shear zones, generally cutting through the Neoproterozoic crystalline basement rocks and trending in different directions. Gold mineralization at the Betam mine area, south Eastern Desert, is related to a series of milky quartz veins along a NNW- trending brittle-ductile shear zone cutting through successions of pelitic schists, next to a small granite intrusion. Gold-sulfide mineralization (pyrite, arsenopyrite, galena, subordinate chalcopyrite and gold) is closely associated with a conspicuous hydrothermal alteration halo. Textural relationships, including replacement and crosscutting of mineral phases and quartz veins record a post-foliation alteration assemblage of quartz+sericite+chlorite+ calcite±albite±epidote.

The hydrothermal alteration halo alongside the auriferous quartz veins comprises three distinct zones, namely: (a) distal chlorite-calcite zone (chlorite+calcite±biotite± pyrite±sericite±epidote), (b) intermediate sericite-chlorite zone (sericite+chlorite+

* A version of this chapter was also published in Chemical Mineralogy, Smelting and Metallization, edited by Eugene D. McLaughlin and Levan A. Breaux, Nova Science Publishers. It was submitted for appropriate modifications in an effort to encourage wider dissemination of research.

† Email: basem.zoheir@gmail.com

pyrite±biotite), and (c) proximal pyrite-sericite zone (quartz+pyrite+sericite±albite). These zones merge to each other gradually, ending outwards into the unaltered metasediments. The pyrite-sericite zone presents the highest gold grade, especially in zones thickly seamed with sulfide-rich quartz veinlets. Mass balance calculations revealed that the pyrite-sericite zone experienced significant metasomatic changes relative to limited mass and volume changes for the chlorite-calcite zone. The overall picture of chemical gains and losses with increase the intensity of hydrothermal alteration is indicative of: (i) addition of SiO_2, K_2O, Na_2O, S, L.O.I., (ii) removal of MgO, and (iii) relatively inert behavior of Al_2O_3, TiO_2, MnO, Fe_2O_3. CaO is variably mobile, slightly gained in the chlorite-calcite and sericite-chlorite zones but depleted in the pyrite-sericite zone. Concnetrations of the trace elements are variable in the different alteration types, but a notable increase in Au, As, Ba, Sr, Rb, V, and Ni in the intensively altered rocks is verified. Investigation of the REE behavior reveals a little modification of their distribution pattern with hydrothermal alteration. Heavy REE are more or less unchanged, whereas light REE are significantly mobile in all alteration types.

New geochemical data provide evidence for progressive silicification, sericitization, and sulfidation as a function of gold mineralization. A proposed model for the hydrothermal alteration system for the Betam deposit includes fluctuation in pH and redox state (f_{O2}), mainly during the wall-rock sulfidation. This might have destabilized gold complexes and lowered gold solubility in solution, hence contributed at least partly in gold deposition in the study area. A decrease in the whole rock $\delta^{18}O$ values from unaltered country metasediments to the distal, intermediate and proximal alteration zones, respectively, might be attributed to rock interaction with an isotopically lighter fluid. In addition, sulfur isotope data of pyrite-arsenopyrite pairs in the mineralized quartz veins and adjacent wall-rock along with the calculated $\delta^{34}S_{\Sigma S}$ values for the ore fluids suggest derivation form non-homogenous (mixed magmatic and metamorphic) fluids.

INTRODUCTION

The Arabian-Nubian Shield (ANS), a large geological ensemble covering vast areas in northeast Africa and west Arabia, is dominated by juvenile crust formed during the Neoproterozoic (950-450 Ma) through accretion of intra-oceanic arcs and/or oceanic plateaux (Kröner et al., 1987; Harris et al., 1993; Stein and Goldstein, 1996). The Eastern Desert of Egypt, the north-western part of the ANS, has long been a mining district for gold since the pre-Dynastic times, with more than 95 gold occurrences mostly confined to the basement rocks (El Ramly et al., 1970; Sabet et al., 1976; Pohl, 1988; Abdel Tawab, 1992; Hassaan and El Mezayen, 1995). At least, 40 occurrences show previous workings of the ancient Egyptians (Pharoans), who likely worked out the richest parts of the auriferous quartz veins (Azer, 1966). Gold mining during the ancient times was likely focused entirely on the near-surface high-grade quartz veins and associated alluvial deposits. Mining activity was extensive during the Pre-Dynastic, Roman, Ptolemaic and Islamic times. Gold production from the major gold deposits, e.g., E1 Sid, Um Rus, Barramiya and Sukari, lasted until 1958 (Neubauer, 1962; Pohl, 1988; Abdel Tawab, 1992). During the Islamic times (i.e. 10^{th} - 11^{th} century A.D.), gold mining in Egypt was concentrated on the southern parts of the Eastern Desert (Klemm et al., 2001). Some 19 gold occurrences and deposits have been located in the Wadi Allaqi district, the majority of them are vein-type and related to brittle-ductile shear zones (El Kazzaz, 1995; El Shimi, 1996; Kusky and Ramadan, 2002).

Many of the Egyptian gold deposits are related to systems of hydrothermal quartz veins cutting through basement rocks of variable composition (pelitic metasediments, metavolcanics, serpentinite and granitoids) and age. Mineralogy of these veins commonly includes pyrite, arsenopyrite, subordinate chalcopyrite, sphalerite, galena, tetrahedrite and rare stibnite. These deposits are interpreted collectively as products of hydrothermal activity (Garson and Shalaby, 1976), induced either by metamorphic or cooling effects of Lower Palaeozoic magmatism (Almond et al., 1984; Pohl, 1988) or Early Cambrian subduction-related calc-alkaline magmatic rocks (El Gaby et al., 1988). Other authors relate gold mineralization to the emplacement of granitoid rocks that intrude mafic/ultramafic rocks (Hume, 1937; Amin, 1955; El Shazly, 1957). Almond et al. (1984) suggested that gold deposition was related to an episode of shearing after the emplacement of all batholithic intrusions and coeval with the regional cooling.

Zones of bleached wallrocks adjacent to the gold-bearing quartz veins in the Eastern Desert are suggestive of distinct mineralogical changes during the percolation of hydrothermal fluids (Osman and Dardir, 1989; Harraz, 1991; Harraz and El Dahhar, 1994; Botros, 2004; Helmy et al., 2004). The metasomatic styles were strongly influenced by variations in the carbon dioxide and alkali contents of the mineralizing fluid (Harraz and El Dahhar, 1994; Harraz et al., 1992). Botros (1993) reviewed the common types of hydrothermal alteration associated with the Egyptian vein-type gold deposits and suggested that sericitization, argillic alteration, silicification are common in the acidic rocks, whereas chloritization, carbonatization, sericitization, pyritization and propylitization prevail in the intermediate and basic host rocks. Harraz (1999) suggested that alteration zones adjacent to the auriferous quartz veins have been formed through addition of CO_2, H_2O, K and lesser Na in the Atud gold deposit, south Eastern Desert. In the Barramyia gold mine, where numerous auriferous quartz veins cutting through highly altered tuffogene metasediments, ultramafites, and listwaenite, Osman and Dardir (1989) described a complex mixture of alteration processes, including sericitization, silcification, sulfidation, carbonatization, ankeritization and chloritization. They reported the highest gold grade in the altered rocks, up to 5 ppm Au, in the carbonaceous wallrocks adjacent to the mineralized veins. The hydrothermal alteration halo enveloping the gold-bearing quartz veins at Hutit mine, south Eastern Desert, grades up to 35 ppm Au, made by mainly of silicified, carbonatized serpentinite (Takla et al., 1995). A narrow alteration halo bounds the main mineralized quartz vein at the Um Tenedba mine, replacing the original granitic/gabbroic material. Sericitization and sulfidation are the main alteration types, with 6 ppm Au at maximum (Takla et al., 1995). In the Dungash gold mine area, Helba et al. (2001) and Khalil et al. (2003) described four alteration zones, mixtures of chloritization, sericitization, carbonatization and silicification overprinting the original volcani-sedimentary host rock mineralogy, in which disseminated gold occur. Accordingly, many of the alteration zones associated with the Egyptian gold deposits are of proven economic value, and on the other side, a significant rule of wallrock alteration in depositing gold in several examples of the vein-type gold deposits of Egypt may be proposed.

The Betam gold deposit is one of several gold occurrences in the Allaqi district at the extreme south Eastern Desert of Egypt. The deposit is located at the head of Wadi Um Teneidib (a tributary of Wadi Defeit), at the intersection of Latitude $22^{o}16'42"$N and Longitude $34^{o}30'31"$E, ~ 7 km west of Gebel El Adrag. Although completely abandoned at present, abundant stone huts, millstones, dumps and tailings observed in the mine area point out significant mining activities in the past. The gold-bearing quartz veins were stopped out

on surface through several trenches (6 m deep from the ground surface) and in the underground through shafts and adits. Gold mineralization is expressed in auriferous quartz veins and veinlets along a brittle-ductile shear zone cutting through schistose pelitic metasediments (Zoheir, 2008). The ore dump at the mine area grades 6 g/t Au (UNDP compilation report by EGSMA, 1986). An elongated (NW-SE) zone of surface alteration is bounded on central shear auriferous quartz veins, especially where bifurcated within the shear zone. The hydrothermal alteration types include pervasive silicification, sericitization, chloritization and albitization. Silicification is confined to zones (few decimeters-wide) adjacent to the auriferous quartz veins. The intensity of alteration correlates positively with the thickness of the silicification zone and quartz veins. Ahmed et al. (2001) described a narrow, NW-trending shear zone characterized by ferrigenation, carbonatization, silicification and associated quartz veins and veinlets at the Betam mine area. They reported gold contents of 2 to 11 ppm in samples from the intensely altered rocks along the shear zone.

The present contribution reports on the petrographic characteristics, mass and mineralogical changes and oxygen and sulfur isotope systematics of the hydrothermal alteration associated with the Betam gold deposit. Bulk-rock geochemical and microprobe studies were conducted to assess the nature and evolution of the ore fluids. Moreover, an attempt to constrain on the ambient temperature, f_{O2} and pH during gold deposition-hydrothermal alteration is based on the available geochemical and isotopic data.

GEOLOGIC AND STRUCTURAL SETTING

The Betam mine area is underlain mainly by thrust-bounded sheets and slices of ophiolitic serpentinite, amphibolite and metabasalt, forming parts of the Allaqi-Hieani suture in the southern Eastern Desert of Egypt (Figure 1).

Successions of basaltic to basaltic andesite volcanoclastic rocks together with metagabbro masses are associated with the ophiolitic rocks east of the mine area. Pelitic to psammopelitic metasedimentary rocks occupy the core of a map scale plunging synform, enfolded between the ophiolitic rocks in the central part of the study area (Figure 2). These metasedimentary rocks show chemical characteristics similar to those of the back arc metasediments (Zoheir, 2004).

Fine to coarse grained mesocratic and melanocratic gabbroic rocks, showing signs of metamorphism under greenschist consitions, are common in the southwestern part of the mine area. Slightly sheared granodiorite masses intruding the pelitic metasedimentary rocks in the northern part of the area are densely dissected by numerous felsic and mafic dikes, quartz and quartz-muscovite pegmatites striking in different directions. Non-deformed monzo- or syeno-granite masses intrude into the metasediments and sheared granodiorite. Olivine gabbro occurs as small bodies forming discontinuous, moderately elevated hills. It intrudes the metagabbro unit south of the mine area.

Rocks close to, and affected by the mineralized shear zone are chiefly pelitic metasediments (mainly garnet-biotite± staurolite±muscovite schist), syeno-granite and metagabbro. These rocks display variable degrees of hydrothermal alteration, generally increase approaching the shear zone.

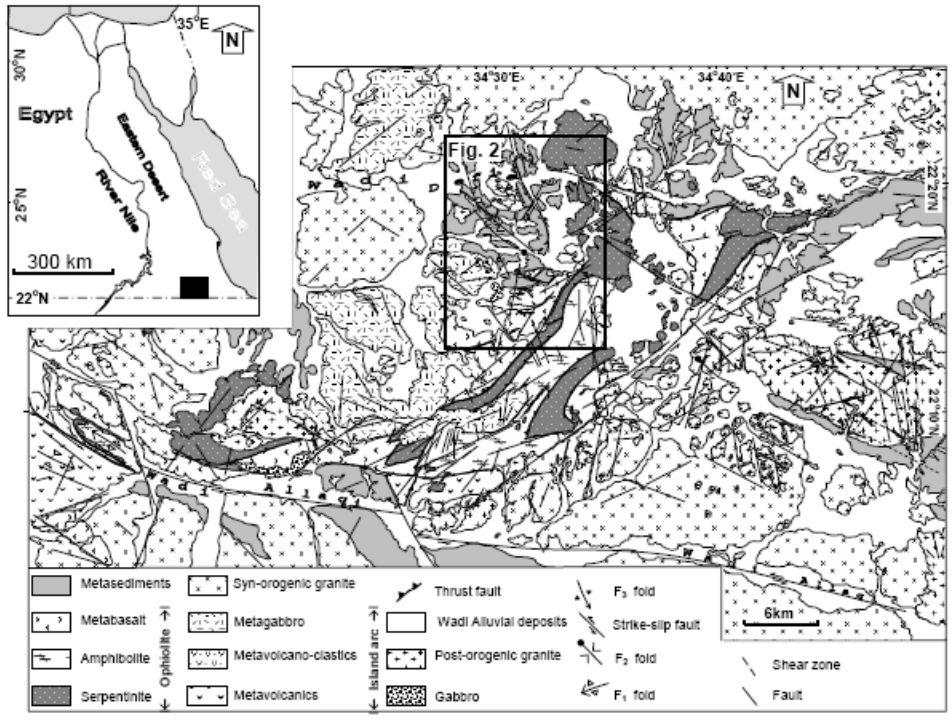

Figure 1. Geological map of the central part of the Allaqi-Heiani Suture, modified from Zoheir and Klemm (2007) and Zoheir (2008). Inset showing the location.

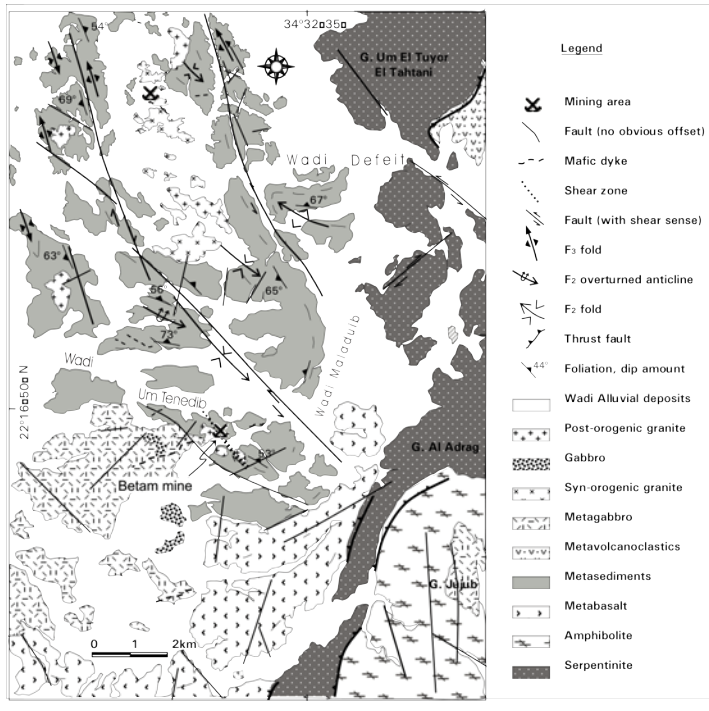

Figure 2. Geological map of the Betam gold mine area (after Zoheir, 2008).

The metasediments are made up of intercalations of quartz-rich bands and dark bands rich in epidote and chlorite. This compositional NW-trending layering (Figure 3A) gradually deflects steeply into the shear zone. Both the brittle faulting and ductile shearing are postdating the layering. The primary metamorphic mineral assemblage includes quartz+biotite+garnet±staurolite±muscovite±hornblende±epidote. Proximal to the shear zone, these rocks show obvious sericitic alteration and sulfidation overprints. In places, these rocks grade into banded quartz biotite-muscovite chlorite schist containing abundant disseminated pyrite and minor carbonate (Figure 3B). Biotite flakes are aligned parallel to the main foliation (S_1-N50^{o}W/60^{o}NE), whereas chlorite is common along the NNW-trending cleavage. Quartz occurs as anhedral elongated grains displaying preferential orientation along to the main foliation. Some quartz crystals contain apatite inclusions aligned parallel to their long dimensions. Recrystallized quartz, constituting ~10 volume percent of the rock, forms stretched ribbons parallel to foliation planes. At the mine area, garnet xenomorphic crystals are more conspicuous in rocks containing muscovite replacing most of the biotite flakes. The auriferous wall rocks are iron-stained schists, thickly seamed with quartz veinlets.

In the southern part of the mine area, metasedimentary rocks are intruded by slightly foliated medium- to coarse-grained metamorphosed gabbroic rocks, which enclose elongate slabs of the metasedimentary rocks. These rocks exhibit variable degrees of alteration at the vicinity of the silicified metasediments and granite. Locally, it is traversed by small scale granite offshoots. Highly altered gabbroic blocks of different sizes are totally enclosed within granite. Small-size blocks are fine grained and exhibit recrystallization and silica invasion. Microscopically, these rocks show subophitic texture and composed essentially of plagioclase, actinolite±relict augite, and minor quartz. If present, augite occurs as subhedral crystals commonly with rims of pseudomorphic actinolite. Plagioclase occurs as large prismatic crystals displaying multiple and polysynthetic twinning and occasionally suffers intensive sausseritization at cleavage planes or massive kaolinitization. Apatite is a common accessory mineral in these rocks and sulfides are associated with chlorite in the altered rocks. Near the mineralization zone, albite replaces plagioclase, and calcite is common. Most of the ferromagnesian minerals are altered into chlorite, calcite and iron oxides ±nodular sphene. Chlorite is commonly associated with fine undulate quartz and encloses euhedral sulfide crystals. Locally, prehnite replaces plagioclase along with zoisite (Figure 3C). Chlorite replaces biotite, hornblende and plagioclase along with calcite and iron oxides±nodular sphene (Figure 3D).

Post-orogenic granite represent discrete exposures of a ~150 m long NNW-trending dike-like body of biotite-muscovite granite, traversing the main foliation of the metasediments (Figure 3E). This granite is medium-grained and composed essentially of quartz, biotite, perthitic microcline, orthoclase, subordinate plagioclase, muscovite and accessory zircon±sphene. Quartz occurs as large anhedral to subhedral crystals myrmekitically intergrown with plagioclase and graphically intergrown with microperthitic microcline. It exhibits undulatory extinction and contains numerous small inclusions of apatite crystals and sericite. Some quartz crystals are recrystallized into aggregates of fine grained un-strained secondary quartz that can be distinguished from the former phase by the absence of sericite inclusions, unstrained nature and their stringer-like and ribbon habit. Near the shear zone, this granite unit has been subjected to hydrothermal alteration which locally causes variations in color into pale pink, pale yellowish brown or red, and variations in mineralogical composition.

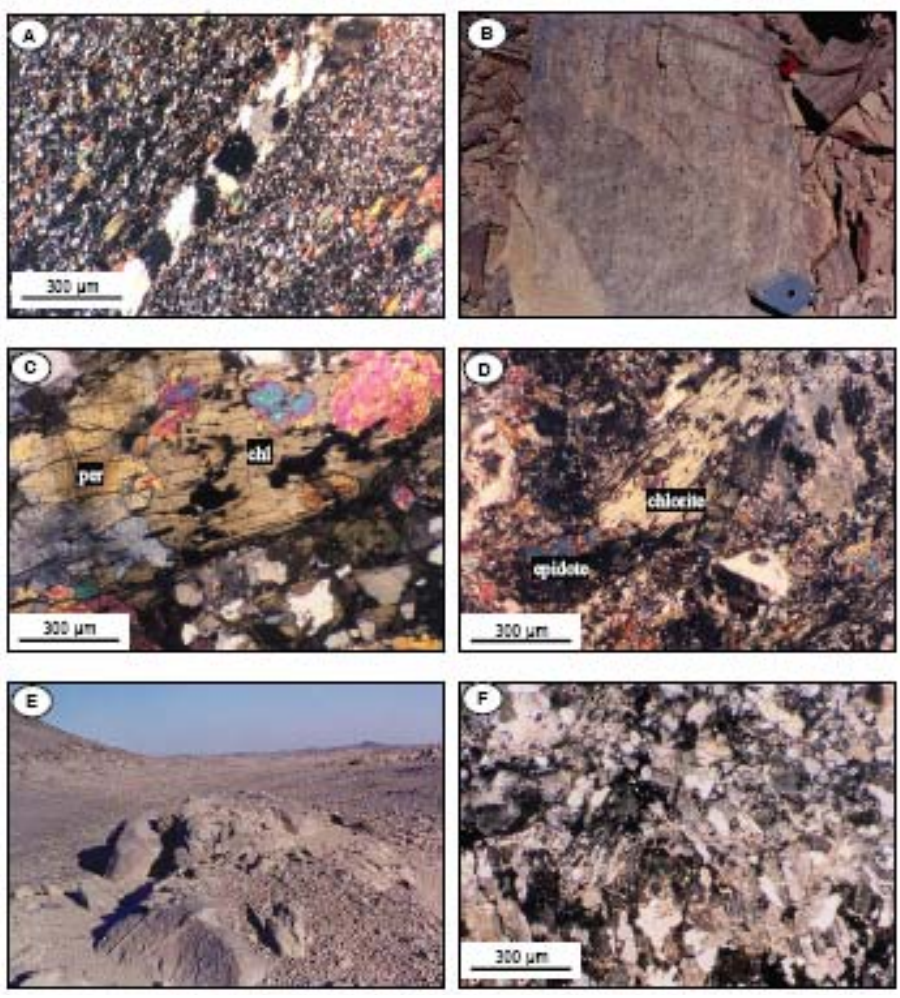

Figure 3. A. Photomicrograph of the least altered metasediments, showing the metamorphic layering with relict hornblende, biotite and recrystallized quartz. XPL. B. Disseminated altered pyrite concentrated at cleavage surfaces of the metasediments. C. Pehrnite (per) develops at the expense of chlorite (chl) in hydrothermally altered metagabbro south of the mine area. D. Chlorite, epidote, calcite and sulphide almost completely replace the original mineralogy of metagabbro from the mine area, XPL. E. Pink granite intruding the metasediments at the mine area. F. Deformed granite clearly suffers sericitic alteration and silicification, XPL.

The hydrothermal alteration intensively develops near the quartz veins. Potash feldspar is replaced by sericite, quartz and iron oxides. Plagioclase crystals are altered into aggregates of sericite and kaolinite or replaced in places by epidote and calcite. In other places plagioclase crystals are completely albitized. Biotite is partially or completely altered into chlorite and hematite with rutile. As the alteration advances, most of the pyrogenic minerals (biotite and plagioclase) are replaced by sericite, chlorite, calcite, and epidote. The destruction of the primary mineral association may proceed so far as the original magmatic texture of the rock is completely obliterated (Figure 3F).

As a part of the central Allaqi-Hieani suture (Figure 1), the mine area has experienced a poly-phase deformation history characterized by several overprinted folding, transpression

and faulting events. Quartz-mineralized shear zones, developed late in the structural evolution of the area, are assumed to have been accompanied by enormous fluid flow, as indicated by the abundant retrograde mineral fabrics and quartz veins (Zoheir, 2004, Zoheir and Klemm, 2007; Zoheir, 2008). The metasedimentary rocks exposed at the mine area represent disrupted blocks of a fold-mosaic extending in a NW-SE direction (Figure 2). These rocks exhibit abundant overturned, recumbent asymmetric meso-and micro-folds associated with a series of contiguous faults, distinctly traced by fractures and by swarms of basaltic dikes. Additional extensional fault-related fractures developed during the re-adjustment of the metasedimentary and ophiolitic rocks (Zoheir, 2008).

The mine area is densely dissected by faults trending in different directions, with a most conspicuous NW-trending left-lateral strike slip faults. The ore-controlling structures are dominated by a ductile to brittle-ductile shear zone (N27-36^{o}W/70-80°NE, with average width of 160 cm), characterised by intensification of N32^{o}W foliations, pervasive brecciation and distinct stretching lineations. Most mineralization occurs in quartz veins that formed within and parallel to the main shear zone along slip surfaces and margins. Discrete quartz lenses are generally parallel to the margins of the shear zone. Dextral asymmetric folds and strain shadows around these quartz boudins suggest that wall rocks as well as the quartz veins were deformed by dextral shear. The lensoid habit of the foliation-parallel quartz bodies within the NNW-trending shear zone suggests a dominant shortening normal to the shear zone.

GOLD MINERALIZATION

Gold is related mainly to a set of quartz veins, along foliation-concordant and foliation-discordant fault segments. These veins represent mainly central shear (fault-fill) shoots and lensoidal bodies, mostly associated with high-angle reverse faults and fracture arrays. They strike generally NNW-SSE and dip steeply to NE (Figure 4). They are mainly dilated, branched milky quartz veins and lenses with maximum width of ~150 cm, commonly restricted to the sheared metasediments, close to the altered granite masses. These veins show anastomozing and undulating geometries, both downdip and along the strike. Commonly, they cut the shear planes, but also are buckled around it, suggesting synchronous timing of vein formation and shearing. Most of the auriferous quartz veins are oriented parallel to the intersection lineation originated where N24ºW/40ºNW crenulation foliation is superimposed on N45-59ºW/44-63ºNE axial planar foliation. A 10 to 30 cm wide zone of densely quartz-veined wall rock bounds the main lode and proportionally correlates with its thickness. In the southern part of the mine area, these quartz veins are commonly associated with highly deformed schists, in which the main foliation (N48^{o}W/29-40^{o}NE) is deformed by crenulation microfolds. Herein, the country metasediments are intensively fractured, silicified, and enriched in disseminated pyrite crystals. These veins have low sulfide contents. Variable combination of carbonate, sulfide and minor kaolinite in-fillings occupy fractures in quartz grains, giving the veins a reddish hue. Fine-grained sulfides occur in fractures, in brecciation zone or along pressure solution seams.

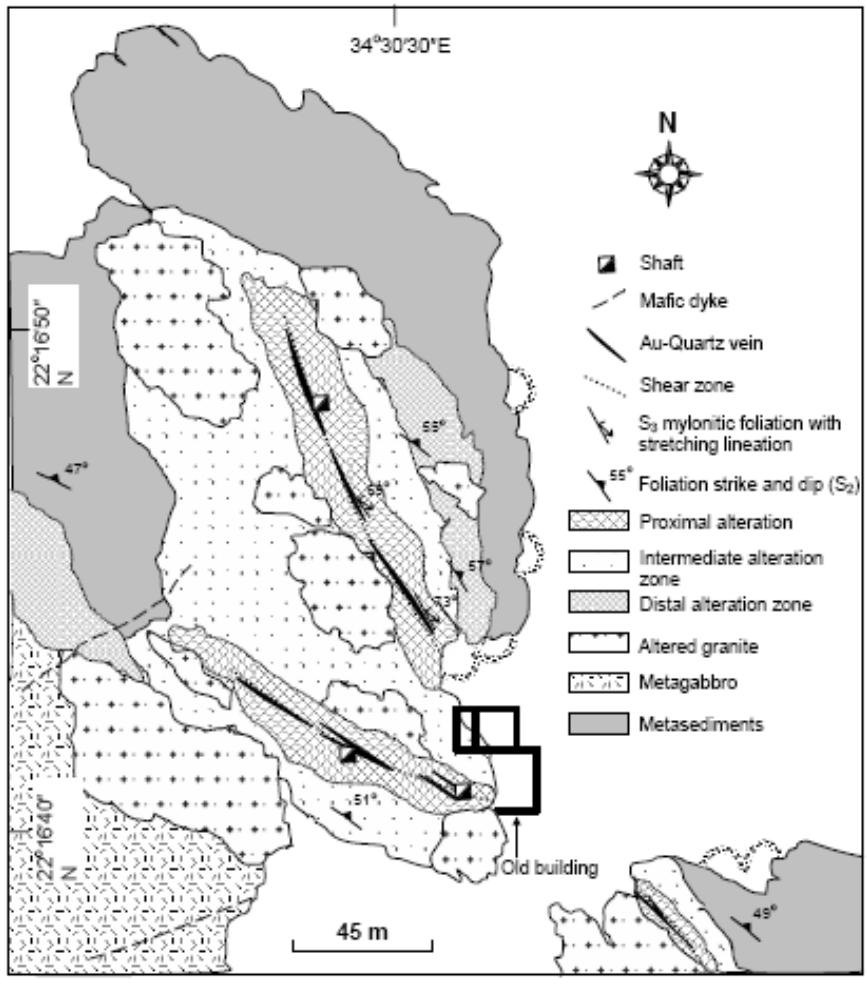

Figure 4. Simplified map of the Betam gold lode and associated alteration zones (Modified from Zoheir, 2008).

Next to these veins, the host rock is frequently bleached in color forming a pale halo varying from few centimeters to meters in width. Intermittent quartz and host rock stringers are common in the marginal parts of the main veins.

The ore mineralogy includes pyrite, arsenopyrite, subordinate chalcopyrite and galena, and minor electrum and free gold grains. Sulfide minerals are notably much concentrated in domains rich in Fe-hydroxides/sericite within the fracture zones. Gold is mainly confined to zones rich in wall rock selvages and iron-stained fractures within the quartz veins or frequently disseminated in the adjacent quartz-sericite alteration zone. Arsenopyrite and pyrite are the most common sulfide minerals, occurring mainly as disseminated individual subhedral grains (70µm - 2mm) or aggregates, usually confined to quartz grain boundaries or occupying microfissures in ore and silicate minerals. Some arsenopyrite crystals contain inclusions of electrum (Figure 5A), ranging in size from 10 to 40µm, and less commonly anhedral pyrrhotite. Pyrite is ubiquitous in all samples, occurring commonly as scattered euhedral grains associated with arsenopyrite. Euhedral arsenopyrite and pyrite grains are

commonly fractured and healed by recrystallized quartz and sulfides, mainly galena, chalcopyrite and altered pyrite.

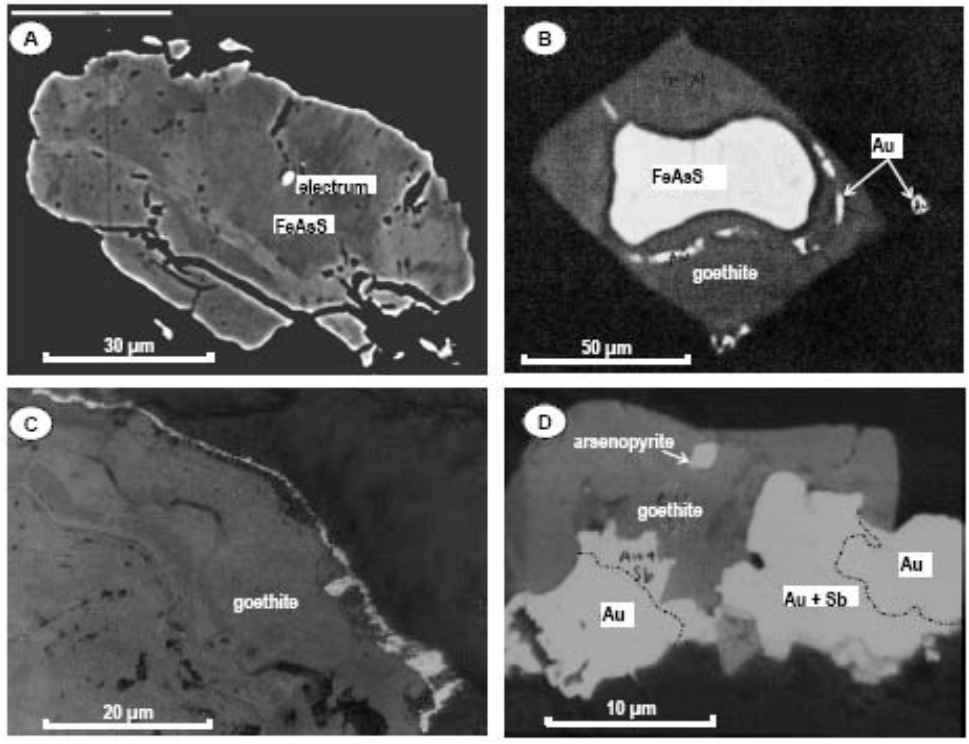

Figure 5. A. Large arsenopyrite grain contains electrum (4 µm) inclusion. B. Gold expelled as arsenopyrite oxidized into goethite. C. Free gold rimming rhythmic goethite grain. D. Aureostibite associated with native gold and goethite completely replacing arsenopyrite.

Various textural features, including juxtaposition and curved boundaries, suggest equilibrated coexistence of pyrrhotite inclusions, euhedral pyrite and arsenopyrite in the quartz veins. In cases, pyrite and arsenopyrite goethite replaces partly or completely the coarse-grained, with survived sulfide remnants and contains remains of the original sulfides still survived (Figure 5B). Chalcopyrite occurs as individual anhedral grains dispersed in the quartz veins, commonly intergrown with galena or associated with goethite. Minor fine anhedral grains of chalcopyrite and patchy galena grains occur in fissure zones and along grain boundaries, occasionally associated with free gold grains. Free gold grains are disseminated in the quartz veins, and associated with partly oxidized pyrites and arsenopyrite in the altered wall rock. It occurs as fracture fillings in deformed arsenopyrite and pyrite and/or as very thin (10-20µm) rims within or around the rhythmic goethite (Figure 5C). Where located in fractures or at grain boundaries, free gold is intergrown with aurostibite, $AuSb_2$ (Figure 5D). Occurrence of aurostibite indicates sulfur-deficiency predominated during the late mineralization (remobilization and oxidation). The ore mineral assemblage and EPMA data of arsenopyrite with gold inclusions, 30.4-30.7 wt. % As, led Zoheir (2008) to estimate 325-344^{o}C and 10^{-10}–$10^{-8.5}$ constraining temperatures and sulfur fugacity (fS_2) of conditions during ore deposition based on the Kretschmar and Scott (1976) diagram (Figure 6).

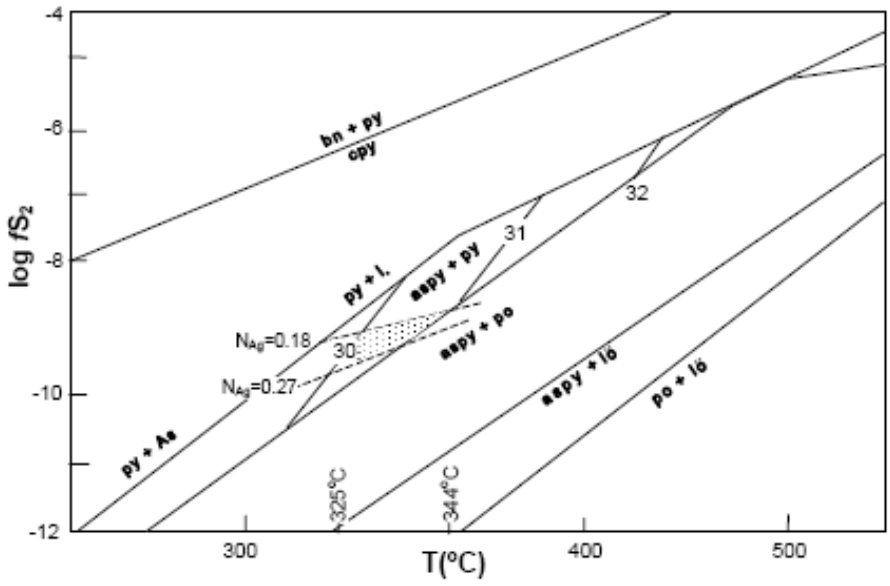

Figure 6. The Fe–Zn–As–S system at low pressure adapted from Scott (1983). Hatched area reflects deposition conditions of arsenopyrite+pyrite±pyrrhotite and electrum assemblage. Arsenopyrite-buffered curves at.% As 31, 32 and 33 (from Kretschmar and Scott,1976), and stability curves of silver; NAg in electrum (Barton and Toulmin, 1964). As: arsenic, aspy: arsenopyrite, bn: bornite, cpy: chalcopyrite, l: liquid, lö: loellingite, po: pyrrhotite, py: pyrite.

HYDROTHERMAL ALTERATION

Chemical interaction between rocks and the circulating hydrothermal solutions is certainly a major factor in precipitation of many ores (Rose and Burt, 1979; Susak, 1994). Hydrothermal alteration encodes information on the intensive (*P,T,* X_{CO2}, etc.) and extensive (fluid flux, mass of ore or gangue) properties of a hydrothermal system within and external to orebodies, and the secular relationship of mineralization to regional deformation, magmatism and metamorphism.

An understanding of the hydrothermal alteration processes is therefore important to obtain information on the physico-chemical conditions, and to characterize the transport and deposition of elements responsible for ore genesis (Reed, 1997; Cathelineau et al., 1993; Noronha et al., 2000).

In the study area, evidence of hydrothermal alteration is commonly limited to a 3-7 m wide halo of discoloration and destruction of primary textures. This halo is characterized by disseminated arsenopyrite, pyrite and carbonate aggregates. Alteration styles include sericitization, carbonatization, sulfidation, chloritization, and silicification.

A positive correlation between intensity of discoloration (bleaching) and thickness of the quartz veins signifies a considerable hydrothermal activity associated with quartz veining in the study area.

Alteration mineralogy documents a post-foliation low grade metasomatic assemblage. The mineralogical composition and intensity of the alteration are dependent, in part, on the host rock composition and, in another, on the proximity to the mineralized horizons.

Hydrothermal alteration around the auriferous shear zone has consistently developed in the metasediments and in the adjacent granite and metagabbro.

Mineralogical studies revealed the presence of three alteration zones, namely: (a) distal chlorite-calcite zone, (b) intermediate sericite-chlorite zone and (c) proximal pyrite-sericite zone. Boundaries among these zones are gradational over centimeter to decimeter-scales. Generally, the degree of quartz veining, gold and base metal enrichment increases from the outer towards inner alteration zones. The inner zone presents the highest gold grade, especially where it is traversed by quartz veinlets.

The alteration mineral assemblages have been determined in a total of 67 samples collected from the altered and fresh host rocks, by the aid of the microscopic investigations and the microprobe analyses.

Mineral percentages, ratios and alteration paragenesis have been estimated by using several thin sections and some doubly polished thin sections. In this respect, mono-mineralic contouring of the alteration data is used to map the wall rock alteration. Sample locations were plotted on a base map prepared from aerial photographs (scale 1:20,000) using the GPS readings and the numerous sketch drawings compiled during the field work.

The geographic distribution of the hydrothermal phases and mineralogical changes throughout the three alteration types are shown in Figure (4), and summarized in Table (1). The following is a detailed mineralogical variation throughout the three alteration zones.

Table 1. Summary of spatial distribution of the hydrothermal alteration phases in the wall-rock metasediments from the Betam gold mine area

Primary phases	ALTERATION ZONE AND ASSEMBLAGE			
	Distal zone	Intermediate zone	Ore zone	
			Proximal zone	Au-qz veins
Biotite	unstable, more or less completely replaced by chlorite	unstable, totally altered into chlorite±pyrite, calcite, hematite and rutile	completely replaced by sericite +pyrite	absent
Hornblende	unstable, all altered into chlorite± biotite, epidote, sericite, and iron oxides	mostly replaced by chlorite± biotite and calcite±pyrite	absent	absent
Feldspar	unstable, partly altered into sericite and kaolinite	almost completely replaced by sericite, quartz and frequent albite		absent
Quartz	stable, locally augmented	fairly developed	largely recrystallized and redistributed	
Garnet	stable in part, partially replaced by sericite and quartz along cracks	almost absent	absent	
Staurolite	unstable, completely replaced by chlorite+sericite±rutile	absent		
Sulphides	confined to chlorite in distribution	disseminated and randomly dispersed fine to medium-grained sulphide grains±gold		individual medium grained crystals, little gold
Total opaques %	<1	~3	2 - 5	~5

The Distal Chlorite-Calcite Zone (Chlorite+Calcite±Biotite±Pyrite±Sericite±Epidote)

The distal alteration zone is generally ubiquitous throughout the mine area, represented by an assemblage of chlorite+calcite±biotite±pyrite±sericite±epidote. An assemblage of quartz-calcite-chorite-sericite-epidote±hematite is, however, common near contacts between the metasediments and gabbroic rocks in the western part of the mine area (Figure 7). In places, the metasediments are densely seamed with micro-veinlets traversing the main foliation (0.5 mm wide), mainly of quartz, epidote and calcite.

Magnetite with hematite intergrowths are observed. Disseminated pyrite is common where alteration is prevasive. Limonite pseudomorphs after pyrite with remnants of pyrite were observed in most samples.

Biotite occurs as preferentially oriented subhedral to anhedral brown flakes with irregular and ragged edges in the intensely altered samples. Replacement of the large biotite plates by fine-grained aggregates chlorite is distinguished.

No petrographic evidence for significant volume change that accompanied the alteration of biotite to chlorite was observed. Chlorite also replaces hornblende and staurolite (if present). It is commonly associated with epidote and calcite. Chlorite flakes show random dimensional orientation and overprint the metamorphic schistosity. Chemically, the Fe/(Fe + Mg) range from 0.42 to 0.46 and Al^{IV} values vary between 1.09 and 2.26 a.p.f.u. This small variability suggests that chemical equilibrium of chlorite and hydrothermal fluid has been attained.

Calcite occurs as disseminated anhedral grains, patches and rims commonly associated with chlorite. Mixtures of calcite and epidote fill the interspaces and replace chlorite and biotite. EPMA data (not presented here) indicated that calcite has a pure composition, as components other than $CaCO_3$ are generally less than 5 percent. Rutile and magnetite occur as tiny globules, blebs and needles associated with titanite and biotite.

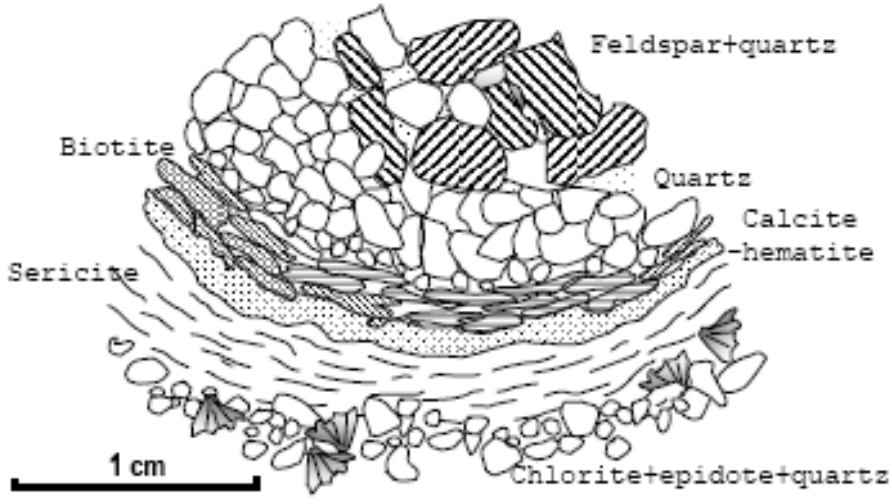

Figure 7. Simplified sketch illustrating distribution of the alteration mineral assemblages in altered metasediments from the distal alteration zone of Betam gold deposit.

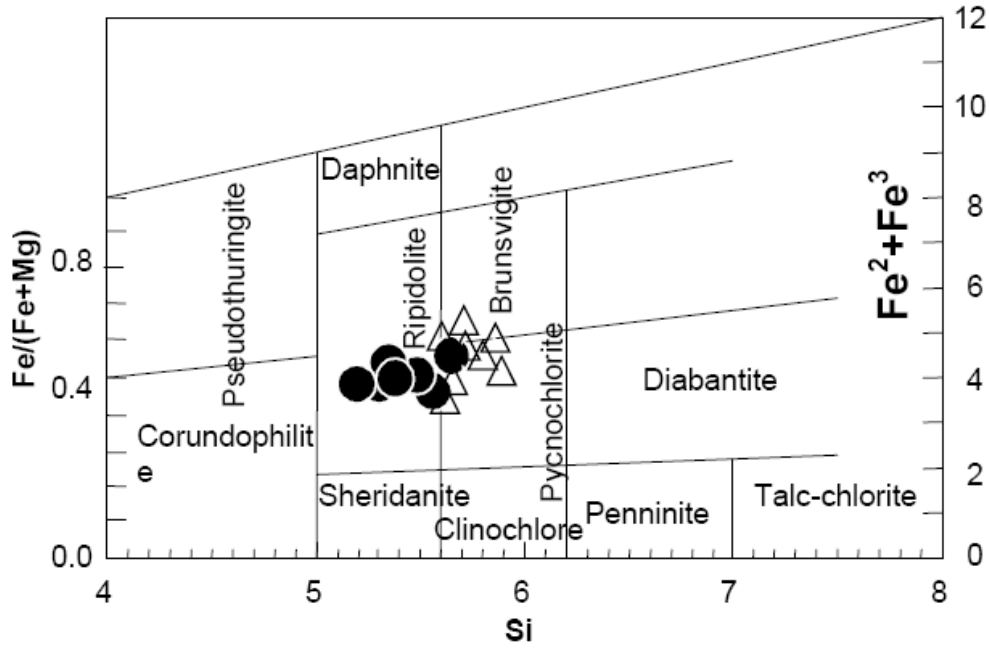

Figure 8. Si vs. (Fe^2+Fe^3) diagram showing plots of chlorites from distal (triangles) and intermediate (circles) alteration zones at Betam mine area. Classification of Hey (1954).

The Intermediate Sericite-Chlorite Zone (Sericite+Chlorite+Pyrite±Biotite)

The distal chlorite+biotite+calcite±epidote±pyrite±sericite zone passes gradually inwards into a greenish or yellowish green intermediate alteration zone. This zone is characterized by a sericite+chlorite±biotite assemblage along with abundant disseminated pyrite. It is manifested by discrete patches within the host metasediments in the central parts of the mine area, and pervasive assemblage throughout the finely laminated metasiltstones in the eastern part. Locally, it reaches some meters in width, surrounding the silicified zone. Alteration minerals typically fill fractures, but are subordinately densely disseminated around major fissure zones.

Sericite forms fine streaks parallel to the rock foliation. Little traces of biotite (or hornblende) have been observed as minerals are more or less completely hydrated and transformed into sericite+iron oxides. The rock is characterized by the presence of appreciable amount of pyrite in association with sericite and lensoidal pyrite.

Where present, biotite occurs as fine subhedral flakes commonly associated with chlorite. The latter occurs as low birefringent, pale to dark olive green subhedral flakes and/or aggregates of cleaved rosette-shaped grains, often filling interstices between xenocrysts in the altered metasediments. Chemical composition of chlorites from both distal and intermediate alteration zones are given in Table (2). The analytical data show that chlorite composition is chemically identical in both zones (rhipidolite to pycnochlorite; Figure 8). Slight compositional variation include slightly lower Al2O3 and FeO, but higher SiO2 and MgO contents in chlorite from the distal alteration zone (Table 2).

Table 2. Representative microprobe data and structural formulae of chlorites from the Betam gold deposit

	from the distal alteration zone								from the intermediate alteration zone							
	b112-5-5	b112-1-13	b112-7-1	b112-1-3	b112-2-3	B78-3-2	B78-4-5	B78-4-6	B7-1-10	b104-1-12	b104-8-4	b104-1-15	b104-1-4	b104-6-3	b104-2-5	b104-4-2
SiO_2	29.63	28.37	28.18	27.82	28.13	27.66	27.82	26.99	26.18	25.52	27.04	26.78	25.80	27.22	26.88	26.91
TiO_2	0.02	0.13	0.02	0.06	0.08	0.05	0.03	0.02	0.08	0.00	0.00	0.12	0.13	0.00	0.08	0.11
Al_2O_3	17.88	17.03	16.43	16.09	18.04	16.11	18.14	16.52	18.73	18.82	18.50	18.06	19.23	19.01	18.64	18.74
FeO	22.60	22.98	23.26	25.17	23.65	26.23	24.35	23.95	23.94	23.93	23.69	24.24	24.51	23.19	23.69	24.64
MnO	0.10	0.05	0.03	0.06	0.03	0.09	0.09	0.07	0.08	0.15	0.28	0.13	0.05	0.06	0.14	0.17
MgO	17.53	17.72	18.36	17.01	18.21	17.51	16.39	18.86	16.95	15.62	17.40	17.47	17.71	17.22	16.67	16.72
CaO	0.11	0.09	0.00	0.09	0.26	0.07	0.14	0.09	0.03	0.43	0.05	0.07	0.12	0.00	0.02	0.07
Na_2O	0.07	0.81	0.05	0.11	0.00	0.02	0.00	0.07	0.02	0.09	0.00	0.00	0.10	0.05	0.06	0.03
K_2O	0.05	0.02	0.01	0.00	0.01	0.00	0.03	0.01	0.03	0.00	0.00	0.00	0.06	0.05	0.01	0.00
F	0.08	0.05	0.11	0.00	0.05	0.00	0.03	0.08	0.00	0.18	0.06	0.26	0.06	0,11	0,08	0.12
Total	87.41	86.61	85.81	85.76	87.82	87.09	86.39	86.02	86.05	84.55	86.95	86.87	87.72	86.79	86.20	87.39
O_F	0.03	0.02	0.05	0.00	0.02	0.00	0.01	0.03	0.00	0.07	0.02	0.11	0.02	0.04	0.03	0.05
formula on 28 anions (anhydrous basis)																
Si	6.09	5.95	5.96	5.95	5.81	5.86	5.87	5.74	5.59	5.57	5.70	5.67	5.43	5.72	5.71	5.67
Al^{IV}	1.91	2.05	2.04	2.05	2.19	2.14	2.13	2.26	2.41	2.43	2.30	2.33	2.57	2.28	2.29	2.33
Al^{VI}	2.42	2.15	2.06	2.01	2.21	1.89	2.37	1.89	2.31	2.41	2.29	2.18	2.20	2.42	2.38	2.32
Ti	0.00	0.02	0.00	0.01	0.01	0.01	0.01	0.00	0.01	0.00	0.00	0.02	0.02	0.00	0.01	0.02
Fe(ii)	3.88	4.03	4.11	4.50	4.09	4.65	4.29	4.26	4.28	4.37	4.18	4.29	4.32	4.08	4.21	4.34
Fe(iii)	0.67	0.00	0.01	0.00	0.06	0.00	0.34	0.00	0.00	0.00	0.00	0.00	0.00	0.17	0.15	0.04
Mn	0.02	0.01	0.01	0.01	0.01	0.02	0.02	0.01	0.02	0.03	0.05	0.02	0.01	0.01	0.03	0.03
Mg	5.37	5.54	5.79	5.43	5.61	5.53	5.15	5.98	5.40	5.08	5.47	5.52	5.56	5.40	5.28	5.25
Ca	0.02	0.02	0.00	0.02	0.06	0.02	0.03	0.02	0.01	0.10	0.01	0.02	0.03	0.00	0.01	0.02
Na	0.03	0.33	0.02	0.04	0.00	0.01	0.00	0.03	0.01	0.04	0.00	0.00	0.04	0.02	0.03	0.01
K	0.01	0.00	0.00	0.00	0.00	0.00	0.01	0.00	0.01	0.00	0.00	0.00	0.02	0.01	0.00	0.00
Cations	19.76	20.10	20.00	20.03	19.98	20.12	19.88	20.20	20.04	20.02	20.00	20.05	20.19	19.94	19.95	19.99
CF	0.05	0.04	0.08	0.00	0.03	0.00	0.02	0.06	0.00	0.25	0.08	0.34	0.08	0.14	0.11	0.16
Fe/(Fe+Mg)	0.42	0.42	0.42	0.45	0.42	0.46	0.45	0.42	0.44	0.46	0.43	0.44	0.44	0.43	0.44	0.45
Mg/(Fe+Mg)	0.58	0.58	0.58	0.55	0.58	0.54	0.55	0.58	0.56	0.54	0.57	0.56	0.56	0.57	0.56	0.55
Si/Al	1.41	1.42	1.45	1.47	1.32	1.45	1.30	1.38	1.18	1.15	1.24	1.26	1.14	1.22	1.22	1.22
$Al^{iv}c$	2.20	2.35	2.33	2.36	2.48	2.46	2.45	2.55	2.72	2.75	2.60	2.63	2.87	2.58	2.60	2.65
T(°C) *	251.6	267.0	264.8	268.5	281.1	278.3	278.0	288.0	305.83	309.8	294.0	297.1	322.7	291.6	293.2	298.6

*Temperature estimated according to Kranidiotis & McLean (1987); correction for the Al^{iv}: $Al^{iv}c = Al^{iv} - 0,88*[Fe/(Fe+Mg)-0,34]$.

Table 3. Representative microprobe data of sericite in hydrothermally altered rocks from the Betam mine area.

In altered metasediments							In altered granite									
	104_1_5	104_1_6	104_1_8	104_1_9	104_2_4	104_3_1	104-5-3	104-6-2	104-7-2	204_3_4	204_3_6	204_3_5	204_3_7	204_3_3	204_3_8	204_1_2
SiO_2	48.24	47.55	47.29	47.19	49.01	48.71	49.26	47.32	48.97	47.85	48.03	48.04	47.82	48.23	48.56	49.81
TiO_2	0.00	0.27	0.36	0.10	0.06	0.31	0.11	0.14	0.05	0.22	0.33	0.35	0.40	0.28	0.10	0.12
Al_2O_3	24.60	25.80	26.46	27.53	24.38	26.00	25.69	25.36	25.51	31.35	32.37	32.38	33.43	31.84	32.57	31.70
FeO	7.55	7.54	6.46	6.92	7.90	7.23	6.42	8.27	6.34	2.36	1.67	1.62	1.64	1.71	1.50	0.63
MnO	0.00	0.00	0.10	0.00	0.00	0.10	0.05	0.01	0.07	0.06	0.00	0.00	0.04	0.00	0.02	0.02
MgO	3.86	3.49	3.80	2.44	3.50	2.41	2.82	4.94	3.33	1.97	1.43	1.43	1.05	1.98	1.84	1.64
CaO	0.02	0.07	0.02	0.07	0.08	0.00	0.01	0.00	0.01	0.13	0.12	0.12	0.04	0.00	0.00	0.03
Na_2O	0.15	0.22	0.22	0.29	0.59	0.31	0.43	0.13	0.26	0.19	0.08	0.15	0.19	0.07	0.05	0.07
K_2O	10.06	9.60	10.03	9.94	9.02	9.55	9.66	8.67	10.31	9.72	9.38	9.38	9.57	9.92	9.75	9.71
Total	94.48	94.54	94.74	94.48	94.54	94.62	94.45	94.84	94.85	93.85	93.41	93.47	94.18	94.03	94.39	93.73
T2	8.33	8.31	8.28	8.30	8.29	8.26	8.25	8.28	8.25	8.11	8.08	8.08	8.03	8.06	8.00	8.01
Formula on basis of 22 anions																
Si	6.69	6.58	6.52	6.52	6.76	6.70	6.76	6.52	6.72	6.46	6.46	6.46	6.39	6.,47	6.47	6.64
Ti	0.00	0.03	0.04	0.01	0.01	0.03	0.01	0.01	0.01	0.02	0.03	0.04	0.04	0.03	0.01	0.01
Al(iv)	1.31	1.42	1.49	1.48	1.24	1.30	1.24	1.48	1.28	1.54	1.54	1.54	1.61	1.53	1.53	1.36
Al(vi)	2.71	2.79	2.81	3.00	2.73	2.91	2.92	2.64	2.85	3.45	3.60	3.59	3.66	3.51	3.58	3.61
Al	4.02	4.21	4.30	4.48	3.97	4.21	4.16	4.12	4.13	4.99	5.13	5.13	5.26	5.04	5.11	4.98
Fe(ii)	0.88	0.87	0.75	0.80	0.91	0.83	0.74	0.95	0.73	0.27	0.19	0.18	0.18	0.19	0.17	0.07
Mn	0.00	0.00	0.01	0.00	0.00	0.01	0.01	0.00	0.01	0.01	0.00	0.00	0.00	0.00	0.00	0.00
Mg	0.80	0.72	0.78	0.50	0.72	0.49	0.58	1.02	0.68	0.40	0.29	0.29	0.21	0.40	0.37	0.33
Ca	0.00	0.01	0.00	0.01	0.01	0.00	0.00	0.00	0.00	0.02	0.02	0.02	0.01	0.00	0.00	0.00
Na	0.04	0.06	0.06	0.08	0.16	0.08	0.11	0.04	0.07	0.05	0.02	0.04	0.05	0.02	0.01	0.02
K	1.78	1.69	1.76	1.75	1.59	1.68	1.69	1.52	1.81	1.67	1.61	1.61	1.63	1.70	1.66	1.65
Total	14.21	14.17	14.21	14.15	14.12	14.04	14.05	14.18	14.15	13.88	13.75	13.76	13.78	13.84	13.80	13.70
Fe/(Fe+Mg)	0.52	0.55	0.49	0.61	0.56	0.63	0.56	0.48	0.52	0.40	0.40	0.39	0.47	0.33	0.31	0.18
Fe+Mg	1.67	1.59	1.54	1.30	1.63	1.34	1.32	1.97	1.42	0.67	0.47	0.47	0.40	0.59	0.54	0.40

The Fe/(Fe+Mg) ratios in chlorite from both zones are more or less identical. However, a slight increase is observed in samples from the intermediate alteration zone. Si/Al ratios are relatively high in the distal zone and gradually decrease slightly towards the intermediate zone. Estimated according to the method introduced by Kranidiotis and McLean (1987), formation temperature of chlorite from the distal alteration zone (251-288oC) is relatively lower than the range estimated for chlorite from the intermediate alteration zone (291-322oC).

The Proximal Pyrite-Sericite Zone (Quartz+Pyrite+Sericite±Albite)

Although not extensive, the quartz+pyrite+sericite±albite alteration represents the most conspicuous alteration type in the mine area. It is manifested by a NW-trending zone of densely quartz-veined, sheared rocks cutting across the country metasediments and granite. A quartz-sericite+pyrite+hematite assemblage is observed close to the granite masses. This alteration zone is intruded by several sulfide-quartz lenses and veinlets with variable lengths (0.5-2 m) and thickness (5mm - 30cm), forming a network structure. Where crosscut by sulfide-bearing quartz veins, this alteration zone presents the highest gold grades among the altered rocks (9 g/t).

Sericite occurs as randomly to weakly-oriented fine-grained flakes and aggregates associated with fine grained quartz, replacing chlorite and biotite (Figures 9A,B). It is generally rich in (Fe+Mg) and poor in Al^{vi}, (Al^{iv} + Al^{vi}) and Na if compared with sericite in the altered granite (Table 3). Sericite in the altered metasediments consists of fine-grained celadonitic muscovite, with phengite content (atomic Fe+Mg per formula) ranging from 1.30 to 1.96. These values are considerably higher than those of the coarse-grained sericite in the altered granite (0.51). Very fine biotite shreds are observed in muscovite flakes in several samples. It is suggested that the relatively large muscovite crystals and their parallel Mg- and Ti-bearing compositions have been formed by different degrees of replacement of original biotite, leaving some biotite remnants as inclusions.

This assumption is emphasized by the high Al content in sericite and the celadonitic overgrowth, implying formation through fluid infiltration and retrogression of biotite. Generally, the Fe/(Fe+Mg) ratios of sericite in the proximal alteration zone adjacent to the gold-bearing quartz veins are very variable, but generally much higher in the metasediments than in granite (see Table 3).

In the silicified shear zone, quartz and feldspar porphyroblasts are brecciated and exhibit some characteristic shear textures, e.g. mortar and augen textures. Coarse-grained quartz crystals exhibit minor conjugate shear planes, along which fine intracrystalline quartz is observed.

The latter is most probably resulted from the dissolution and recrystallization of quartz due to shearing and heat effect (Passchier and Trouw, 1996). Away from the silicified shear zone, disseminated pyrite and destruction of primary texture decrease.

Albite occurs as fine-grained, subhedral crystals dispersed in the altered metasediments adjacent to the main gold-bearing quartz veins. Texturally, albite forms clear, twinned subhedral crystals in the altered metasediments and irregular rims around k-feldspar crystals in the granite. Microscopic and SEM observations constrain on the overgrowth of albite at the

expense of relict andesine crystals and chlorite flakes in samples from the proximal alteration zone.

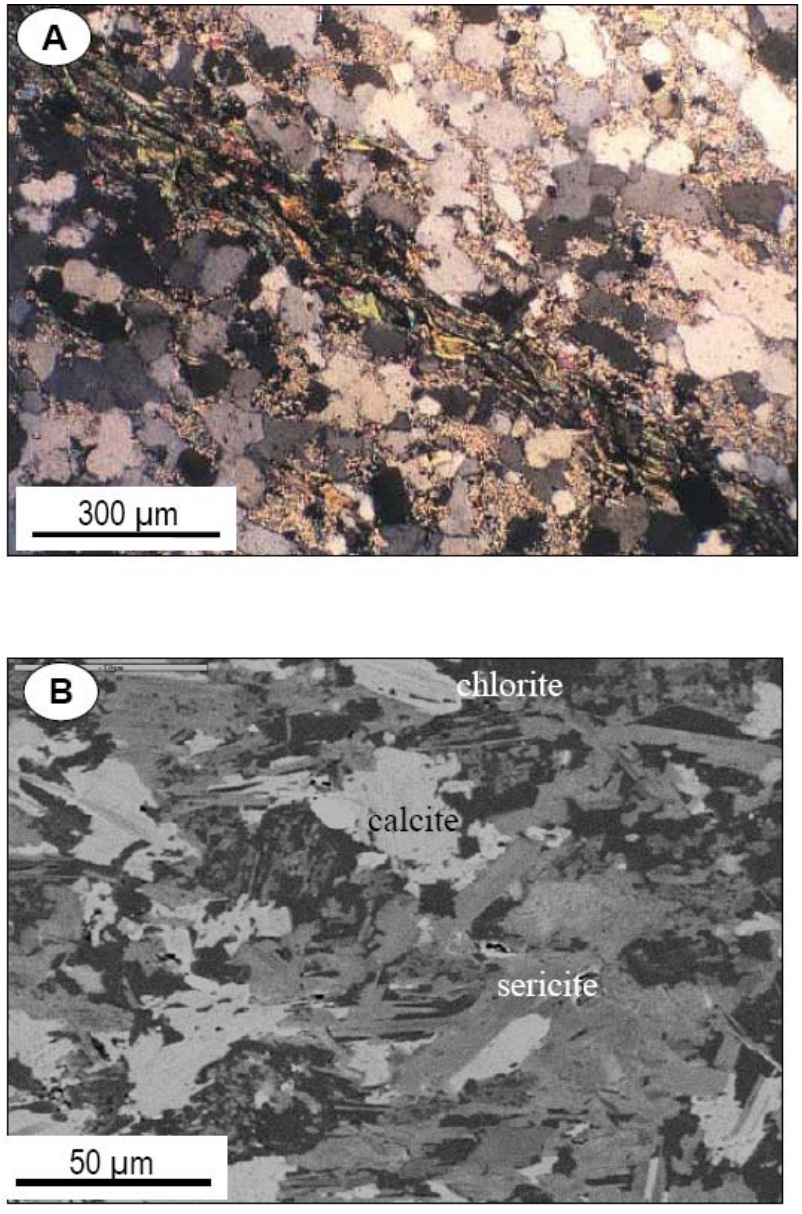

Figure 9. Photomicrographs showing intensely sericitized metasediments from the proximal alteration zone A. Interstitial sericite replacing biotite flakes, XPL. B. Sericite and calcite replacing chlorite, BSE.

GEOCHEMISTRY OF THE ALTERED WALLROCKS

A geochemical study is intended to characterize the chemical changes which might have been undertaken by the host rocks during alteration. Mass balance calculations are used to

evaluate the mobility of elements during alteration and to understand the chemical modifications associated with the hydrothermal alteration.

Theoretically, chemical changes occurred during the fluid-wall rock interaction can be quantified by comparing the chemical analyses of the least and most altered rock types. A number of bulk rock analyses of the hydrothermally altered and least/un-altered metasediments from the mine area was used for this study (Table 4). Whole rock analyses were done by ACTLABS Laboratories (Canada) using X-Ray Fluorescence (XRF) and Inductively Coupled Plasma-Emission Spectrometer (ICP-ES) for major elements reported as oxides and selected trace elements, and Inductively Coupled Plasma- Mass Spectrometer (ICP-MS) for trace and rare earth elements.

Elemental Changes Associated with Different Types of Alteration

Direct comparison between chemical analyses of the least-altered and intensely altered rocks using wt% of the major constituents are not useful, as it does not take into account the volume changes that accompany mass transfer. One widely used method for establishing a way of normalizing the data so that relative elemental gains and losses during hydrothermal alteration can be determined has been that of Gresens (1967). In this method Gresens argued that, if those components that are likely to have been immobile during alteration can be identified, they can be used to establish any volume change that has taken place, thereby allowing gains or losses of other components to be calculated based on that assumed volume change. Consequently, he considered composition- volume relations during alteration, and derived equations for calculation of gains and losses from chemical analyses and specific gravities of altered and unaltered rocks. His equation was later modified by Grant (1986) to one relating the concentration of a component in the altered rock to that in the original through a mass change term such that

$$C_i^A = M^O/M^A\,(C_i^O + \Delta C^i)$$

where C_i^A = concentration of component i in the altered rock; M^O = mass of the original, fresh rock; M^A = mass of the altered rock; C_i^O = concentration of component i in the original rock; and ΔC^i = change in concentration of component i.

If the analytical data are plotted as C_i^A *vs*. C_i^O, those elements that are immobile (i.e., $\Delta C^i = 0$) will define a mass change term (M^O/M^A) or "isocon" that can be used to calculate gains and losses of other components through a series of simple equations. Since "relative immobility" can be the result of either no mass transfer of an element or geochemically similar behavior of certain elements during alteration, it is preferable to base determination of the isocon on as many geochemically dissimilar species as possible (Grant, 1986). In this method, analyses have to be arbitrarily scaled to fit on a single plot of concentrations of elements in altered rock *vs*. their concentration in the fresh precursor. Depending on the scaling factor used, this results in points getting closer to or farther from a best-fit line through the "immobile" elements, depending on their distance from the origin.

Table 4. Geochemical data) used for the mass balance calculations of Betam gold deposit

	Unaltered host rocks				Median	Distal alteration zone			Intermediate alteration zone			Proximal alteration zone			
wt%	b_212	b_83	b_124	b_115		b_112	b_111	b_78	b_106	b_104	b_113	b_84in	b_154	b_222	b_123
SiO_2	52.51	51.34	51.35	53.55	52.51	54.36	53.51	51.19	52.36	57.14	53.16	59.79	61.35	60.21	58.02
Al_2O_3	12.81	13.42	12.98	12.91	12.81	12.68	13.04	12.69	12.52	12.43	11.73	11.94	10.95	11.15	12.12
Fe_2O_3	9.12	9.19	8.97	9.12	9.12	8.49	9.88	9.62	9.31	8.03	9.82	9.47	9.88	9.47	10.06
MnO	0.25	0.24	0.33	0.21	0.25	0.27	0.39	0.24	0.41	0.15	0.27	0.28	0.31	0.39	0.33
MgO	13.16	13.08	13.91	11.94	13.16	9.98	7.75	12.87	8.54	5.84	7.65	2.05	2.53	2.45	3.05
CaO	3.29	3.33	3.01	3.25	3.29	3.99	4.64	3.80	5.11	3.19	4.53	2.69	3.05	3.14	3.25
Na_2O	0.91	0.98	0.86	0.83	0.91	0.99	1.07	1.00	1.10	1.96	1.66	1.08	0.95	1.19	2.05
K_2O	3.61	3.55	2.97	2.89	3.61	2.94	3.96	2.91	4.84	4.72	4.29	5.78	4.13	4.49	5.12
TiO_2	0.69	0.63	0.64	0.66	0.69	0.63	0.64	0.62	0.61	0.63	0.58	0.59	0.60	0.56	0.59
P_2O_5	0.50	0.47	0.40	0.45	0.50	0.55	0.42	0.60	0.55	0.12	0.47	0.45	0.49	0.43	0.51
L.O.I	3.63	4.04	4.01	3.88	3.63	4.26	4.93	4.42	5.31	4.96	5.63	4.93	5.07	5.21	5.01
S	0.04	0.08	0.09	0.05	0.04	0.10	0.36	0.13	0.51	0.37	0.28	0.46	0.49	0.48	0.48
Total	100.52	100.34	99.53	99.74	100.52	99.22	100.58	100.10	101.17	99.53	100.09	99.51	100.65	99.17	100.69
ppm															
Au	0.0	0.0	0.0	0.0	0.0	2.0	2.0	1.0	3.0	6.0	4.0	8.0	9.0	12.0	11.0
Ag	0.0	0.0	0.0	0.0	0.0	0.0	0.0	1.0	1.0	2.0	2.0	2.0	3.0	4.0	3.0
Ba	74	93	87	57	80	123	253	96	286	167	57	247	281	257	157
Sr	88	116	83	67	85.31	95	185	131	240	140	250	172	190	331	190
Rb	52	35	66	67	59.02	85	50	56	95	78	29	60	68	123	65
Cr	65	69	47	63	63.92	78	113	58	93	142	124	45	24	21	45
V	31	43	28	29	30.13	47	92	56	210	115	120	102	107	101	58
Co	17	21	22	16	19.19	18	16	27	23	21	17	13	16	15	9
Ni	15	22	21	14	18.32	18	27	23	267	34	151	30	38	32	32
Cu	12	14	10	11	11.42	12	8	16	33	14	23	11	12	23	22
Zn	31	47	44	22	37.31	27	29	30	91	36	56	25	33	37	28
As	345	307	248	316	311.50	330	942	341	1087	644	810	2167	2223	2223	2167
Sc	5	5	5	3	5.00	11	8	3	10	9	13	11	13	6	9

	Unaltered host rocks				Median	Distal alteration zone			Intermediate alteration zone			Proximal alteration zone			
wt%	b_212	b_83	b_124	b_115		b_112	b_111	b_78	b_106	b_104	b_113	b_84in	b_154	b_222	b_123
Zr	49	48	47	54	48.60	48	46	38	51	45	43	36	36	42	41
Y	7	6	9	7	6.88	8	9	8	7	11	10	7	7	8	8
Nb	9	7	9	7	8.00	10	6	9	12	6	12	4	6	8	6
La	22.11	23.50	21.24	24.65	22.80	23.07	21.67	26.60	26.77	19.59	24	26.28	28.18	27.85	27.85
Ce	43.0	45.7	52.1	42.0	44.4	47.8	47.5	48.8	52.6	42.9	48.6	50.0	55.6	54.3	54.0
Nd	18.0	14.2	13.9	16.7	15.47	18.96	17.50	20.67	20.92	18.73	20.75	19.75	21.25	21.49	21.47
Sm	5.10	4.80	4.26	4.68	4.74	5.02	4.51	5.55	5.26	3.78	5.46	5.04	5.37	5.21	5.25
Eu	0.82	0.81	0.69	0.80	0.80	0.89	0.84	0.85	0.88	0.96	1.90	0.92	0.93	0.70	1.00
Tb	0.58	0.57	0.56	0.57	0.57	0.61	0.60	0.57	0.74	0.68	0.90	0.92	0.88	0.65	0.79
Yb	0.09	0.13	0.12	0.07	0.11	0.84	2.21	0.53	2.61	2.23	0.69	2.65	0.86	1.06	1.30
Lu	0.04	0.03	0.04	0.07	0.04	0.12	0.15	0.05	0.18	0.29	0.05	0.15	0.18	0.21	0.20
density (gr/cm3)	2.94	2.94	2.96	2.91	2.94	2.92	2.88	2.93	2.91	2.87	2.88	2.83	2.85	2.82	2.85

In the present work, and in order to provide better visualization of relative immobility of elements, we have chosen to remove the visual effects of arbitrary scaling by scaling all the data to be the same distance from the origin (i.e., normalizing so that the sums of squares = 1), a method suggested by Humphris et al. (1998). The result is a plot in which all of the data points lying along an arc of a circle centered on the origin. By evaluating which points group together (and hence are behaving similarly) and combining this with consideration of their geochemistry, we can evaluate which elements to use for calculation of the mass change term (M^O/M^A), which can then be used to calculate elemental gains and losses. Chemical comparisons have been made among data of the altered rocks and median of the four unaltered rock samples. The use of the statistical median instead of the absolute concentration in a specific sample of the altered and least-altered rocks minimizes the error introduced by heterogeneity which might be expected in the host metasedimentary rocks. The median values are noticed to be similar to the chemical analyses corresponding to the most representative sample of the un-altered rocks, selected on basis of petrographic observations.

On the x-y plots of fresh/fresh and fresh/altered rock samples, TiO_2, Al_2O_3, Zr, Y, Sc and Tb are noticed to be consistently grouped together, therefore assumed to be similarly immobile during alteration (Figures. 10A→D). On basis of their immobility, these elements are used to monitor mass transfer in the isocon calculations (c.f. Selverstone et al., 1991; Leitch and Lentz, 1994; Humphris et al., 1998; Kolb et al., 2000). Their use to define the isocon allowed calculation of the net mass changes in the altered wall rock.

Mass changes of each alteration zone with respect to the un-altered precursor are summarized in Table (5). Based on the mass balance calculations, volume and mass changes (ΔV, ΔM) associated with hydrothermal alteration in the mine area increase gradually from the distal through intermediate to proximal alteration zone. Chemical gains and losses that are attributed to the hydrothermal alteration in the three alteration zones indicate: (i) addition of SiO_2, K_2O, Na_2O, S, LOI; (ii) removal of MgO; (iii) relatively inert behavior of Al_2O_3, TiO_2, MnO, Fe_2O_3, whose slight variations can be attributed to the original protolith. CaO is variably mobile, slightly gained in the distal and intermediate alteration zones but lost in the proximal alteration zone. The trace elements behave variably in the different alteration types, but a notable increase in As, Ba, Sr, V, and Ni in the intensively altered rocks is verified. Investigation of the REE behavior reveals a little modification of their distribution patterns with hydrothermal alteration. Heavy REE are more or less unchanged, whereas light REE show mobility in all alteration types, where their concentration generally increases.

Alteration Diagrams

Based on the conclusion that Al and Ti were immobile during alteration, or their mobility was not significant, correlation between their concentrations in the analysed samples should draw a general overview of alteration. A single alteration trend, obtained by plotting TiO_2 *vs.* Al_2O_3 contents in the altered samples and the un-altered precursors, is considered as indicative of an initially homogeneous precursor (Figure 11). Notably, samples from the proximal alteration zone are reasonably more intensively altered (distant from the precursor) if compared with those collected form the distal alteration zone. This observation demonstrates that fluid-wall rock buffering is attained close to the Au-quartz veins, whereas in the distal zone the system was out of equilibrium.

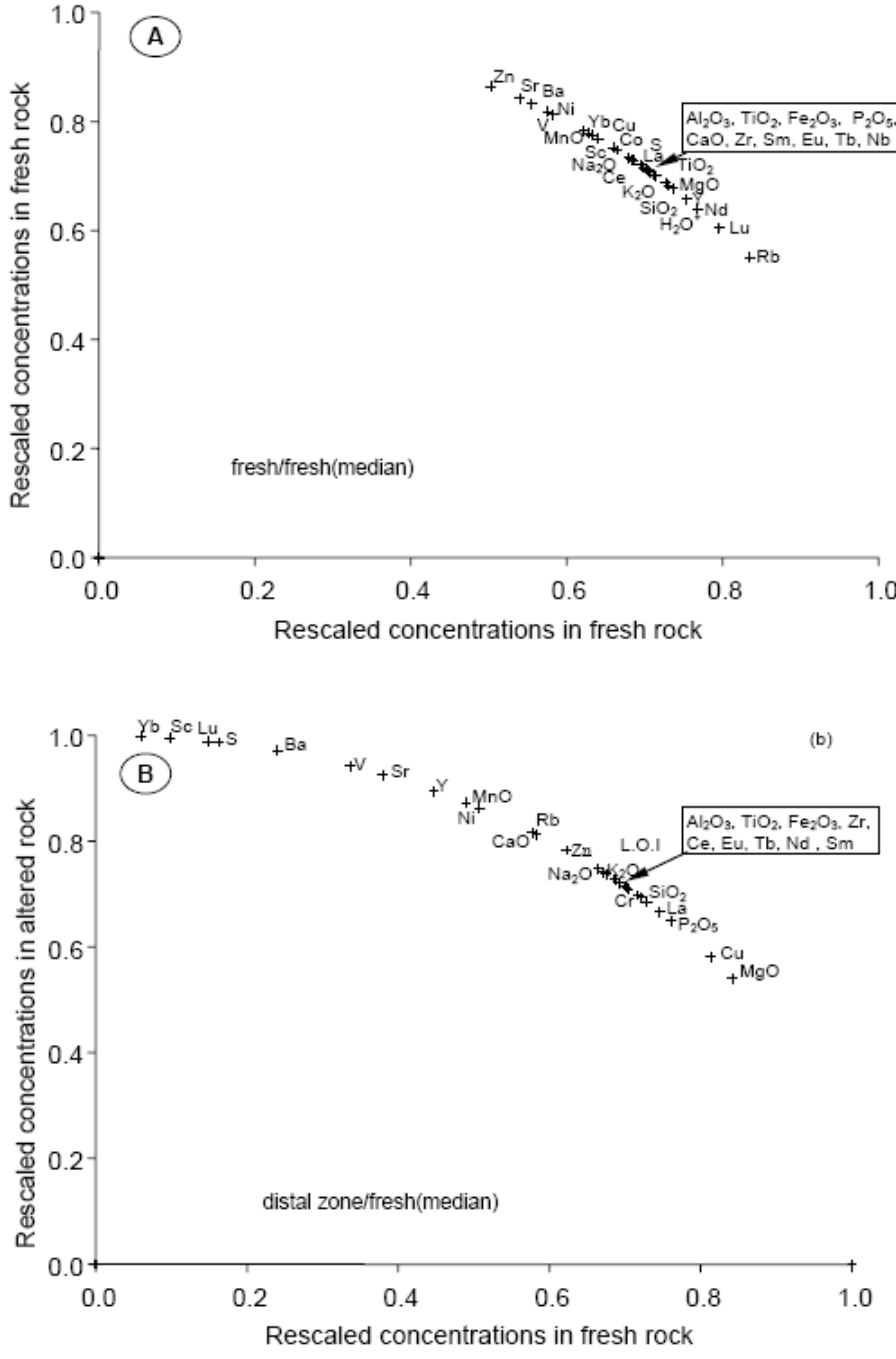

Figure 10. (Continued).

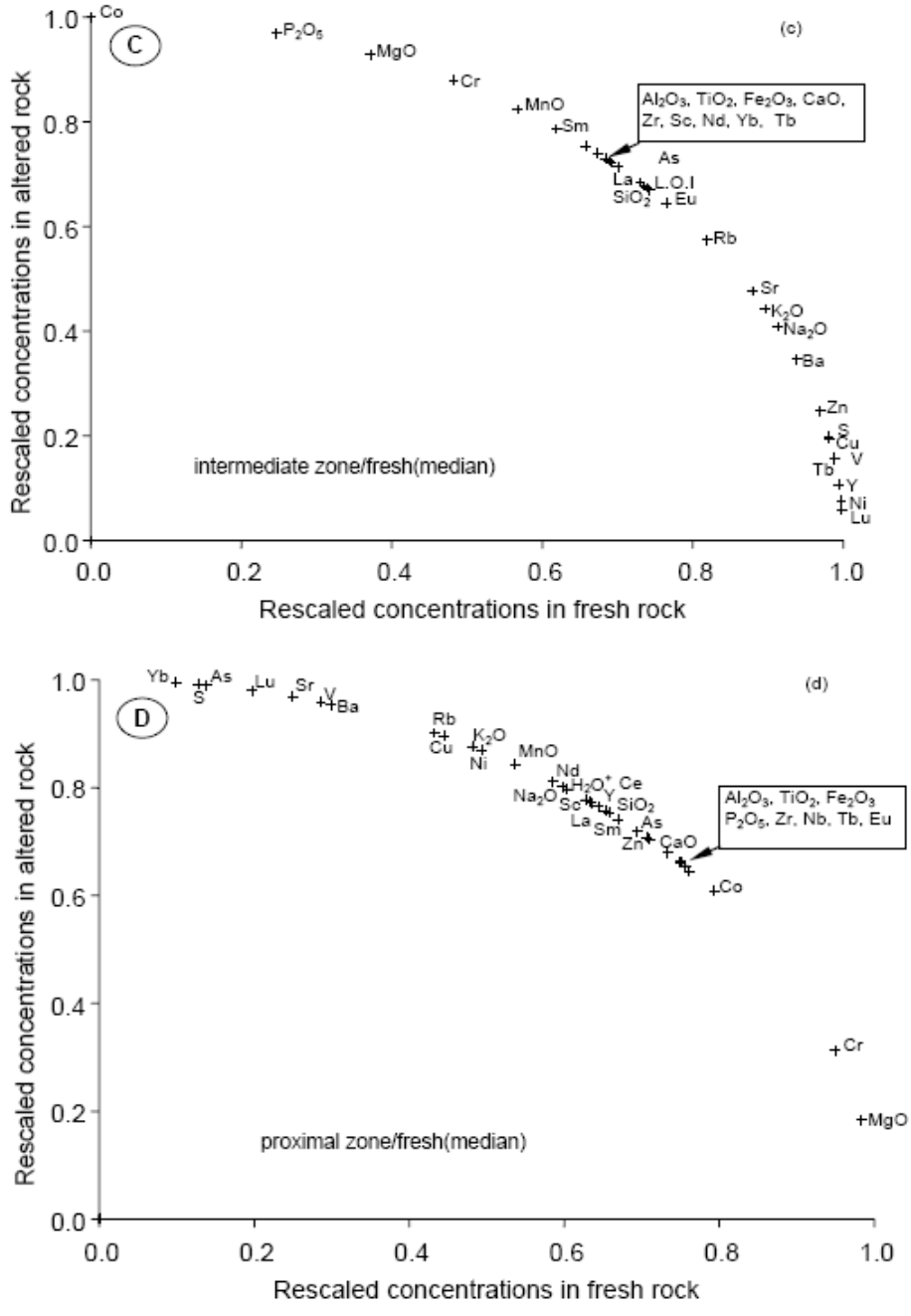

Figure 10. Plots of data of a host rock metasediments fresh precursor/median of the four fresh samples (A) and altered-unaltered pairs from the different alteration zones (B, C, D) rescaled to allow evaluation of which elements may be considered "relatively immobile" during alteration. The concentration data have been standardized so that the sum of squares equals 1, thereby resulting in all data points lying along the arc of a unit circle (see text for further discussion).

Table 5. Major and trace element mass changes in the three alteration zones associated with the Betam gold deposit

	Distal alteration zone			Intermediate alteration zone			Proximal alteration zone			
	b_112	b_111	b_78	b_106	b_104	b_113	b_123	b_84in	b_154	b_222
g/100 g										
SiO_2	4.56	3.67	1.27	2.48	7.45	3.31	8.36	10.20	11.82	10.64
Al_2O_3	0.23	0.60	0.24	0.06	-0.03	-0.75	-0.35	-0.54	-1.57	-1.36
Fe_2O_3	-0.30	1.15	0.88	0.56	-0.77	1.09	1.33	0.72	1.15	0.72
MnO	0.03	0.16	0.00	0.18	-0.09	0.04	0.10	0.04	0.07	0.16
MgO	-2.75	-5.07	0.26	-4.24	-7.05	-5.17	-9.95	-10.99	-10.49	-10.57
CaO	0.87	1.55	0.68	2.04	0.04	1.44	0.11	-0.47	-0.10	0.00
Na_2O	0.14	0.23	0.16	0.26	1.15	0.84	1.24	0.23	0.10	0.35
K_2O	-0.21	0.85	-0.24	1.76	1.64	1.20	2.06	2.74	1.03	1.41
TiO_2	0.02	0.03	0.01	0.00	0.02	-0.03	-0.02	-0.02	-0.01	-0.05
P_2O_5	0.11	-0.02	0.16	0.11	-0.34	0.03	0.07	0.01	0.05	-0.02
L.O.I	0.48	1.18	0.65	1.57	1.21	1.90	1.26	1.18	1.32	1.48
S	0.04	0.31	0.07	0.47	0.32	0.23	0.44	0.42	0.45	0.44
g/1000 kg										
Au	2	2	1	3	6	4	11	8	9	12
Ag	0	0	1	1	2	2	3	2	3	4
Ba	47	182	19	217	93	-21	83	176	211	186
Sr	13	107	51	164	60	175	113	93	112	259
Rb	29	-8	0	40	22	-29	8	3	11	69
Cr	17	54	-4	33	84	65	-17	-17	-39	-42
V	19	66	28	188	89	94	30	75	81	75
Co	0	-2	9	5	3	-1	-10	-6	-2	-4
Ni	1	9	6	259	17	139	15	13	21	15
Cu	1	-4	5	23	3	13	11	-1	1	12
Zn	-9	-7	-6	57	0	20	-8	-12	-4	1
As	31	667	43	818	358	531	1940	1940	1999	1999
Sc	6	3	-2	6	4	9	4	7	8	1
Zr	1.28	-0.80	-9.11	4.40	-1.84	-3.91	-5.99	-11.19	-11.19	-4.95
Y	1.35	2.48	1.44	0.83	4.56	3.66	1.61	0.14	0.66	1.61
Nb	2.39	-1.76	1.35	4.47	-1.76	4.12	-1.76	-3.84	-1.76	0.31
La	1.18	-0.28	4.84	5.02	-2.45	2.25	6.14	4.50	6.49	6.14

Table 5. (Continued)

	Distal alteration zone			Intermediate alteration zone			Proximal alteration zone			
	b_112	b_111	b_78	b_106	b_104	b_113	b_123	b_84in	b_154	b_222
Ce	5.27	4.98	6.34	10.24	0.28	6.20	11.76	7.58	13.45	11.76
Pr	0.00	0.00	0.00	0.00	0.00	0.00	0.00	0.00	0.00	0.00
Nd	4.24	2.72	6.01	6.27	4.00	6.10	6.83	5.06	6.62	6.83
Sm	0.47	-0.05	1.03	0.73	-0.81	0.93	0.72	0.49	0.84	0.72
Eu	0.12	0.07	0.08	0.11	0.19	1.17	0.23	0.15	0.16	-0.08
Tb	0.07	0.06	0.02	0.20	0.14	0.36	0.25	0.39	0.35	0.11
Yb	0.77	2.19	0.45	2.61	2.21	0.61	1.25	2.65	0.79	0.99
Lu	0.09	0.11	0.01	0.14	0.26	0.01	0.16	0.11	0.14	0.17
mass change term										
Slope Ti,Al	0.99	1.01	0.98	0.97	0.98	0.91	0.93	0.93	0.89	0.87
ΔM =	-1.22	0.79	-1.80	-3.46	-2.27	-8.91	-6.56	-7.40	-10.51	-12.73
ΔV =	-1.89	-1.27	-2.13	-4.44	-4.59	-10.77	-9.41	-10.87	-13.25	-16.29

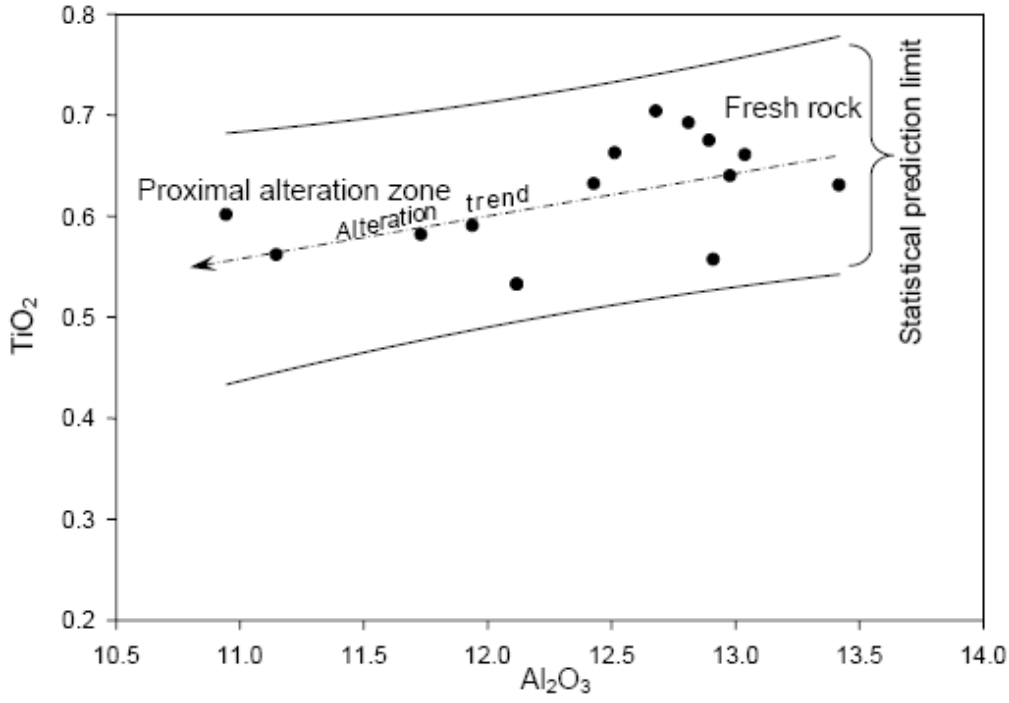

Figure 11. TiO_2 vs. Al_2O_3 (wt.%) binary plot of the un-altered (fresh) and altered rocks from the Betam gold deposit. Alteration trend is the best fit line among all samples.

Undulating anhedral quartz grains and sub-grains increase notably in zone densely seamed with quartz veinlets. To examine the mutual relation between veining and silicification, contents of SiO_2 are plotted versus Al_2O_3 in samples from the alteration zones (Figure 12). The plot shows a progressive silicification from the distal to proximal alteration zone, where gold grade increases.

This increase may be induced by the mineralizing fluid or simply attributed to redistribution of silica in the host rocks. For example, if SiO_2 decreases by 5 wt% in the 10 to 20 m wide zone of the host rock during alteration, a vein of approximately 1 to 1.5 m width could form if all the SiO_2 are re-deposited. However, mass balance calculations indicate that silica is gained in the three alteration zones if compared with the un-altered host rock, and not depleted. This leads to conclude that quartz veining and alteration in the mine area are derived by a silicification process, through which silica was derived form circulating SiO_2-rich hydrothermal fluids.

In order to eliminate the lithologic effect, the alumina normalization method (element/Al_2O_3, Fenton, 1987) is adopted. This method is based upon the observation that there is a strong correlation between most of the elements and Al_2O_3. If an element is bonded by aluminous minerals (e.g. muscovite, chlorite, feldspar), the ratio of element/Al_2O_3 will not vary with alumina concentration. On the other hand, if the ratio of element/Al_2O_3 does vary with Al_2O then this suggests either that alteration occurred or that the element is not bonded by alumina minerals. K is known to be bonded with alumina minerals; therefore, variation in K_2O/Al_2O_3 with alumina concentration is only caused by alteration. Figure (13) shows that K

was significantly mobile through hydrothermal alteration in the investigated deposit, with more K_2O enrichment close to the ore body.

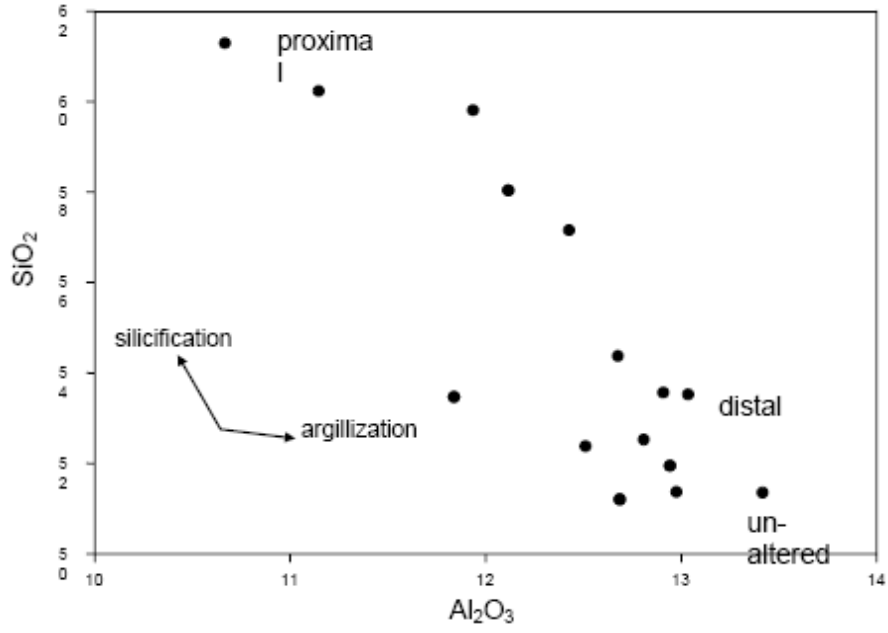

Figure 12. Plot of wt.% SiO_2 vs. wt.% Al_2O_3 showing data distribution of the hydrothermally altered rocks from Betam gold deposit.

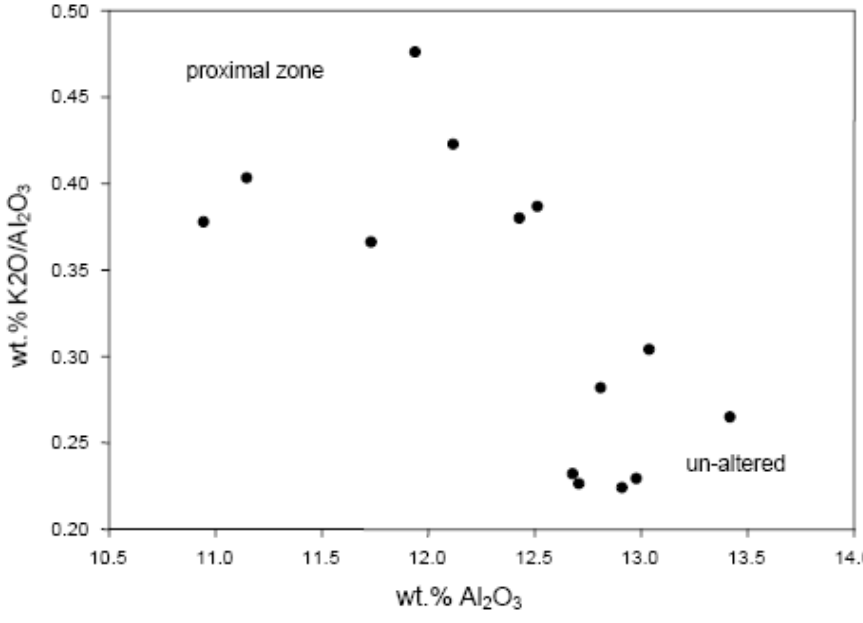

Figure 13. Plot of wt.% K_2O/Al_2O_3 vs. wt.% Al_2O_3 showing data distribution of the hydrothermally altered rocks from Betam gold deposit.

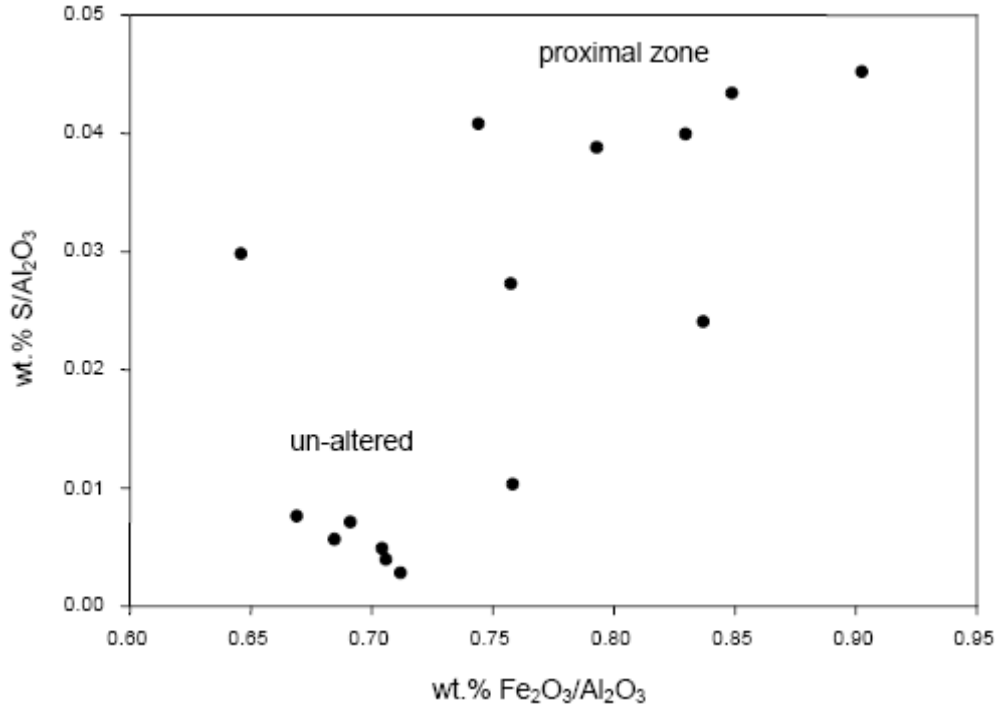

Figure 14. Plot of wt.% S/Al_2O_3 vs. wt.% Fe_2O_3/Al_2O_3 showing data distribution of the hydrothermally altered rocks.

Although progressive sericitization is ob served in samples from distal to proximal alteration zone, loss in total wt% Al_2O_3 might be due to replacement of aluminous minerals by silica through pervasive silicification.

The S/Al_2O_3 versus Fe_2O_3/Al_2O_3 plot can be very useful to measure the degree of sulfidation and to distinguish mechanisms of pyrite precipitation (Hofstra and Cline, 2000). Pyrite that forms by sulfidation of host rock iron has a vertical trajectory, whereas pyrite that forms by other mechanisms lies along a trajectory with a slope of 0.8. Data of the analyzed samples plot along a generally more or less vertical trajectory, or locally along and inclined line, with very small inclination (~0.06). This small slope value may indicate a sulfidation process, in which non-significant amounts of iron was added (Figure 14).

Whole Rock $\delta^{18}O$ Values

In order to obtain information on the fluid–rock interaction, 23 whole-rock samples were analyzed for their oxygen isotopic composition. The method followed was that of Clayton and Mayeda (1963), but using CIF_3 as the oxidizing reagent. Mass spectrometric measurements have been performed on a Finnigan MAT 252 mass spectrometer at the University of Tübingen (Germany). Accuracy of the analyses lies within ±0.2 per mil. Values are reported in the conventional δ-notation in permil relative to SMOW (Standard Mean Ocean Water).

For the host rock pelitic metasediments, whole rock $\delta^{18}O$ values of 18.4-16.6 per mil are determined, which are typical for metamorphosed and slightly altered pelitic rocks (Savin and Epstein, 1968; Hoefs, 1997). The sheared and mineralized rocks deviate significantly from the host rock to a lighter oxygen isotopic composition. The isotopic compositions of the distal, intermediate and proximal alteration zones are distinct (Table 6). The whole rock $\delta^{18}O$ values of the distal chlorite-calcite alteration zone are 13.7-12.3 per mil. For the intermediate sericite-chlorite alteration $\delta^{18}O$ values of 12.8-10.7 per mil were determined. The proximal pyrite-sericite alteration is characterized by a marked decrease in values with $\delta^{18}O$ = 11.2-9.6 per mil.

Table 6. Whole rock $\delta^{18}O$ values of hydrothermally altered rocks from Betam gold deposits

sample	Distance to quartz veins (m)	$\delta^{18}O$‰ (SMOW)
b_15	510	18.4
b_16	335	17.7
b_17	120	18.0
b_19	23	17.2
b_121	14	16.9
b_77	12	18.1
b_124	11	17.4
b_102	10	16.8
b_83	8	16.6
Distal zone		
b_112	7	13.5
b_134	6	13.7
b_111	6	13.6
bx12	5	12.9
b_78	4	12.7
b_72	4	12.3
Intermediate zone		
b_106	3.5	12.8
b_44	3	11.2
b_104	2.5	11.6
b_113	2	10.7
Proximal zone		
b_81	1.75	11.2
b_123	1.5	11
b_84in	1	9.9
b_154	0.5	10.1
b_222	0.15	9.6

$\delta^{34}S$ Values of Sulfides

Thirty three separates of sulfides associated with gold mineralization (16 pyrite and 17 arsenopyrite separates) have been hand-picked under a binocular microscope from samples collected from the mineralized quartz veins and different alteration types.

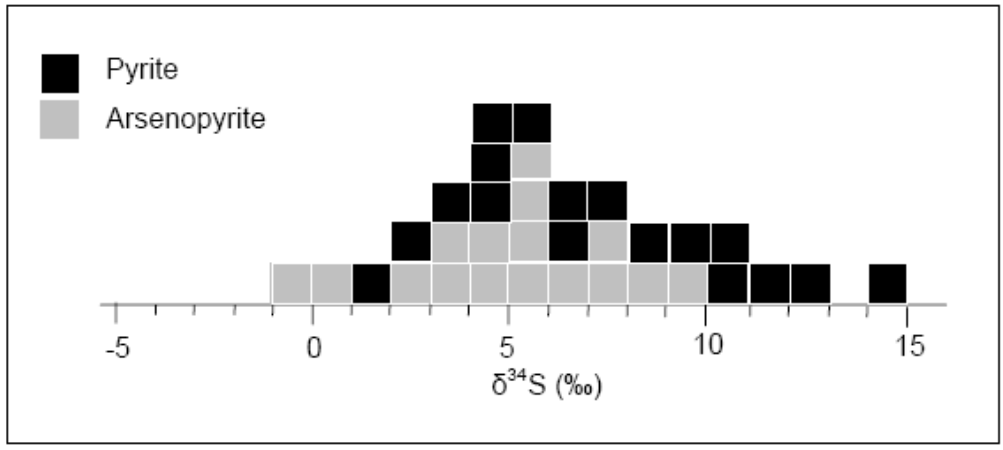

Figure 15. Distribution $\delta^{34}S$ values of pyrite and arsenopyrite associated with gold in the mineralized vein and wall-rock samples.

Pyrite and arsenopyrite are chosen for this study as their concentrations allows collecting the separates and because of their intergrowth textures which are suggestive of coexistence (cogenesis).

Purity of the analyzed separates is in excess of 95%. Analyses were performed using a gas-ion mass-spectrometer equipped with an element analyser (Optima, Micromass) at the Institute of Mineralogy and Geochemistry, Universität Karlsruhe (TH). The overall analytical error is less than +0.2 per mil.

The present analytical data are presented in The $\delta^{34}S$ values for pyrite range from -0.6 to 9.7 per mil, with a mean value of 5.6 per mil. For arsenopyrite, $\delta^{34}S$ values vary from 1.3 to 14.1 per mil, with a mean value of 4.3 per mil (Figure 15). These comparable values likely imply isotopic homogeneity induced by equilibrium conditions during gold-sulfides deposition.

Thus, for three pyrite-arsenopyrite pairs from the auriferous quartz veins, the $\Delta_{py\ -\ aspy}$ values range from -0.2 to 0.4. The equilibrium fractionation factors for pyrite-H_2S (Ohmoto and Rye, 1979) are -1 per mil at ~320°C, average estimate of chlorite and arsenopyrite thermometry (comparable with temperatures of fluid inclusions entrapment, Zoheir, 2008). The equilibrium isotope fractionation factor for arsenopyrite-H_2S is assumed to be similar (Layne et al., 1991). Assuming that sulfur was predominant as H_2S in the ore fluids, the $\delta^{34}S_{H2S}$ values from -1.6 to 13.1 per mil may be taken as the bulk sulfur isotope composition of the hydrothermal fluids ($\delta^{34}S_{\Sigma S}$) using mineral- H_2S fractionation factors and chlorite temperatures.

Alteration Model

A genetic relationship between the hydrothermal alteration and gold mineralization is inferred from observations including the presence of mineralized quartz veins within a volume of altered rocks, and increase of wall rock alteration and density of veining towards the main Au-bearing quartz veins.

Table 7. Simplified, elementary chemical reactions assumed to have been responsible for mineral transformations by hydrothermal alteration in Betam gold deposit

$(Fe^{++},Mg)_2Al_9(Si,Al)_4O_{20}(O,OH)_4 + 2K(Fe,Mg,Ti)_3AlSi_3O_{10}(OH)_2 + 2SiO_2 + 6H^+ + K^+ + 4O^{2-} \rightarrow (Fe,Mg,Ti)_5Al_2Si_3O_{10}(OH)_8 + 3KAl_3Si_3O_{10}(OH)_2 + TiO_2 + 3(Fe,Mg)^{2+}$
staurolite biotite fluid chlorite muscovite rutile (aq) ...(1)

$2K(Fe,Mg,Ti)_3AlSi_3O_{10}(OH)_2 + 4H^+ + 12O^{2-} \rightarrow (Fe,Mg,Ti)_5Al_2Si_3O_{10}(OH)_8 + 3SiO_2 + 6TiO_2 + (Fe,Mg)^{2+} + 2K^+$
biotite fluid ch

$2Ca_2(Mg,Fe,Al)_5Si_8O_{22}(OH)_2 + 6H_2O + 4CO_2 + 3O_2 \rightarrow 2(Fe,Mg)_5Al_2Si_3O_{10}(OH)_8 + 4CaCO_3 + 10SiO_2$
hornblende fluid chlorite calcite quartz ...(3)

$(Fe,Mg)_3Al_2(SiO_4)_3 + 2K(Fe,Mg,Ti)_3AlSi_3O_{10}(OH)_2 + H^+ + 2O^{2-} \rightarrow (Fe,Mg,Ti)_5Al_2Si_3O_{10}(OH)_8 + 3KAl_3Si_3O_{10}(OH)_2 + 3SiO_2$
garnet biotite fluid chlorite muscovite quartz ...(4)

$2K(Mg,Fe)_3(AlSi_3O_{10})(OH,F)_2 + 4H^+ + 2H_2S^- \rightarrow (Mg,Fe)_5Al(AlSi_3O_{10})(OH)_8 + 3SiO_2 + FeS_2 + 2K^+ + 4F^-$
biotite fluid chlorite quartz pyrite aq. ...(5)

$3K(Fe,Mg,Ti)_3AlSi_3O_{10}(OH)_2 + 18H_2S + 10O_2 \rightarrow KAl_3Si_3O_{10}(OH)_2 + 9FeS_2 + 3SiO_2 + 9TiO_2 + 9Mg^{2+} + 2K^+ + 20H_2O$
biotite fluid sericite pyrite quartz rutile (aq.) .....(6)

$(Fe,Mg,Ti)_5Al_2Si_3O_{10}(OH)_8 + 10H_2S + 8O_2 \rightarrow 5(Fe,Mg)S_2 + 3SiO_2 + 5TiO_2 + 10H_2O + 2Al(OH)^{2+}$
chlorite fluid pyrite quartz rutile (aq.) .....(7)

$3K(Fe,Mg,Ti)_3AlSi_3O_{10}(OH)_2 + 18HS^- + 5.5O_2 \rightarrow KAl_3Si_3O_{10}(OH)_2 + 9FeS_2 + 3SiO_2 + 9TiO_2 + 11H_2O + 9Mg^{2+} + 2K^+$
biotite fluid sericite pyrite quartz rutile (aq.) .....(8)

$(Fe,Mg)_5Al_2Si_3O_{10}(OH)_8 + 10HS^- + 3.5O_2 \rightarrow 5FeS_2 + 3SiO_2 + 5TiO_2 + 9H2O + 5Mg^{2+}$
chlorite fluid pyrite quartz rutile (aq.) ....(9)

$K(Mg,Fe)_3AlSi_3O_{10}(OH,F)_2 + K^+ + Al^{3+} + 2Au(HS)_2^- \rightarrow KAl_3Si_3O_{10}(OH,F)_2 + 2FeS_2 + 2Au + 4H^+ + Mg^{2+}$
biotite fluid sericite pyrite (aq.) .....(10)

The gradational contacts between the alteration zones imply progressive interaction during and after infiltration of the ore-forming fluids into the host rocks. In this context, changes in the host rock composition, mineral microanalyses and modal mineralogy are used to decipher the type and extent of fluid-wall rock interactions during alteration.

Given the investigations of Meyer and Hemley (1967), Mueller and Saxena (1977), Barton and Skinner (1979), Kishida and Kerrich (1987) and Groves and Forst (1991), a group of simplified chemical reactions are assumed to have been responsible for the main mineral transformations induced by hydrothermal alteration in the mine area (Table 7). These reactions are not intended to represent actual fluid-mineral reactions nor realistic identification of the mobile components. The reactions, however, integrate the mineralogical and whole-rock chemical effects of the alteration process.

The incipient mineralogical transformations are typified by a nearly complete conversion of the Fe-Mg silicates into chlorite and muscovite by means of hydrolysis, probably according to one or more of the reactions 1, 2, 3 and 4 (Table 7).

The spatial association of chlorite and iron sulfides with hydrothermal quartz is consistent with chloritization due to reaction 4. However, the presence of biotite relics in the intermediate alteration zone implies an incomplete transformation if the paragenesis described by reaction 5 has taken place.

Sulfidation might be attributed to the conversion of biotite to sericite in the presence of H_2S (reaction 6), which is evident by development of thin envelopes of sericite-chlorite adjacent to the sulfide-rich zones, and bordering the quartz-pyrite veinlets. It might also have taken place by oxidation of chlorite or magnetite by H_2S-bearing solutions (reaction 7).

Alternatively, if HS^- was the main sulfur species in the solution instead of H_2S, the pyrite forming reaction might directly involve acid-base equilibria, equations 8 and 9. The last two reactions are redox changes-induced (S^{2-} is oxidized to S^-) and, therefore, tend to reduce the interacting fluids particularly where the fluid/rock ratio is low, thus providing favorable conditions for gold deposition (Phillips and Groves, 1983). Buchholz et al. (1998) described a similar paragenesis formulated as in equation 10 (Table 7).

DISCUSSION

Mineralization Type and Hydrothermal Alteration Characteristics

The disseminated style of gold-sulfide mineralization and alteration mineral assemblages, including chlorite, sericite, calcite and pyrite are characteristic of orogenic gold deposits (Groves et al., 1998) formed under upper greenschist to lower amphibolite facies conditions (Eilu et al., 1999 and references therein). Combining the field and petrographic observations indicate that formation of the auriferous quartz veins was spatially and temporally linked to the development of the brittle-ductile shear zone at the mine area.

The systematic distribution of alteration types is attributed to temporal and lateral evolution in composition of the fluid through interaction with the wall rock. Generally, addition of SiO_2, H_2O, CO_2, K_2O, and S is accentuated by the widespread association of chlorite, calcite, sericite, and sulfides.

The calculated mass changes typically exhibit a good correlation with the modal changes in the analyzed samples.

Further, the progressive losses of MgO are consistent with the modal decrease of mafic minerals as the veins are approached.

Such a correlation strongly suggests that the mass transfer was closely coupled with the fluid-mineral reactions during alteration. For a similar sericite-carbonate-sulfide alteration associated with gold deposits, Kishida and Kerrich (1987) have proposed that the alteration would result in the release of H^+ from the fluid which decreases the fluid pH, probably reducing the solubility of gold.

Coexistence of pyrite+arsenopyrite±pyrrhotite±chalcopyrite and calcite in the alteration domains denotes that f_{O2}, reduced sulfur and CO_2 (and the activities of other components) were internally buffered via mineral reactions (Henley et al., 1984; Mikucki and Ridley, 1993). The presence of microscopic and sub-microscopic gold particles in intensely altered wall-rock and the close association of this gold with the Fe-sulphides, points towards the importance of the wall-rock alteration (sulfidation) in depositing gold.

Sulfidation by reaction of sulfur in the ore fluid with Fe-Mg-bearing minerals (biotite and/or amphiboles) of the host rock led to breakdown of the S-complex and gold precipitation (reaction 10 in Table 7, e.g. Klein et al., 2005). Variation in pH conditions is likely have taken place due to the formation of sericite (release of H+ to the fluid) and while the carbonatization of the host rock (removal of CO_2 from the fluid). As a consequence, destabilization of gold-bisulfide complexes and lowering of gold solubility through interplay of cooling, changes in pH and fluid-wall rock interaction was, at least partly, responsible for gold deposition in the area.

Stable Isotope Systematics

Stable isotope ratios have long been integral to the study of hydrothermal systems, and have in many instances provided the key to constraining the origin and evolution of the mineralizing fluids in these systems. Variations in $\delta^{18}O$ values have been used to map the extent of fossil hydrothermal systems in silicate rocks (Engel et al., 1958; Taylor, 1973, 1974; Criss et al., 1985).

Hydrothermal alteration in most common silicate rocks produces $\delta^{18}O$ values that are lower than those of the original host rock. This depletion in $\delta^{18}O$ occurs when hydrothermal fluids with low $\delta^{18}O$ values interact and exchange with host rocks with high $\delta^{18}O$ values, causing progressive enrichment of $\delta^{18}O$ in the hydrothermal fluid and associated $\delta^{18}O$ depletion in the country rock.

Less commonly, the $\delta^{18}O$ values of the hydrothermally altered rocks are higher than those of the fresh precursor.

On the other hand, sulfur isotope compositions of hydrothermal S -bearing minerals are controlled by the total sulfur isotope composition of the fluids and by the temperature, Eh, and pH at the site of mineralization (Rye and Ohmoto, 1974; Ohmoto and Rye, 1979; Ohmoto, 1986). The first parameter can be regarded as a characteristic of the source, whereas the remaining three relate to the environment of deposition.

Accordingly, interpretation of the distribution of $\delta^{34}S$ values relies on a knowledge of the sulfur isotope characteristics of the various possible sulfur reservoirs and of parageneses that constrain the ambient temperature, Eh and pH.

The decrease in $\delta^{18}O$ whole rock values from around 18 per mil for the un-altered host rocks to ~12.6 per mil, 11.4 per mil, 10.4 per mil for the distal, intermediate and proximal alteration zones, respectively, suggests hydrothermal alteration by external fluids and progressive fluid–rock interaction.

Changes in $\delta^{18}O$ value are unlikely to result from changes in the mineralogy only, as the changes in bulk chemistry are too small to account for a significant change in isotopic compositions.

The isotopic compositions of the three alteration zones are different, suggesting different degrees of fluid-wall rock interaction due to variability in shear intensity from proximal to distal zones.

Notably, the deviation of the $\delta^{18}O$ whole rock values for the distal alteration from the host rock composition is stronger than for the proximal alteration zone. The opposite should be expected, however, a more complex fluid–rock interaction can be anticipated in the center of the shear zone because of stronger deformation and fluid flow.

Values of $\delta^{34}S$ for pyrite and arsenopyrite point out to rather mixed magmatic and metamorphic genesis for these sulfides.

The relatively wide range of $\delta^{34}S_{\Sigma S}$ values for the ore fluids indicates that sulfur was derived from heterogeneous sources or different sulfur components that have not fairly well mixed in the hydrothermal solutions. This implies the contribution of both magmatic and metamorphic sources in the ore fluids.

CONCLUSIONS

Gold mineralization and hydrothermal alteration zones at the Betam mine area are manifestations of a shear zone-related hydrothermal system linked spatially and genetically with the NW-SE brittle-ductile shear zone.

Gold-sulfide mineralization (pyrite, arsenopyrite, galena, minor chalcopyrite and gold) is closely associated with pervasive hydrothermal alteration, quartz+sericite+chlorite+ alcite±biotite ±epidote±albite. Based on the petrographic and micro-analytical investigations, the hydrothermal alteration halo enveloping the auriferous quartz veins is classified into three distinct hydrothermal alteration zones, namely: (a) distal chlorite-calcite zone, (b) intermediate sericite-chlorite zone, and (c) proximal pyrite-sericite zone.

These zones merge to each other gradually, ending outwards into unaltered schist. Mass balance calculations reveal that, although generally more or less conserved (not exceeding ~13%), rocks from the proximal alteration zone experienced significant metasomatic changes relative to limited mass and volume changes for the distal alteration zone. Chemical gains and losses with increase the intensity of hydrothermal alteration is indicative of addition of SiO_2, K_2O, Na_2O, S, LOI, removal of MgO and relatively inert behavior of Al_2O_3, TiO_2, MnO, Fe_2O_3, whose slight variations can be attributed to the original protolith. CaO is variably mobile throughout the three alteration zones. An increase in Au, As, Ba, Sr, Rb, V, and Ni in the intensively altered rocks is verified.

Investigation of the REE behavior reveals a little modification of their distribution patterns with hydrothermal alteration. Heavy REE are more or less unchanged, whereas light REE show mobility in all alteration types, where their concentration generally increases. Alteration diagrams, i.e. X–Y plots of wt% SiO_2/Al_2O_3, $[K_2O/Al_2O_3]/Al_2O_3$ and $[S/Al_2O_3]/[Fe_2O_3/Al_2O_3]$, provide evidence for progressive silicification, sericitization, and sulfidation as a function of gold mineralization. These alteration characteristics reflect the interaction between the wall-rocks and a carbonic-rich solution, similar to the orogenic gold deposits elsewhere.

Components other than CO_2 and gold added to the altered rocks are K_2O, H_2O, S and As with either introduction or redistribution of SiO_2, and more localized introduction of Na_2O, Rb and Ba. There is a distinctive suite of immobile elements (e. g., Al, Ti, Zr, V, Y) and relatively mobile elements (Fe, Mg, Cr, Ni, Sc), and there is commonly a volume increase in mineralized zones (e.g. Groves and Foster, 1991).

The proximal (inner) alteration zone reflect fluid-dominated (unbuffered) metasomatic reactions, whereas, the distal and intermediate zone reflect a decreasing gradient of fluid to rock ratio, as well as chemical gradients, and represent progressive infiltration of the fluid into the wall-rock.

The hydrothermal alteration system of the studied deposit is best indicated by a conspicuous increase in volume and mass changes, and a systematic decrease in whole-rock oxygen stable isotope values from the distal through intermediate to proximal alteration zone (Figure 16). Contribution of a light isotopic source (magmatic?) is based on the decrease in oxygen isotopic values approaching the mineralized quartz veins. Furthermore, sulfur isotope values of sulfides associated with gold from the mineralized quartz veins and adjacent wall-rock and the calculated $\delta^{34}S_{\Sigma S}$ values for the ore fluids suggest derivation form mixed magmatic and metamorphic fluids.

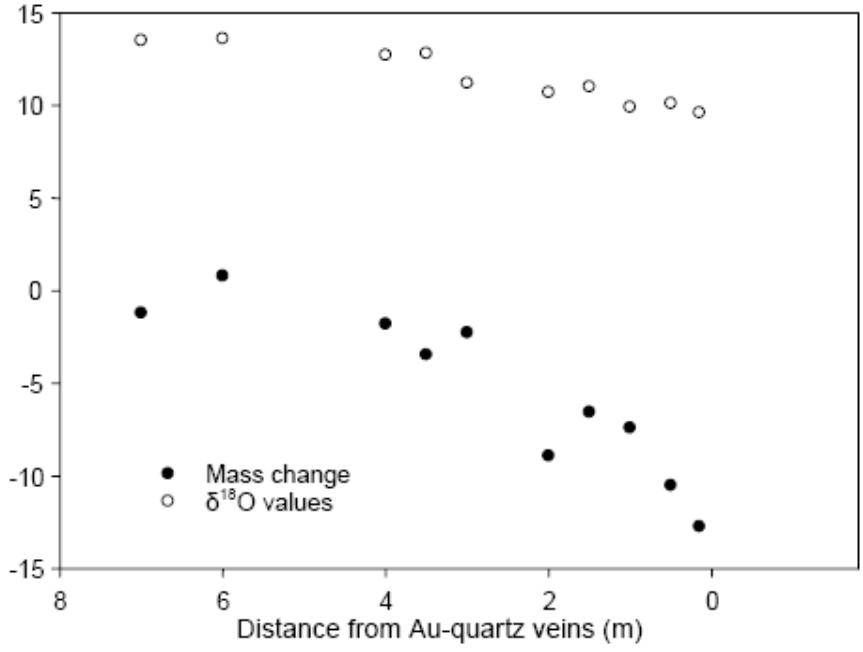

Figure 16. Variation in mass changes and $\delta^{18}O$ values with distance from the Au-quartz veins. The three alteration zones are indicated by discontinuous curves joining the data points.

ACKNOWLEDGMENTS

The authors acknowledge the help of Drs. A. Matzke (Universität Tübingen), Z. Berner (Universität Karlsruhe, TH) and R. Kaindl (University of Graz, Austria) during the laboratory work. We are also grateful for the European commission for supporting a short time visit to Germany for the first author in the summer 2006, through which the Mass spectrometric and microprobe analyses have been conducted. Dr. Susan Humphris, Woods Hole Oceanographic Institution, is greatly thanked for her critical reading and enlightening comments on the initial version of this manuscript.

REFERENCES

Abdel Tawab, M.M., 1992. Gold exploration in Egypt from Pharoanic to modern times. *Zentralbl. Geol. Paläont. Teil* 1. 1991, 2721-2733.

Ahmed, A.M., Said, M.M., El Baghdady, M.M., Abdel Wahab, G., 2001. Mineral potential of the eastern part of Wadi Allaqi, South Eastern Desert, Egypt. *Annals of the Geological Survey of Egypt XXIV*, 451-462.

Almond, D.C., Ahmed, F., Shaddad, M.Z., 1984. Setting of gold mineralization in the northern red Sea hills of Sudan: *Econ. Geol*. 79, 389–392.

Amin, M.S., 1955. Geological features of some mineral deposits in Egypt. *Bull Inst Desert* Egypt, 5, 208–239.

Azer, N., 1966. Remarks on the origin of Precambrian mineral deposits in Egypt (U.A.R.). *Mineralogy and Petrology*, 11 (1-2), 41-64.

Barton, P.B.Jr., Skinner, B.J., 1979. Sulfide mineral stabilities. Geochemistry of Hydrothermal Ore Deposits. In: Barnes, H.L., (Ed.), 278–403, Wiley Intersci., New York.

Barton, P.B.Jr., Toulmin, P., 1964. The electrum-tarnish method for the determination of the fugacity of sulfur in laboratory sulfide system: *Geochimica et Cosmochimica Acta*, 28, 619–640.

Botros, N.S., 1993. New prospects for gold mineralization in Egypt. *Ann. Geol. Surv.* Egypt 19, 47–56.

Botros, N.S., 2004. A new classification of the gold deposits of Egypt: *Ore Geol. Rev*. 25, 1-37.

Buchholz, P., Herzig, P., Friedrich, G., and Frei, R., 1998. Granite-hosted gold mineralization in the Midlands greenstone belt: a new type of low-grade large scale gold deposit in Zimbabwe. *Mineral. Depos*. 33, 437-460.

Cathelineau, M., Boiron, M.C., Essarraj, S., Barakat, A., Garcia Palomero, F., Urbano, R., Toyos, J.M., Florido, P., Pereira, E.S., Meireles, C., Ferreira, N., Castro, P., Noronha, F., Dȍria, A., Ribeiro, M.A., Barriga, F., Mateus, A., Yardley, B. Banks, D., 1993. Major structural factors of Au concentrations in the northwestern Iberian Massif (Spain-Portugal): a multidisciplinary and multiscale study. In: Hach-Ali, P.F., Torres-Ruiz, J.,Gervilla, F. (Eds.), Proceedings of the second biennial SGA meeting Current research in geology applied to ore deposits, Granada, 613–616.

Clayton, R.N., Mayeda, T.K., 1963. The use of bromine pentafluoride in the extraction of oxygen from oxides and silicates for isotopic analysis. *Geochimica et Cosmochimica Acta*, 27, 43–52.

Criss, R.E., Champion, D.E., McIntyre, D.H., 1985. Oxygen isotope, aeromagnetic, and gravity anomalies associated with hydrothermally altered zones in the Yankee Fork mining district, Custer County, Idaho: *Econ. Geol*. 80, 1277–1296.

Eilu, P., Mathison, C., Groves, D.I., Allardyce, W., 1999. Atlas of alteration assemblages, styles and zoning in orogenic lode-gold deposits in a variety of host rock and metamorphic settings. Geology and Geophysics Department and UWA Extension, The University of Western Australia, Publ 30, 50 p.

El Gaby, S., List, F.K., Tehrani, R., 1988. Geology, evolution and metallogenesis of the Pan-African Belt in Egypt. In: El Gaby, S., Greiling, R.O. (Eds.), The Pan-African Belt of

northeast Africa and adjacent areas. Friedr. Vieweg and Sohn, *Braunschweiglwiesbaden*, 17-68.

El Kazzaz Y.H., 1995. Tectonics and Mineralization of Wadi Allaqi, south Eastern Desert, Egypt: Ph.D. thesis, University of Luton, 220 p.

El Ramly, M.F., Ivanov, S.S., Kochin, G.C., 1970. The occurrence of gold in the Eastern Desert of Egypt. Studies on Some Mineral Deposits of Egypt. Part I, Sec. A, Metallic Minerals. Geological Survey of Egypt, 21: 1 –22.

El Shazly, E.M., 1957. Classification of Egyptian mineral deposits: *Egyptian Journal of Geology,* 1 (1), 1– 20.

El Shimi, K.A., 1996. Geology, structure and Exploration of Gold Mineralization in Wadi Allaqi area (SW, Eastern Desert, Egypt), PhD Thesis (unpub.), Ain Shams Univ., 326 p.

Engel, A.E.J., Clayton, R.N., Epstein, S., 1958. Variations in isotopic composition of oxygen and carbon in Leadville Limestone (Mississippi, Colorado) and its hydrothermal and metamorphic phases. *Journal of Geology* 66, 374–39.

Fenton. M.W., 1987. The Geochemistry and Petrology of Selected Lower Paleozoic Sedimentary Rocks from Victoria. Australia.Unpubl. PhD thesis, Univ. of Melbourne.

Garson, M.S., Shalaby, I., 1976. Precambrian-lower Paleozoic plate tectonics and metallogenesis in the Red Sea region. Geological Association Canada, *Special Paper* 14, 573-596.

Grant, J.A., 1986. The isocon diagram - A simple solution to Gresens' equation for metasomatic alteration. *Econ. Geol*. 81, 1976–1982.

Gresens, R.L., 1967. Composition-volume relationships of metasomatism. Chemical Geology 2, 47–65.

Groves, D.I., Forster, R.P., 1991. Archean lode-gold deposits. In: Fortes, R.P., (Ed.), Gold Metallogeny and Exploration, Blackie, Glasgow, 63–103.

Groves D.I., Goldfarb, R.J., Gebre-Mariam, M., Hagemann, S., Robert, F., 1998. Orogenic gold deposits: a proposed classification in the context of their crustal distribution and relationship to other gold deposit types: *Ore Geo. Rev*. 13, 7–28.

Harraz, H.Z., 1991. Lithochemical prospecting and genesis of gold deposit in El Sukari gold mine, Eastern Desert, Egypt. PhD thesis, Faculty Science, Tanta University, Egypt, 494 p.

Harraz, H.Z., 1999. Wall rock alteration, Atud gold mine, Eastern Desert, Egypt: processes and P–T-XCO2 conditions of metasomatism. *Journal African Earth Sciences* 20, 527–551.

Harraz, H.Z., El Dahhar, M.A., 1994. Fluid-wall rock interaction and its implication in gold mineralization at the Umm Rus gold mine area, Eastern Desert, Egypt: *Egyptian Journal of Geology*, v. 38, p. 713-747.

Harraz, H.Z., Hassanen, M.A., El Dahhar, M.A., 1992. Fluid inclusions and stable isotopic studies at El Sid gold mine, Eastern Desert, Egypt: *Egyptian Journal of Geology*, 36, 323-343.

Harris, N., Inger, S., Massey, J., 1993. The role of fluids in the formation of High Himalayan leucogranites. In: Treloar, P.J., Searle, M.P. (Eds.), *Himalayan Tectonics*. Spec. Pap. - Geol. Soc. Am. 74, 391– 400.

Hassaan, M.M., El Mezayen, A.M., 1995. Genesis of gold mineralization in Eastern Desert, Egypt. *Al-Azhar Bulletin of Sciences*, 6, 921-939.

Helba, H.A., Khalil, K.I., Abdou, N.M., 2001. Alteration patterns related to hydrothermal gold mineralization in meta-andesites at Dungash area, Eastern Desert, Egypt. *Resource Geology*, 51, 19–30.

Helmy, H.M., Kaindl, R., Fritz, H., Loizenbauer, J., 2004. The Sukari Gold Mine, Eastern Desert-Egypt: structural setting, mineralogy and fluid inclusion study. *Mineral. Depos*. 39:495–511.

Henley, R.W., Truesdell, A.H., Barton P.B.Jr., Whitney J.A., 1984. Fluid-Mineral Equilibria in Hydrothermal Systems. El Paso, U.S.A. *Society of Economic Geologists*, 267 p. (Reviews in Economic Geology 1).

Hey, M.H., 1954. A new review of the chlorites: *Mineralogical Magazine* 30, 277-292.

Hoefs, J., 1997. *Stable Isotope Geochemistry*. Springer, Berlin. 201 p.

Hofstra, A.H., Cline, J.S., 2000. Characteristics and models for Carlin-type gold deposits. In: Hagemann, S.G., Brown, P.E.(Eds.), *Reviews in Economic Geology, Society of Economic Geologists*, 13, 163– 214.

Hume, W. F., 1937. The minerals of economic value associated with the intrusive Precambrian igneous rocks. *Geology of Egypt. 3,* 689-990.

Humphris, S.E., Alt, J.C., Teagle, D.A.H., Honnorez J.J., 1998. Geochemical changes during hydrothermal alteration of basement in the stockwork beneath the active Tag hydrothermal mound. In: Herzig, P.M., Humphris, S.E., Miller, D.J., and Zierenberg, R.A. (Eds.), Proceedings of the Ocean Drilling Program, *Scientific Results*, 158, 255-276.

Khalil, K. I., Helba, H. A., and Mucke, A., 2003. Genesis of the gold mineralization at the Dungash gold mine area, Eastern Desert, Egypt: a mineralogical – microchemical study, *Journal of African Earth Sciences*, 37: 111 – 122.

Kishida, A., Kerrich, R., 1987. Hydrothermal alteration zoning and gold concentration at the Kerr Addison Archean lode gold deposit, Kirkland Lake, *Ontario. Econ. Geol*. 82, 649-690.

Klein, E.L., Harris, C., Giret, A., Moura, C.A.V., Angélica, R.S., 2005. Geology and stable isotope (O, H, C, S) constraints on the genesis of the Cachoeira gold deposit, Gurupi Belt, northern Brazil: *Chem. Geol*. 221, 188–206.

Klemm, D., Klemm, R., Murr, A., 2001. Gold of the Pharaohs—6000 years of gold mining in Egypt and Nubia. *African Earth Sciences* 33, 643–659.

Kolb, J., Kisters, A.F.M., Hoernes, S., Meyer, F.M., 2000. The origin of fluids and nature of fluid– rock interaction in auriferous mylonites of the Renco Mine, southern Zimbabwe: *Mineral. Depos*. 35(1), 109–125.

Kranidiotis, P., McLean, W.H., 1987. Systematics of chlorite alteration at the Phelps Dodge massive sulfide deposit, Matagami, *Quebec. Econ. Geol*. 82, 1898–1911.

Kretschmar, U., Scott, S.D., 1976. Phase relations involving arsenopyrite in the system Fe-As-S and their application: *Canadian Mineralogist* 14, 364-386.

Kröner, A., Greiling, R., Reischmann, T., Hussein, I. M. Ster, R. J., Durr, S., Kruger, J., Zimmer, M., 1987. Pan- African crustal evolution in the Nubian segment of Northeast Africa. American Geophysics Union, Special Publication, 17, 235-257.

Kusky, T.M., Ramadan, T.M., 2002. Structural controls on Neoproterozoic mineralization in the South Eastern Desert, Egypt: an integrated field, Landsat TM, and SIR-C/X SAR approach, *Journal of African Earth Sciences* 35(1), 107-121.

Leitch, C.H.B., Lentz, D.R., l994. The Greisen approach to mass balance constraonts of alteration systems: methods. Pitfalls and examples. In: D.R. Lentz (Editor). Alteration

and Alteration Processes associated with Ore-forming Systems. Short Course Notes, Vol. II, Geological Society of Canada, Waterloo. Ontario, 161-192.

Meyer, C., Hemley, J.J., 1967. Wall rock alteration. In: Barnes, H.L. (Ed.), Geochemistry of Hydrothermal Ore Deposits. Holt, Rinehart and Winston, New York, 166–235.

Mikucki, E.J., Ridley, J.R., 1993. The hydrothermal fluid of Archaean lode-gold deposits at different metamorphic grades: compositional constraints from ore and wall rock alteration assemblages: *Mineral. Depos*. 28, 469–481.

Mueller, R.F., Saxena, S.K., 1977. Chemical Petrology, with Application to the Terrestrial Planets and Meteorites. New York, Springer-Verlag. 396 p.

Neubauer, V.H.W., 1962. Geologic der Goldlagerst~itte von E1 Sid in Ober~igypten mit einem Beitrag zur Geologic der zentralen Arabischen Wiisk. *Geol. Jahrb*. 80:117-160 (in German)

Noronha, F., Cathelineau, M., Boiron, M.C., Banks, D.A., Dória, A., Ribeiro, M.A., Nogueira, P., Guedes, A., 2000. A three-stage fluid flow model for Variscan gold metallogenesis in northern Portugal. *Journal of Geochemical Exploration*, 71, 209– 224.

Ohmoto, H., 1986. Stable isotope geochemistry of ore deposits: J.W. Valley, H.P. Taylor, Jr., and J.R. O'Neil, eds., Reviews in Mineralogy Volume 16: Stable Isotopes in High Temperature Geological Processes: *Mineralogical Society of America*, 491-560.

Ohmoto, H., Rye, R.O., 1979. Isotopes of sulfur and carbon: in H.L. Barnes ed., Geochemistry of Hydrothermal Ore Deposits, Second Edition: John Wiley and Sons, 509-567.

Osman, A., Dardir, A., 1989. On the mineralogy and geochemistry of some gold-bearing quartz veins in the central Eastern Desert of Egypt and their alteration wall rocks. *Annals of the Geological Survey of Egypt*, 16, 17-25.

Passchier, C.W., Trouw, R.A.J., 1996. *Microtectonics*. Springer, Berlin, 289 p.

Phillips, G.N., Groves, D.I., 1983. The nature of Archaean gold bearing fluids as deduced from gold deposits of Western Australia: Geologic Society Australia Journal 30, 25-40.

Pohl, W., 1988. Precambrian Metallogeny of NE-Africa. In: The Pan-African Belt of NE Africa and Adjacent areas (edited by El Gaby S. and Greiling R. O.), *Earth Evolution Sci.(*Vieweg), Wiesbaden, 319-341.

Reed, M.H., 1997. Hydrothermal alteration and its relationship to ore fluid composition. In: H.L. Barnes (ed.) *Geochemistry of Hydrothermal Ore Deposits*. New York, John Wiley and Sons, Inc., 303-365.

Rose, A.W., Burt, D.M., 1979. Hydrothermal alteration. In: H.L. Barnes (ed.) Geochemistry of Hydrothermal Ore Deposits: New York, John Wiley and Sons, 173-235.

Rye, R.O., Ohmoto, H., 1974. Sulfur and carbon isotopes and ore genesis: A review. *Econ. Geol.* 69, 826-842.

Sabet, A.H., Tscogoev, V.B., Bondonosov, V.P., Babourin, L.M., Zalata, A.A., Francis, M.H., 1976. On gold mineralization in the Eastern Desert of Egypt. *Annals of the Geological Survey of Egypt,* 6, 201-212.

Savin, S. M., and Epstein, S., 1968. Oxygen and hydrogen isotope variations in sedimentary rocks and minerals: Geological Society of America Special Paper 101, 190 p.

Scott, S.D., 1983. Chemical behaviour of sphalerite and arsenopyrite in hydrothermal and metamorphic environments: *Mineralogy Magazine*, 47, 427–435.

Selverstone, J., Morteani, G., Staude, J.M., 1991. Fluid channelingduring ductile shearing: transformation of granodiorite into aluminous schist in the Tauern Window, Eastern Alps. *Journal of Metamorphic Geology*, 9, 419–431.

Stein, M., Goldstein, S.I., 1996. From plume head to continental lithosphere in the Arabian-Nubian Shield. *Nature* 382, 773–778

Susak, N.J., 1994. Alteration factors affecting ore depoSítion. In: D.R. Lenz (ed.) Alteration and Alteration Processes Associated with Ore-Forming Systems. St. John's, Canada, *Geol. Assoc*. Canada, 115-130 (Short Course Notes 11).

Takla, M.A., El Dougdoug, A.A., Gad, M.A., Rasmay, A.H., El Tabbal, H.K., 1995. Gold-bearing quartz veins in mafic and ultramafic rocks, Hutite and Um Tenedba, south Eastern Desert, Egypt. *Annals of the Geological Survey of Egypt* 20, 411-432.

Taylor, H.P.Jr., 1973. $^{18}O/^{16}O$ evidence for meteoric-hydrothermal alteration and ore deposition in the Tonopah, Comstock lode, and Goldfield mining districts, Nevada: *Econ. Geol.* 68, 747–764.

Taylor, H.P. Jr., 1974. The application of oxygen and hydrogen isotope studies to problems of hydrothermal alteration and ore deposition: *Econ. Geol*. 69, 843-883.

UNDP compilation report. 1986. document no. 6/87 in the *Egyptian Geological Survey and Mining Authority* (EGSMA), Cairo, Egypt.

Zoheir, B.A., 2004. Gold mineralization in the Um El Tuyor area, South Eastern Desert, Egypt: geologic context, characteristics and genesis. Ph. D. Thesis, Ludwig-Maximilians-Universität München, Germany, 159 pp.

Zoheir, B.A., 2008. Structural controls, temperature-pressure conditions and fluid evolution of orogenic gold mineralisation in Egypt: a case study from the Betam gold mine, south Eastern Desert. Mineralium Deposita. *Mineralium Deposita* 43:79–95.

Zoheir, B.A., Klemm, D.D., 2007. The tectono-metamorphic evolution of the central part of the Neoproterozoic Allaqi-Heiani suture, south Eastern Desert of Egypt. *Gondwana Research* 12, 289-304.

In: Gold Mining: Formation and Resource Estimation ISBN: 978-1-60741-096-6
Editors: M. D. Corral, J. L. Earle

Chapter 8

EVOLVING ECONOMIC MARGINALITY AND LOCAL ECONOMIC DEVELOPMENT RESPONSES IN SELECTED SOUTH AFRICAN GOLD AND COAL MINING AREAS*

E. Nel[1†] and J. A. Binns[2]
[1]Department of Geography, Rhodes University, Grahamstown, South Africa
[2]Department of Geography, Univesity of Otago, Dunedin, New Zealand

ABSTRACT

This paper discusses the recent and dramatic rationalization of key sectors of South Africa's once powerful mining industry and the effects on former mining towns. Whilst older coalfields have been replaced by new areas of production, the same is not true for gold. A key challenge for mine towns facing job loss and mine closure is how to respond through appropriate local actions which can diversify local economies and create jobs. The paper draws on the experience of different South African centres in this regard.

INTRODUCTION

For a century and a half the South African economy has been skewed in terms of an extraordinary dependence on the mining industry and on gold and coal production in particular, creating what has been termed the Mineral-Energy Complex (MEC) as a dominant spatial and economic entity (Fine and Rustomjee, 1996). In recent years, the fall in the price

* A version of this chapter was also published in Globalization and Africa, edited by James L. Maruba, Nova Science Publishers. It was submitted for appropriate modifications in an effort to encourage wider dissemination of research.

† E-mail: E.nel@ru.ac.za; This paper draws on and synthesises material published in two papers previously [one about each of the two case studies outlined above – *International Development Planning Review* – 2002; *Economic Geography* - 2003].

and the demand for gold, depletion of existing gold resources in certain areas and mechanised coal mining in newer coalfields has witnessed the loss of tens of thousands of mining jobs and the effective economic collapse of the original base of once prosperous mining centres. Two of the worst affected areas are those of the Free State goldfields and the KwaZulu-Natal coalfields. Evolving economic marginalisation in these areas has, on a positive note, helped to catalyse a variety of local responses to the severe economic hardship and job loss which prevails. Collectively referred to as Local Economic Development and in line with current government policy, local governments and other stakeholders are attempting to identify and pursue alternate development strategies for their areas. This paper briefly examines the key principles of mining closure and deindustrialisation and Local Economic Development, with respect to mining areas in decline, before moving on to an examination of recent trends in the gold and coal mining industry in South Africa with particular reference to the two areas identified for particular investigation. The core focus of the paper is on the developmental responses which are being pursued in the now economically marginal mining towns of Welkom in the Free State Goldfields and Utrecht in the KwaZulu-Natal coalfields.

DE-INDUSTRIALISATION, JOB LOSS AND LOCAL RESPONSE

De-industrialisation was a key feature of the economic geography of Western Europe and North America from the 1960s to the 1980s. De-industrialisation refers to either an absolute fall in manufacturing value-added, and/or an absolute decline in manufacturing employment in manufacturing (Blackaby, 1979; Bazen and Thirlwall, 1989). These processes were particularly apparent in the areas associated with the early Industrial Revolution where there was a concentration of the iron and steel and coal industries. Factors such as ageing industrial infrastructure, depletion of raw materials, cheaper and more efficient production from elsewhere, labour instability and reduced demand all played a role in the demise of once prosperous economic hearths. Areas in which closure and job loss were most apparent include, among others, the Ruhr in Germany, Appalachia in the USA, Lorraine in France and the industrial belts of the Midlands, North-West and North-East of the UK (Barr, 1969; Camagni, 1991; Spooner, 1981).

In the case of the Ruhr, the number of active coal mines reduced from 140 in 1956 to 24 in 1984 and by 1985, 38% of all jobs in iron and steel production had also been lost (Hennings and Kunzman, 1990). In the case of the UK coal industry, between 1947 and 1993 the number of coal-mining jobs fell from 718,000 to 32,500. In the USA, in the decade preceding 1991, the number of coal-miners fell from 230,000 to 130,000, whilst 15 million jobs in heavy manufacturing were lost by 1976 (McKenzie, 1984). Protracted de-industrialisation has entrenched economic stagnation and ensured long-term structural poverty and unemployment in the worst affected regions, leading to the stigmatisation and marginalization of so-called ‘rust-belt’ areas (Massey, 1984; Cooke, 1995).

In the twenty years which have elapsed since the era of de-industrialisation reached its peak in the western world, many of those areas which faced severe job-loss have gradually, either through their own or state initiatives, started to identify and pursue alternate forms of employment and wealth creation (Cooke, 1995). Innovative local initiatives have either led to industrial restructuring (Stohr, 1990), the transformation of redundant landscapes and

industrial infrastructure into tourist and heritage features (Edwards and Coit, 1996) or the creation of new economic activity (Hudson, 1995). Economic transformation has clearly been painful and slow and many of the old industrial regions have never regained the economic pre-eminence which they once enjoyed. These initiatives can broadly be classified as LED (Local Economic Development), which, according to Zaaijer and Sara (1993, p.139) 'is essentially a process in which local governments and/or community based groups manage their existing resources and enter into partnership arrangements with the private sector, or with each other, to create new jobs and stimulate economic activity in an economic area'.

Whilst the literature tends to suggest that the phenomena of de-industrialisation and mine closure were part of an historical era which has since passed in the western world, the reality is that in elsewhere in the world similar processes are now taking place, with equally devastating impact on affected communities. For example, in sub-Saharan Africa it has been suggested that structural adjustment reforms have, since the 1980s, undermined a weak manufacturing base, and a process of de-industrialisation has been noted (Jalilian and Weiss, 2000).

In 1994, the South African economy emerged from decades of international isolation and internal protection, however, full exposure to the world economic system aggravated many deep structural weaknesses within the economy, including weak international competitiveness, low levels of productivity and inefficiencies in production. By 1999, 500,000 jobs were reported to have been lost in the preceding 5 years. This despite, or perhaps because, the government in 1996 adopted a neo-liberal economic policy known as the Growth, Employment and Redistribution [GEAR] strategy (Lester, Nel and Binns, 2000).

Whilst many sectors of the South African economy have been hard hit by rationalisation and closure in the last decade, the worst affected sectors are probably those of gold- and coal-mining. In the Free State Goldfields alone, nearly 100,000 jobs were lost during the 1990s (Binns and Nel, 2001). In parallel with international evidence, economic crises often encourage innovative local responses (Stohr, 1990), with attempts being made to revive local economies and create employment. A wide range of innovative local economic development initiatives are emerging in South African localities contending with recession and redundancy which are seeking to restructure their economies and create employment (Nel, 2001). In recognition of the importance of such endeavours, the South African Government through its Local Economic Development Fund [LEDF] instituted in 1999, is now actively supporting those local initiatives which are seen to have significant growth and job creation potential (DPLG, 2000).

RECENT TRENDS IN SOUTH AFRICA'S GOLD AND COAL INDUSTRY

In South Africa, as a result of the country's spectacularly rich mineral resources, the existence of the MEC and the critical regional importance of mineral production in areas such as the Rand, Free State Goldfields, Mpumulanga and KwaZulu-Natal, mining has been a key anchor in both the national and regional economies. Arguably two of the most critical mineral products in the South Africa, both historically and at present are those of gold and coal. Whilst the latter has traditionally been the key earner of foreign exchange and the past driving

force of the economy, coal has served to power the local economy and, in recent years, production has increased making the country a key global supplier.

However, when changes occur within a particular region or mineral sub-sector the ramifications on a local economy or region can be catastrophic. Declining gold production, as a result of changes in global demand and resource availability in certain goldfields has had a particularly severe impact on areas such as the Free State Goldfields, weakening the local economy and causing considerable uncertainty (Seidman, 1993; Nattrass, 1995). Between 1987 and 1999, the number of gold mining jobs in the country fell by some 58%, whilst production has fallen by nearly 40% over the last twenty-five years (StatsSA, 1975-2000). Although South Africa has the world's largest known reserves and highest production of gold, the industry is engaged in a struggle for survival. Production and employment in the industry have been on a downward trend for some time. Between 1975 and 1999 gold production declined by nearly 38%.

The effects of these changes have been acutely felt in the country's major goldfields, with the two worst affected areas being those of the Free State and Klerksdorp in the North West province. In these two areas the loss of mining jobs has been 100,000 and 30,000 jobs respectively (van der Walt, 1999). In particular centres, such as Stilfontein and Welkom, which were developed as new towns during the boom in gold mining, the loss or radical decline in production has been catastrophic. Unemployment rates, particularly amongst low-skilled black labourers, have increased from almost zero up to 65% in such areas. The effective absence of a state welfare system, has aggravated the situation.

A similar process is a playing itself out in many of the coal-mining areas where aging mines, resource depletion and changes in the demand for different grades of coal has led to the effective cessation of coal-mining throughout the northern part of KwaZulu-Natal (KZN). By contrast output has in fact increased in the newer coalfields in Mpumulanga where mechanised production predominates (SA Mining World, 1993; Strydom and Vrey, 1993). Despite the fact that South Africa is the fifth largest producer of coal in the world and the third largest exporter (Editors Inc., 2000), production factors do not favour the KZN producers. National coal output has risen from 52 million tons in 1969 to 223 million tons in 1999, however the number of coal mining jobs fell from 76 090 to 60 845 in the same period (StatsSA, 1975-2000). What these figures mask is the almost total loss of some 30 000 jobs in KwaZulu-Natal in the last 30 years; the national figures are moderated by the increased employment in the other coalfields. Between 1981 and 1983, the number of working coal mines in KZN had declined from 44 to 21 and the region's total sales of coal fell from 14 to 9 million tons (Talana Museum, 1998).

LOCAL RESPONSE TO ECONOMIC CRISES

Within these areas, as result of the local economic and employment crises, with or without external support, local authorities and other local agencies are obliged to try and address the economic marginalisation which has taken place and to try and steer the economy in a new direction. Attention now shifts to examine the situation and the response in one gold and one coal mining area.

The Response of Welkom in the Free State Goldfields

The city of Welkom is the largest urban centre in a region of some one million people and the centre of what came to be known as the Free State Goldfields, a fabulously rich field when discovered and exploited in the 1940s and 1950s. Now, with exhaustion of the easily accessible gold and the falling world market prices, the area and the towns which it created are in major crisis. From the late-1980s, mining operations have been significantly curtailed and some 100 000 mining jobs have been lost, with devastating effects on the local economy. A range of differing, but often related development endeavours have been embarked on, as detailed below.

The Response of the Local Authority

As a direct result, a comprehensive response has been pursued by city of Welkom, which established a dedicated development centre, the Free State Goldfields Development Centre, in 1992, to try and draw in new investment, to encourage local economic restructuring and to investigate alternative economic activity (http://welkom.co.za, 1997; van der Walt, 1999, 2000). The centres' mission is to 'promote the successful management of change from a mining economy to one characterised by a diversified economy based on diversified, competitive and export driven enterprises' (van der Walt, pers. com., 1999).

Though not having met with absolute success, key achievements of the Centre are worth noting. In collaboration with a local tertiary college and a mine, retraining of retrenched miners has been undertaken and workspace provided for small businesses. There has been encouragement of new economic activities, including tourism promotion, gold jewellery production, provision of facilities for informal sector traders and support for agricultural activities and agro-industry. In addition, the Development Centre offers guidance and incentives to 'Micro Enterprises' and incentives to larger establishments. Planned activities include moves to turn the town airfield into an international cargo airport and to initiate urban farming (Nieuwoudt, 1999).

By 1999, nearly 80 firms, most of them small, had been assisted by the Development Centre (van der Walt, 1999). Unfortunately, the long-term results experienced have been mixed with most of small firms eventually failing and no major firm has invested to date.

Other Initiatives

In addition to the activities of the local authority there are other noteworthy activities in the region geared to refocus the local economy. Key amongst these is the support given by the Harmony gold-mining group to establish a jewellery cluster based on sales from their gold refinery. A gold factory known as `Via de Oro' opened its doors in 1998, and now employs 350 staff; this will rise to 850. Two additional firms are also considering starting operations in the area. In addition, in 2000 a gold-jewellery school was opened (Bosman, pers com., 2001).

The most impressive project in the Welkom area is that of the Phakisa Freeway, which was set up by the provincial government to address development issues through sporting activities. High unemployment levels in the Welkom area prompted Phakisa to develop an

innovative development intervention (Phakisa Freeway, 1999). A world class motor racing track has been built, using international funds. Significantly, the track secured a five year contract, which started in 1999, to host one of the annual international formulae one motor-bike grandprix races. In addition, the circuit includes one of only four oval racing tracks in the world [outside of the USA]. The circuit is booked virtually every weekend of the year. The spinoffs of this project and the potential of such a major intervention to restructure the local economy are enormous. 28 000 temporary jobs and 2 800 permanent jobs have been created as a result (Goosen, pers. com., 1999).

A noteworthy intervention is that of the Mine Worker's Development Agency [a branch of the National Union of Mineworkers]. In parallel with similar initiatives elsewhere in the country it has undertaken training of ex-mine-workers and is trying to establish small businesses for them (Molefi, pers. com., 1999).

Summary

Despite an impressive range of programmes which have been launched, it would be difficult to assert that more than a small fraction of lost jobs have been restored and the local economy has not yet been returned to previous levels of prosperity. The launching of a range of crisis responses is however, praiseworthy and it is important to note that the most successful - the Phakisa freeway has relied on significant external intervention, support and funding. This suggests, as Stock (1995) asserts that local initiatives can never achieve more than small, sporadic victories and that significant external support is usually needed to revive a local economy in crisis (Stohr, 1990).

The Response of Utrecht in the KwaZulu-Natal Coalfields

The development of the town of Utrecht has been closely linked to the coal mining industry. The town, established in 1854 (Smook, pers.com. 2001), used to contribute 13% of Natal’s coal production from its four mines. At their most productive time, in the late 1970s , these mines employed nearly 10 000 workers. From the late-1980s, exhaustion of easily accessible coal seams, aging infrastructure, closure of the regional iron and steel industry which had absorbed the bulk of local production and competition for the export market from the large, mechanised mines in Mpumulanga led to the closure of two of the four mines and radical reductions in operations at the remaining two mines. By 2001 less than 300 of the original 10 000 jobs remained and an unemployment rate of 50% was reached in the town (Ross, pers. com., 2001). The decline of coal mining has had a drastic effect on the employment situation and general prosperity of Utrecht and its hinterland. As recently as 1999, approximately 40% of the residents of Utrecht town were mine employees and many other residents relied on income generated by the mine to support their businesses.

The Initial Local Government Response

In 1995, in the light of the worsening situation, local officials decided that something had to be done to re-build the economy and confidence of the community of Utrecht. In the words of a consulting group, '...the Utrecht Transitional Local Council [TLC], realising that the future of the town was in the balance, took the bold step of creating a new focus of the town away from the coal mining industry and towards the huge tourism potential of the Utrecht area. This move has been partially responsible for the survival of the town after the collapse of the coal mining industry' (P&N Environment and Development Consultants, 2000, p. 3). It is significant, that in pursuit of this tourism alternative that the mine has been particularly supportive.

Local leaders realised that the town was not well placed to compete with larger towns in the region for new firm investment (Myburgh, pers.com. 2001). It was however recognised that Utrecht did have peace and tranquillity, as well as an unusually high level of collaboration and spirit of partnership between the municipality, the mine, business and community interests and the tribal authorities. The 'Utrecht renaissance' focuses on the development of tourism, and a number of tourism-related initiatives, notably a game park, game farm and the production and sale of local arts and crafts, as detailed below.

The Game Reserve

In the 1990s, a caravan park with chalets was established adjacent to the municipal dam, a short distance to the north-east of the town. Across the dam, on the Balele mountains , the Balele Nature Conservancy was established, and with the support of the mine, the reserve was stocked with a variety of game species, thereby creating a Game Reserve as an additional tourist attraction. The game park covers some 1500ha, 700ha of which are under the ownership of the municipality, with the remaining land being owned by a co-operative neighbouring farmer. Adjacent to the caravan park, the mining company had established for its workers a leisure club with swimming pool, bowling green, tennis courts, rugby field, restaurant and bar. The leisure club was handed over to the municipality and is now another tourism asset, the Utrecht Country Club. On the Balele mountains, disused mine buildings have been converted into a youth camp for use by school and other youth groups. A wetland area close to the dam is to be created to encourage bird watching (Stannard pers. com. 2001). Innovatively, the Council has decided to adopt the marketing logo on its stationery as being 'The village in a game park'

Arts and Crafts Association

Building on local skills in both the black and white communities, it was decided to establish an arts and craft centre based on the production and sale of pottery, sewing and leather goods, using local skills and raw materials (Smook, 1998). A Traditional Arts and Crafts Village has been built, which is strategically sited at the main entrance to the town at the junction of the High Street and main road by-passing the town.

The 'Mangosuthu Arts and Crafts Village', as it is now known, has an adjacent pottery and a shop, where craft products are sold. Previously unemployed people have been trained in pottery, sewing, printing and beadwork. In 2001, the number of potters had increased from 8 to 14, 15 women were being trained in sewing and 5 leather workers were being trained (Smook, pers.com., 2001). When it is in full operation, the Centre will provide self-employment to previously unemployed people in at least 10 different crafts. The project has attracted significant funding from the government's Local Economic Development Fund (LEDF).

The Game Farm

The successes achieved have encouraged the community to embark on other tourist-related initiatives. The most noteworthy of these are the marketing of Utrecht as 'The village in a game park' and the decision taken in 2000 by the Utrecht local government to demarcate an area for the development of the 'Utrecht Community Game Farm' and to link the game park with the game farm (Myburgh, pers.com., 2001). The project has led to the establishment of an economically viable game farm on municipal land to the east of the town. On the farm, animals will be reared for breeding purposes and also for processing of their meat, hides and horns under controlled hunting conditions. Initially allocated 700ha , it will ultimately incorporate 5000ha (Stannard, pers.com., 2001). A game lodge, bush camp and the development of roads are planned. The game farm project was successful in receiving a grant of R1.2million in 2000 from the central government and a further R1.5million in 2001 for a two-year period.

This project also involves a joint venture with the Utrecht Arts and Crafts Village which will be a retail point for products generated by the Game Farm such as hides, skins, hooves, horns and biltong (dried meat), much of which will also be processed by the Arts and Crafts Association. Both the council and the mine have helped to build a small abattoir, next to the game farm. During 2000-2001 some 31 jobs will be created, and in the long-term the game farm will employ about 50 people. By 2006 there should be some 445 game animals and it is expected that the project should be economically self-sustaining by 2004. The mayor of Utrecht felt that although the project will not create many jobs, he recognised that the spin-offs from tourism could create a significant number of jobs (Mtshali, pers. com., 2001).

When combined with the pre-existing game park [to the west of the town), the Game Farm project [to the east] will mean that the whole town of Utrecht will be surrounded by and be part of the project, as it will lie within the game farm area. The entrance to the game farm will be at the entrance to the town itself (Stannard, 2000, p.4).

Summary

The developments which have happened in Utrecht provide some valuable lessons for many other towns in South Africa and beyond, which have experienced de-industrialisation and associated job losses. In Utrecht, with the demise of the coal industry the 'bottom fell out of' the local economy. Fortunately, the seriousness of the situation was recognised by a number of key actors in the community, and a visionary plan of action was formulated. This

has led one of the key role-players to state, 'the town has moved a long way from being a typical coal mining town to one which is teetering on the brink of becoming a tourism epicentre' (Stannard, pers. com., 2001).

The success of Utrecht has been dependent on the availability of both natural and human resources, and an injection of appropriately targeted external funding. According to the Mayor 'The changes will take time...but we must work together to get something better for all of us in Utrecht' (Mtshali, pers. com., 2001).

CONCLUSION

Dramatic changes have taken place in selected sectors and sub-regions of South Africa's mineral economy, which have prompted what are often quite dramatic and innovative responses in an attempt to regenerate local economies and to find new sources of employment. Though employment has not been restored to pre-existing levels, LED does, none the less, offer an alternative in a time of depression and crisis. The gold- and coal-mining areas of South Africa have suffered from the process of de-industrialisation which, in relative terms, has been as severe as that faced in some of the old industrial heartlands of Europe and North America. Whilst there are a range of possible policies which might be introduced by government, initiatives which also have a strong 'grassroots' and 'bottom-up' motivation are often more likely to succeed (Stohr, 1990). In developing and implementing new initiatives which might create jobs and alleviate poverty, it seems that in the South African context, where there is so much to do to redress the legacies of apartheid policies and only limited funds available, much depends on the vision and innovation inspired by local leaders and entrepreneurs. Wherever possible, they must engage external support and funding which can, hopefully, ensure the sustainability of worthwhile development programmes.

REFERENCES

Barr, J. (1969). *Derelict Britain*. Pelican, Harmondsworth.

Bazen, R.J. and Thirlwall, A. (1989). *De-industrialisation: studies in the UK economy*. London: Heinemann .

Binns, T., and Nel, E. (2003). Gold loses its lustre - decline and response in the South African goldfields, *Geography* , 79, *141-66.*

Blackaby, F. (Ed.). (1979). *De-industrialisation*. London: Heinemann.

Bosman, D. (2001). Personal communication. Harmony Gold Mines, Virginia.

Camagni, R. P. (1991). Regional de-industrialisation and revitalisation processes in Italy. (136-166). In: Rodwin, L. and Sazanami, H., *Industrial change and regional economic transformation: the experience of Western Europe*. London: Harper Collins.

Cooke, P. (Ed.). (1995). *The rise of the rust belt*. London: UCL Press.

CSS (Central Statistical Services). (1981, 1993), *Census of mining*. CSS, Pretoria.

DPLG (Department of Provincial and Local Government). (2000*). Local Economic Development Fund*. DPLG, Pretoria.

Editors Inc. (2000). *South Africa at a glance*. Craighall: Editors Inc.

Edwards, J A. and Coit, J.C.L. (1996). Mines and quarries: industrial heritage tourism. *Annals of Tourism Research*, 23, *341-363*.

Fine, B. and Rustomjee, Z. (1996). *The political economy of South Africa: from mineral-energy complex to industrialisation*. London: Hurst.

Goosen, E. (1999). Personal communication. Race Track Manager, Phakisa Freeway, Welkom.

Hennings, G., and Kunzmann, K.R. (1990). Priority to local economic development: Industrial restructuring and local development responses in the Ruhr area - the case of Dortmund. (190-223). In: Stohr, W.B.. (Ed.). *Global challenge and local response*. London: Mansell.

http://www/ welkom.co.za . (1997). *Free State Goldfields Development Centre*.

Hudson, R. (1995). Making music work? Alternative regeneration strategies in a deindustrialized locality: the case of Derwentside. *Transactions of the Institute of British Geographers*, 20, *460-473*.

Jalilian, H. and Weiss, J. (2000). De-industrialisation in sub-Saharan Africa: myth or crisis? (137-158). In: Jalilian, H., Tribe, M., and Weiss, J. (Eds.). *Industrial development and policy in Africa: issues of de-industrialisation and development strategy*. Cheltenham: Edward Elgar.

Johnstone, I. (1999). Personal commnication. Co-ordinator Goldfields Metro. Development Corporation, Welkom.

Lester, A., Nel, E. and Binns, T. (2000). *South Africa past, present and future*. Harlow: Longman.

Massey, D.B. (1984). *Spatial divisions of labour: Social structures and the geography of production.* London: McMillan.

McKenzie, R.B. (1984). *Fugitive industry: the economics and politics of de-industrialisation*. Cambridge: Ballinger.

Molefi, N. (1999). Personal communication. Mineworkers Development Agency, Welkom.

Mtshali, B. W. (2001). Personal communication. Mayor, Utrecht.

Myburgh, L. (2001). Personal communication. Town Secretary, Utrecht.

Nattrass, N. (1995). The crisis in South African gold mining. *World Development*, 23, *857-868.*

Nel, E. L. (2001). Local economic development: a review and assessment of its current status in South Africa. *Urban Studies*, 38, *1003-1024*.

Nieuwoudt, F. (1999). Personal communication. Town Planner: Development, Welkom City Council.

P & N Environmental Development Consultants (2000). *Development Plan.* Utrecht.

Phakisa Freeway. (1999). *Africa's raceway*. Phakisa, Welkom.

Ross, D. (2001). Personal communication. Mine Manager, Welgedacht Exploration Co.Ltd., Utrecht.

S.A. Mining World. (1993). Vryheid Coronation winds down. *S.A. Mining World*, 12, *26-27*.

Seidman, G. W. (1993). Shafted: the social impact of down-scaling on the Free State Goldfields. *SA Sociological Review,* 5, *14-34*.

Smook, G. (2001). Personal communication. Project Manager, Utrecht Arts and Crafts Village, Utrecht.

Smook, G. (1998). *Development of Utrecht Arts and Crafts Village: Business Plan*. Utrecht.

Spooner, D. (1981). *Mining and regional development*. Oxford: Oxford University Press.

Stannard, R. (2000). *Development of Utrecht Community Game Farm and Wildlife Products: Business Plan.* Utrecht..

Stannard, R. (2001). Personal communication, Community Game Farm Manager, Utrecht.

Statistics South Africa (formerly Department of Statistics). (1975-1999). *Quarterly Bulletin of Statistics.* Pretoria.

Stock, R. (1995) *Africa South of the Sahara.* New York: Mansell.

Stohr, W. (Ed.). (1990). *Global challenge and local response*. London: Mansell.

Strydom, A.J. and Vrey, W.J.H. (1993). Die bedreiging van ‘n dorp se ekonmiese basis vereis pro-aktiewe optrede: Vryheid as gevallestudie. *Town and Regional Planning,* 34, *20-25*.

Talana Museum. (1998). *Natal coal industry, 1888-1998*. Dundee: Talana Museum.

van der Walt. (1999-2001). Personal communication. The Manager: Development, Frees State Goldfields Development Centre, Welkom.

Zaaijer, M. and Sara, L.M. (1993). Local economic development as an instrument for urban poverty alleviation: a case from Lima, Peru. *Third World Planning Review*, 15, *127-142*.

In: Gold Mining: Formation and Resource Estimation ISBN: 978-1-60741-096-6
Editors: M. D. Corral, J. L. Earle

Chapter 9

PHYTOCHELATINS IN WILD PLANTS FROM GUANAJUATO CITY – AN IMPORTANT SILVER AND GOLD MINING CENTER IN MEXICO*

Kazimierz Wrobel, Julio Alberto Landero Figueroa and Katarzyna Wrobel*

Instituto de Investigaciones Científicas, Universidad de Guanajuato,
L. de Retana N° 5, 36000 Mexico

ABSTRACT

Phytochelatins (PCs) are a group of small, metal-binding peptides that are biosynthesized by higher plants, some fungi and algae in the response to heavy metal exposure. One actual research topic focuses on better understanding the global effect that all elements present in natural environments exert on the PCs production by plants.

In this work, PCs levels were evaluated in the wild plants, chronically exposed to low or moderate levels of heavy metals. The quantification of total PCs in plant extracts was carried out by HPLC with fluorimetric detection, after derivatization of free –SH groups with monobromobimane. Additionally, the distribution of metals in molecular mass (MM) fractions of these same extracts was studied by size exclusion chromatography with on-line UV and ICP-MS detection. All samples were collected in Guanajuato city (Mexico), which has long been an important silver and gold mining area. Among different metals reported in Guanajuato soils, lead, cadmium, copper and silver were selected in this study, because of their capability to induce phytochelatins in plants. The common plants from this region were analyzed, namely: *Ricinus communis* (castor bean), *Tithonia diversifolia* (Mexican sunflower) and *Opuntia ficus* (nopal). The analytical approach involved the ICP-MS analysis of total elements in soil, soil fractions and wild plants and also the evaluation of relationships between PCs, metal levels found in plants/soil and different soil parameters.

---

* A version of this chapter was also published in Causes and Effects of Heavy Metal Pollution, edited by Mikel L. Sánchez, Nova Science Publishers. It was submitted for appropriate modifications in an effort to encourage wider dissemination of research.

* Corresponding autor: katarzyn@quijote.ugto.mx.

In the analysis of plants, PC-2, PC-3 and PC-4 were detected in nopal, PC-2 in castor bean, while in Mexican flower no phytochelatins were found. In further development, the extracts of soil humic substances were obtained and the distribution of metals in molecular mass (MM) fractions was studied by size exclusion chromatography with on-line UV and ICP-MS detection. The soil humic substances (HS) were also assessed.

In search of possible relationship between the parameters measured, the statistical analysis of correlation was performed. The results obtained indicate that the binding of metals to soil HS contributes in lowering their uptake by castor bean plant. On the other hand, the soils collected at nopal roots presented low HS levels and no correlation with metals in plant was found. The results obtained in the sequential extraction of soils and the abundance of sulfide minerals in Guanajuato indicate that the sulfide bound metals were the primary forms of Pb, Cu and Cd in soil adjacent to nopal roots. Owing to their generally poor solubility, rizosphere processes should be important in mobilizing metals and their uptake by nopal.

Our results provide further evidence on the role of environmental conditions in the accumulation of heavy metals in relation to PCs production in different plant genotypes. In particular, multi-elemental approach is necessary in studies on PCs induction in actual field situations, where plants (or other organisms) are exposed to a variety of metals and metalloids.

INTRODUCTION

Phytochelatins (PCs) are a group of small, metal-binding peptides of the general structure $(Glu\text{-}Cys)_n$-Gly, where n varies from 2 to 11 (Figure 1a) [1,2]. Other families of PCs, differing in the type of C-terminal amino acid have also been characterized [3]. PCs are biosynthesized by higher plants, some fungi and algae in the response to heavy metal exposure, which is considered a major detoxifying pathway for heavy metals in these organisms [4]. The PCs role in maintaining the homeostasis of intracellular levels of essential metal ions has also been highlighted [5]. Depending on the coordination capacity of metal ion and on the specific ability of plant for PCs synthesis, up to four sulfur atoms can be coordinated from either single or multiple PC molecules, resulting in PC-1, PC-2, PC-3 and PC-4 complexes (Figure 1b). The formation of PC-5 and PC-6 has also been reported, but only in transgenic plants [6], in cell cultures [7] and freshwater green alga [8].

The term phytochelatins was introduced by Zenk et al. in 1985, after isolation of novel metal-bining peptides from cell suspension cultures of a higher plant after exposure to Cd [9]. Since then, the extensive studies have been carried out aiming structural characterization of PCs and their metal complexes [10,11] as well as the elucidation of induction mechanisms [12,13]. In the first approach, the isolation and characterization of PC synthases from different organisms have been carried out. Most commonly, the experimental approach has involved plant growth (or other types of culture) under controlled exposure conditions, typically using the salt of one element at relatively high concentrations.

The expression of PCs not only enhances the tolerance to heavy metals but also causes their accumulation in plant tissues, so the feasibility of PCs for phytoremediation of toxic heavy metals from contaminated soil and water has been explored [14,15]. In particular, plant engineering to assure higher rates of PCs induction has been studied [16-18].

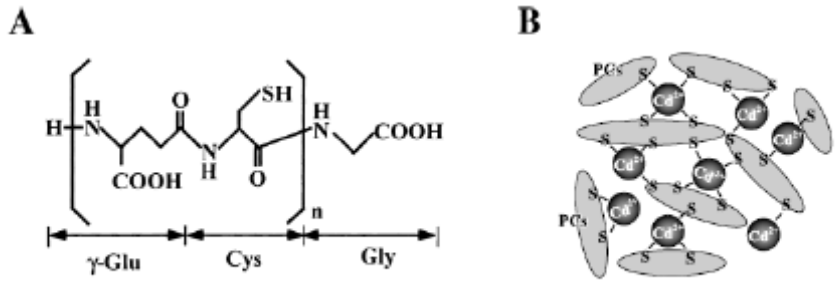

Figure 1. Primary structures of PCs (A) and PC-Cd complexes (B) [2].

However, before the routine use of plants in phytoremediation becomes possible, several questions regarding genetic regulation of PC synthase, its localization in plants and interaction of PCs and PCs synthase with different metal/metalloid forms, need to be answered. Furthermore, the mechanisms responsible for metal uptake and accumulation in plants in relation to PCs production are not fully understood. It should be realized that, in natural environments, plants are exposed to many elements and their forms at different concentration levels. In general, processes occurring in the soil-root system are considered important [19,20], yet the role of environmental parameters, possibly affecting metal bioavailability to plants, remains unclear. The increased production of phytochelatins has been observed in the presence of various organic chelators (ethylene diamine tetraacetate, ethylene diamine disuccinate, citric acid, etc.) as added to nutrient solution and/or soil [21-24]. On the other hand, metal binding by humic matter in soils has been shown to affect the mobility of metals in the environment. Depending on the experimental design and the type of metal, the increased or decreased uptake of Cd, Cu, Pb have been observed [25-30]. Importantly, the data relating soil humic substances with phytochelatin production in plants exposed to heavy metals are lacking.

In order to gain further insight on the induction of PCs and element complexation by these compounds in real-field situation, the global effect of different elements present at low concentrations should be studied together with possible effects of relevant environmental parameters.

Within this context, the present work has been focused on the wild plants growing in Guanajuato city, located in central Mexico. Guanajuato city has long been an important silver and gold mining center and the leaching of several metals and metalloids from the mine tailings to different environmental compartments has been reported [31,32]. Consequently, the plants growing in this area are chronically exposed to various metals, that are present in soils in relatively wide range of concentrations. Among those elements, we have focused on lead, cadmium, copper and silver, because of their capability to induce phytochelatins in plants [3,10,33-37] and also because of their abundance in the region of Guanajuato [31,32]. For the purposes of this work, three wild plants have been selected, namely *Ricinus communis* (castor bean), *Tithonia diversifolia* (Mexican sunflower) and *Opuntia ficus* (nopal). These plants are common in Guanajuato and they can grow within small distance one from another, which is important to assure similar exposure conditions of different plants. The accumulation of metals in castor bean has already been reported [38,39]. Its possible application in

phytoremediation has been explored [38,40], yet data available for Mexican sunflower and nopal are scarce [41]. Quite importantly, no information on possible induction of PCs in any of the three plant types has been found.

In a course of this study, we have focused on answering the following questions:

1. Do the wild plants chronically exposed to low/moderate concentrations of Ag, Cd, Cu and Pb induce PCs?
2. How to distinguish among elements that are important for PCs induction and those that are simply bound to PCs already existing?
3. Are the soil parameters important in PCs induction?

In the following sections, the experimental design and the results obtained in this study are systematically presented.

EXPERIMENTAL DESIGN

The sampling sites were selected in order to cover a wide range of element concentrations in soil. Thus, the site 1 corresponded to the place where the silver ores had been processed in the past; the site 2 was located at the Guanajuato river close to the mine tailing; the site 3 was at a hill, relatively distant from the mines; the site 4 was in the urban area developed on main tailing; the site 5 was in the part of city far from the mines and the site 6 was at the riverside, but far from the mining zone. Additionally, nopal samples were also collected in the "clean area", which corresponded to the countryside, about 40 km from Merida city, peninsula of Yucatán.

The plants were collected in November 2005 (just after the wet season), taking at each site three samples of roots and three samples of leaves from plants of similar size and color of leaves. To avoid possible variations of soil parameters, the area of any sampling site did not exceed 9 m^2 At each sampling site, the pH of topsoil (0 - 30 cm) was measured. The relative variability of pH values for several measurements at one site did not exceed 2 % and the values found at different sites were in the range pH 7.7 to pH 8.0 (pH 8.0 – 8.1 in the soil from Merida).

For each plant species, the roots and leaves collected at one site were pooled. Roots were carefully separated from the adjacent soil and pooled. Three washing agents were tested, namely deionized water, 0.05 M $CaCl_2$ and 0.05 M EDTA (with and without ultrasonication). Since the washing procedure had no significant effect on the results, the roots were washed with deionized water in ultrasonic bath (10 min). Both, roots and leaves were cut into small pieces, freeze-dried and homogenized by mortar grinding in liquid nitrogen.

The soil samples were collected in these same sites, from which the plants were taken. (six samples of about 250 g per 9 m^2 site). For the determination of total Ag, Cd, Cu and Pb, the samples from each site were pooled and dried. Soil fractionation was carried out according to the simplified Tessier method [42]. Fresh soils, without pooling, were used for the assay of humic substances.

In plant material, total element concentrations were determined by inductively coupled plasma mass spectrometry (ICP-MS) after wet acid digestion. The extraction of PCs from

freeze-dried root and leave homogenates was carried out with ammonium acetate (pH 7.4) [43]. Metal binding to PCs was studied by size exclusion liquid chromatography (SEC) with on-line UV and ICP-MS detection. Total PCs were assayed by reversed phase high performance liquid chromatography (RPHPLC) with fluorimetric detection [44,45].

The analytical approach in soil involved: (i) the determination of total element concentrations by ICP-MS after acid digestion; (ii) ICP-MS determination of elements in soil fractions after Tessier sequential extraction, (iii) assessment of soil humic substances (HS) by UV/Vis spectrophotometry [46] and (iv) SEC – UV/Vis – ICP-MS analysis of HS extracts for examination of metal binding to HS.

In search of possible relationship among parameters measured, the statistical analysis of correlation was performed, based on the results obtained in six sampling sites (software package Statistica for Windows, StatSoft Inc. 2000, Tulsa OK).

CAPABILITY OF THE WILD PLANTS CHRONICALLY EXPOSED TO LOW OR MODERATE CONCENTRATIONS OF METALS IN SOIL FOR THE INDUCTION OF PHYTOCHELATINS

In the first approach, cadmium, copper, silver and lead were determined in the pooled soils and plant roots. As an example, the results obtained in sites 1-3 are presented in Table 1. The metal levels found in soil were in agreement with the ranges reported previously [31,32], yet substantial differences can be observed among different sampling sites. Among four metals, lead was found to be the most abundant in soil (maximum concentration 362 ± 8 μg g^{-1}, site 1), copper levels were generally lower with the highest value also at the site 1 (221 ± 7 μg g^{-1}), Ag levels were about 4 to 5 times lower that those for Cu (highest value 42.2 ± 0.7 μg g^{-1}, site 1) and cadmium presented concentrations below 1.0 μg g^{-1} at any site. Even though the three plant species were collected simultaneously from these same sites, the highest concentrations of metals were found in *Opuntia f.,* followed by *R. communis* and *T. diversifolia*, (Table 1). As could be expected, the concentrations of metals in roots were higher in plants collected from more contaminated sites (site 1 and 2 versus site 3).

In order to examine if any of three wild plants can produce PCs, the root and stem extracts were obtained and analyzed for phytochelatins by reversed phase chromatography. It should be stressed that, at this point, we were interested in the total content of PCs and not in specific metal – PCs binding. Thus, in the analytical procedure applied, metals bound to PCs were eliminated by DPTA complexation and, after reduction, the fluorescent derivatization of the free thiol groups was achieved [44,45,47]. In the analysis of plant extracts, phytochelatins were found in *Opuntia f.* and in *R. communis*, but not in *T. diversifolia* [36]. Furthermore, nopal extracts contained PC-2, PC-3 and PC-4 and castor bean extract only PC-2. Total PCs levels in the plant samples collected at sites 1-4 are presented in Table 2. It can be observed that nopal contained relatively high concentrations of PCs as compared to castor bean. Also, the PCs levels in roots were always higher than in leaves.

In the context of the first question put in this work, the results obtained indicate that the wild plants, chronically exposed to low or moderate metal levels in soil do biosynthesize phytochelatins. However, our results seem to confirm that this process is genotype - dependent [18,48].

Table 1. Total cadmium, copper, lead and silver levels in soils and plant roots collected from three different sites in Guanajuato (1 - Hacienda when the silver ores had been processed in the past, 2 - Riverside close to the mine tailing, 3 – Site at a hill, relatively distant from the mines, each analysis was performed in triplicate)

Sample	Site	Mean concentration of heavy metal ± SD, μg g^{-1} (dried weight)			
		Ag	Cd	Cu	Pb
Soil	1	42.20 ± 0.65	0.373 ± 0.018	221 ± 7	362 ± 8
	2	3.40 ± 0.07	0.483 ± 0.010	20.6 ± 1.0	194 ± 7
	3	3.20 ± 0.32	0.296 ± 0.011	17.0 ± 0.5	19.4 ± 0.5
Mean concentration of heavy metal ± SD, ng g^{-1} (freeze-dried roots)					
R. communis	1	131 ± 6	16 ± 3	2580 ± 80	2740 ± 60
	2	141 ± 9	123 ± 8	2600 ± 70	1720 ± 50
	3	85 ± 6	12 ± 2	992 ± 17	198 ± 6
T. diversifolia	1	23 ± 2	9 ± 1	530 ± 16	805 ± 18
	2	35 ± 4	15 ± 2	592 ± 20	445 ± 10
	3	< 5 (DL)	< 0.5 (DL)	187 ± 7	20.5 ± 0.6
Opuntia f.	1	27 ± 2	224 ± 9	5030 ± 110	3250 ± 87
	2	8.8 ± 1.2	173 ± 7	4050 ± 98	2190 ± 84
	3	5.3 ± 1.5	124 ± 7	5750 ± 103	854 ± 46

nf – not found.

Table 2. Total PCs in the extracts from plants collected at three sampling sites characterized by different soil metal contents. (1 - Hacienda when the silver ores had been processed in the past, 2 - Riverside close to the mine tailing, 3 – Site at a hill, relatively distant from the mines, 4 – urban area developed on the mine tailing, each analysis was performed in triplicate)

Sampling site	μg of total PCs per gram of the freeze-dried plant homogenates		
	Nopal roots	Nopal leaves	Castor bean roots
1	12.2 ± 0.4	8.4 ± 0.6	2.3 ± 0.2
2	16.8 ± 0.4	10.0 ± 0.3	5.1 ± 0.3
3	27.7 ± 0.3	10.4 ± 0.2	2.2 ± 0.4
4	74.3 ± 0.3	20.3 ±0.2	28.3 ± 0.8

SPECIFIC ROLE OF METALS IN THE PRODUCTION OF PHYTOCHELATINS IN PLANTS, NATURALLY EXPOSED TO A WIDE RANGE OF ELEMENTS

In this work, four metals (Ag, Cd, Cu, Pb) were selected because of their abundance in the Guanajuato region and because of their known capability to induce phytochelatins in plants [10,33-35]. Since the highest levels of total phytochelatins were found in nopal (Table 2), the extracts of this plant were used to study specific metal-PCs binding. As an example, the chromatograms obtained for the plant material from site 3 in Guanajuato are presented in

Figure 2 (cadmium could not be detected). For lead, lower element levels were observed in stems than roots. Furthermore, it eluted mainly as bound to high molecular mass compounds (between 75 – 95 % of total area of chromatogram), but also in the low molecular mass fraction. For copper, only one elution peak was observed in the region of low molecular mass (Figure 2b). Contrary to lead, in many samples the copper abundance in stems was higher than in roots. The elution profile of silver (Figure 2a) indicates its association with high molecular weight compounds; however, the chromatographic peaks were relatively broad suggesting non-specific binding. The results obtained indicate different profiles of metal association with PCs. Based on peak area measurements, the relative distribution of three metals between high and low molecular mass fractions was estimated for each plant sample.

It should be stressed that the procedure by SEC – ICP-MS enabled to get data on specific binding of each metal to PCs, while RPHPLC with fluorimetric detection provided complementary quantitative information on total pool of PCs in plant material (Table 2). In the context of the second question to be answered in this work, which regards the role of individual metals in PCs production, it was considered that the correlation between total PCs and a metal bound to PCs would indicate that this metal is important in the induction of PCs. On the contrary, when no relationship between these two parameters exists, a metal would be just bound to PCs already existing.

The correlation analysis was performed taking the data obtained in the analysis of PCs-rich plant extracts by SEC – ICP-MS and RPHPLC with fluorimetric detection. For lead, significant correlation was found between total PCs and SEC-ICP-MS areas ($r = 0.7026$, $p = 0.088$ for roots and $r = 0.8581$, $p = 0.071$ for stems). Furthermore, total PCs correlated with lead eluted in SEC high molecular mass fraction ($r = 0.6835$, $p = 0.023$ for roots and $r = 0.8818$, $p = 0.048$ for stems). These results confirm the association of Pb with nopal phytochelatins and suggest its possible role in PCs induction. For copper, correlation was observed between total PCs and entire SEC–ICP-MS area in roots ($r=0.7568$, $p = 0.129$) and between total PCs and high molecular mass fraction of SEC in roots ($r= 0.7455$, $p=0.138$). Apparently, copper could be involved in the induction of PCs in roots, however the translocation of lead and copper through the plant is apparently different. No statistically important correlation was found for silver indicating that it is not associated with phytochelatins production.

SOIL PARAMETERS IN RELATION TO THE INDUCTION OF PCS IN WILD PLANTS

As discussed in the Introduction, various processes occurring in the soil-root system are considered important for PCs induction, however the role of environmental parameters, possibly affecting metal bioavailability to plants, remains unclear [19,20]. Binding of polyvalent cations to humic substances derived from different environmental compartments has often been reported and the following order of decreasing affinity has been proposed: Cu(II) > Ni(II) > Co(II) > Pb(II) > Cd(II) > Cr(III) >> (Mn(II), Mo(VI), Zn(II)) [49-51].

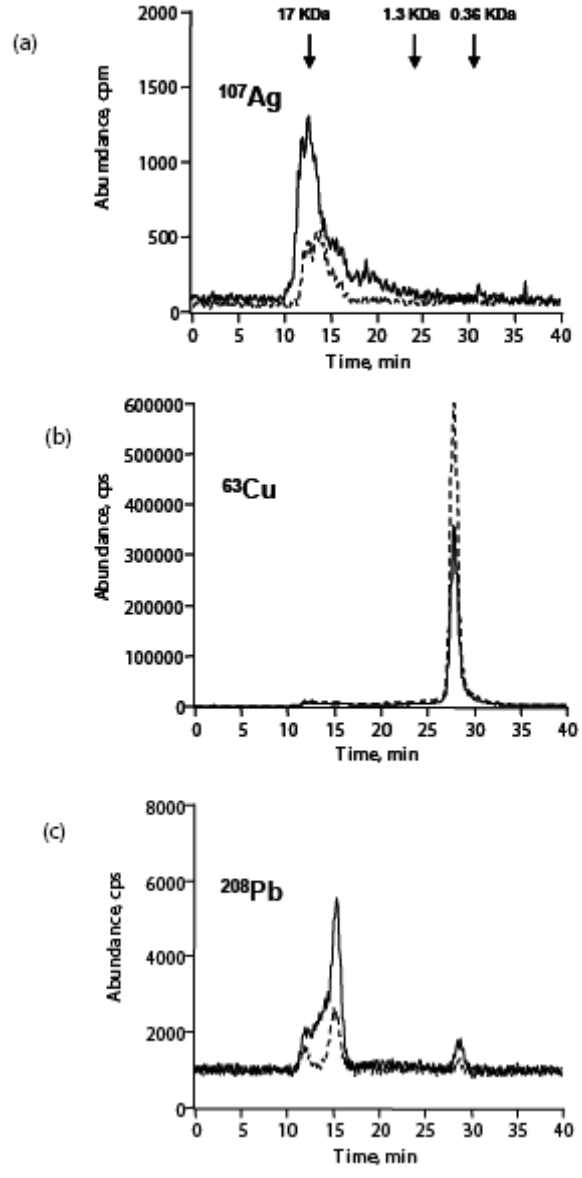

Figure 2. SEC – ICP-MS chromatograms of the (----) nopal stem extract; (_____) nopal root extract: (a) ^{107}Ag; (b) ^{63}Cu; (c) ^{208}Pb .

Several authors observed that humus matter is capable to reduce the bioavailability of certain metals in soils [25,30,52,53]. Based on the above reports, the focus of this work was to evaluate possible relationship between soil humic substances (HS) and PCs.

The HS were assayed in fresh soil samples taken at the roots of nopal and castor bean (two plant synthesizing PCs) and the results obtained are summarized in Table 3. As can be observed, the HS levels were significantly lower in the samples collected at cactus roots, which is in agreement with literature data [54,55]. Consequently, possible relationship between soil HS and PCs production was studied in castor bean plant.

Table 3. The concentrations of soil humic substances found at the roots of two plants in different sampling sites

Sampling site	Soil humic substances, mg g^{-1} (fresh soil)	
	Nopal	Castor bean
1	75 ± 13	481 ± 38
2	453 ± 19	415 ± 42
3	175 ± 23	1345 ±100
4	43 ± 8	553 ± 47
Merida	10 ± 6	-

The statistical analysis of correlation was performed, using all data obtained for Ag, Cd, Cu, Pb in soils and in plant roots, PC-2 in plant extracts and HS in soils. For Cd and Ag, the statistically important positive correlation between metal concentration in soils and in plants was observed ($r = 0.8092$, $p = 0.051$; $r = 0.9261$, $p = 0.009$), while for lead and copper this relation presented low statistical significance ($r = 0.5232$, $p = 0.287$ and $r = 0.5849$, $p = 0.223$ respectively). Strong positive correlation can also been observed between cadmium and lead levels in plant ($r = 0.9664$, $p = 0.002$). On the other hand, the inverse correlation of metal in plants and soil humic substances was found. The statistical significance of such relation decreased in the following order: Cu > Pb > Cd > Ag ($r = -0.7457$, $p = 0.089$; $r = -0.6558$, $p = 0.157$; $r = -0.5280$, $p = 0.282$; $r = -0.2084$, $p = 0.692$, respectively). It should be stressed that the decreasing order of the statistical significance observed in this work is in agreement with the order of heavy metals affinity to humic substances, cited above [49-51]. In the view of our results, the binding of metals to soil humic substances contributes in lowering their uptake by *R. communis*. Apparently, the metals presenting strong affinity to HS have lower bioavailability to this plant. Indeed, there was no important relationship between soil and plant levels for Cu and Pb, but statistically important correlation between these parameters was found for other two elements, presenting lower affinity to HS (Ag and Cd).

On the other hand, the inverse correlation between soil HS and plant PC-2 was found ($r = -0.7825$, $p = 0.066$). Among four metals studied, cadmium levels in soil and in plant presented strong positive correlation with PC-2 ($r = 0.7857$, $p = 0.064$; $r = 0.9395$, $p = 0.005$, respectively). For lead, the correlation was significant only between PC-2 and metal in plants ($r = 0.9573$, $p = 0.003$) and other two metals (Cu, Ag) did not correlate with PC-2 in plants. These results suggest that both, cadmium and lead promote phytochelatin induction in *R. communis*. The lack of correlation between soil Pb and plant PC-2 ($r = 0.4261$, $p = 0.400$) suggest that soil humic substances contribute in lowering the metal uptake by *R. communis*.

To examine the association of metals with soil humic substances, these compounds were extracted from soil with 0.1 M sodium pyrophosphate and analyzed by SEC – ICP-MS as described elsewhere [46]. As an example, two chromatograms are presented in Figure 3 that were obtained in the analysis of soil from site 5 and 6 (HS concentrations 553 mg g^{-1} and 143 mg g^{-1} respectively). The relative distribution of metals in molecular mass fraction corresponding to HS was estimated at each sampling site, by calculating the fraction of metal co-eluted with HS in size exclusion chromatography (peak area between 10 and 18 min of chromatogram with respect to total area of ICP-MS chromatogram) and the results obtained are presented in Table 4.

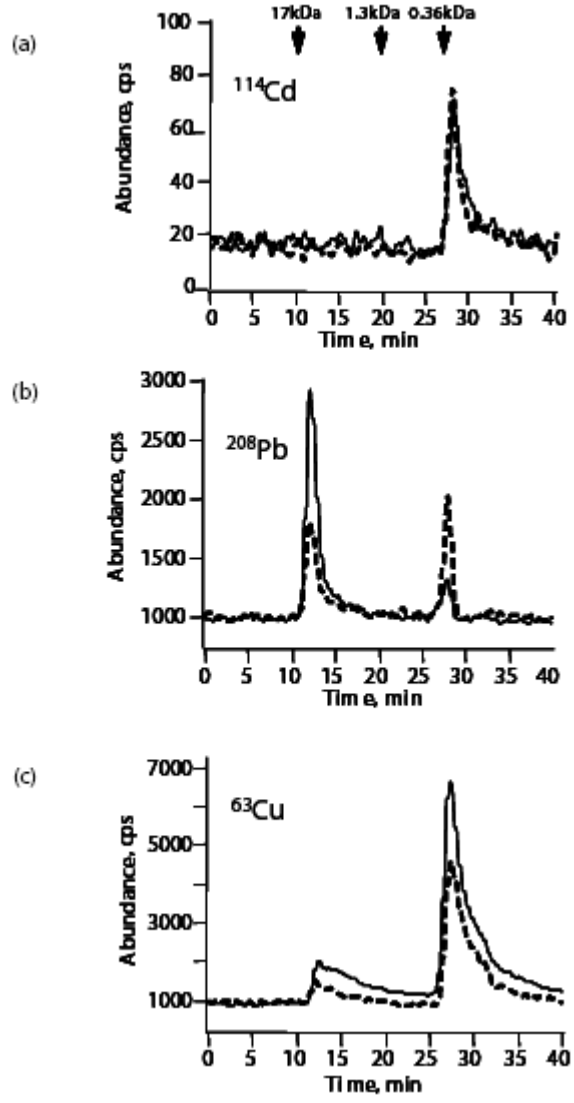

Figure 3. SEC – ICP-MS chromatograms of the soil extracts from site 5 (—) and site 6 (----): (a) ^{114}Cd; (b) ^{208}Pb; (c) ^{63}Cu.

It can be observed that, independently of the HS level, cadmium co-eluted with low molecular mass fraction, so this metal apparently is not bound to HS (Figure 3a, Table 4). For copper and lead, their elution occurred in different molecular mass fractions of the soil extracts (Figure 3b, 3c). As shown in Table 4, higher relative contributions of lead with respect to copper were always observed in the elution region of high molecular mass. Furthermore, the relative distribution of lead was clearly affected by the concentration of HS (Figure 3b). In particular, for higher HS concentrations in soil extract, relatively lower contributions of metal in low molecular mass fractions was observed. These results provide further evidence that the soil humic substances contribute in lower bioavailability of Pb and Cu, that present high affinity to HS.

Table 4. Humic substances in soils and a fraction of metal co-eluted with HS in size exclusion chromatography (based on the peak area measurement vs total area of chromatogram).

Sampling site	HS, mg g^{-1}	Metal association with soil HS[(a)]		
		Cd	Cu	Pb
1	481	0	1.4	14
2	415	0	15	100
3	1345	0	24	72
4	372	0	7.4	59
5	553	0	17	94
6	143	0	32	27

[(a)]- % of metal in soil extract, which co-eluted with HS in size exclusion chromatography.

Since soils adjacent to the nopal roots contained low concentrations of humic substances, it cannot be expected that this parameter would affect metal uptake by plant. To get more information on the bioavailable metal forms, sequential extraction of soils from sites 1 – 6 was performed and the four metals of interest were determined in each fraction. The simplified Tessier method enables to extract the following fractions: F1 – exchangeable; F2 - fraction bound to carbonates; F3 - associated with oxides of iron and manganese; F4 - organic matter and sulfides and F5 – residual. The results obtained showed that the major fractions of Pb and Cu were bound to F4 at any sampling site (62.9 % - 86.3 % of total soil Pb and 60.4 % - 65.1 % of total soil Cu respectively) Significantly lower levels of these two metals were found in carbonate fractions (F2: less than 10 % of total Pb and less than 10 % of Cu in soil) and only minute amounts corresponded to “free” Pb or Cu (F1). For Ag, practically all the metal was bound to the organic matter and sulfides (F4, more than 95 % of total soil Ag). As already mentioned, the Cd soil levels were lower as compared to other metals, however, relatively uniform metal distribution among F1 – F5 fractions was observed. At sites 1 and 4, the relative distribution of “free” Cd was 36 % and 32 % respectively.

In search of any relationship between Pb, Cu and Ag levels in soil fractions F1 – F5 and root/leave concentrations of these metals, the statistical correlation analysis was carried out taking analytical data obtained at six sampling sites (Cd was excluded, because of its low concentrations in soil and in plant tissues). No statistically important correlation was found between metal levels in soil versus leaves. The correlation parameters obtained for roots and soil data are presented in Table 5. At first, for Pb and Cu, total (acid-digested) metal in soil did not correlate strongly with its concentration in plant ($r = 0.7321$, $p = 0.176$ and $r = 0.8169$, $p = 0.091$, respectively). Furthermore, no statistically important correlation was found between any metal in the fractions F1 (exchangeable), F2 (carbonates), F3 (manganese and iron oxides) or F5 (residual) and root metal, indicating that these fractions were not important for the uptake of Cu, Pb and Ag by nopal. On the other hand, statistically significant correlations found between metal in F4 and root metals ($r = 0.8436$, $p = 0.072$ for Pb; $r = 0.8648$, $p = 0.058$ for Cu; $r = 0.8842$, $p = 0.046$ for Ag, Table 5) suggest that organic matter and sulfide bound metals (fraction F4) should be bioavailable to nopal. The results obtained in spectrophotometric assay revealed low levels of humic substances (primary soil organic matter) in soils adjacent to the roots of nopal (Table 3). On the other hand, sulfide minerals are abundant in Guanajuato region [56].

Table 5. Statistical analysis of correlation between total metal concentrations in soil and soil fractions F1 – F5 and their levels found in nopal roots

metal in soil vs metal in roots	Pb	Cu	Ag
soil *vs.* root	0.7321	r = 0.8169	r = 0.9368
	0.176	p = 0.091	p = 0.019
F1 *vs.* root	nf	nf	nf
F2 *vs.* root	nf	nf	nf
F3 *vs.* root	nf	nf	nf
F4 *vs.* root	r = 0.8436	r = 0.8648	r = 0.8842
	p = 0.072	p = 0.058	p = 0.046
F4 *vs.* root	nf	nf	nf

nf – no statistically important correlation was found.

Our results suggest that sulfides are primary Pb, Cu and Cd forms in soil close to the cactus roots (at least 20 cm from the roots). The solubility of these compounds is generally poor, so the rhizosphere processes and, in particular root exudation of low-molecular weight carboxylic acids should be important in mobilizing sulphide bound metals [57,58]. However, the literature data on these processes in nopal or other cactaceous is scarce. Puente et al.[59] proposed the contribution of bacteria and fungi in the rhizoplane of nopal roots (the area at the plant and soil interface) as a factor increasing metal bioavailability.

CONCLUSION

The results obtained in this study enable to answer the interrogations set up at the beginning. In particular it can be concluded that the wild plants, chronically exposed to low/moderate metal levels in soil biosynthesize phytochelatins. In the analysis of three different plants collected simultaneously at these same sites, PCs were found in nopal and in castor bean, but not in Mexican sunflower, which seems to confirm that phytochelatin induction is genotype dependent. Furthermore, lead and cadmium were found to be important for PCs induction in nopal. It is proposed that the uptake of these metals could be controlled by rizosphere processes. In the case of castor bean, the metals promoting PCs induction in plant were also cadmium and lead, however, their uptake is apparently controlled by the association of metals with soil HS.

In general, the results obtained provide evidence that PCs induction in plants growing in natural environments depends on: (i) total element concentrations in soil; (ii) actual physicochemical forms of elements in soil; (iii) organic matter content in soil and (iv) different processes occurring in rizosphere.

REFERENCES

[1] Zenk, M.H. *Gene* 1996, 179, 21-30.
[2] Hirata, K.; Tsuji, N.; Miyamoto, K. *J Biosci Bioeng* 2005, 100, 593–599.

[3] Persson, D.P.; Hansen, T.H.; Holm, P.E.; Schjoerring, J.K.; Hansen, H.C.B.; Nielsen, J.; Cakmak, I.; Husted, S. *J. Anal. At Spectrom.* 2006, 21, 996-1005.
[4] Clemens, S. *Planta* 2001, 212, 475-486.
[5] Thumann, J.; Grill, E.; Winnacker, E.L.; Zenk, M.H. *FEBS Lett* 1991, 284, 66-91.
[6] Takagi, M.; Satofuka, H.; Amano, S.; Mizuno, H.; Eguchi, Y.; Hirata, K.; Miyamoto, K.; Fukui, K.; Imanaka, T. *J Biochem* (Tokyo) 2002, 131, 233-239.
[7] Yen, T.Y.; Villa, J.A; DeWitt, J.G. *J. Mass Spectrom.* 1999, 34, 930-941.
[8] Le Faucheur, S.; Behra, R.; Sigg, L. *Environ.Toxicol. Chem.* 2005, 24, 1731-1737.
[9] Grill, E.; Winnacker, E.L.; Zenk, M.H. *Science* 1985, 230, 674–676.
[10] Scarano, G.; Morelli, E. *Biometals* 2002, 15, 145-151.
[11] Spain, S.M.; Rabenstein, D.L. *Anal. Chem.* 2003, 75, 3712-3719.
[12] Cobbett, C.S. *Curr. Opin. Plant. Biol.* 2000, 3, 211-216.
[13] Clemens, S. *J. Plant. Physiol.* 2006, 163, 319-332.
[14] Mejare, M.; Bülow, L. *Trends Biotechnol* 2001, 19, 67-73.
[15] Meagher, R.B. *Curr. Opin. Plant Biol.* 2000, 3, 153-162.
[16] Bovet, L.; Feller, U.; Martinoia, E. *Environ. Int.* 2005, 31, 263-267.
[17] Yang, X.; Feng, Y.; He, Z.; Stoffella, P.J. *J. Trace Elem. Med. Biol.* 2005, 18, 339-353.
[18] Clemens, S. *Int. J. Occup. Med. Environ. Health* 2001, 14, 235-239.
[19] Koster, M.; Reijnders, L.; van Oost, N.R.; Peijnenburg, W.J. *Environ. Pollut*. 2005, 133, 103-116.
[20] Lucho Constantino, C.A.; Prieto García, F.; del Razo, L.M.; Rodriguez Vazquez, R.; Poggi Varaldo, H.M. *Agric. Ecosys. Environ.* 2005, 108, 57-71.
[21] Piechalak, A.; Tomaszewska, B.; Baralkiewicz, D. *Phytochemistry* 2003, 64, 1239-1251.
[22] Sun, Q.; Wang, X.R.; Ding, S.M.; Yuan, X.F. *Chemosphere* 2005, 60, 22-31.
[23] Meers, E.; Ruttens, A.; Hopgood, M.J.; Samson, D.; Tack, F.M. *Chemosphere* 2005, 58, 1011-1022.
[24] Turgut, C.; Katie Pepe, M.; Cutright, T.J. *Environ. Pollut.* 2004, 131, 147-154.
[25] Lorenzo, J.I.; Beiras, R.; Mubiana, V.K.; Blust, R. *Environ. Toxicol. Chem.* 2005, 24, 973-980.
[26] Voets, J.; Bervoets, L.; Blust, R. *Environ. Sci. Technol.* 2004, 38, 1003-1008.
[27] Garcia-Mina, J.M.; Antolin, M.C.; Sanchez-Diaz, M. *Plant. and Soil.*2004, 258, 57-68.
[28] Misra, V.; Pandey, S.D. *Bull. Environ. Contam. Toxicol.* 2005, 74, 725-731.
[29] Inaba, S.; Takenaka, C. *Environ. Int.* 2005, 31, 603-608.
[30] Kungolos, A.; Samaras, P.; Tsiridis, V.; Petala, M.; Sakellaropoulos, G. *J. Environ. Sci.* Health A Tox Hazard Subst *Environ. Eng.* 2006, 41, 1509-1517.
[31] Garcia-Meza, V.; Ramos, E.; Carrillo-Chavez, A.; Duran-de-Bazua, C. *Bull. Environ. Contam. Toxicol.* 2004, 72, 170-177.
[32] Morton-Bermea, O.; Carrillo-Chavez, A.; Hernandez, E.; Gonzalez-Partida, E. B*ull. Environ. Contam. Toxicol.* 2004, 73, 770-776.
[33] Morelli, E.; Scarano, G. *Mar. Environ. Res.* 2001, 52, 383-395.
[34] Keltjens, W.G.; Van Beusichem, M.L. *Plant and Soil* 1998, 203, 119-126.
[35] Maitani, T.; Kubota, H.; Sato, K.; Yamada, T. *Plant Physiol.* 1996, 110, 1145-1150.
[36] Landero Figueroa, J.A.; Wrobel, K.; Afton, S.; Caruso, J. A.; Gutierrez Corona, J.F.; Wrobel, K. *Chemosphere* 2008, 70, 2084-2091.

[37] Mehra, R.K.; Tran, K.; Scott, G.W.; Mulchandani, P.; Saini, S.S. *J Inorg Biochem* 1996, 61, 125-142.
[38] Giordani, C.; Cecchi, S.; Zanchi, C. *Environ Manage* 2005, 36, 675-681.
[39] Khan, A.G.; Chaudhry, W.J.; Hayes, W.J.; Khoo, C.S.; Hill, L.; Fernández, R.; Gallardo, P. *Water Air Soil Poll* 1998, 104, 389-402.
[40] Gupta, A.K.; Sinha, S. *Bioresour. Technol.* 2006, 98, 1788-1794.
[41] Olivares, E.; Peña, E.; Aguiar, G. *J. Plant Physiol.* 2002, 59, 743–749.
[42] Tessier, A.; Campbell, P.G.C.; Bisson, *N.J. Anal. Chem.* 1979, 51, 844.
[43] Pereira Navaza, A.; Montes-Bayon, M.; LeDuc, D.L.; Terry, N.; Sanz-Medel, A. *J. Mass Spectrom.* 2006, 41, 323–331.
[44] Doring, S.; Korhammer, S.; Oetken, M.; Markert, B. Fresenius *J. Anal. Chem.* 2000, 366, 316-318.
[45] Sneller, F.E.; van Heerwaarden, L.M.; Koevoets, P.L.; Vooijs, R.; Schat, H.; Verkleij, J.A. *J. Agric. Food Chem.* 2000, 48, 4014-4019.
[46] Wrobel, K.; Sadi, B.B.M.; Wrobel, K.; Castillo, J.R.; Caruso, *J.A. Anal. Chem.* 2003, 75, 761-767.
[47] Tang, D.; Shafer, M.M.; Vang, K.; Karner, D.A.; Armstrong, D.E. *J. Chromatogr.* A 2003, 998, 31-40.
[48] Hall, J.L. *J. Exp. Bot.* 2002, 53, 1-11.
[49] Evangelou, V.P.; Marsi, M. *Plant and Soil* 2001, 229, 13-24.
[50] Pandey, A.K.; Pandey, S.D.; Misra, V. *Ecotoxicol. Environ. Safe* 2003, 47, 195.
[51] Sadi, B.B.M.; Wrobel, K.; Wrobel, Z.; Kannamkumarath, S.S.; Castillo, J.R.; Caruso, J.A. *J. Environ. Monit.* 2002, 4, 1010-1016.
[52] Lamelas, C.; Wilkinson, K.J.; Slaveykova, V.I. *Environ. Sci. Technol.* 2005, 39, 6109-6116.
[53] Remon, E.; Bouchardon, J.L.; Cornier, B.; Guy, B.; Leclerc, J.C.; Faure, O. *Environ. Pollut.* 2005, 137, 316-323.
[54] Galizzi, F.A.; Felker, P.; Gonzalez, C.; Gardiner, D. *J Arid Environ* 2004, 59, 115-132.
[55] Burke, I.C.; Lauenroth, W.K.; Riggle, R.; Brannen, P.; Madigan, B.; Beard, S. *Ecosystems* 1999, 2, 422-438.
[56] Carrillo-Chavez, A., Morton-Bermea, O.; Gonzalez-Partida, E.; Rivas-Solorzano, H.; Oesler, G.; Garcia-Meza, V.; Hernandez, E.; Morales, P.; Cienfuegos, E. Ore *Geol. Rev.* 2003, 23, 277–297.
[57] Wenzel, W.W.; Lombi, E.; Adriano, D.C. in: *Heavy Metal Stress in Plants*, 2004, pp. 313-344 (Prasad, M.N.V., Ed.) Springer-Verlag, Berlin, Germany.
[58] Jones, D.L.; Hodge, A.; Kuzyakov, Y. *New Phytologist* 2004, 163, 459-480.
[59] Puente, M.E.; Bashan, Y.; Li, C.Y.; Lebsky, V.K. *Plant Biol.* (Stuttg) 2004, 6, 629-642.

INDEX

A

B

C

D

E

F

G

H

I

J

K

L

M

N

O

P

Q

R

S

T

U

V

W

Y

Z